VALDAI PERIGLACIAL FIELD SYMPOSIUM GUIDEBOOK

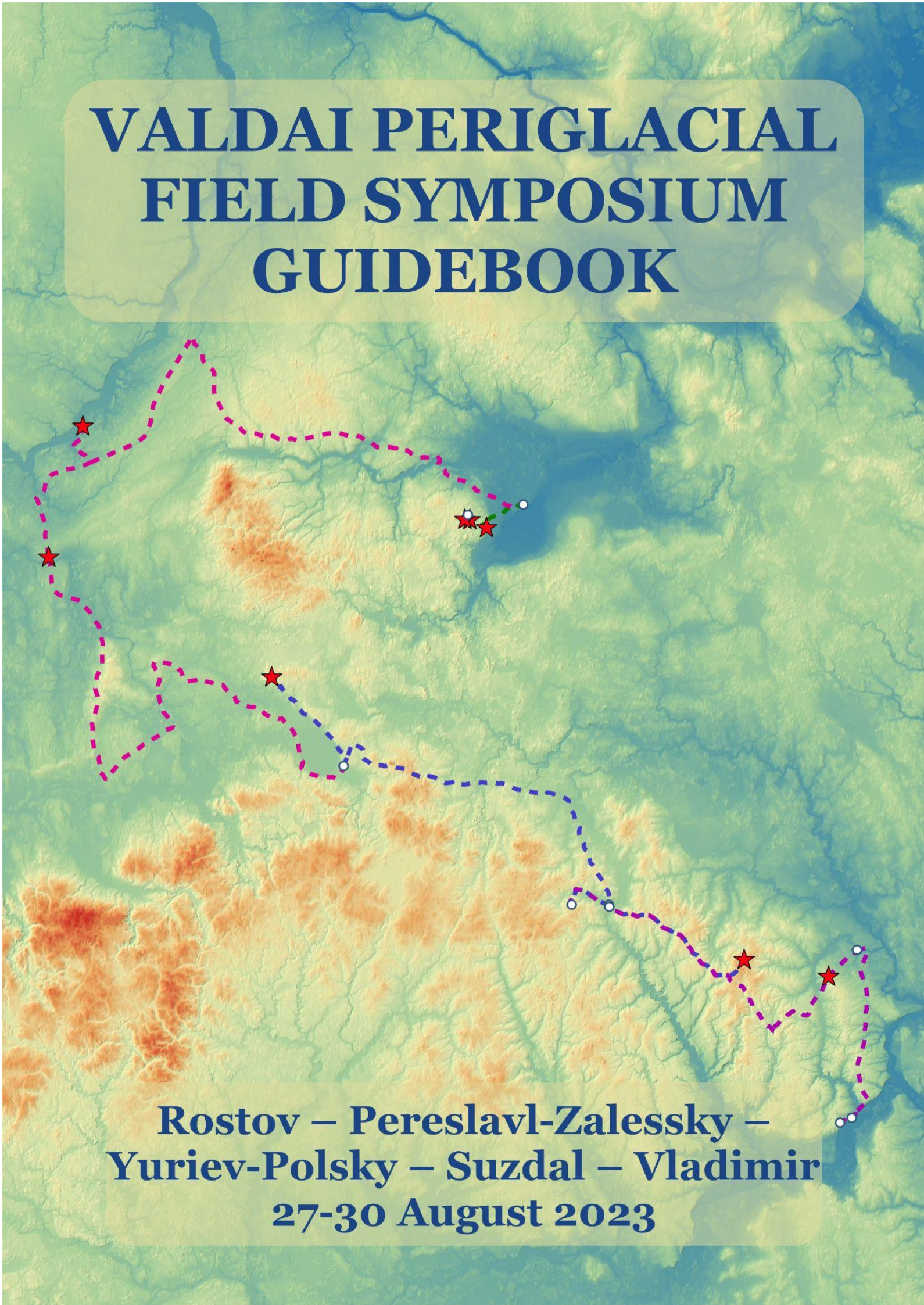

Rostov – Pereslavl-Zalessky – Yuriev-Polsky – Suzdal – Vladimir

27-30 August 2023

VALDAI PERIGLACIAL FIELD SYMPOSIUM GUIDEBOOK

Rostov – Pereslavl-Zalessky – Yuriev-Polsky – Suzdal – Vladimir

27–30 August 2023

ПЕРИГЛЯЦИАЛ ВОСТОЧНО-ЕВРОПЕЙСКОЙ РАВНИНЫ

ПУТЕВОДИТЕЛЬ ПОЛЕВОГО СИМПОЗИУМА

Ростов – Переславль-Залесский – Юрьев-Польский – Суздаль – Владимир

27–30 августа 2023

УДК 551.89
ББК 26.82
DOI: 10.15356/periglacial978-5-89658-071-3

Approved for publication by
the Academic Council of the Institute of Geography, Russian Academy of Sciences

Valdai Periglacial Field Symposium Guidebook, 27–30 August 2023 [Electronic edition] – IG RAS, Moscow, 2023. 160 p.

This issue considers new and only partially previously published data on the Late Pleistocene landscapes and deposits of the Moscow glaciation marginal zone, which has experienced dynamic periglacial conditions during the Valdai epoch. The manuscript is arranged as a guidebook for the Valdai Perglacial Field Symposium, which was held on 27–30 August 2023 embracing the Upper Volga and Vladimir Opolie regions in the center of the East-European Plain. The field route captured the unique landscapes of Borisoglebsk Upland and Rostov Lowland, Volga Valley terraces and surrounding moraines, Shikhobalovo and Suzdal plateaus.

Reconstructions of environmental settings of the former periglacial zone accomplished by several scientific teams are presented based on the studies of lacustrine and palustrine paleoarchives, palimpsest records of cover deposits, and fluvial channel morphology and alluvial infills. The structure of postglacial sedimentary cover embedding relict cryogenic phenomena and paleosols, both buried and surface, is examined. Thus, the origins and age of mantle (loess-like) loams and the input of cryogenic relicts on the soil cover spatial organization and paleosol structure are discussed, and problems of the paleohydrological development of the Upper Volga Basin are raised.

This issue targets specialists in the fields of Quaternary geology and paleogeography, paleopedology and soil geography, geomorphology, cryolithology, and paleolimnology, as well as undergraduates and graduates studying Earth Sciences.

ISBN 978-5-89658-071-3

Moscow, 2023

УДК 551.89
ББК 26.82
DOI: 10.15356/periglacial978-5-89658-071-3

Утверждено к печати Ученым советом Института географии РАН

Перигляциал Восточно-Европейской равнины. Путеводитель к полевому симпозиуму, 27–30 августа 2023 г. [Электронное издание] – М.: ИГ РАН, 2023. 160 с.

В издании представлены новые и лишь частично ранее опубликованные данные о позднеплейстоценовых ландшафтах и отложениях краевой зоны московского оледенения, испытавшей в валдайскую эпоху динамичные преобразования в перигляциальных условиях. Книга оформлена как путеводитель к полевому симпозиуму “Перигляциал Восточно-Европейской равнины”, который прошёл с 27 по 30 августа 2023 г. по территории Верхневолжья и Владимирского Ополья. Полевой маршрут захватил уникальные ландшафты Борисоглебской возвышенности и Ростовской низменности, террас долины Волги и окружающих моренных гряд, Шихобаловского и Суздальского плато.

Представлены реконструкции природных обстановок бывшей перигляциальной зоны, выполненные несколькими научными коллективами на основе изучения озерных и болотных палеоархивов, палимпсестовой памяти покровных отложений, морфологии речных русел и аллювиальных выполнений. Рассмотрено строение послеледникового осадочного чехла, вмещающего реликтовые криогенные горизонты и палеопочвы, как погребенные, так и поверхностные. Таким образом, обсуждаются происхождение и возраст покровных (лёссовидных) суглинков, вклад криогенных реликтов в пространственную организацию почвенного покрова и структуру палеопочв, а также поднимаются проблемы палеогидрологического развития бассейна Верхней Волги.

Этот выпуск предназначен для специалистов в области четвертичной геологии и палеогеографии, палеопочвоведения и географии почв, геоморфологии, криолитологии и палеолимнологии, а также студентов и аспирантов, изучающих науки о Земле.

ISBN 978-5-89658-071-3

Москва, 2023

CONTENTS

PREFACE

"Valdai Periglacial" scientific conference and field symposium (Fig. 1) was organized by the Institute of Geography, RAS with the support of the Soil Science Faculty, Lomonosov Moscow State University; Institute of Earth Sciences, Saint-Petersburg State University; Faculty of Geography, Herzen State Pedagogical University; Commission for Study of the Quaternary; agricultural enterprise Red Mayak LLC; and the State Museum-Reserve "Rostov Kremlin", in which premises the in-doors events were held. The geography of participants stretched from Kaliningrad to Tyumen, and from Orenburg to Karelia, with two capitals – Moscow and Saint-Petersburg – providing the largest delegations (Makeev et al., 2023).

Landscapes of the Rostov Lowland and Borisoglebsk Upland have been the focal attention of Russian scientists since the mid-XIX century. There, at the well-renowned Early Medieval Sarsky Gorodische, Meryan settlements and burial mounds near the village of Shurskol, the efforts of Count A.S. Uvarov's expedition laid the core stone of the Russian school of archeology in 1851. Almost three decades later, in 1878, dark-colored soils of the Lake Nero low terraces – the notorious "Rostov chernozems" – were studied by the founder of pedology Prof. V.V. Dokuchaev. He determined their ultimate lacustrine origin and dispelled the myth of their relationship with the fertile soils of steppes.

Figure 1. Participants of the Valdai Periglacial Field Symposium against the Borisoglebsk Upland landscapes.

The first half of the XX century is associated with the classic works of soil scientists and Quaternary geologists, e.g., scientific groups of A.A. Krasyuk, K.K. Markov, I.P. Gerasimov. Found in the late 1930s by N.V. Chizhikov (1956), unique postglacial deposits have been

studied in the gully incisions near the village of Cheremoshnik (Figs. 2 & 3). Without exaggeration, those late Quaternary sections have gained international acclaim and even were depicted in fiction art pieces (Dorosh, 1973). At the dawn of the radiocarbon age determination of organic matter in the late 1950s, some of the first dates in the USSR were obtained for certain peat, wood, and soil samples from the NE Borisoglebsk Upland (Serebryanny, 1965).

The current Symposium pursues a series of scientific events dedicated to the geomorphology, Quaternary geology, and paleogeography of the Upper Volga Region. In August 1969, the International Symposium "Paleogeography and Pleistocene Periglacial Phenomena" was organized by the Commission for Study of the Quaternary, USSR Academy of Sciences (Markov et al., 1969; Ivanova, 1972) as one of the VIII INQUA Congress events (Paris, 30 August – 5 September, 1969) on the initiative of K.K. Markov, Chairman of the INQUA Paleogeographical Commission, USSR AS Corresponding Member. The symposium was reminiscent of the current conference. Assembly of no further than 20 oral presentations was crowned with an extensive three-day field excursion around the Upper Volga (Fig. 2) and another tour to Yakutia.

Figure 2. Title page of the Guidebook "Moscow – Upper Volga" for the International Symposium on Paleogeography and Pleistocene Periglacial Phenomena (Markov et al., 1969) and the following year photo featuring V.A. Novsky in front of the Cheremoshnik-B section (Moskvitin, 1976).

In 1981, the XI INQUA Congress was held in Moscow with a couple of excursions visiting the Upper Volga and the Golden Ring touristic route (Shik & Tseytlin, 1981). Just three years later at the XXVII International Geological Congress, a two-day bus excursion followed in the footsteps (4–14 August 1984, Moscow) (Sudakova et al., 1984) led by N.G. Sudakova (MSU) and V.V. Dashevsky (Ministry of Natural Resources RSFSR). At the turn of the millennia, in July 2001, another symposium of the RAS Commission for Study of the Quaternary "Problems of the stratigraphy of Quaternary deposits and geoecology of the Yaroslavl Volga Region" was held in Yaroslavl (Lavrushin & Chistyakova, 2001). Researchers of the Yaroslavl and adjacent regions took part in the symposium coming from Moscow, Saint-Petersburg, Syktyvkar, Saransk, and Cherepovets. Three scientific excursions were conducted to examine the Quaternary sections in the vicinity of Rybinsk, Uglich, and Rostov.

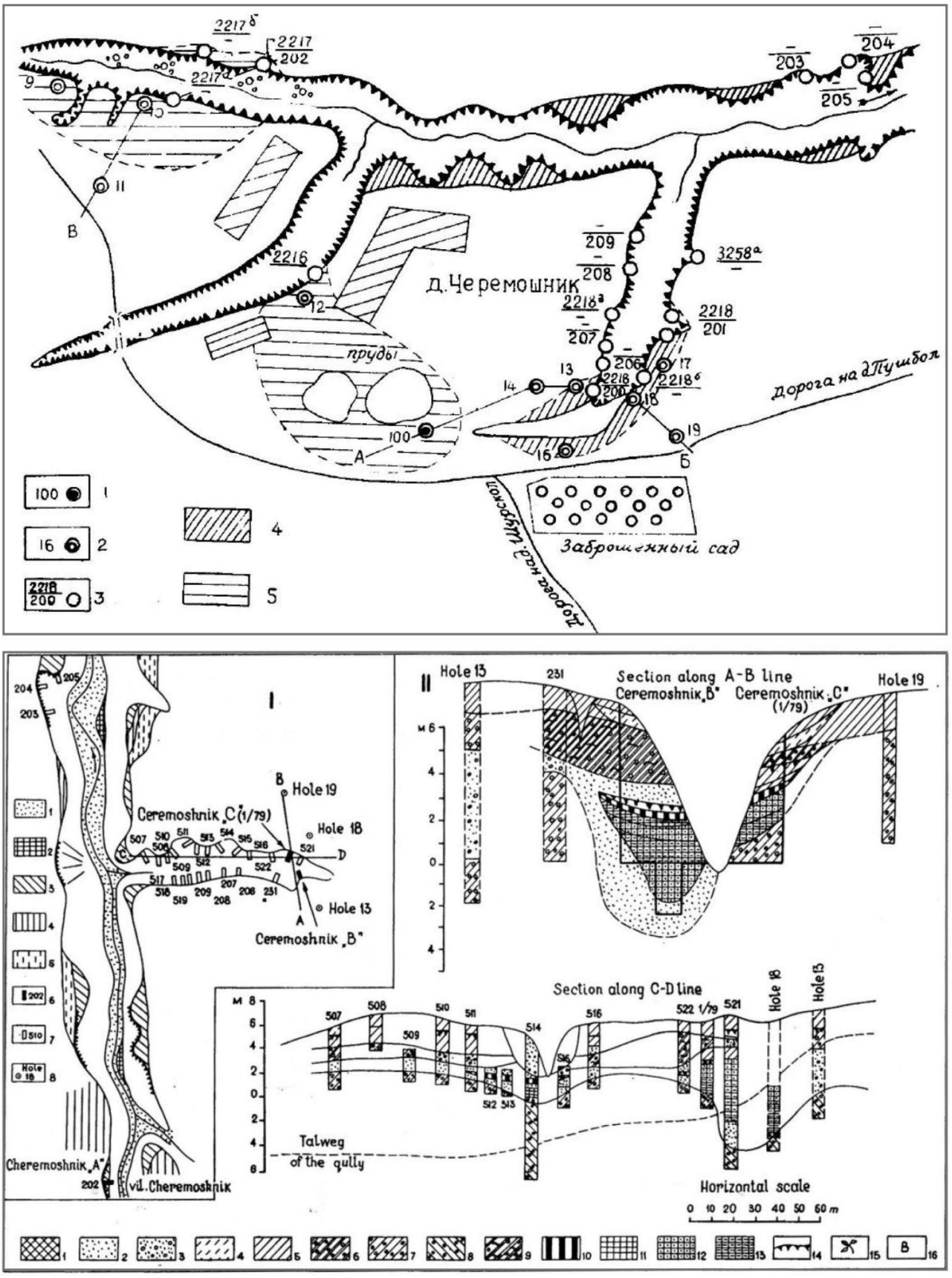

Figure 3. Sketches of geological exposures and their positions in the Cheremoshnik-Puzhbol gully system presented in the guidebook "Moscow – Upper Volga" for the International Symposium on Paleogeography and Pleistocene Periglacial Phenomena (Markov et al., 1969) and Excursion 10–B guidebook "Quaternary deposits near the town of Rostov-Yaroslavsky" for the XXVII International Geological Congress (Sudakova et al., 1984).

In fine traditions, the current Symposium comprised scientific sessions, workshops, and a four-day field tour embracing a wide range of issues of Quaternary geology and paleogeography, geomorphology, pedology, paleoclimatology, paleolimnology, cryolithology, and other related scientific fields with an emphasis on the Late Valdai environments conditioned by the dynamic climatic rhythms of cold and warm, arid and humid oscillations (Palacios et al., 2022). Those rhythms constrained the sedimentation and pedogenesis against the widespread permafrost and erosion phenomena and lake environments. Episodes of surface stabilization associated with the paleosol development were rhythmically disturbed by slope and subaerial sedimentation and cryogenic deformations.

Formed in periglacial settings and polygenetic in nature, loamy deposits largely governed the organization of modern soil bodies and soil cover. So far, reconstructions of complex dynamics of the Late Pleistocene sedimentation and pedogenesis have been based on the infills of depressions of the initial glacial topography (i.a. Markov et al., 1969; Moskvitin, 1967, 1976; Novsky, 1975; Sudakova et al., 1984; Lavrushin & Chistyakova, 2001; Rusakov et al., 2015, 2017, 2019; Shishkina et al., 2019; Garankina et al., 2019, 2022 Belyaev et al., 2020; Sheremeskaya et al., 2022). However, in autonomous and subordinate paleolandscape positions, the integrity of paleogeographic records varies significantly. That issue emphasizes the relevance of studying interfluvial landscapes of the Moscow glaciation marginal zone while the reconstruction of Last Deglaciation and Late Glacial events (21–11 ka) (Palacios et al., 2022) remains the most controversial reflecting the increasing frequency and contrast of environmental changes.

On the first day (25 August), a thematic workshop at the Museum of Rostov Merchantry was dedicated to the paleogeographical issues of the Rostov Lowland, Borisoglebsk Upland, and Upper Volga Valley (Fig. 4a).

Figure 4. Thematic workshop "Paleogeographical issues of Rostov Lowland, Borisoglebsk Upland, and Upper Volga Valley" at the city estate of Kekin merchants (a) and welcoming speech of A.V. Panin during the opening of the conference at the Stable Yard of Rostov Kremlin (b).

On 26 August, oral and poster sessions proceeded in the Stable Yard of the Rostov Kremlin (Fig. 4b). V.I. Astakhov opened the plenary session by comparing the Last Periglacial of the Russian Plain with the adjacent regions. It was followed by presentations of D.A. Subetto (On the issue of glaciolacustrine deposition); O.K. Borisova (An attempt at reconstructing vegetation and climate in the periglacial region of the Late Valdai glaciation based on paleofloristic data); I.D. Streletskaya (Polygonal structures and associated deformations in deposits); A.O. Makeev (Soils on Moscow Cryochron tills as an archive of paleogeographic information); E.V. Garankina (Mantle loams as a periglacial phenomenon: origin and age); A.A. Gol'yeva (Phytolithic complexes of soils and cultural layers of Vladimir Opolye), S.I. Larin (Periglacial relicts of Sartan Cryochron in the

SW of Western Siberia); E.Yu. Novenko (Interstadial Late Pleistocene vegetation of Middle Desna Basin: reconstruction based on paleobotanical data from Khotylevo I section); A.G. Ryabukha (Paleocryogenic origin of microdepression landscape of Orenburg Region); and A.V. Panin (On existence of a hypothetical Tver proglacial lake in context of the primary settlement of Dubninskaya Lowland). The following sessions put an emphasis on the reports by young researchers and students against the results of profound scholars yielding an enriched discussion.

In-door debates were followed by a four-day field trip familiarizing the attendees with the topography, geological sections, buried soils, and relict cryogenic horizons of the Valdai periglacial zone (Fig. A). Field sites were presented by E.A. Konstantinov (IG RAS), A.V. Rusakov (SPbSU), E.V. Garankina (MSU), I.G. Shorkunov (IG RAS), A.O. Makeev (MSU), V.A. Lobkov (IG RAS), and L.S. Frolova (MSU). Students and graduates of the Faculties of Geography and Soil Sciences, MSU, and PhD students and young scientists of the Institute of Geography, RAS took a major part in organizing the field tour and preparing the key sections for the field presentation.

On the first day of the field tour (27 August), the participants engaged with the fluvial history of the Nero Lake basin (Fig. 5) as well as the glacial topography of the Borisoglebsk Upland (Figs. B–C). Lake sedimentation as the leading driver of its postglacial transformation was presented in the quarry walls showing the complex relationship of lacustrine and glacial deposits (Fig. 6). Structure of the interfluvial sedimentary cover including buried soil horizons, pedosediments, and their cryogenic deformations was displayed in a large soil pit on the flat top of the highest hill in the vicinity (Fig. 7).

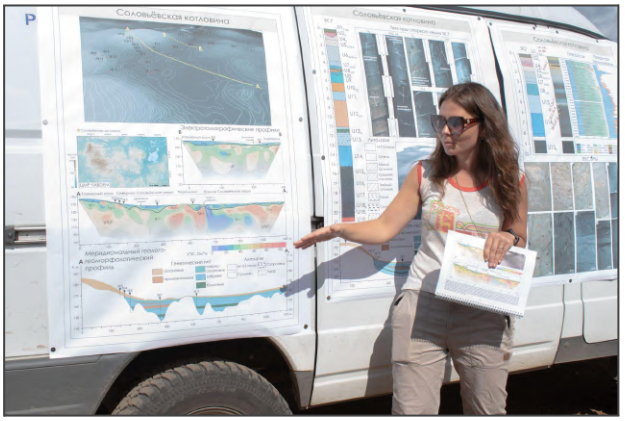

Figure 5. Katerina Garankina showcases lacustrine sedimentary sequences of NE Borisoglebsk Upland.

Figure 6. Discussion concerning the contact of lacustrine and glacial deposits in the Solovey Quarry.

Figure 7. Ilya Shorkunov demonstrates the cover deposits of the Borisoglebsk Upland interfluves.

Second and third days (28–29 August) were spent examining terraces of the Volga Valley and adjacent moraine ridges in the elevation range of 117 to 180 m a.s.l. (Fig. 8). Participants observed the relict glacial landscape of Moscow age and soils in bipartite deposits. The absence of river terraces in the Upper Volga Valley was emphasized with attention drawn to the Late Glacial eolian reworking of the upper layer above till on bedrock terraces.

Figure 8. Alexander Makeev presents the geological structure of terraces of the Upper Volga Valley and a soil profile in bipartite sediments.

On the third and fourh field days (29–30 August), participants got acquainted with the landscape (Figs. D–E) and geological structure of the Vladimir Opolie (Figs. 9 & 10). Its soil cover majorly inherited relict permafrost features – block-and-through paleocryogenic topography. Issues of the early human settlement and later agricultural development were also raised during the excursion.

Figure 9. Irina Streletskaya elaborates on the nature of permafrost features in the soil profile of the Shikhobalovo Plateau.

Figure 10. Vasily Lobkov and Lyubov Frolova present the soil cover heterogeneity and buried paleosols of the Suzdal Plateau.

Centered on the environmental history of the periglacial zone, the Symposium route was accompanied by the monuments of ancient Russian history and culture widely represented along the Golden Ring (Fig. A).

Photos in Figs. 6 & 8–10 are courtesy of Dmitry Baranov, Figs. 1 & 4 of Ilya Shorkunov, Figs. 7 & 11 of Ekaterina Garankina, Fig. 5 of Lubov Frolova.

Those wishing to learn more about the Symposium backstage may visit social media of the Department of Paleogeography, Institute of Geography RAS: https://vk.com/quaternary_science, and the Laboraory of paleoarchives https://web.telegram.org/a/#-1729705721.

Conference materials "Periglacial of East-European Plain and Western Siberia" (released in Russian) can be downloaded here: http://eg.igras.ru/ru/quarternea2023/.

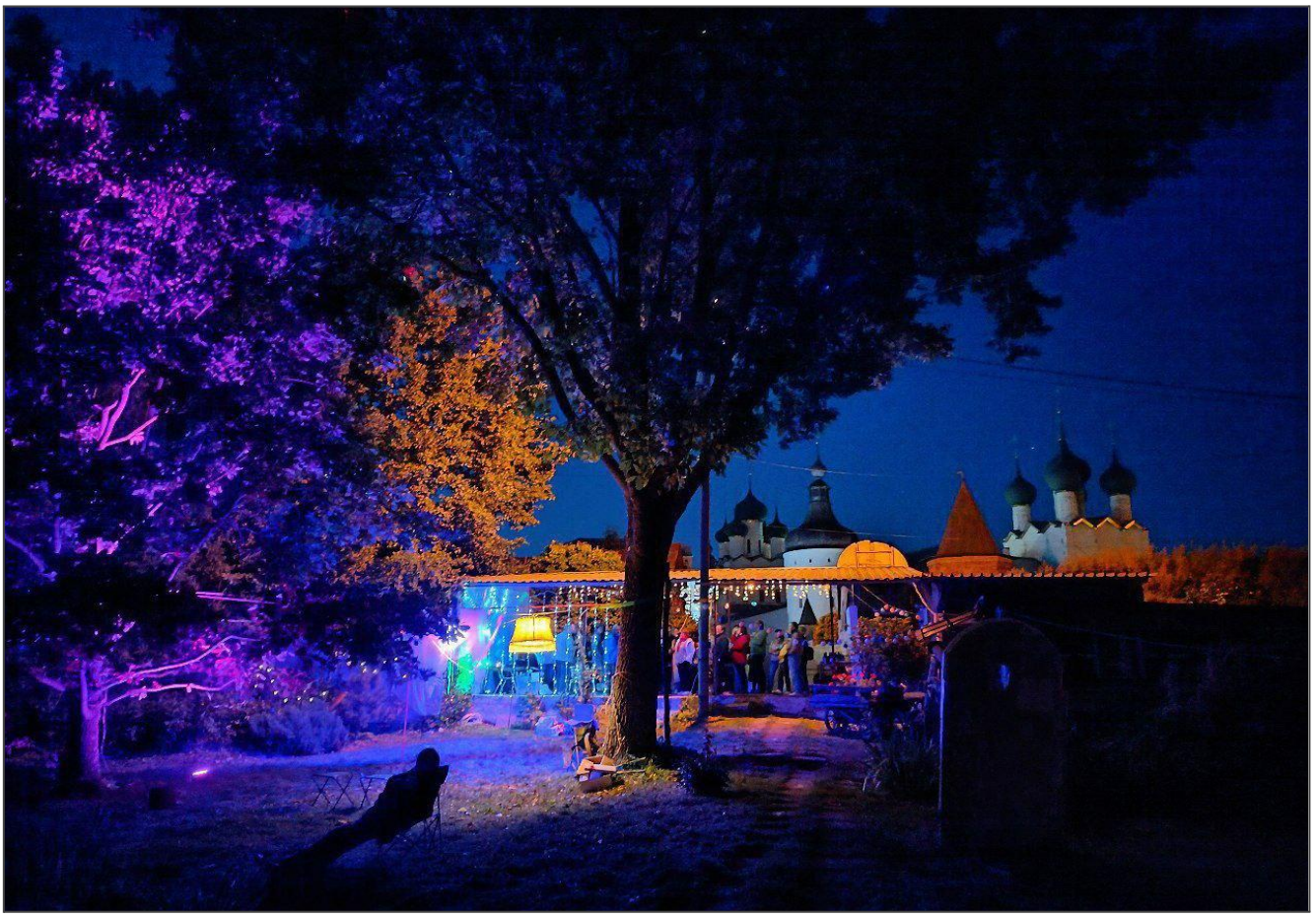

Figure 11. Valdai Periglacial ice-breaker party at the backyard of Rostov Kremlin, Hors art gallery.

FIELD TOUR MAPS

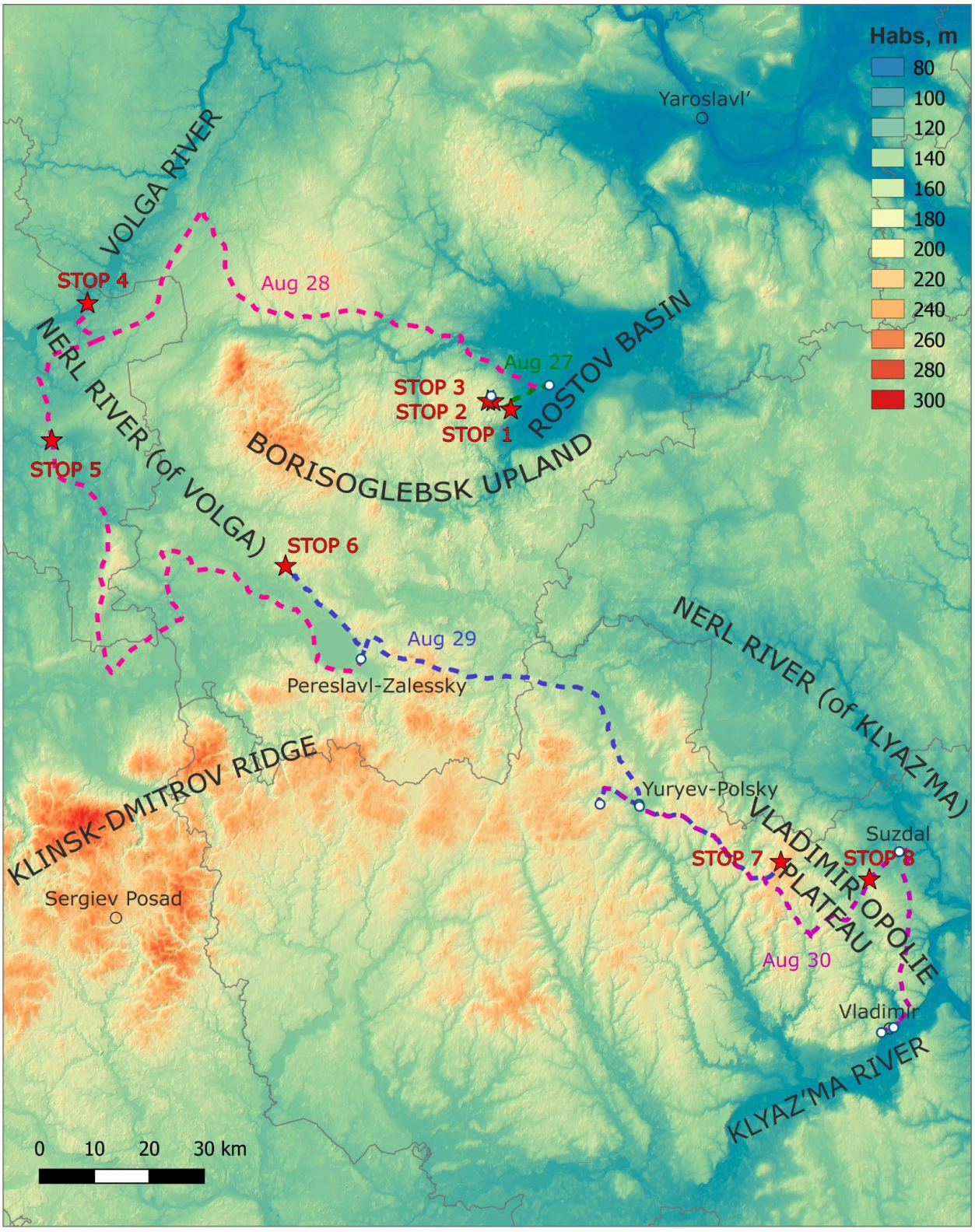

Figure A. Map of the conference field tour, 27–29 August 2023

(here and below – FABDEM in the background)

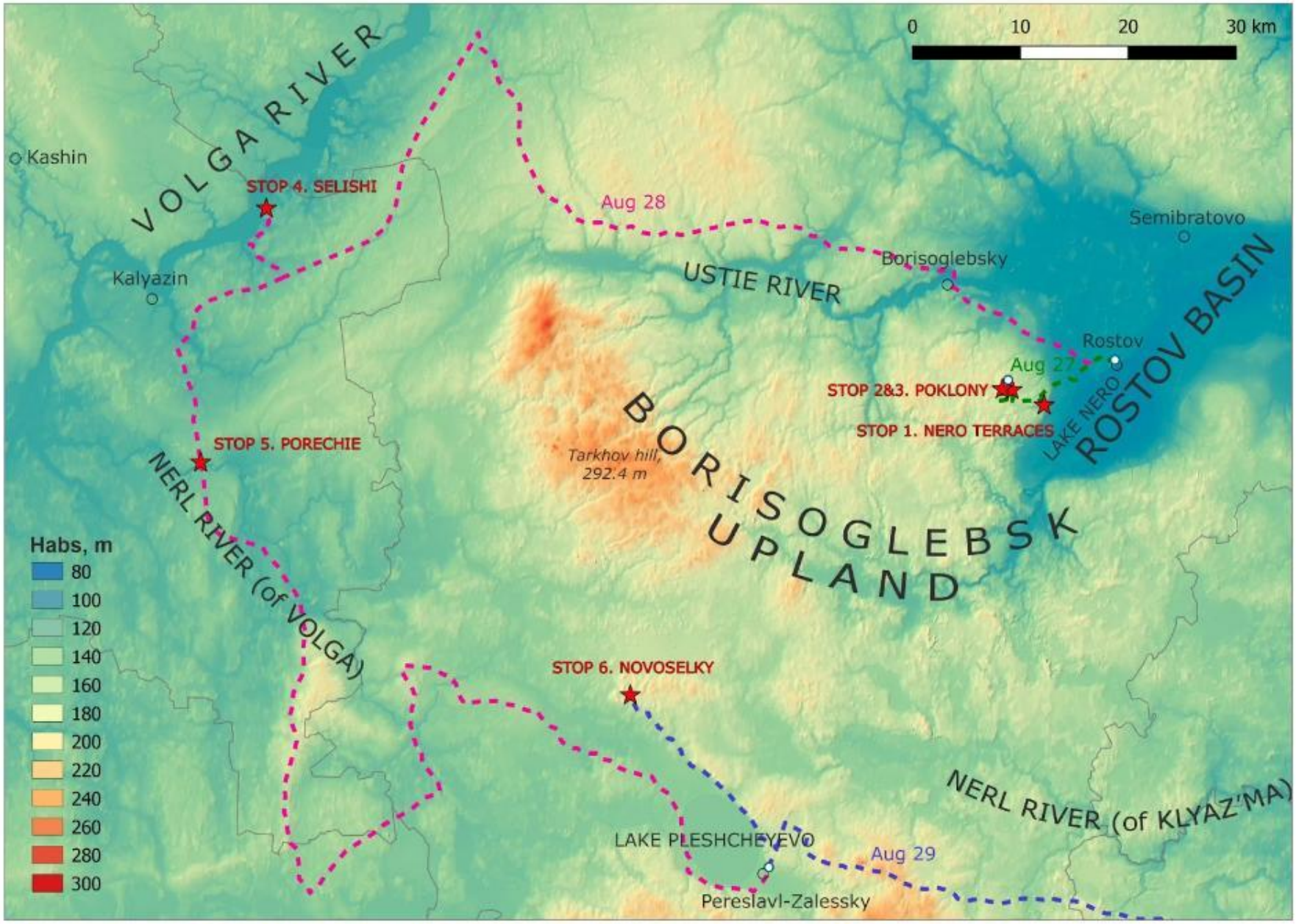

Figure B. Map of the first three days of the conference field tour, 27–29 August 2023

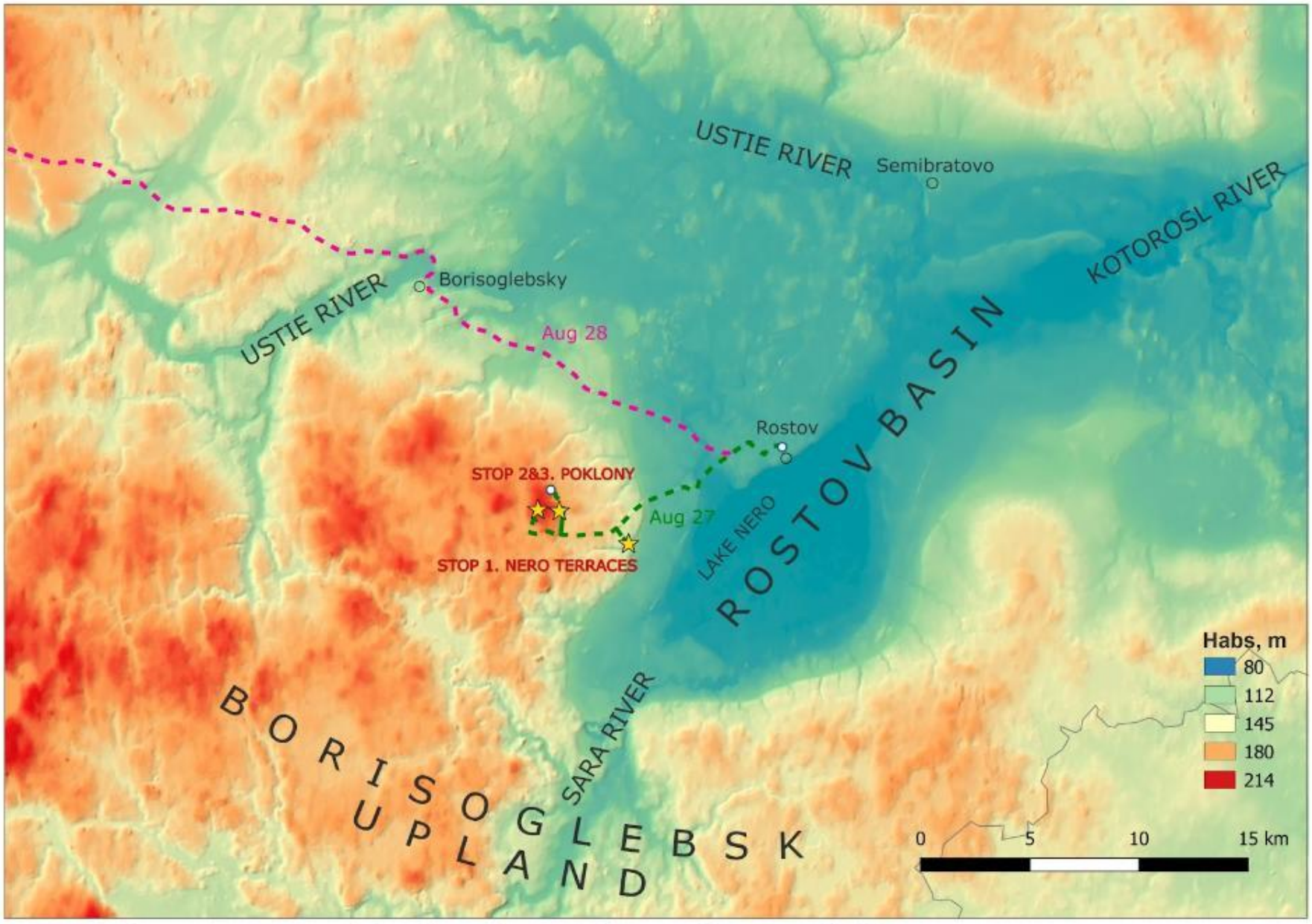

Figure C. Map of the first day of the conference field tour, 27 August 2023

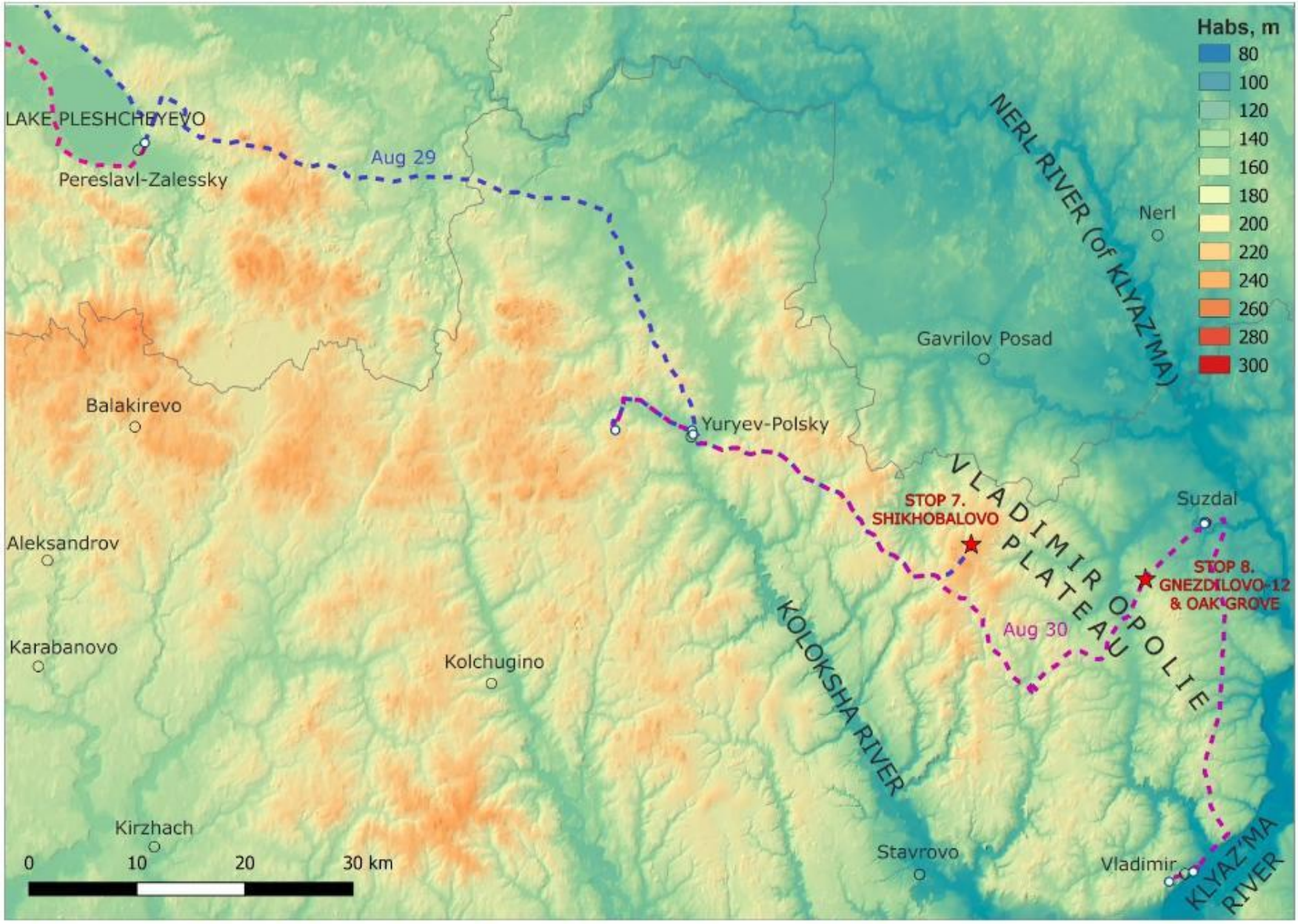

Figure D. Map of the last two days of the conference field tour, 29–30 August 2023

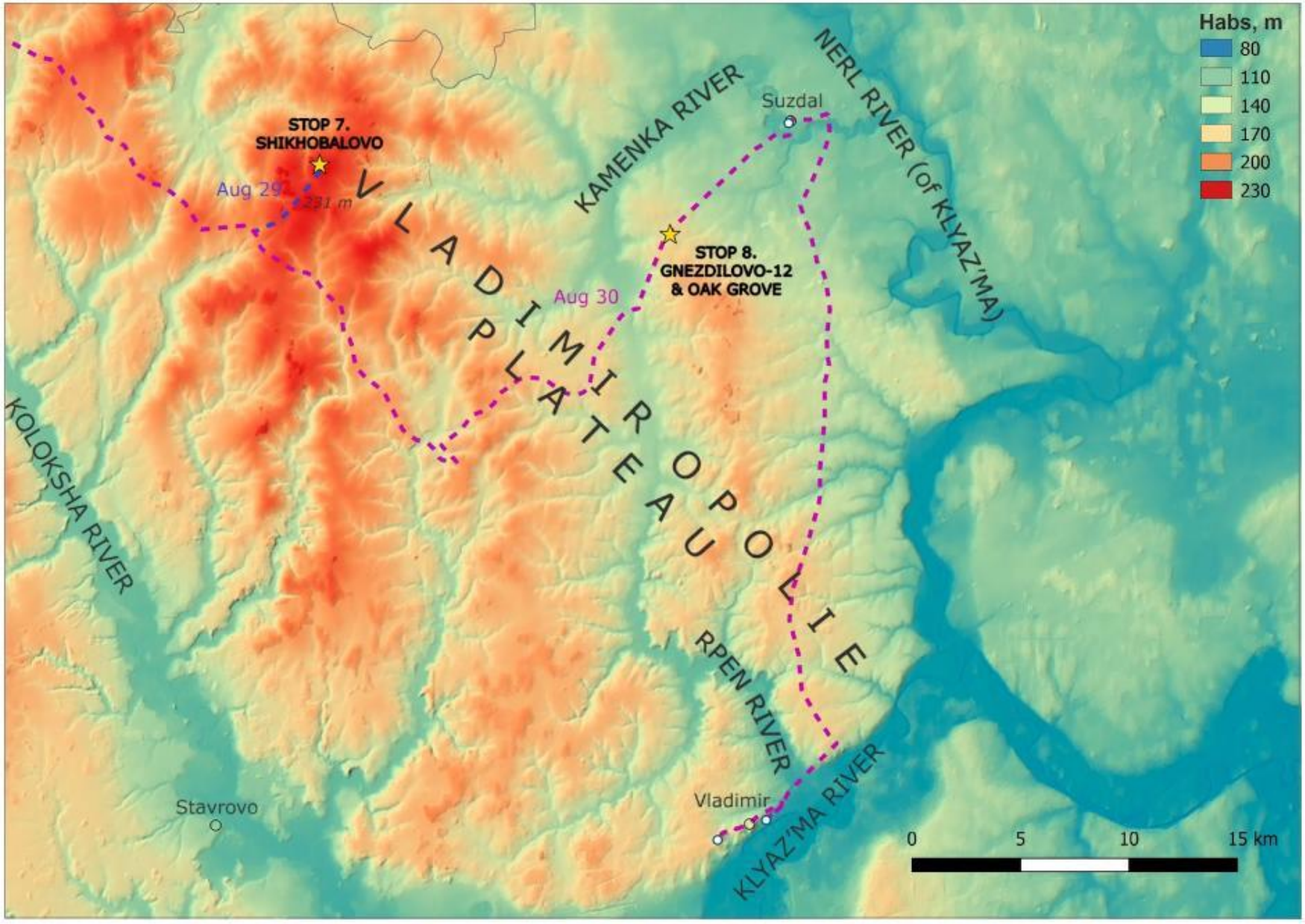

Figure E. Map of the last day of the conference tour, 30 August 2023

BORISOGLEBSK UPLAND AND ROSTOV LOWLAND: THE INTERVENING HISTORY OF ENVIRONMENTAL CHANGE
August 27, 2023

STOP 1. ROSTOV BASIN AND LAKE NERO: GEOLOGY, GEOMORPHOLOGY, AND PALEOGEOGRAPHY
August 27, 2023, morning

Topography. The Rostov Basin (Lowland) is a depression 60–80 m deep with an area of about 750 km² (Fig. 1.1), located approximately 180 km NE of Moscow. It has an irregular shape with a wide northern and a narrow southern margin. The maximum width (north to south) is 28 km and the length (west to east) is 35 km. From the west and SW, the basin is canvased by the Borisoglebsk Upland, from the NW by the Uglich Upland, from the north by the Talitsa Upland, from the east by spurs of the Klin-Dmitrov Ridge. The elevation of the Rostov Basin floor varies from 90.7 m (near the confluence of Kotorosl and Lakhost rivers) to 105 m at the footslopes of surrounding uplands.

On the floor and the sides of the Rostov Basin, three to six terrace levels are distinguished in the range of 94 to 145 m a.s.l. The most accepted scheme of the terrace complex is presented on the State geological map of USSR. Quaternary deposits, O-37-XXVIII, 1968 (Fig. 1.2.). Terrace T0 94–97 m high is a lake floodplain subjected to periodic flooding during heavy floods. Terrace T1 100–105 m high occupies most of the Rostov Basin floor. At the footslopes, along the rear seam of the T1 terrace, there are extensive alluvial-colluvial trains. Alluvial fans of neighboring rivers and streams descending from the uplands often merge. Terrace T2 of 107–115 m is fragmentary expressed manifesting best on the SE and W sides of the Rostov Basin. Terrace T3 of 118–125 m is well expressed on the eastern side of the lowland near the Utkino Village and the western side near the villages of Poddybie and Shulets. Another terrace T4 is often identified at a height of ~145 m (Aleshinskaya & Gunova, 1997).

Hydrography. Several dozen rivers flow into the Rostov Basin, the largest of which are Ustye, Kotorosl, Sara, Lakhost, Veksa, and Mogza. The basin runoff is through the Kotorosl River, which flows into the Volga River in the city of Yaroslavl. On the Rostov Basin floor, riverbeds are meandering. Kotorosl River meanders reach extraordinary proportions in between the confluences with the Veksa and Lakhost rivers. Intense horizontal riverbed deformations led to a great number of abandoned channels, in which oxbow lakes developed. Up to half of the Rostov Lowland is occupied by marsh landscapes. A dense artificial drainage network shows the scale of marsh reclamation, which took place in the first half and mid-XX century.

Lake Nero is located in the south of the Rostov Basin (Fig. 1.1) being the largest lake of the Yaroslavl Volga Region. It is a flowing water body. The water surface area (58 km²) is only about 8% of the total basin area. The lake is SW–NE elongated and pear-shaped – extending to the south. The Sara River and another 20 small rivers (Vorzhenka, Voksitsa, Sulost, Seletskaya, Vorobylovskaya, Glubokaya, Serebryanka, Vanoga, Mazikha, Ishnya, Kuchebezh, etc.) flow into Lake. The Veksa River drains the lake giving rise to the Kotorosl River downstream of the confluence with the Ustye River.

The lake is 13.2 km long with a maximum width of 8.3 km and an average depth of 1.6 m peaking at 4.7 m (Bikbulatov, 2003). Before the Veksa River damming mean long-term level was 93.75 m (Fortunatov & Moskovskiy, 1970). In years with average water level, fluctuation amplitudes are 1.2–1.3 m. In dry years with little precipitation, it could reach 3 m. During the observation period, the maximum level was recorded at 96.37 m, and the minimum – at 93.09 m (Bikbulatov, 2003).

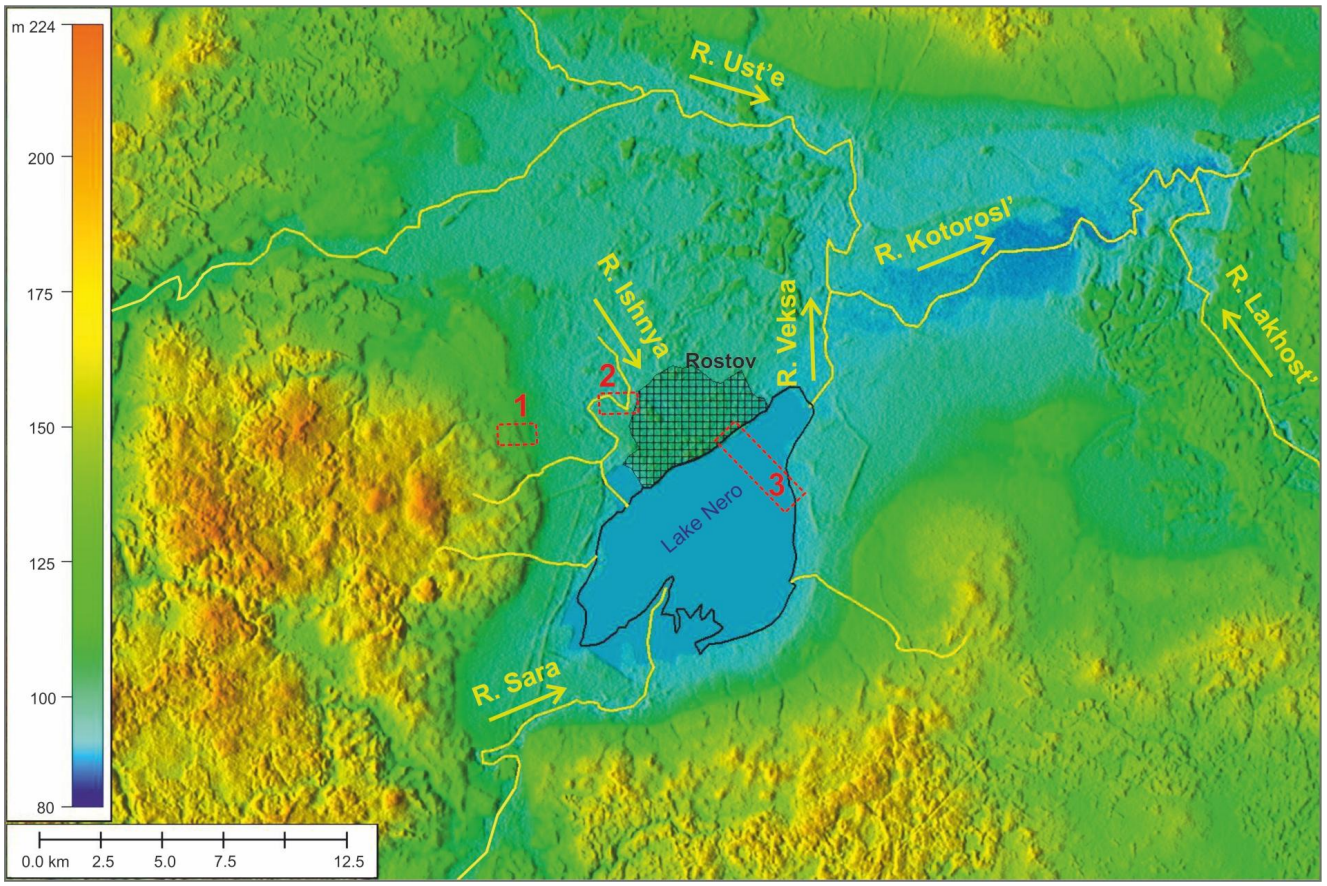

Figure 1.1. Topography and hydrography of the Rostov Lowland. The red frames show the key sites: *1* – Poddyb'ye; *2* – Ishnya; *3* – Rostov-Ugodichi.

In the late 1980s, a dam was built to straighten the riverbed of the Veksa River to regulate the water level in Lake Nero and prevent floods occurring during the snowmelt period as a result of water rising in the Ustye River and backwater on the Veksa River. According to the authors' measurements carried out in November 2021, the water level in the upper pool of the Veksa River dam was 94.3 m, and in the lower pool – 93.0 m. Measurements of the low water level of the lake in February 2020 showed a value of 94.2 m. The measurements were made by the EFT M4 GNSS receiver in RTK mode, the heights are given according to the EGM 08 geoid.

The shores of the lake are low and swampy. In the north, near the Veksa River source in the "throat" of the lake, as well as in its southern bays, there are many small marshy swampy islands. Off the western shores, there are the islands of Rozhdestvensky (opposite the Rostov Town) and Levsky (opposite the L'vy Village). In the southern part of the lake, there is a large beak-shaped delta (more than 2 km long) of the Sara River, which divides that part of the lake into two bays – the southwestern one (Varus), which has fairly smooth shore outlines, and the southeastern one, indented with small bays and bays (Klyuchi, Makarikha, Boteev, Volchikha, Plotska, Gertsukha, Ozereshnya, Plavia, etc.).

Lake Nero belongs to the highly eutrophic type. In summer, with abundant plankton blooms, the water takes on a shade from green to brownish. About 80% of the water area of the lake is covered with macrophyte communities dominated by pierced-leaved pondweed, dark green hornwort forming underwater meadows, and yellow egg-pods. In the coastal strip, communities of reeds, large manna, lake reeds, and cattails are widespread.

Geological structure. The Rostov Basin is of tectonic nature and originated in the Lower Cretaceous (Somov, 1939). In the Paleogene and Neogene, the initial tectonic depression was significantly deepened as a result of intense erosion, and a deep valley arose on the site of

Lake Nero. In the Pleistocene, an inherited landscape developed with repeated glacial advances largely leveling the pre-glacial landscape of the territory.

Pre-Quaternary formations are represented by Permian, Triassic, Jurassic, and Cretaceous rocks.

Permian gypsum clays, siltstones, sands, and sandstones of the Tatarian stage outcrop in the floors of deep paleovalleys. Lower Triassic clays interbedded with sands are exposed on the sides of paleovalleys. The Upper Jurassic and Lower Cretaceous clays, sands, and silts line up most of the Rostov Lowland floor.

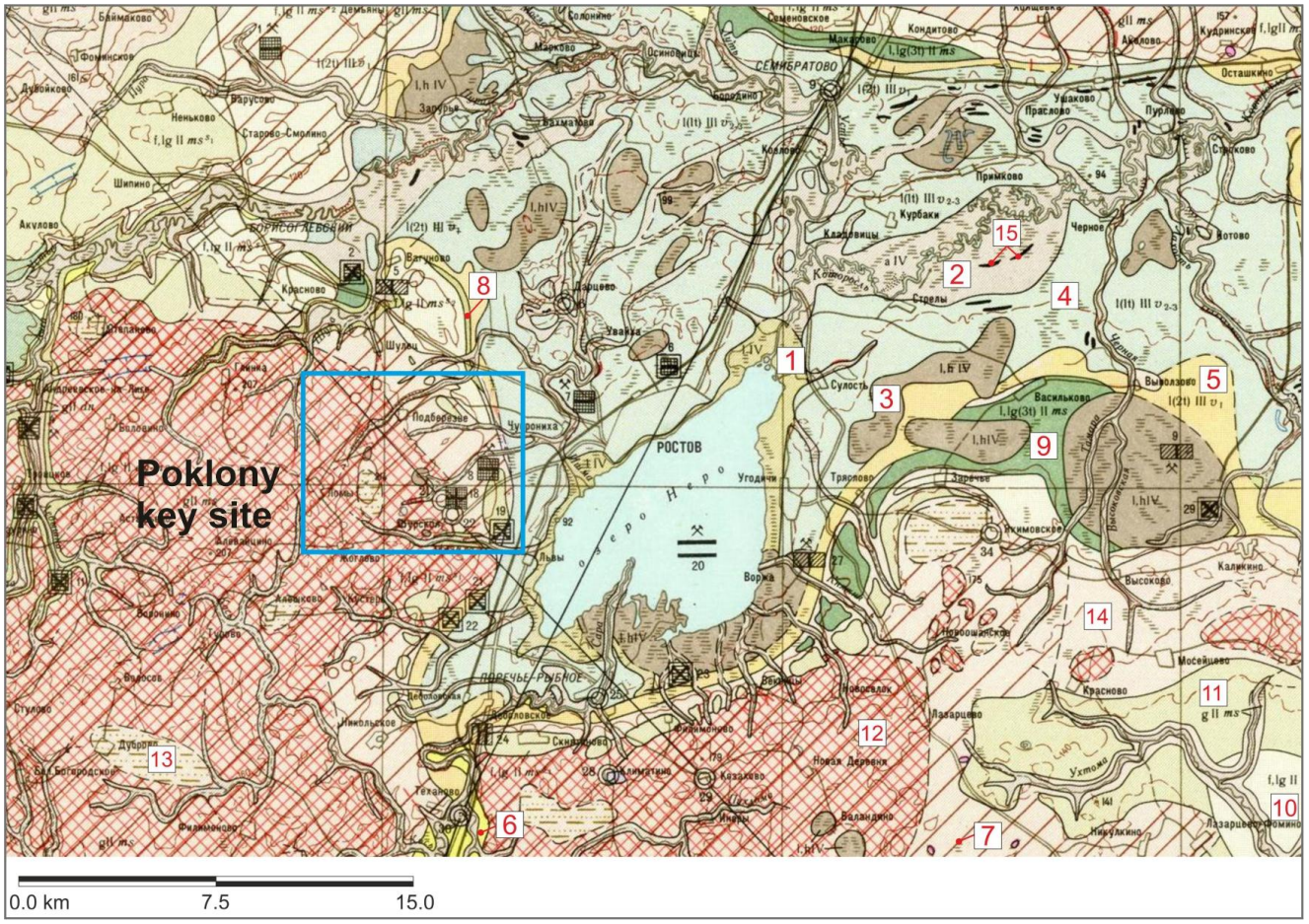

Figure 1.2. Fragment of State geological map of USSR. Quaternary deposits. 1:200000, O-37-XXVIII, 1968. *1* – lacustrine deposits, Holocene, sand, loam, sandy loam, gyttja; *2* – alluvial deposits, Holocene, sand; *3* – lacustrine and palustrine deposits, Holocene, loam, peat; *4* – deposits of the 1st lake terrace, middle and upper Valdai time, loam, clay, sand; *5* – deposits of the 2nd lake terrace, late Valdai time, loam, clay, sand; *6* – alluvial deposits of the 1st river terrace, middle and late Valdai time, sand, loam; *7* – watershed cover formations of problematic origin, Valdai time, loam; *8* – slope deposits, Valdai time, loam; *9* – lacustrine deposits of the 3rd lacustrine terrace, Moscow time, sand, loam, silt; *10* – glaciofluvial deposits of the later stages of glacier retreat, Moscow time, loam, sand; *11* – glaciofluvial deposits of the early stages of glacier retreat, Moscow time, sand; *12* – terminal moraines, Moscow time; *13* – deposits of glacial meltwater channels and lakes, Moscow time, sand; *14* – glacial till, Moscow time, boulder loam, sandy loam, sand, pebbles, gravel; *15* – natural levees.

Quaternary deposits and Pleistocene paleogeography. In the Rostov Basin, the thickness of Quaternary deposits reaches 160 m (Aleshinskaya & Gunova, 1997) represented by a complex of glacial, glacioluvial, lacustrine, alluvial, and palustrine formations (Figs. 1.3 & 1.4). More than 100 m of the sedimentary stratum accounts for the lake sediments accumulated over the past 150 ka since the Moscow ice sheet retreated.

Large-scale geological studies of Quaternary deposits were carried out in the 1950–1970s.

Those works included the drilling of deep exploratory wells, the drilling of Holocene bottom sediments of Lake Nero, as well as various analytical studies: lithological and geochemical, diatom analysis, spore-pollen analysis, thermoluminescent dating, radiocarbon dating. A generalization of the results of those studies is given in works by Z.V. Aleshinskaya and V.S. Gunova from the Faculty of Geography, Moscow State University.

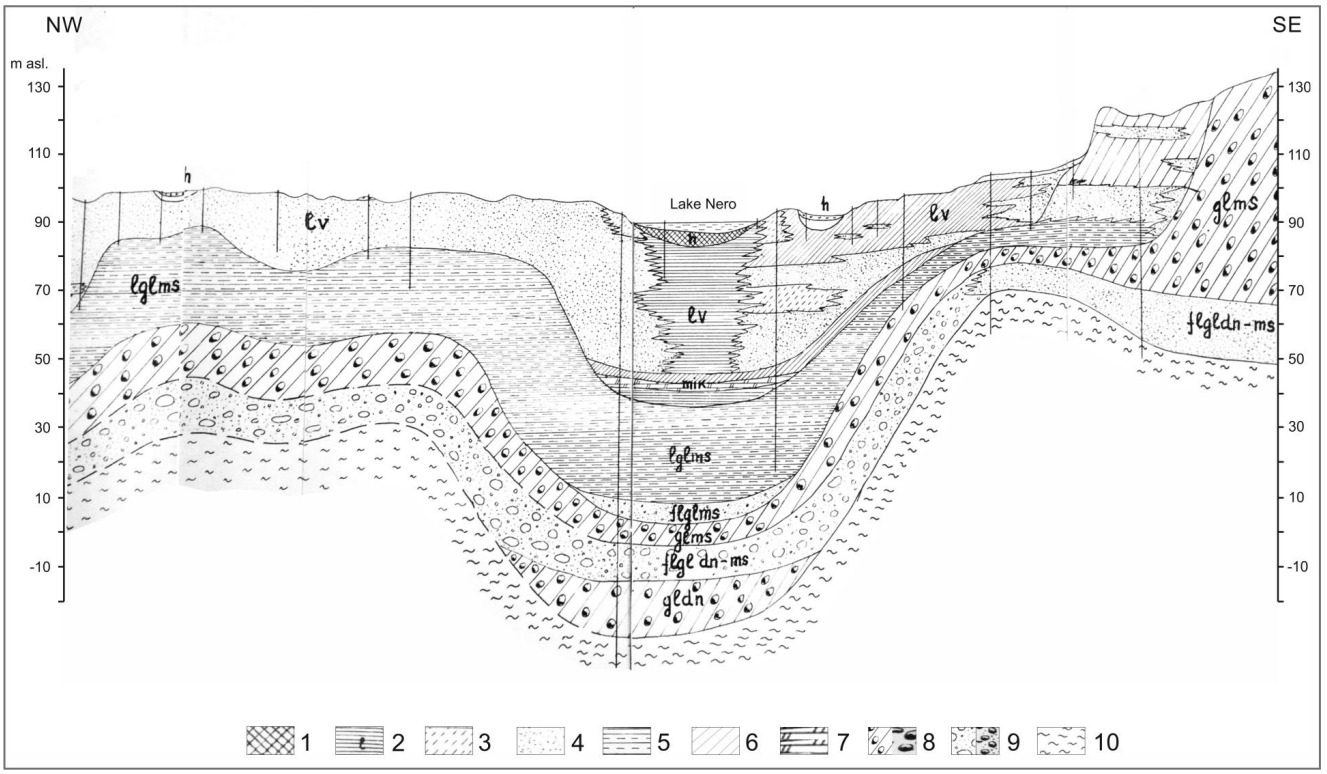

Figure 1.3. Geological profile of the Lake Nero basin along the Rostov-Ugodichi transect (fragment) compiled by Z.V. Aleshinskaya and V.S. Gunova (Gunova, 1975). The ratio of horizontal and vertical scales is 1:50.
1 – peat & sapropel; *2* – clay; *3* – sandy loam; *4* – sand; *5* – varved clays; *6* – loam; *7* – gyttja; *8* – boulder loam; *9* – sand with gravel, pebbles and boulders; *10* – pre-Quaternary bedrock.

Below the main results of the studies (Gunova, 1975; Aleshinskaya & Gunova, 1997) are briefly summarized with authors' additions. The main features of structure, composition, and age of the Pleistocene deposits are given with paleogeographic interpretations.

Dnieper-Moscow glaciation. Dnieper till is represented by dark-brown highly compacted loams. Reaching 40 m thick within the lowland it lies over the bedrock with erosive contact. It is covered by 10-m thick glaciofluvial pebbles with boulders and sand matrix of the Dnieper age. Above, the Moscow till is composed of reddish-brown and brown boulder loams and sandy loams up to 14 m thick.

End of the Moscow glaciation. During the late Moscow, melting of the glacier led to the formation of a vast glacial lake in the basin. A deep ultraoligotrophic water body enabled the deposition of varved clays up to 27 m thick in its center upon the glaciofluvial sands underlain by the Moscow till. Lining up the Rostov Basin floor, varved clays are laterally substituted towards the sides by sand and gravel-pebble facies, which compose the highest levels of glaciolacustrine terraces with elevations of 118 to 145 m a.s.l.

Palynological studies testify to the severe Late Moscow climatic conditions. Tundra and forest-tundra associations dominated near the lake represented by pine-birch woodlands. Open spaces with tickets of shrub birches and moss-herbaceous associations occupied significant areas.

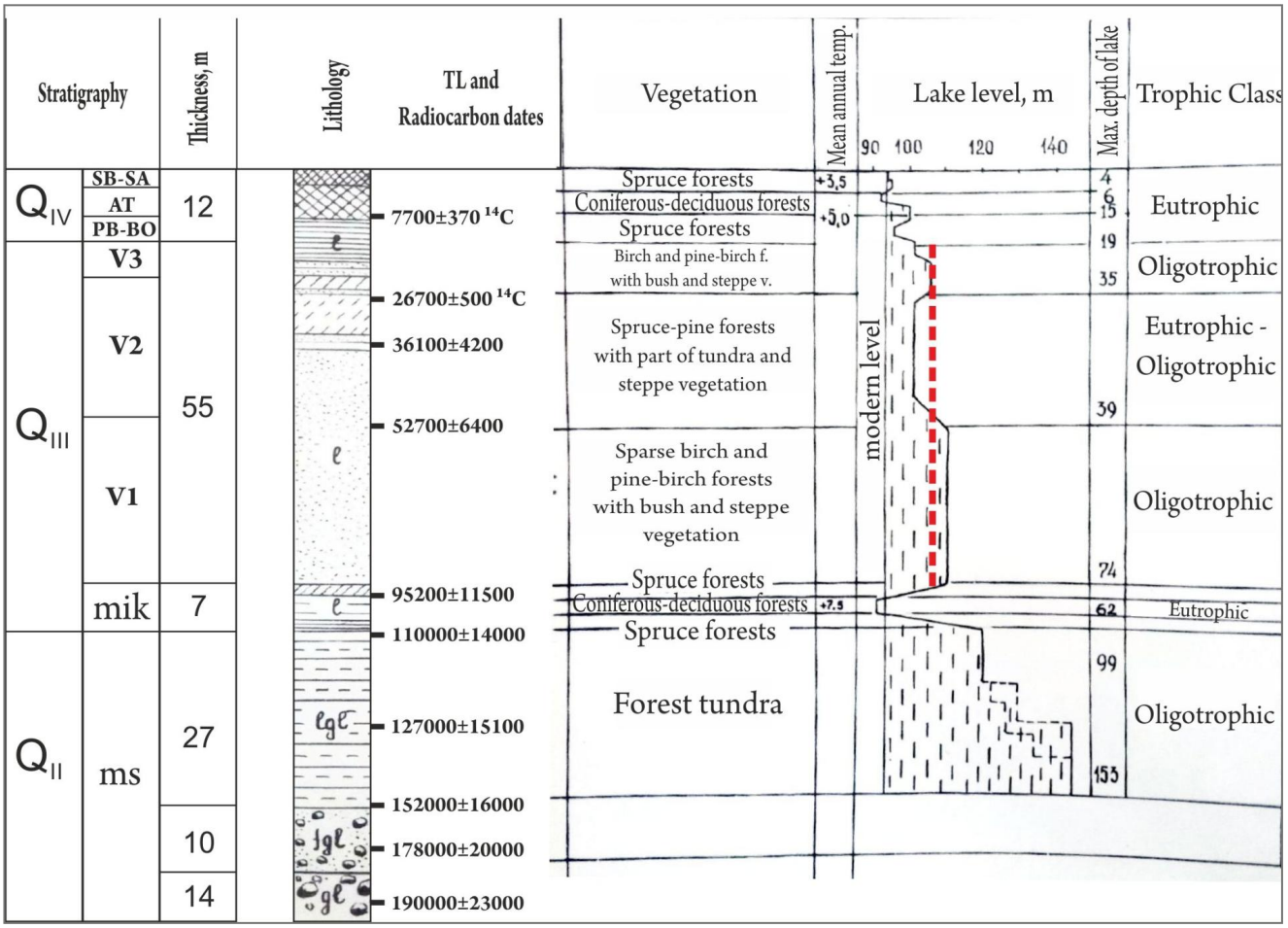

Figure 1.4. Consolidated stratigraphic scheme of Quaternary deposits in the basin of Lake Nero and its paleogeographic interpretation (fragment compiled by V.S. Gunova (1975)). See the legend in Fig. 1.3. *The red dashed line* is the maximum probable level of the lake after the Mikulino interglacial.

Mikulino interglacial. During the Mikulino, clays and later marls and loams accumulated in the center of the lake. The total thickness of interglacial sediments ranges from 2 to 7 m. Spruce forests grew in the vicinity of the lake, then substituted by birch and pine forests with few broad-leaved species.

During the Mikulino climatic optimum, the physicochemical regime of the lake and surrounding landscapes changed significantly. The climate was slightly warmer than present with broad-leaved and coniferous-broad-leaved forests common in the vicinity of the lake. Lake Nero was a shallow well-heated life-rich water body, which remained a flowing reservoir during the entire Mikulino interglacial, according to geomorphological, geochemical, and diatom data. Its level dropped significantly compared to the late Moscow. It was probably close to the modern one or even somewhat lower that is evidenced by the limited distribution of its Mikulino sediments at elevations of 40 to 66.6 m a.s.l.

Valdai epoch. The absence of glacial and glaciofluvial sediments in the post-Mikulino stratum unequivocally indicates the Moscow glaciation to be the last in that area. Northern taiga, tundra, and steppe elements in the spore-pollen spectra of the Valdai deposits indicate the periglacial zone to be spread there during the entire Valdai epoch.

During *the early Valdai*, a 25 m thick layer of non-carbonate silty sands accumulated in the center of Lake Nero indicating the high sedimentation rates and significant depth of the reservoir. Simultaneously, less than 3 m of loams with a carbonate content of up to 30% accumulated in the warmer shallow coastal

zone. The lake level could have risen above 100 m a.s.l. yet not exceeding 107 m, generally characterized by the oligotrophic features.

At the early stages of the early Valdai, pine-birch and birch light forests with spruce were common in the vicinity of Lake Nero. Open landscapes with shrubs and xerophytic forb associations were of great importance.

During *the Middle Valdai*, there was a slight warming and a decrease in the Lake Nero level. Two regressive stages were noted with the latter being more prominent. Yet the lake preserved the features of an oligotrophic reservoir although to a lesser extent than at the previous and subsequent stages of the Valdai era. Sediments quite diverse in lithology and thickness were formed. In the central part of the lake, 8 m thick clays of low carbonate content with plant remains and 10 m thick silty fine sands accumulated. Contrastingly, in the well-heated shallow coastal zone with abundant aquatic vegetation, marls deposited at the onset of the Middle Valdai with the carbonate content reaching 94.2% (almost 10 times higher than in the sediments of the central part of the basin).

Palynological data indicate landscapes combining forest, steppe, and tundra associations. In the first half of the Middle Valdai, forest groups were dominated by coniferous (spruce and pine) species, while in the second half, birch tended to predominate, tentatively implying a cooler climate.

In *the late Valdai*, two stages are distinguished in the history of the lake. During the first stage, up to 6 m of clays with plant detritus accumulated in the center of the lake against sands in the peripheral zone. Sediments are non-carbonate. The lake level rise, which onset was noticed at the end of the Middle Valdai, reached its maximum exceeding the modern one by several meters. Paleobotanical, geochemical, and lithological data testify to the oligotrophy of the lake. The vegetation cover of the lake catchment was dominated by pine, birch, and spruce light forests. Along with forest groups, steppe communities were widespread, in which sagebrush played the major role, as well as tundra associations with the predominance of shrub birches.

The second late Valdai stage corresponds to the degradation of the Valdai glacial cover characterized by frequent and abrupt changes in environmental conditions. Frequent changes in lithological composition testify to the repeated shifts in the lake regime and fluctuations of its level. At the end of the stage, the Lake Nero level decreased reaching a minimum in the Late Glacial, which was probably lower than the modern one. Thus, the lake water surface significantly reduced.

Terrace complex on the western side of the Rostov Basin. In 2019, work was carried out to study the structure of the western side of the Rostov Depression near the village of Poddyb'ye (Fig. 1.5a). A geodetically constrained topographic profile and two machine-drilled cores – K7 and K7-B – were accomplished. The profile traverses the area where terrace T2 (107–115 m) is best expressed while terrace T1 (100–105 m) is least complicated by alluvial-colluvial deposits.

Terrace T2 has an inclined surface of 115 to 110 m a.s.l. with indistinct rear seam and edge. In core K7 (Fig. 1.5c), rhythmically layered sandy loams and loams with single gravels were recovered in the depth range of 6.5–22.5 m. Individual layers are 2 to 5 mm thick. Probably, rhythmites accumulated in the peripheral part of a large deep oligotrophic water body that existed in the late Moscow (Aleshinskaya & Gunova, 1997). Rhythmites are overlain by a sand layer (up to 2 m thick) with gravel and angular pebbles. Overlying thin (0.3 m) dark gray-brown organic loam (loamy gyttja) was assigned to the Mikulino deposits. Sediments above the rhythmites correspond to the stage of lake level drop leading to the formation of an abrasion terrace. During the Mikulino, local shallow lakes could develop on that terrace. The upper 4.3 m of core K7 represent a slope train of mottled yellow-gray loams with dark clods and sand. The absence of Valdai lacustrine deposits on the terrace indicates the lake level of the Rostov Basin not exceeding 108 m in the post-Moscow time.

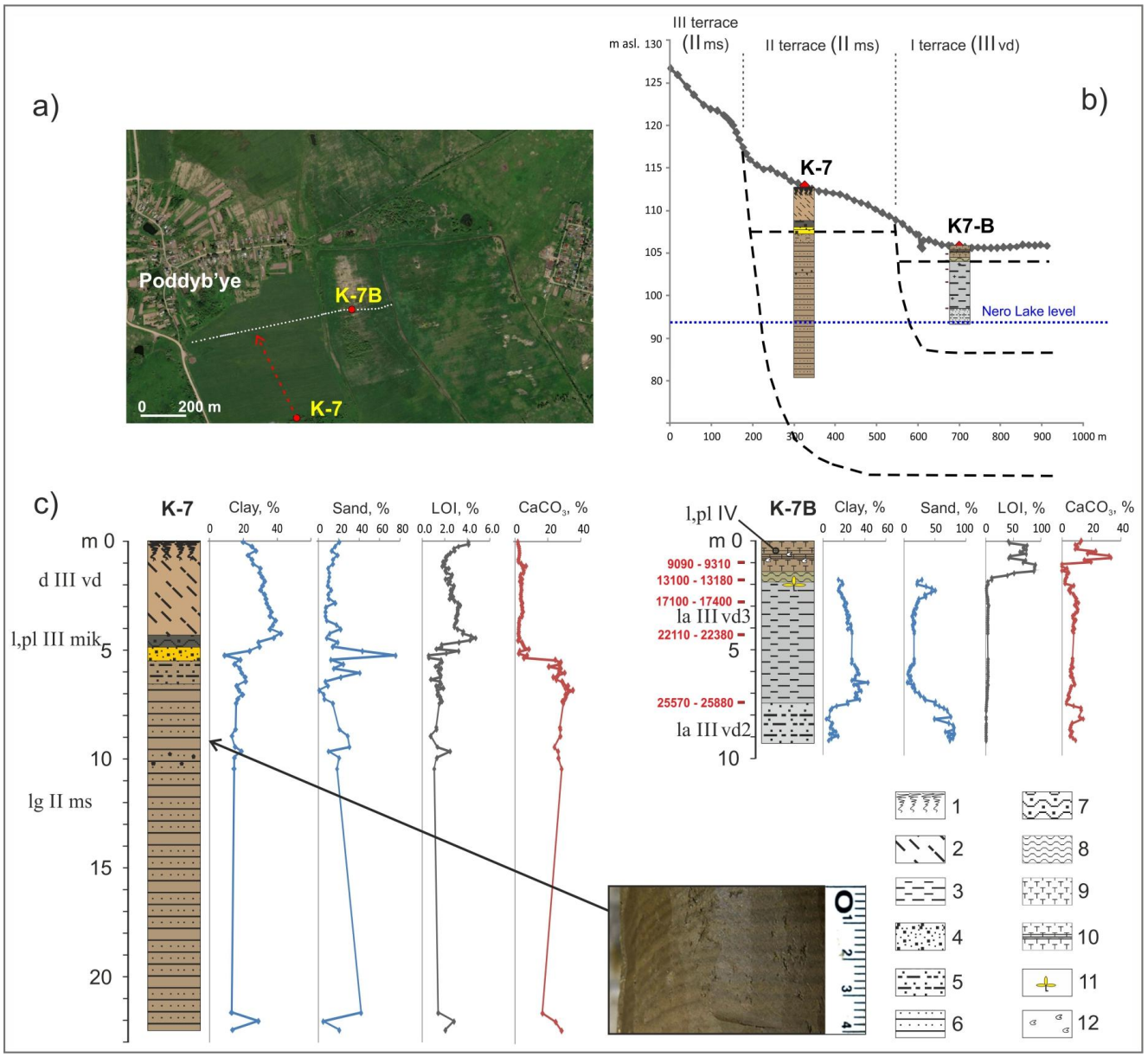

Figure 1.5. Structure of the terrace complex at the Poddyb'ye key site, the western Rostov Depression: a) positions of cores and topographic profile with a satellite image at the background; b) geological profile; c) geological structure and analytical data of K7 and K7B cores. *1* – soil; *2* – slope loam; *3* – massive loam; *4* – sand with gravel; *5* – silty sand; *6* – varves; *7* – loamy gyttja; *8* – gyttja; *9* – peat; *10* – peat with calcareous gyttja; *11* – plant remains; *12* – shell detritus. The colors are close to natural.

Terrace T1. At the base of core K-7B (Fig. 1.5b), located on terrace T1, massive silty sands, probably of lacustrine-alluvial origin, were recovered. The top of the sands lies at 98.4 m a.s.l. 667 diatom valves were counted in a sample taken from a 9.0 m depth. 78% of the diatom flora consists of planktonic species. *Stephanodiscus neoastraea* predominates (51%), *Pantocsekiella ocellata, Aulacoseira ambigua* are present with some *Stephanodiscus alpinus* (4.8%). Among the periphytonic species, there are *Tabellaria fenestrata* and *T. floculosa*. Such a set of diatoms suggests an oligo-mesotrophic relatively deep reservoir with water temperatures below modern ones.

The sands are overlain by massive gray loams 5.5 m thick with three AMS radiocarbon dates obtained for total organic carbon. There are no date inversions. The bottom of loams is about 25.7 ka, and its roof is 15.0–17.0 ka. Thus, the loam layer formed during the late Pleniglacial, including the last glacial

maximum. In the sample from a depth of 7.0 m, 1243 diatom valves were found. The diatom flora is dominated by planktonic species (about 95%). *Aulacoseira granulata* and *Stephanodiscus alpinus* predominate (36 and 31% respectively), *S. neoastraea, Cyclotella radiosa,* and *Pantocsekiella ocellata* are present. Of the periphyton species *Cavinula scutelloides* was found. Such a diatom complex corresponds to a cold oligotrophic reservoir.

Gray loams are overlain by 0.25 m thick gyttja with an organic matter content of 5 to 40%. Its age, according to the date from a depth of 1.8 m (13100–13180 cal yrs BP), corresponds to the Bølling–Allerød interstadial. A sample from a depth of 1.6 m contained 354 diatom valves. Attention is drawn to the dominance of periphyton diatom species and the complete absence of planktonic ones. Thus, we can conclude that the reservoir was very shallow. The entire complex of diatoms is characteristic of an oligotrophic acidic reservoir. The presence of *Hantzschia amphioxis*, an aerophilic species, indicates that the reservoir was drying up, probably representing a local isolated reservoir on the terrace. Species *Eunotia biconstricta, Stauroneis gracilis, Rexlowea parasemen, Eunotia praerupta var. bidens* testify to more severe climatic conditions than modern ones.

Above the gyttja, sedge-reed peat with a thin layer of carbonate silt indicates a lowland bog existed throughout the Holocene, periodically transforming into a shallow local lake (Samus & Konstantinov, 2022).

The presence of marine species *Paralia sp.* in the samples from depths of 7.0 and 9.0 m speaks in favor of partial redeposition of the material. The facies interpretation of layer 2 (massive loams) is very complex. It is not completely clear whether that was a reservoir occupying the entire Rostov Basin or a small isolated lake on the lake terrace. Recent revision of lacustrine paleobasins in the Upper Volga basin speaks against the existence of a single lacustrine reservoir (Borisova et al., 2022). The studies showed that at the end of the Late Pleistocene a large lake reservoir in the Yaroslavl and Kostroma lowlands, connected to the Rostov Basin by the Kotorosl River, did not exist at levels of about 105–110 m.

Fluvial landforms on the Rostov Basin floor. On the floor of the Rostov Basin, one can observe a wide variety of fluvial landforms (Fig. 1.6): meandering riverbeds, oxbow lakes, macromeanders, and deltas. Fluvial processes are the leading exogenous processes in the Rostov Basin; they determine the main features of the relief of the basin floor. Without taking into account the dynamics of fluvial processes, it is impossible to understand the reasons for the change in the level of Lake Nero.

The intensity of alluvial accumulation on the Rostov Basin floor is directly related to the volume of sediment carried by the river and the parameter, *ceteris paribus*, is related to the area of the drainage basin. The largest rivers flowing into the Rostov Basin have the following basin sizes: Ustye – 2530 km², Lakhost – 922 km², Sara – 791 km² (State Water Register). The difference in the river basin sizes explains the height distribution of the Rostov Basin floor. Thus, its most elevated part is located in the NW part that is an area of intense alluvial accumulation of the Ustye River, being, in fact, its internal delta. Complicated by a network of abandoned channels it shows the river positions in the recent past. The town of Rostov is located within that delta.

At the south of the Rostov Basin, the major sediment supply is by the Sara River, which accumulated a rather large beak-shaped delta protruding for several kilometers into Lake Nero (Fig. 1.6-1). However, the accumulation intensity is significantly lower than at the Ustye River delta constraining the topographic depression existence in the southern part of the basin where Lake Nero is located.

The upper Kotorosl Valley is of interest. Down the confluence of the Ustye and Veksa to the mouth of the Lakhost River (Fig. 1.6-2) extreme meandering constrained by low longitudinal slopes and the wide valley floor left a large number of abandoned channels occupied by oxbow lakes. In spring satellite images, the floodplain is located below the

riverbanks; so-called embanked channels are a sign of active riverbed accumulation and growth of its elevation. The riverbed elevation of the Ustye-Kotorosl River system plays a great part in controlling the Lake Nero level constraining its runoff threshold. During floods, the water level in the Ustye-Kotorosl system often reaches the level of Lake Nero, occasionally exceeding it. Such a level rise causes backwater or even countercurrent in the Veksa River, which is accompanied by intensive accumulation in its riverbed and the throat of Lake Nero.

Lakhost River, which flows into the Kotorosl from the SE, has formed an internal delta. The delta prevents the Kotorosl runoff that is seen in the channel morphology change (Fig. 1.6-3). Westward of the Lakhost River delta, an area of intense meandering of the Kotorosl channel is described above. Eastwards, down the delta section, the Kotorosl channel straightens and deepens sharply. Thus, alluvial accumulation in the inner delta of the Lakhost River is one of the leading drivers of the existence of a large lake in the Rostov Basin at present.

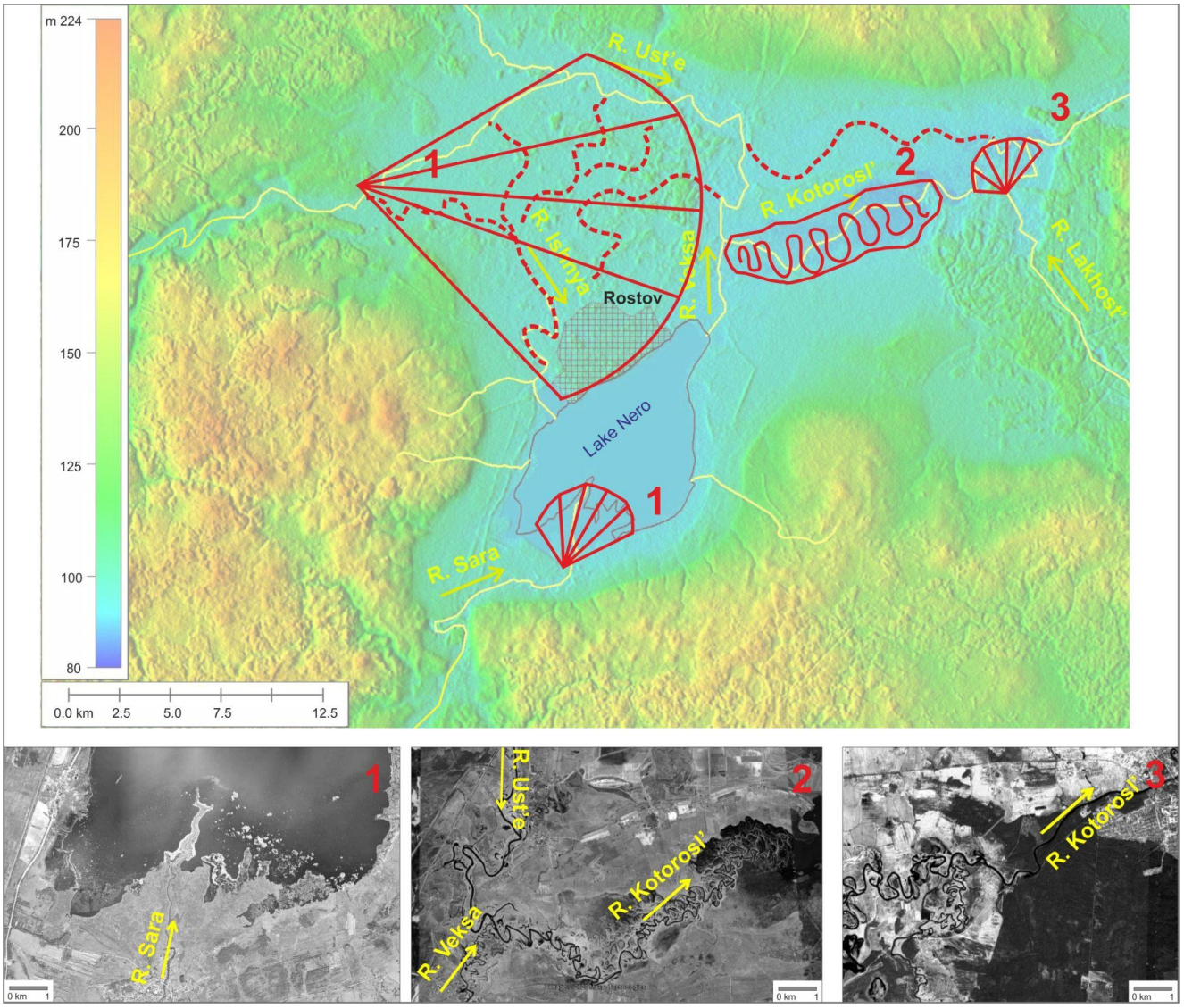

Figure 1.6. Fluvial landforms of the Rostov Lowland. Solid red lines are areas of alluvial accumulation (internal deltas and areas of intense meandering). Dashed red lines – macromeanders (large paleochannels).

Ishnya River valley – a large paleochannel of the end of the Pleistocene – beginning of the Holocene. The modern valley of Ishnya River is a swampy macromeander (Fig. 1.7a,b) – i.e. paleochannel left by the river, which greatly exceeded the Ishnya River in terms of runoff. Interpretation of satellite images shows that in the past the

paleochannel belonged to the Ustye River system. Likely, the Ustye River, at some stage of its existence, flowed directly into Lake Nero. According to the channel morphometry (Ukraintsev et al., 2020), that paleoriver was 1.5 times larger than the modern Ustye River, according to peak water discharges.

Near the Varnitsky Convent, a coring transect was accomplished by crossing the Ishnia River valley twice (Fig. 1.7b,c). Core ISHNYA-1227 in the paleochannel floor, exposed an intercalation of peat, gyttja, sandy loam, and sand with wood fragments at the depth of 1.1 to 6.3 m, which was interpreted as old alluvium facies. Below, in the 6.3 to 8.1 m interval, fine and very fine well-sorted layered sand with interlayers of sandy loam and single wood fragments was interpreted as riverbed alluvium. Two AMS dates were obtained from a depth of 5.95 m for total organic carbon – 10140±90 cal yrs BP and from a depth of 7.3 m for a wooden fragment – 9500±20 cal yrs BP.

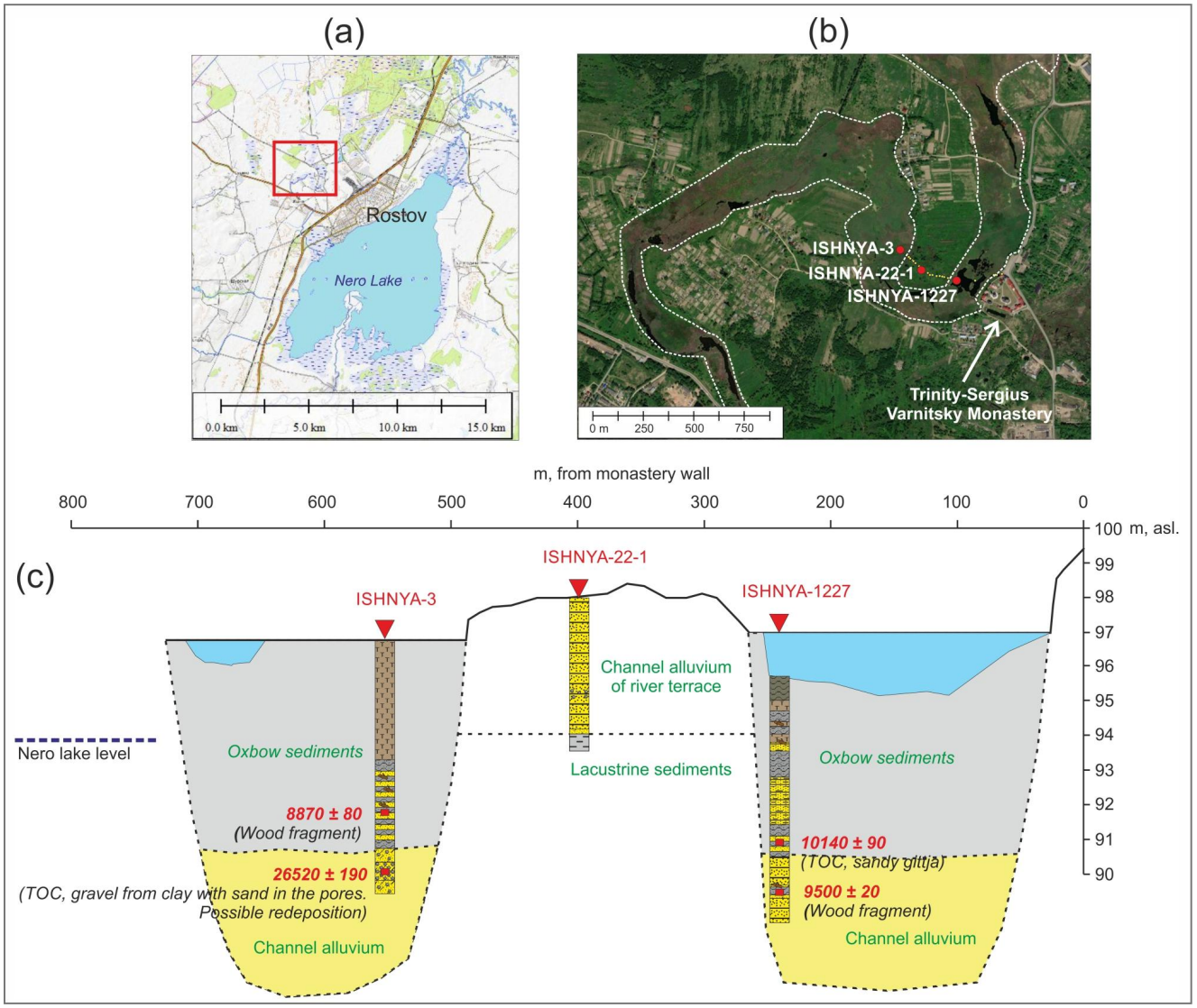

Figure 1.7. Ishnya River valley – large paleochannel: a) location of the key section; b) satellite image with large paleochannel (white dash line); c) geological profile. See symbols for cores in Fig. 1.10.

A similar structure of the paleochannel is observed in core ISHNYA-3. Under a layer of lowland peat (0.0–3.8 m), there is an interbedding of sandy gyttja and fine sand with woody fragments (branches). It is interpreted as a transition from channel to oxbow alluvium. In the interval of 6.1–7.4 m, medium and coarse sands occur with the inclusion of clay pellets 0.5–1 cm in diameter. Two AMS dates were received for core ISHNYA-3. The upper date for

wood from the oxbow facies (8870±80 cal BP) does not contradict the dating results of core ISHNYA-1227. The lower date for TOC from the channel facies (26520 ± 190 cal BP) differs significantly, which can be explained by an admixture of clay pellets – redeposited erosion products of Pleistocene lacustrine loams.

The structure of the river terrace located 1.5 m above the water level in the paleochannel (98 m a.s.l.) was exposed in core ISHNYA-22-1. From the surface down to 4.0 m, yellow-red layered fine and medium sand is interpreted as an alluvial channel facies. Below, a medium-layered gray loam with interlayers of sand and a sharp contact is interpreted as Valdai lacustrine deposits. Similar loams are widely distributed along the Rostov Basin floor at terrace T1 and occur under the Holocene gyttja in Lake Nero.

Dating results of deposits make it possible to estimate the age of the onset of siltation and death of the paleochannel at about 9–10 cal ka. The process was not abrupt – cessation of full-fledged river flow occurred gradually. Thus, the functioning stage of the paleochannel probably fell in the Late Glacial and Preboreal times. Channel alluvium recorded at 88.0 m a.s.l. (and probably even deeper as the base was not reached) suggests the level of the receiving basin even lower than the present of Lake Nero.

Structure of bottom sediments and Holocene history of Lake Nero. To refine the bathymetric map, depths in the NE part of Lake Nero were measured from ice in February 2020 (Fig. 1.8). The contemporary water level was 94.2 m (according to geoid EGM08). Using the Livingstone piston corer, nine cores were drilled from ice along the Rostov-Ugodichi line (Fig. 1.8b). Corresponding ground-penetrating radar (GPR) survey was carried out using the Zond 12e radar with 300 MHz antenna and Python3 radar with 100 MHz antenna (Fig. 1.9). Loss on ignition at 550 and 950 °C, magnetic susceptibility, and grain size distribution were determined for samples in cores NER-3 and NER-5 (Fig. 1.10). Based on radiocarbon dates for cores NER-5 and W-2006 (after Wohlfarth et al., 2006) sedimentation age-depth models were constructed in the Bacon v.2.4.0. package in R-studio using the Bayesian method.

There are several features in the structure of lacustrine sediments (Konstaninov et al., 2023). The cores are shown against the GPR data in Fig. 1.9 while the composition and correlation of the key cores are provided in Fig. 1.10.

1. The structure and thickness differ significantly near the shore, in areas of medium depths, and at the axial part of depression.

2. In the axial trough (NER-5), Pleistocene sediments are represented by gas-saturated loams and sandy loams. The thickness of Holocene deposits is almost twice as high as the average one in the lake. Calcareous mud of the first half of the Holocene (11.7–6.0 ka) lacks hiatuses. The upper organic gyttja layer of the second half of the Holocene is almost eroded.

3. In areas of medium depths (NER-2, NER-3, W-2006), the structure of deposits is replicated. Pleistocene dense gray loams are overlain by a thin layer of sandy loam or sand with shell detritus aged 15.0–14.5 cal yrs BP. Holocene calcareous mud and silty gyttja occur above with a series of hiatuses.

4. On the GPR profile, the lake bottom boundary, bottom of organic gyttja, and coastal sands are recognizable with the deeper boundaries poorly distinguished (Fig. 1.9). First probable reason for that is a partial fading of the signal passing through thick (up to 0.5 m) layered ice. Secondly, there is a smooth, gradual transition of the layers – from weakly consolidated organic sediment to denser terrigenous-calcareous mud, which dissipates a significant part of the wave energy. Thirdly, the water of Lake Nero is relatively highly mineralized (240–600 mg/l), which increases the electrical conductivity.

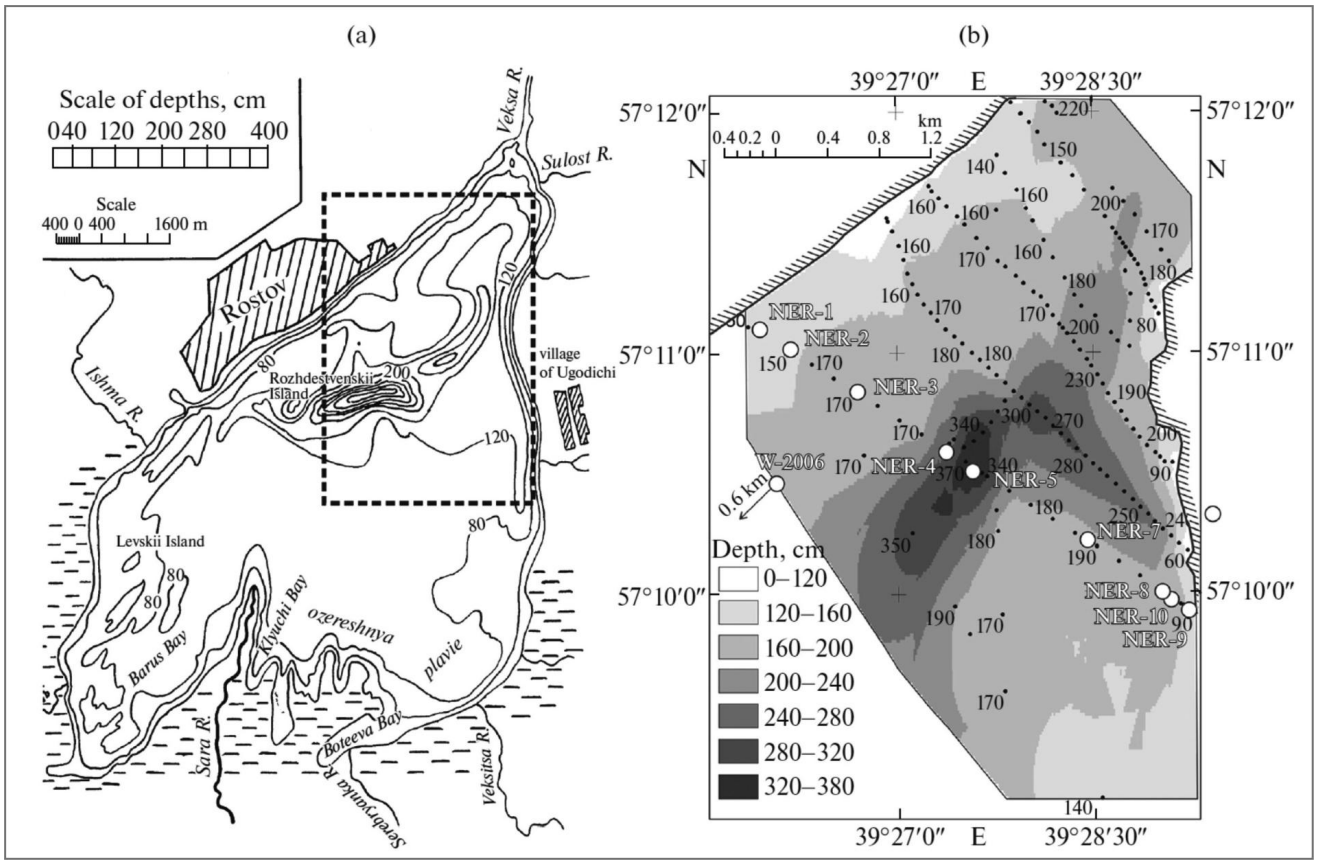

Figure 1.8. Depth distribution in Lake Nero: a) bathymetric scheme (Barysheva, 1953); b) bathymetric map of the NE part of the lake compiled from 2020 winter measurements. Symbology in b): *black points* – depths at measuring sites, cm; *white circles* – cores; cores with the «NER» indices are the author's results; W-2006 core is from Wohlfarth et al., 2006.

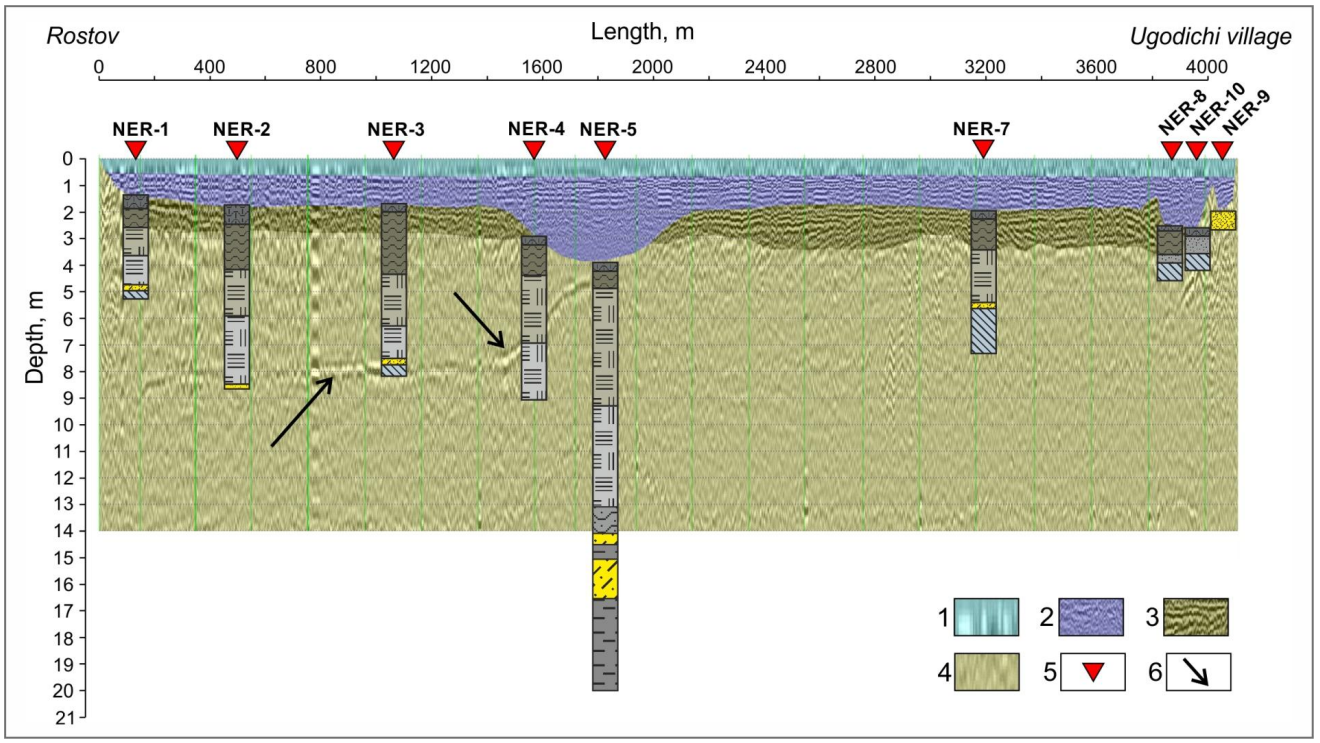

Figure 1.9. Rostov-Ugodichi GPR profile 100 MHz and the bottom sedimentary structure (Konstaninov et al., 2023). *1* – ice; *2* – water; *3* – wet organic gyttja; *4* – wet mineral loams; *5* – cores; *6* – distortions (horizontal interference due to the transformation of time into depth). See symbols for cores in Fig. 1.10.

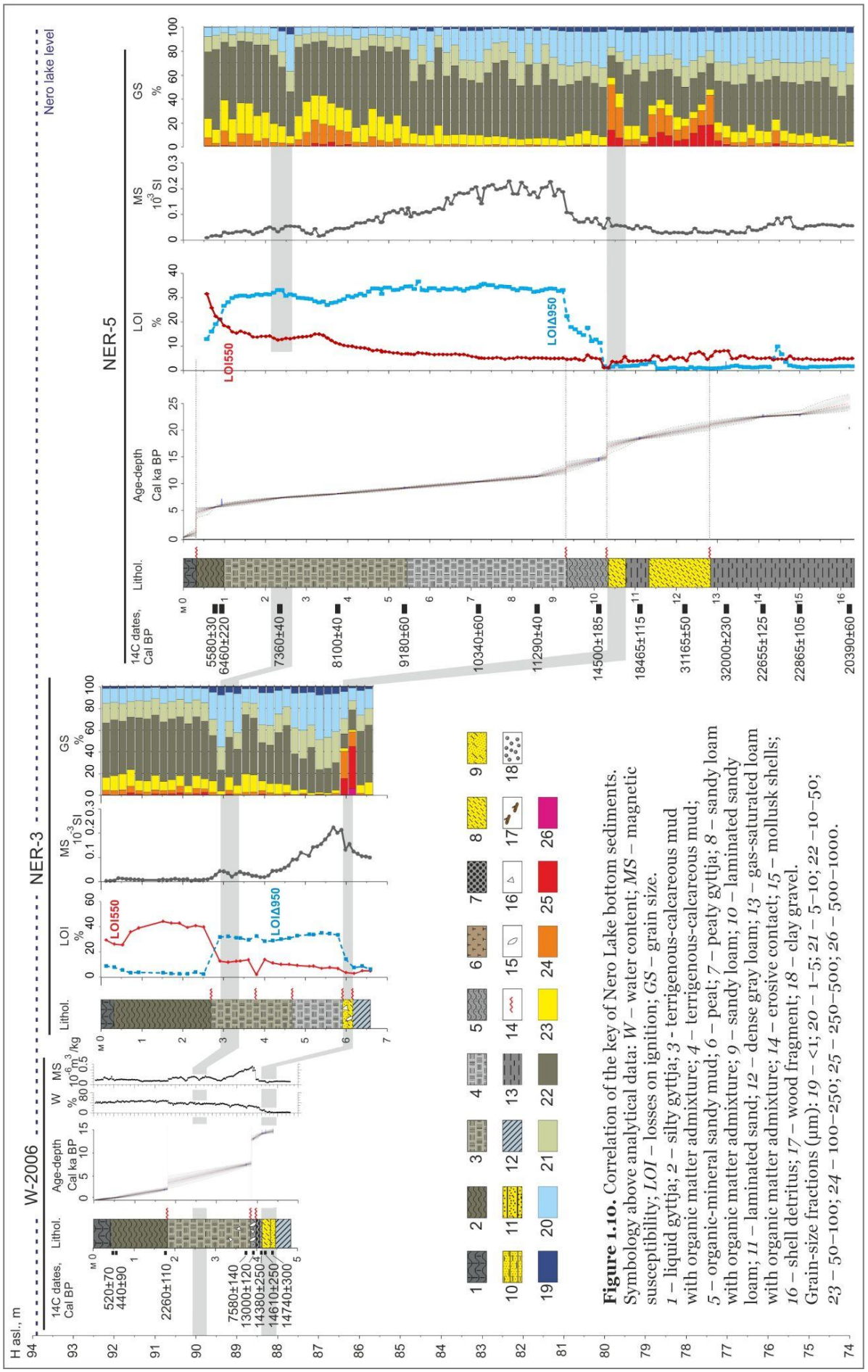

Figure 1.10. Correlation of the key of Nero Lake bottom sediments. Symbology above analytical data: *W* – water content; *MS* – magnetic susceptibility; *LOI* – losses on ignition; *GS* – grain size. *1* – liquid gyttja; *2* – silty gyttja; *3* - terrigenous-calcareous mud with organic matter admixture; *4* – terrigenous-calcareous mud; *5* – organic-mineral sandy mud; *6* – peat; *7* – peaty gyttja; *8* – sandy loam with organic matter admixture; *9* – sandy loam; *10* – laminated sandy loam; *11* – laminated sand; *12* – dense gray loam; *13* – gas-saturated loam with organic matter admixture; *14* – erosive contact; *15* – mollusk shells; *16* – shell detritus; *17* – wood fragment; *18* – clay gravel. Grain-size fractions (μm): *19* – <1; *20* – 1–5; *21* – 5–10; *22* –10–50; *23* – 50–100; *24* – 100–250; *25* – 250–500; *26* – 500–1000.

To build a level fluctuation scheme, integration of age models was performed for three cores of bottom sediments W-2006, NER-3 (correlation), and NER-5. That integration made it possible to construct a bottom height growth curve and fix the stages of a possible lake-level drop (hiatuses). Those data, together with the facies analysis of the deposits, formed the basis for constructing a curve for level changes in the Late Glacial and Holocene (Konstaninov et al., 2022). Data from previous studies, in particular paleobotanical and archeological materials, were taken into account (Fig. 1.11a,b,c). The upper limit of the mean annual level beyond the stages mentioned was estimated based on the results of the Rozhdestvenskii Island survey, where no Holocene lacustrine sediments were recorded in the structure of the surface cover.

Large hiatuses and associated sandy deposits indicate the regressive stage in the history of the lake in the interval of 20.8–10.0 cal ka BP. The main part of the regression (20.8–14.4 cal ka BP) was accompanied by a dramatic increase in sand input into the lake, which may indicate an increase in the river water discharge. Our estimates show that during the regression the lake level dropped below 87 m a.s.l. That is almost 7 m below the mean annual level (93.75 m). During the regression, the lake reduced by several times with the water body preserved only in the deepest axial part of the basin.

The deep Late Pleniglacial – Early Holocene regression was followed by a rather rapid growth of the lake level at the end of the Boreal period. At the beginning and middle of the Atlantic period (9.0–6.5 cal ka BP), the lake level could have reached 91–94 m a.s.l., which corresponds to the modern one. The established transgression is generally consistent with the diatom analysis results (Gunova & Leflat, 1997) that showed the high content of planktonic species in the first half of the Atlantic period, indicating relatively deep-water conditions.

Starting from 6.5 cal ka BP, the lake level decreases rather rapidly, eutrophication grows, and the organic matter content increases significantly. At the lowest point of the regressive phase, the level did not exceed 90.6 m. At about 5.2 cal ka BP, it started slowly recovering but did not reach the modern levels. The Late Atlantic – Early Subboreal regressive stage is confirmed by cultural layer finds and soils below the modern lake level in the low terrace sections (Alexandrovskiy, 2011). In the middle of the already low level at the beginning of the Sub-Atlantic, short-term shoaling to about 91.7 m was recorded. From 2.4 cal ka BP, the lake level was slowly rising, reaching the present levels about 300–500 years ago.

Considering the flow-through type of Nero Lake during the entire Holocene and the absence of a significant underground flow, the mandatory condition for a significant drop in the water level should be the decrease in the height of the flow threshold, i.e., erosion in the channel of an outflowing river (the Veksa River). However, the Veksa River channel deepening under the conditions of extremely low gradients of the Ustye and Kotorosl rivers is not possible without the downcutting of the latter. At present, the Ustye-Kotorosl channel (Chizhikov, 1956) at the site of the Veksa River, judging on the erosion and accumulation regime, is in the Ustye-Kotorosl River system. A comparison of the level fluctuation curve of Nero Lake (Fig. 1.11d) with the fluvial intensity diagram (Fig. 1.11e) reveals a significant relationship. Likely, the large regression of the lake in the Late Glacial and Early Holocene was caused by the extremely high discharges and deep downcutting of river channels (Panin & Matlakhova, 2015; Ukraintsev et al., 2020). The consequence of that was a significant drop in the height of the runoff threshold and the actual transformation of Nero Lake into a small lake-like extension at the confluence of the Sara and Ishnya rivers. The transgression of Nero Lake in the Atlantic period coincides with the minimum level of fluvial activity in the Holocene, which created the preconditions for intensive accumulation in the Ustye-Kotorosl valley. Subsequent small regressions generally coincide in time with the growth of fluvial activity.

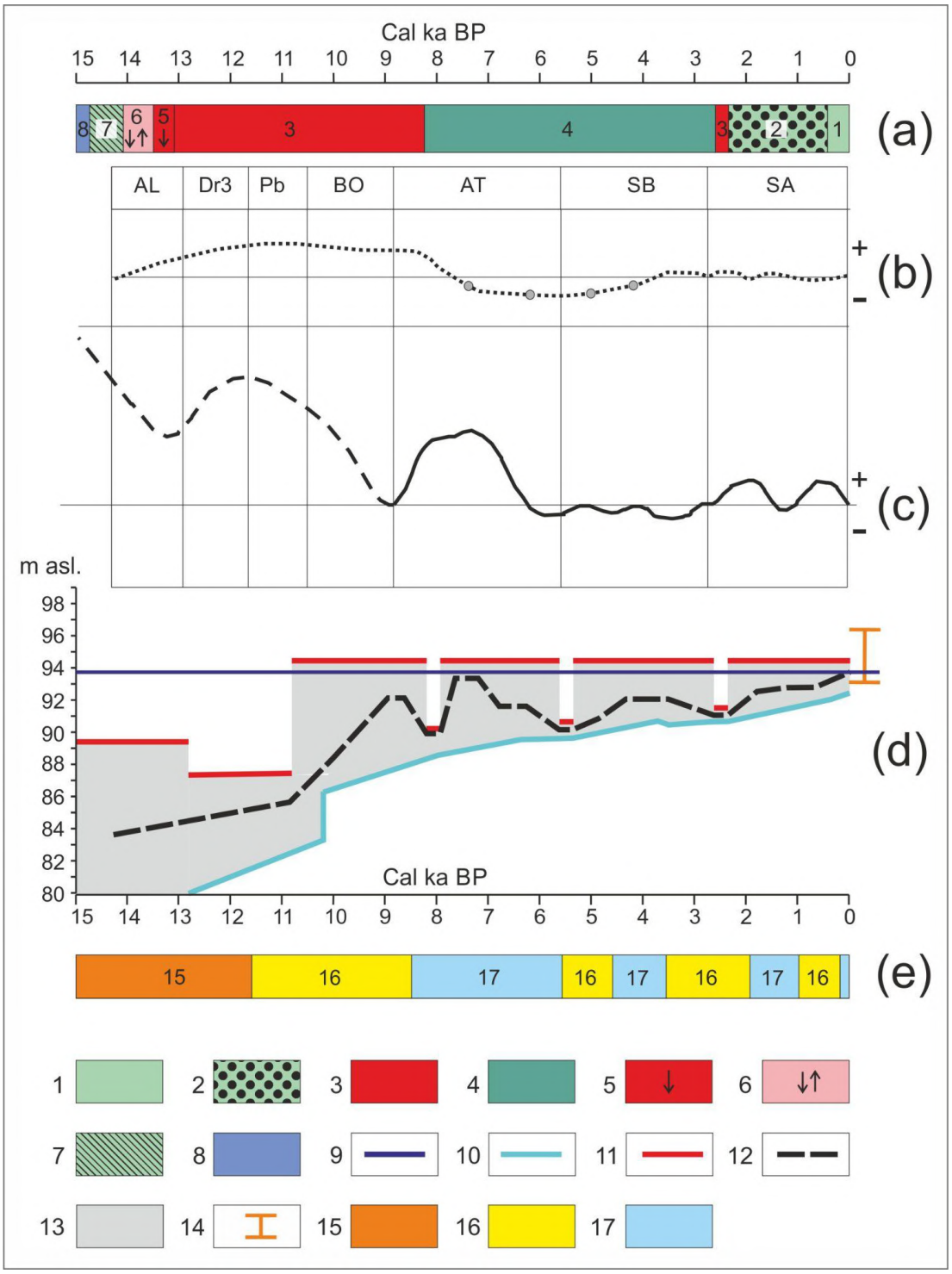

Figure 1.11. Fluctuations of Lake Nero in the Holocene (Konstaninov et al., 2022, 2023), comparison of the results of different authors: a) scheme from Wohlfarth et al., 2006; b) scheme from Alexandrovskiy, 2011; c) scheme from Gunova & Leflat, 1997; d) author's reconstruction; e) change in fluvial activity in the center of the East European Plain (Panin & Matlakhova, 2015). *1* – shallow eutrophic lake; *2* – shallow anoxic lake with high acidity; *3* – hiatus in sediments (drop in level); *4* – shallow lake; *5* – possible shallowing of the lake / shoreline; *6* – level fluctuations and gradual shallowing; *7* – shallow eutrophic / mesotrophic lake; *8* – shallow oligotrophic lake; *9* – mean annual level according to the data for the middle of the XX century (Bikbulatov et al., 2003); *10* – minimum probable mean annual level; *11* – maximum probable mean annual level; *12* – author's estimate of the change in the mean annual level; *13* – probable area of fluctuation mean annual level; *14* – recorded amplitude of level fluctuations for 1930–1980s (Bikbulatov et al., 2003); *15* – epoch of an extreme river runoff; *16* – high fluvial activity; *17* – low fluvial activity.

CONCLUSIONS

– The deep regression of the level of Nero Lake in the Late Pleniglacial and Early Holocene was established. Stratigraphic unconformities in the sediments point to the stage of the low-level position (below 87 m a.s.l.) between 20.8 and 10.0 cal ka BP The lake decreased in size several times; the water body was preserved only in the axial deepest part of the basin.

– The large transgressive phase was recorded at the beginning and in the middle of the Atlantic period from 9.0 to 6.5 cal ka BP The lake level reached 91–94 m a.s.l., which is close to the current values. The mean annual level did not rise above the 94.2 m a.s.l. in the Holocene.

– In the interval of 6.5–2.4 cal ka BP, the regressive position of the mean annual level was reconstructed; it is lower than the modern one by about 1–3 m. (4) From 2.4 ka BP, the level of Nero Lake grew slowly, reaching modern levels about 300–500 years ago.

– The transformation of channel systems was the main factor of Nero Lake level fluctuation in the Holocene causing changes in the height of the runoff threshold of the lake. That transformation was caused by both the climatic changes in fluvial activity and the internal self-development of river channels.

STOP 2. GLACIAL INHERITANCE VS POSTGLACIAL METAMORPHOSES OF BORISOGLEBSK UPLAND INTERFLUVES
August 27, 2023, morning

2A. GLACIAL DEPOSITS AND ASSOCIATED TOPOGRAPHY

Career Hill and Wedding Glade quarries. The glacial topography of the NE Borisoglebsk Upland is represented by low-amplitude hilly plains alternating with pronounced flat-topped hills and shallow flat-bottomed kettle holes ranging 0.5 to 4 km in diameter (Fig. 2.1). The Solovey Kettle (600 m x 800 m) is canvased from the north and west by large hills elevated 25–50 m above its bottom while smaller knobs 5–7 m high are spread along its southern and eastern margins (Fig. 2.1). To the north, Career Hill rises 8–20 m above the adjacent plain being elongated WSW – ENE. The thickness exposed in quarry walls and coring sites was about 25 m. Wedding Glade cut by another quarry was a part of the larger Poklony Hill represented by a gentle ledge on its E slope. There ~15 m of sediments were exposed, however, on much greater spatial coverage. Thus, the thoroughly studied sedimentary sequence of the Career Hill (Fig. 2.2, Table 2.1) coupled with a more generalized spatial investigation of the Wedding Glade (Fig. 2.4) allowed to unveil the complex polygenetic inner structure and geomorphic transformations of such large hills.

They are majorly constituted by thick glaciolacustrine finely laminated light-yellowish sands (Fig. 2.4b,c) and reddish-brown ("chocolate") loams (Figs. 2.2b,c & 2.3g) (unit D) accumulated in a rather deep-water intra- or subglacial environments. However, that thickness is significantly overthrown and folded probably by a powerful glacier advance. On the flanks of that upturned stratum, reddish glacial diamicts with large dislocated sandy blocks (Fig. 2.2c) are found, also addressing the glaciotectonic nature. Yet it is unclear if the deposition of those facies occurred synchronously with the glacially induced deformations or reflected a later superimposed episode of glacial accumulation as was proposed by A.I. Lobanov (Lobanov, 2001).

Regardless, that highly laterally variating stratum is uniformly truncated and disconformly overlayed by another glaciolacustrine unit yet of much thicker and contrasting bedding (Figs. 2.2b, 2.3a, & 2.4a). Well-sorted loam, sand, and gravel beds each tens of cm thick (Fig. 2.3a,b) reflect deposition in an intraglacial environment of higher energy and sedimentation rates (unit C). Intra-bed plastic deformations of gravitational type (small-scale folding, water-escape structures, load casts, etc. Fig. 2.3e–h) are probably of syn- and meta-sedimentary origin due to high sedimentation rates of material with a reverse density gradient. Yet a certain influence of low-magnitude earthquakes associated with the general deglaciation could not be excluded. At the top, they are partially eroded by a certain glacifluvial flow (Fig. 2.3b) accompanied by subaqueous slumps and debris flows (Unit B, Fig. 2.3a). The entire stratum is significantly faulted with amplitudes up to 1–2 m increasing southwards (Fig. 2.3b), the fault planes being emphasized by clastic dykes of the overlying material (Fig. 2.3f). The origin of faulting relates to the uneven melting of the underlying glacial ice (ice lake bottom). Those events were followed by the final episode of thin but almost uniform deposition of flow till with debrites (Figs. 2.2a,b & 2.3d) lacking faults but deformed by narrow inclined cryogenic wedge casts (Fig. 2.3c) probably of thermal contraction nature.

Figure 2.1. DEM of the Solovey Kettle and surrounding glacial hills derived from the digitized contours of the land-planning map of 1:10000 scale with key geological exposures, cores, and profiles.

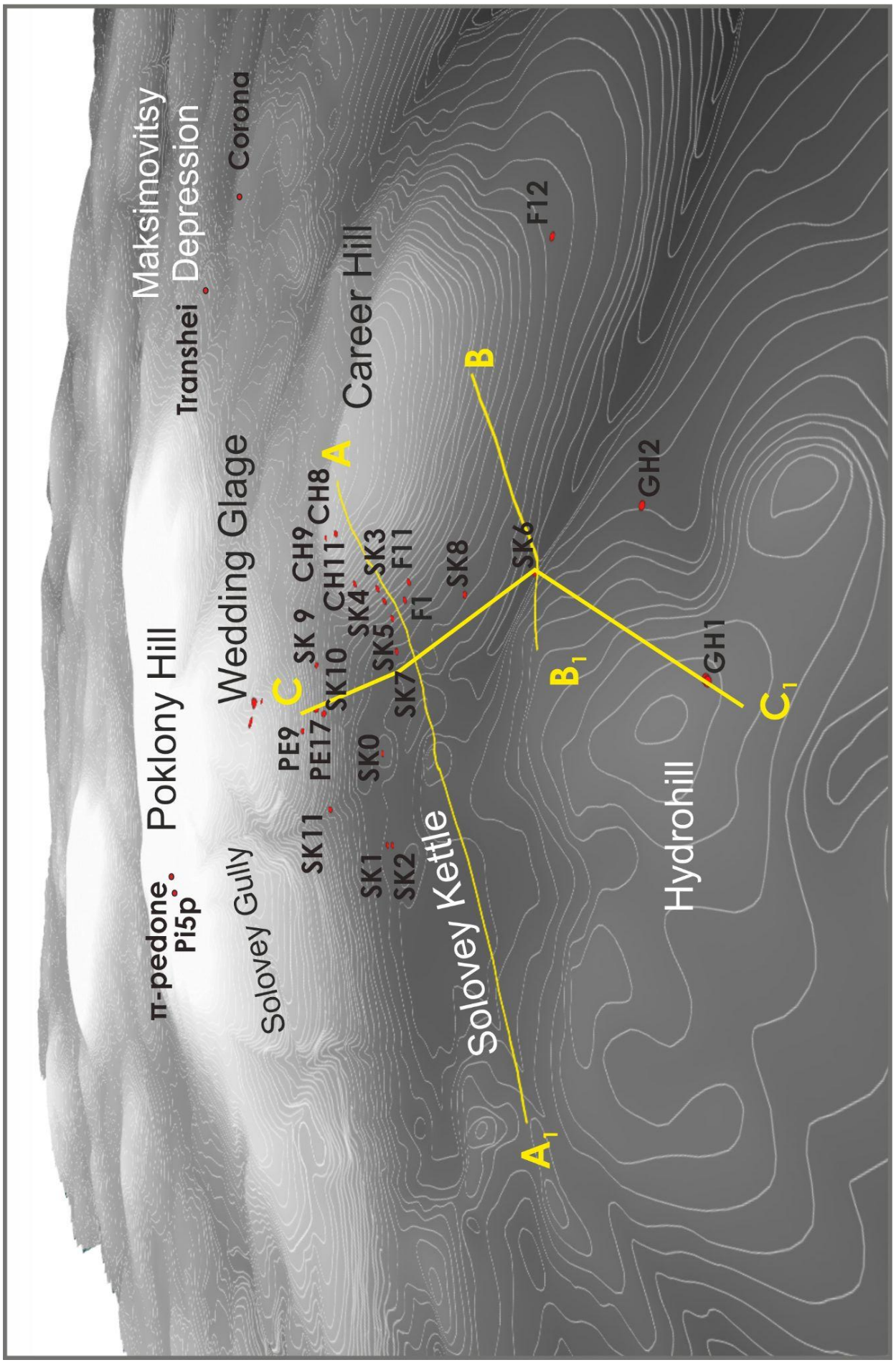
Maksimovitsy
Poklony Hill
Transhei Depression
Corona
Wedding Glage
Career Hill
π-pedone
Pi5p
Solovey Gully
Solovey Kettle
Hydrohill
A
B
C
A1
B1
C1
PE9
PE17
SK11
SK1
SK2
SK0
SK10
SK7
SK5
SK4
SK3
SK9
CH11
CH9
CH8
F1
F11
SK8
SK6
F12
GH2
GH1

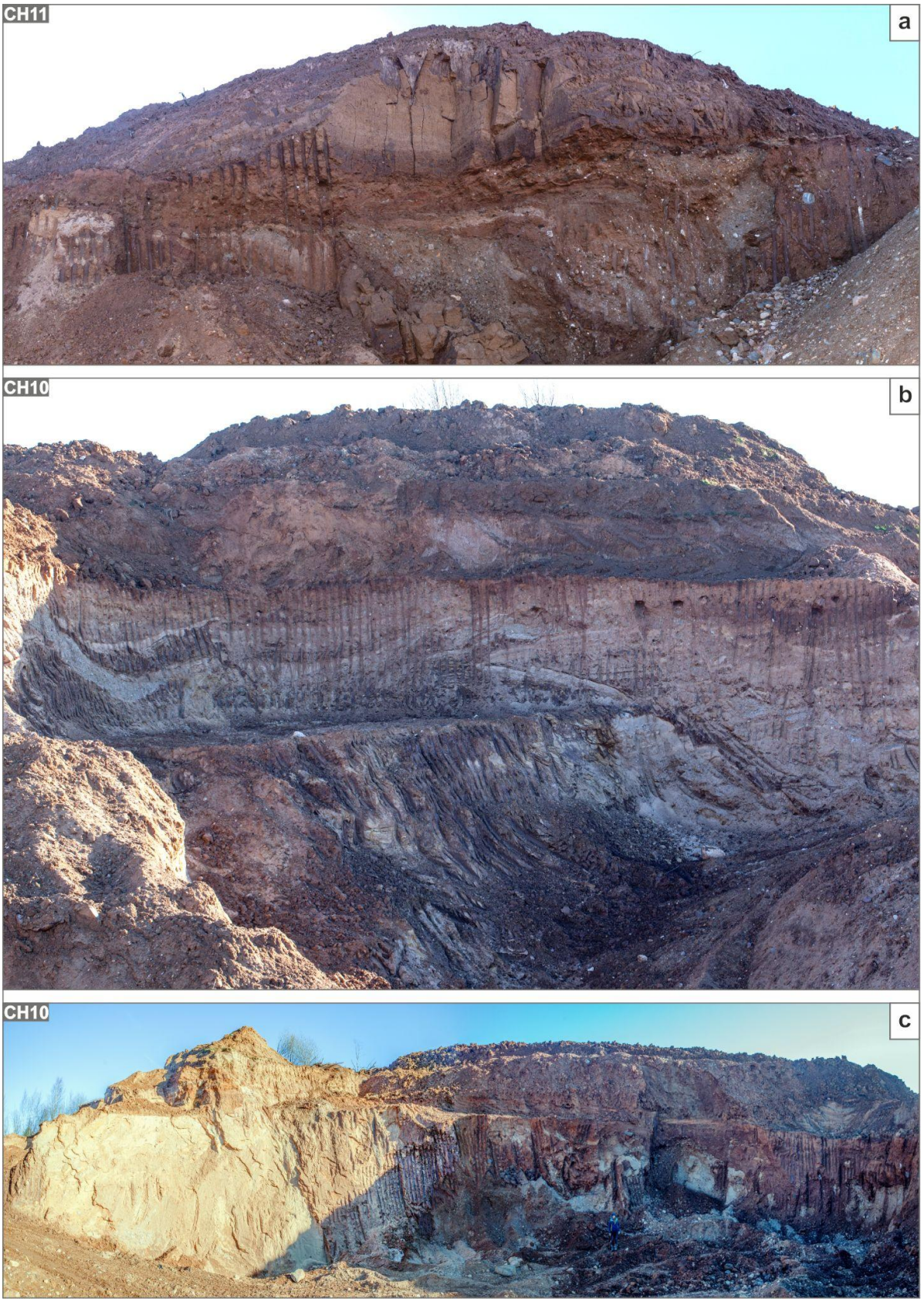

Figure 2.2. Geological structure of the Career Hill quarry: a) "Mantle loams" with blocky structure on top of the flow till above glacial diamicts; b) glacially dislocated laminated glaciolacustrine loams (unit D) below heterogeneous intraglacial lake deposits (unit C) with subaqueous slope disturbances (unit B). Note the sharp disconform contact of the units; c) Vertically laminated glacially dislocated glaciolacustrine loams (on the left) and reddish glacial till with large detached blocks of poorly consolidated lighter sands and gravels (on the right).

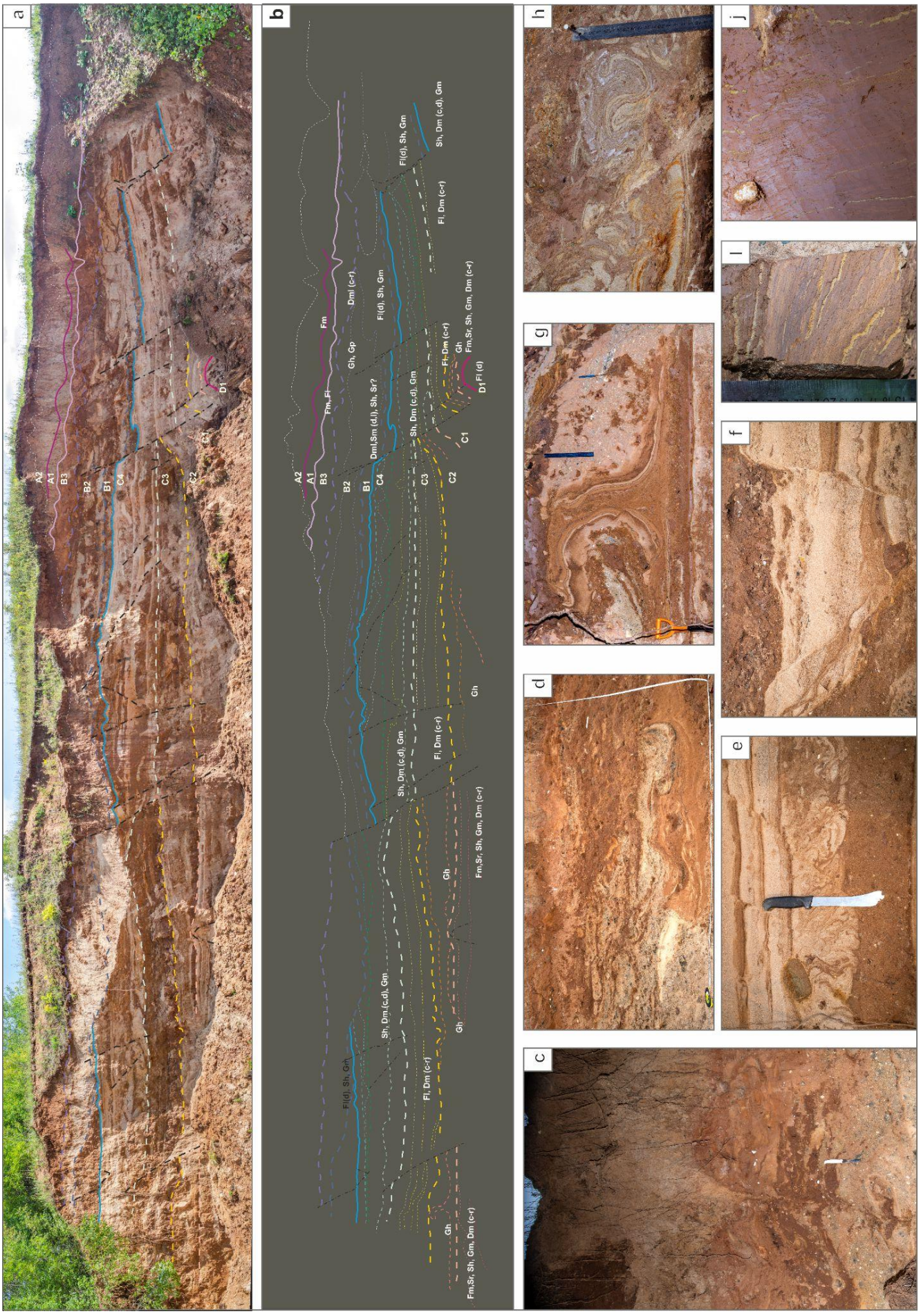
a
b
c
d
e
f
g
h
i
j
A2
A1
B3
B2
B1
C4
C3
C2
C1
D1
Fm
Fm, Fl
Gh, Gp
Dml (c-r)
Dml,Sm (d,l), Sh, Sr?
Fl(d), Sh, Gm
Sh, Dm (c,d), Gm
Fl, Dm (c-r)
Gh
Fm,Sr, Sh, Gm, Dm (c-r)
D1 Fl (d)
Fl(d), Sh, Gm
Sh, Dm (c,d), Gm
Fl, Dm (c-r)
Gh
Fm,Sr, Sh, Gm, Dm (c-r)

Figure 2.3. Structures of glaciolacustrine stratum exposed in the eastern wall of the Career Hill quarry: a) general structure of the glacial base (units D–B) and overlying mantle loams (unit A) with main geological boundaries and lithological interpretations by N.V. Karpukhina; b) detailed interpretation scheme of the same exposure reflecting the stratigraphical sequence (colored lines, the line's width matches its hierarchical significance) pronouncedly deformed both by intra-bed plastic deformations and larger faulting (emphasized by black dashed lines) propagating through different units and subunits; c) narrow wedge cast penetrating from the top of glacial sediments; d) flow and load-casting structures in low till (unit B3); e) flame structures and f) small-scale graben-like faults with clastic dykes in well-sorted sandy beds of unit C4; g) diapir of sandy material into the overlying gravel-rich bed. Note the preserved inner lamination of the former; h) small-scale faulting in contrastingly-layered sands and loams of unit C3; i) microfaulting of the contrastingly laminated sandy loams (unit C4); j) vertical sandy fine lamination disrupted by microfaulting in the dense basal loams (unit D).

Figure 2.4. General geological structure of the Wedding Glade quarry (a) with basal light yellowish sands overlaid by contrastingly stratified glaciolacustrine loams and sands with angular disconformity; b-c) show the details of the inner structure of majorly deformed basal sands.

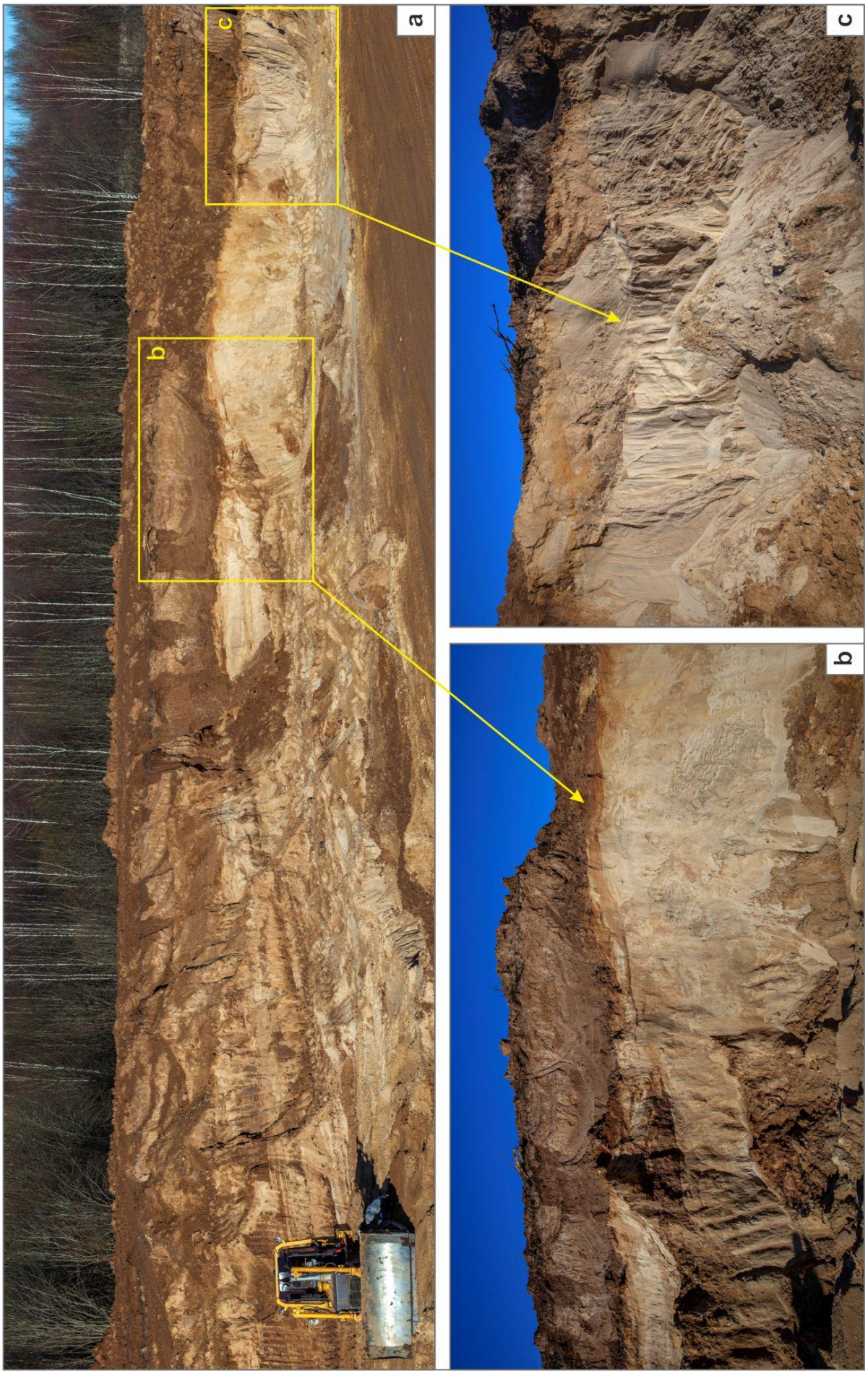
a
c
b
c
b

Table 2.1. Lithology of the Career Hill, CH1-8 exposures

Unit	Depth, m*	Thickness, m**	Texture	Lamination	Sedimentary structures: syn- and meta-	Sedimentary structures: post-	Lower contact	Genetic interpretation	Sedimentary conditions
A2	0.0(1.0)–1.5(2.7)	1.5–2.0	**Fm** Homogenous silt loams	–	–	Polygonal network of ice-wedge pseudomorphs (1–2 m spacing) inheriting older polygonal network. Structural organization due pedogenesis	Gradual to sharp (on predominance of silt content and structural density) wavy (A~0.5 m, P~5–7 m and A~0.2–0.3 m, P~1–2 m – reflecting difference in spatial distancing of older and younger wedge cast networks)	'Mantle loams' with distinct eolian input and varying slope redeposition	Subaerial environment
A1	1.5(2.7)–1.9(3.2)	0.3–0.4(0.2–0.7)	**Fm, Fl** Loams ↓slightly sandy loams with gravel	Non-contrast subhorizontal (h~mm) wavy (A~mm-cm, P~n*10cm) lenticular	–	Polygonal network of ice-wedge pseudomorphs (≥5–7 m spacing) with inclined to subvertical lenticular lamination of the infill of A1 & A2 deposit	Sharp contrast to low-contrast irregular wavy of two orders (A~0.2–0.3 m, P~0.5–1 m & A~0.5 m, P~5–10 m (infill with angular disconformity of B3 top undulations and wedges with stepped contacts h~1–3 cm)	Lacusrine deposits with eolian input	Stagnant shallow water body (residual pool of glaciokarsic or thermos-karstic nature)
B3	1.0(...)–2.1(2.7)	1.7 / 0.2–1.1	**Dml (c-r)** Slightly cemented sandy to sand loams rich in gravel, pebbles and rounded boulders of carbonate and magmatic rocks (D≤1 m), with sandy interlayers and small lenses	Irregular lenticular-wavy (A~cm, P~cm & n*10cm) of 2 orders (h~cm & n*10cm) Oblique to infill structures in B2 top undulations (depositional, erosional and faulting in origin) with angular disconformity	Small features of suspension flow, small load casts, water-escape structures clastic dykes	Subvertical and steeply inclined (70–80°) thermal contraction cracks, occasionally filled with A1 material	Sharp to gradual inclined (~7–10° to SSW) gently wavy to stepped (P~0.2–0.7 m)	Flow till	Shallow residual lake in ice banks

B2 2.1(2.7)–2.8(4.4) 0.6–1.9 / 1.3–2.7	**Gh, Gp** Lenses of silt-loam matrix supported gravels and pebbles with interlayers of B1 material	Inclined to horizontal irregular (P~0.1–0.5 m) lenticular and wavy (A&P~n*(0.1–1) m). Rare coarse oblique lamination	Features of sliding and viscoplastic to liquid flow (h~0.5–1.5 m, A ≥1 m, P~1–3 m). Rolling of loamy interlayers in the frontal zone of the flows (incl. overturned folds)	Some of major trans-unit faults (A~1–2.5 m, P~5–10 m) inclined to SW at ~60°. Some of thermal-contraction cracks from A1 and infilled with B3 material	Sharp erosional inclined (dipping WSW at ~15–20°) wavy to conform gently inclined (dipping at 3–7° NNW) and stepped (along faults in the underlying units)	Subaqueous gravitational debrites	Shallow residual supraglacial lake
B1 2.8(4.4)–3.6(4.0) 1.2(0.0)/0.1–0.2(0.6)	**Dml, Sm (d, l), Sh, Sr (?)** Alternation of gravel loams and gravel sands with rounded dropstones	Inclined to subhorizontal wavy (A<5 cm, P~8–15 cm) of 2 orders (h~cm&n*10cm)	Small features of suspension flow, small water-escape structures, ripples (?)	Series of large trans-unit faults (A~1–3 m, P~5–10 m, dipping S-SSE at ~60°). Occasional systems of smaller (A~n*0.1–1.5 m, P~(1–10)*n cm) subparallel (in B1, 60–80° to NNW) and graben-like (in C2, 20–70° to N & S) faults with clastic dykes of B2 & B1 material and smaller feathering faults (A&P~1–10 cm). Most faults do not affect the overlying B3 and only the major ones protrude into B2. Sporadic thermal-contraction cracks from A1(2) (where B2 has lower thickness); others run from B1 (top is truncated) down to C4. When penetrating dense loamy beds cracks branch into subhorizontal sand apophyses first cm long	Sharp (on the predominance of sand beds over loamy ones and lighter color) subhorizontal slightly wavy and undulating, conform to bedding of underlying unit C4	Flow till	
C 3.6(4.0)–>10.0 >6.0/ 3.5(<6.0)	Alternation of loamy, sandy, gravel-loamy and pebbly-gravel beds with dropstones	Horizontal to gently inclined of multi-order (at least 4 – from mm & cm to n*(0.1–1) m) - predominant laminar flow			Sharp disconform (erosional) with the underlying unit D, sharp conform between the subunits	Glacio-lacustrine deposits with subaqueous gravitational flows	Shallow supraglacial lake of rather high energy and dynamics
C4 3.6(4.3)–5.1(6.2) 1.6(2.5) / 1.6(2.7)	**Fl(d), Sh, Gm** Alternation of sand and gravel-loam beds (h~10–20 vs 30–40 cm), dropstones laterally substituted by gravel & pebbly lenses at the base of C4	Horizontal of 2–3 orders (P~5–10, 1–2 & 0.1 cm), including graded layering (h~2–3 cm) Massive (in gravel loams)	Small water-escape (ball-and-pillow and flame) structures. Disrupted loamy interlayers (h~1 cm), loamy clasts (D~2–10 cm) in sands. In the lower part (gravel-pebbly facies) – features of sliding, viscoplastic flowing and rolling	Systems of small (A~n*(0.1)–1–1.5 m, P~n*(1–10) cm) asymmetric graben-like (dipping at 20-70° S & N) faults with echelon faulting (A&P~1–10 cm). Clastic dykes. Sporadic thermal-contraction cracks from A1(2) & B2 down to C4. When penetrating dense loamy beds cracks branch into subhorizontal sand apophyses first cm long	Sharp horizontal conform, erosional (by debris flow) gently concave at the north	Turbidites, flow till, debrites	

C3 **5.1(6.2)–6.8(7.9)** **1.4(1.7)** / 1.8(0.1–0.2)	**Sh, Dm (c,d), Gm** Alternation of gravel-loam (h~20–30 cm) & clay (h~10–20 cm) beds	Horizontal of 2–3 orders (P~5–10, 1–2 & ~0.1 cm) on sand interlayers (h~10–15, 0.5–1 & 0.1–0.2 cm) and probably even finer in seemingly massive clays. Massive (in gravel-loam beds)	Overturned and standing folds preserving the initial fine lamination. Disrupted loamy and sandy interlayers. Small load casts (in gravel-loam beds)	Diagenetic deformations due to consolidation and compression: - micro-faults and cleavages producing prismatic-blocky structure in contrast finely laminated sand and clay beds (A~1–10 mm, P~0.5–2 cm) – blocky structure dipping SSE at 30° with angular & shell-like cleavage emphasized by Mn in very-fine laminated clays	Sharp gently inclined (infill of erosional lows in C2 top with angular disconformity) to subhorizontal	Glacio-lacustrine deposits	Deeper supraglacial lake of a relatively low dynamics, favorably with perennial ice cover
C2 **6.8(7.9)–8.2(8.6)** **0.7(1.7)** / 0.5(>2.0)	**Fl, Dm(c-r)** Pebbly-gravel bed (h~0.1–1 m) with small interlayers (h~1–10 cm) of clays and loams at the base	Graded horizontal of four orders (h~10, 5, 1 & 0.1 cm enlarging northwards)	Diapir h~40–45 cm of fine-laminated clay-sand bed into sandy-gravel bed. Flow features in gravel-loam beds with fine sandy interlayers and water-escape structures (vertical intrusions h~25 cm of underlying sands)	Systems of small (A~1–2 cm, P~5 cm) symmetric graben-like (60–70°) faults and sporadic singular faults. Cross-cutting micro-faulting (80° & 35°) in contrast finely-laminated sandy-loam beds at the base	Sharp convex upwards (infill of erosional lows in C1 top with angular disconformity) to horizontal	Turbidites laterally substituted by debrites	
C1 **8.2(8.6)–>9.0(>10.0)** **>0.5(>1.4)** / 0.1(0.3)	**Gh** All the facies. Large pebbly-gravel face (infill of pronounced depression in D1 top) almost completely wedges out to S	Multi-order (h from 30–10 to 1–0.1 cm) texturally contrast subhorizontal slightly wavy (A~5–10 cm, P~0.1–0.2 to 1 m)	Ball-and-pillow, small overturned folds in loam-sand beds	Systems of small symmetric low-amplitude (A~1–2 cm) horst-like reverse faults (80° to N & S)	Clear disconform highly undulating (A>0.5–1 m, P~2–10 m), occasionally with small steps, steeply dips >2–3 m to NW (D1 top cleavaged by micro-faults with progressively flattening layering)	Glacio-lacustrine deposits with debrites and flow till lenses	Shallow supraglacial lake

D2	**>15.0**	**Fm, Sr, Sh, Gm, Dm(c-r)** Dense clayey loams with uneven sand content, sporadic pebbles and loamy clasts D~2–10 cm	Fine horizontal due to sandy-silt laminas (h~1–2 mm) and laminasets (h≳0.5–2 cm), highly deformed	–	Pronounced folding and faulting at the contact with D2 & C1. Lamination is vertically upturned and fragmentary contorted into standing folds highlighted by subvertical sandy laminas). Diagenetic deformations and reworking (Mn on prism sides, circular Liesegang structures)	–	Glacially dislocated older glacio-lacustrine deposits	Deep intraglacial lake of stagnant low-energy sedimentary environment against yet contrasting dynamics
D1	**9.0<(10.01)<24.5**	**Fl(d)** Dense clayey face with uneven sand content, sporadic small rounded gravel	Horizontal of 2–3 orders: large (h~m – more or less sandy beds), fine (sand & silt laminas h~1–2 mm) and small (laminasets h≳0.5–2 cm), highly deformed	–	Steeply inclined to vertical lamination, occasionally wavy. Frequent alteration of horizontally and inclined lamination in adjacent micro-blocks fragmented by micro-faults. Diagenetic reworking signs	–		

*Depths are given for the N part of the exposure less disturbed by faulting, with normal bed thicknesses

Thicknesses are given separately for the N and S parts of the exposure **(less disturbed by faulting, with normal bed thicknesses / more disturbed by faulting, with increased bed thicknesses due to subsidence infill)

Thus, the sequence above the prominent erosive contact with the underlying glaciotectonically deformed unit D resembles the final stages of regional glacial cover and particularly its degradation that was constrained by widespread dead-ice distribution (Shishkina et al., 2019). Separate rather small supraglacial lake basins were characteristic for that stage, which is indicated by the pronounced episedimentary faulting (evidence of the ice floor) and general highly variegated textures and structures. If unit C reflects highly dynamic yet relatively steady supraglacial lake development then unit B suggests a short-term and drastic adjustment to the sequential melt-out, first, of the ice floor and, then, ice banks of the lake that, thus, ceased to exist. Hence reddish clast-rich loamy diamicts traditionally considered an archetype of the MIS6 tills, account, in fact, for only a minor part of the entire facial variability of the Late Moscow glacial environments. Being quite sparsely distributed in the study area, that facies almost does not participate in its modern landscape structure usually manifesting only in subdued positions as gully incisions or at the core bottoms. That yields a place for the glacially dislocated older glaciolacustrine deposits, or "local till" (A.I. Moskvitin, 1967) to be the major lithological and geomorphological phenomena of the area and to greatly influence the postglacial landscape evolution.

After the final disappearance of ice banks, the glacial lake ceased to exist producing a prominent flat-topped hill with quite steep slopes. Postglacial evolution generally preserved the hilltop morphology covering it with a rather uniform loamy mantle. At the lower part (subunit A1), it shows higher variability and was probably accumulated in small residual waterbodies on the undulating top of glaciolacustrine unit B. Drainage regime and sedimentary environments of such shallow pools differed significantly, probably, due to varying paleogeomorphic positions against the steep hillslopes.

Hence major topographic highs of the key site owe to the pronounced glaciolacustrine deposition on top of large-scale glacially dislocated blocks. However, their gentle convex-concave hillslopes have experienced significant transformation during the postglacial evolution. The stepped elongated E slope of Poklony Hill supported by the larger watershed was prone to gully erosion while the steeper slopes of Career Hill are still devoid of incisions. Their sedimentary cover includes several colluvial units, which are going to be regarded in connection with the geological structure of the Solovey Kettle infill.

2B. POSTGLACIAL LACUSTRINE SEDIMENTATION

Solovey Kettle key site. In contrast to prominent glacial highs at the north and west, the eastern and southern sides of the Solovey Kettle are obscure in the modern landscape (Fig. 2.1). Round-topped gently sloping glacial hills (600–800 m in diameter) rise only 6–7 m above its bottom. In-between the hills linear depressions do not currently drain the basin, except for an artificially deepened drainage channel in its NE corner. The flat slightly concave bottom of the kettle (1 x 0.7 km) has semi-separated S and NE hollows, while at the NW it is slightly elevated and has a specific hummocky pattern of 1–1.5 m height amplitudes. 13 cores (SK), ranging in thickness from 4 to 21.5 m, were recovered from the bottom and sides of the Solovey Kettle. The coring depth closely corresponds to the thickness of postglacial sedimentary fill, in different parts of the basin varying from 20 m in the deepest parts (Fig. 2.5) to the first meters at the sides. Coupled with electric resistivity tomography data (Fig. 2.6), it revealed a buried paleodepression generally following the outlines of the modern one to be much deeper and its sides much steeper than in the actual landscape. Beneath the smooth concave modern toe slopes of the surrounding hills, the paleodepression reveals steeply dipping southern and western sides, with an approximate slope of 17–20°.

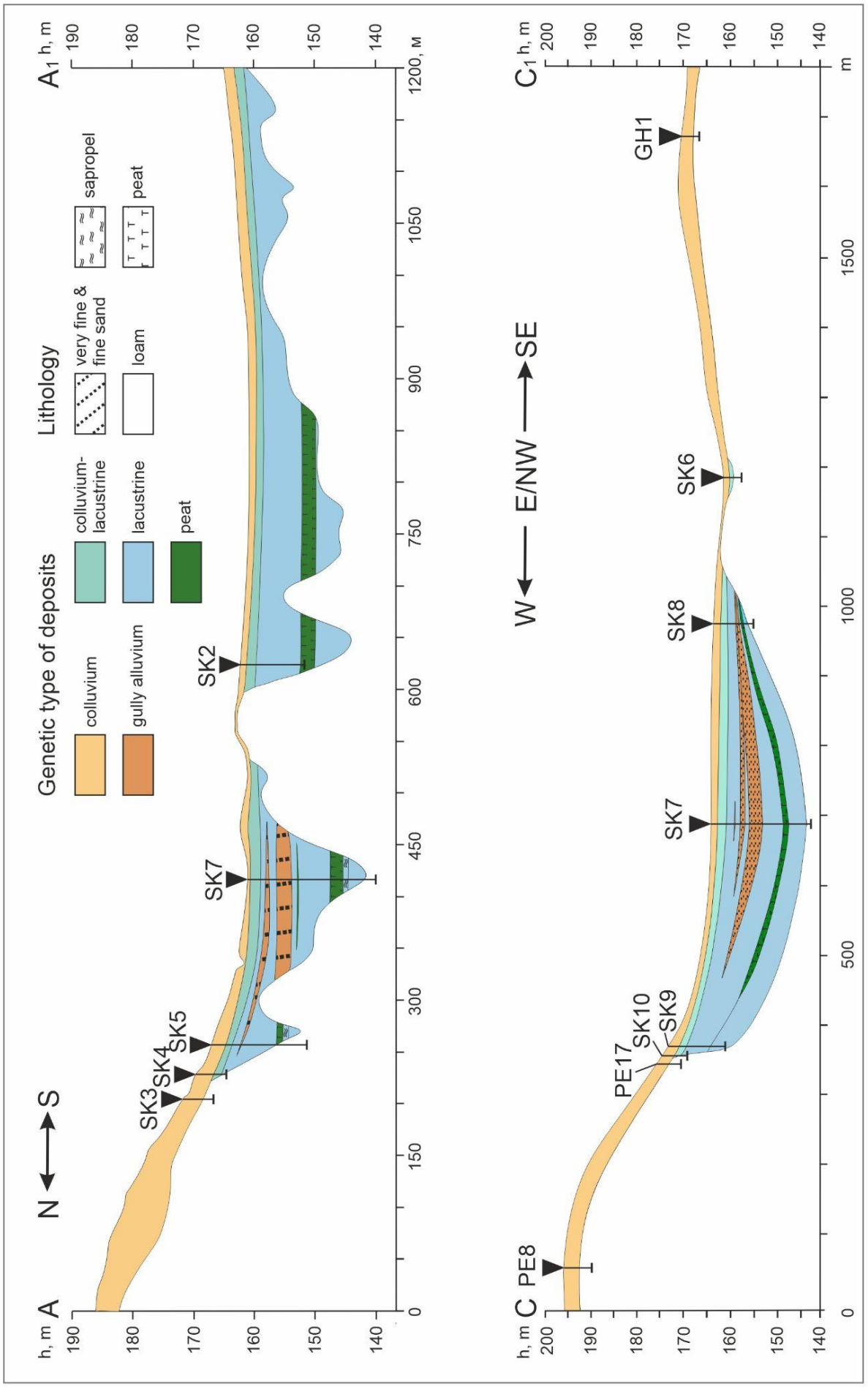

Figure 2.5. Geological profiles of the Solovey Kettle: a) meridional cross-section; b) sub-latitudinal cross-section (see Fig. 2.1 for locations). The bottom of loamy postglacial infill refined in accordance with the ERT data (see Fig. 2.6).

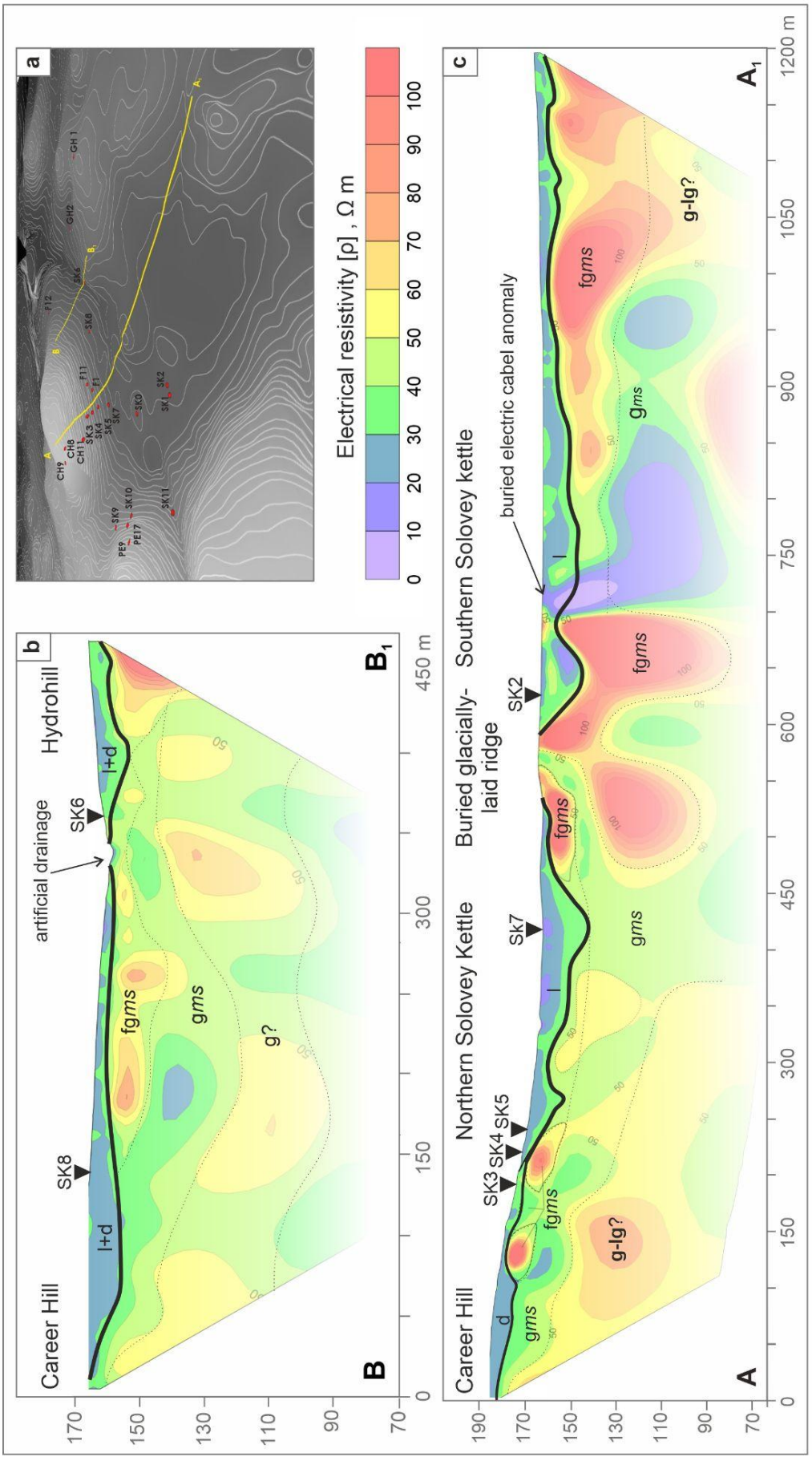

Figure 2.6. Electrical resistivity tomography profiles (SibER-48, 48 electrodes with 5 m spacing) of the Solovey Kettle: a) DEM of the kettle derived from the digitized contours of the land-planning map of 1:10000 scale with positions of the profiles and geological cores and exposures; b) profile crossing the potential drainage pathway at the NE part of the kettle; c) longitudinal cross-section of the Career Hill and Solovey Kettle. Bold black line indicates the bottom of the loamy postglacial infill (low ρ-values) on top of the more resistive glacial deposits (higher ρ-values). Note the high amplitudes of ρ-values below the line well-aligned with the high variability of glacial facies (basal till, flow till, glaciolacustrine, glaciofluvial) recovered in the Career Hill quarry walls (Figs. 2.2 & 2.3). Also note the steep gradients of the line close to the Career Hill footslope reflecting much steeper sides of the buried paleodepression and that the glacial base rises almost to the surface in the central part of the kettle (profile A–A1) showing a glacially-laid ridge almost buried by the superimposed accumulation of the finer material. See comments on the next page.

No incision or associated infill is found in the B–B1 cross-section whereas the more resistive glacial base comes up to the surface at the lowest point of the modern dry hollow. That contradicts the hypothesis of the Solovey Kettle being drained by that pathway to the West Cheremoshnik Gully and rather argues for its prolonged existence as a semi-closed basin isolated from the general drainage network of the NE macroslope of the Borisoglebsk Upland.

ERT showed that the geomorphic structure of paleodepression was much more complex – with several (semi-)separate kettle holes inside its outlines. Paleoridges with even steeper slopes dividing those buried kettle holes are emphasized by the highest electric resistivity values (Fig. 2.6c). They are probably composed of glacifluvial or glaciolacustrine pebbly sands and gravels analog to those exposed in the Career Hill quarry. That is corroborated by the rock clasts outcropping on the eastern flank of the Solovey Kettle where a low westerly spur of a knob (GH1) dives gently into its floor.

According to the ERT data, the greatest sedimentary thickness is associated with the central part of the Solovey Kettle (SK2) and the present-day toe slope of the Career Hill (SK7). As only the latter core has reached the glacial floor of the depression, it was selected for reconstructing the general stratigraphic sequence of paleobasin. Combined with the interpretation of other cores, it helped establishing the facies diversity of rather deep-water to lake shore sedimentary conditions of basin infill, reconstructing general environmental characteristics of the catchment, as well as assessing the contribution of slope processes and linear erosion to the sediment supply and tracing its sources along the sides.

The paleodepression within the Moscow (MIS6) glacial sedimentary complex ($U19_{lg\text{-}fg\text{-}g}$, see the description above) is filled with a thick (up to 20.5 m) stratified loamy stratum with sandy, peaty, and gyttja interlayers distinguished into 18 lithological units (Table 2.2, Figs. 2.7 & 2.8). Its bottom is lined up with rhythmically laminated silts with contrasting thicker sand interlayers ($U18_l$). Microfaults (Fig. 2.7) indicate uneven settling, likely due to the melting of buried glacier ice under the warming effect of a relatively deep-water basin as evidenced by the (sub)millimeter lamination. An accommodated lens of sandy diamict ($U18_{sl}$) (Fig. 2.7) is quite similar to the underlying sandy tills ($U19_g$) while its fragmentary placement and sharp contacts allow to interpret it as a result of rapid slumping along the steep unstable sides of paleodepression. Above a multi-order (sub)mm to cm lamination with microfaulting and multiple angular disconformities persists in $U17_l$. However, a significant content of fine organic matter and plant remains (Fig. 2.7), incl. wood fragments, against the decrease in the sand fraction, suggests improving climatic conditions and reducing energy of the depositional environment while indirectly pointing to the stabilization of the adjacent watersheds. The organic content increases even further upwards in laminated carbonate sapropels ($U16_l$) (Fig. 2.7) likely formed under warm interglacial conditions in a low-energy eutrophic shallow-water basin. It was followed by a stage of superaqueous accumulation of relatively thick (>1 m) dense peats ($U15_b$) of an upwards decreasing degree of decay (Fig. 2.7).

On top of Moscow till, a rather compressed but alike sedimentary sequence was repeatedly described (i.a. Markov et al., 1969; Sudakova et al., 1984) outcropping on the sides of Puzhbol and Eastern Cheremoshnik gullies a couple of kilometers to the east. The onset of organogenic accumulation marked by thin lenses of well-decayed peats was ^{230}U-Th dated to 122–144 ka (Rusakov et al., 2019), which was followed by varved clay sedimentation shortly substituted by gyttjas alternating with peats of 114–115 ka ^{230}U-Th age at the top. Thus, those deposition ages encompassing the entire MIS5e are consistent with the Mikulino palynological interpretation (Gorlova, 1968; Markov et al., 1969; Sudakova et al., 1984; Lavrushin & Chistyakova, 2001; Novenko et al., 2005; Rusakov et al., 2015, 2017; Sheremetskaya et al., 2022), allowing them to be correlated with the investigated units U18–U15.

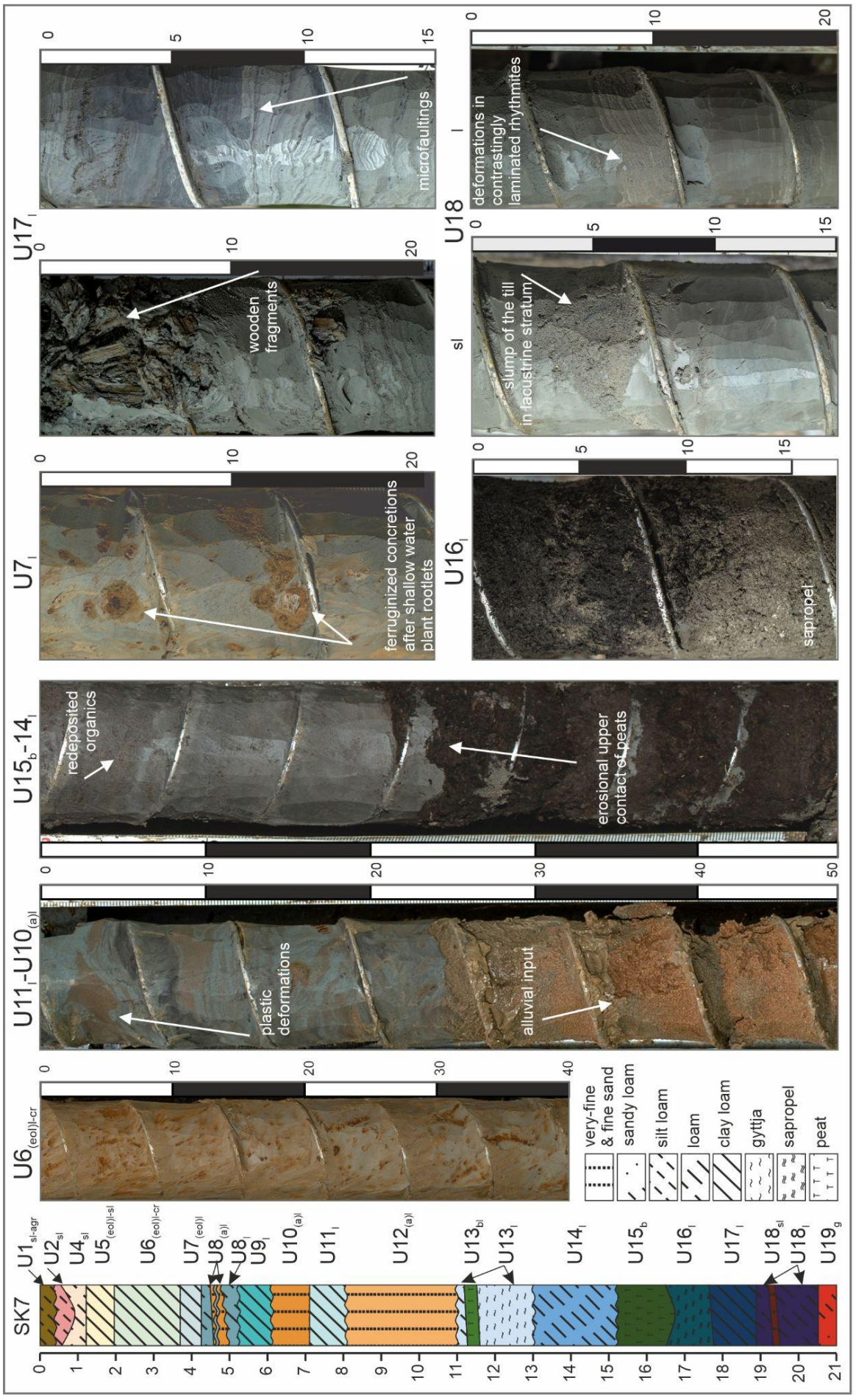

Figure 2.7. Lithological structure of the SK7 reference core, Solovey Kettle key site. See Table 2.2 for an interpretation of color in stratigraphical legend. Photos show specific structures of different units allowing genetic interpretations.

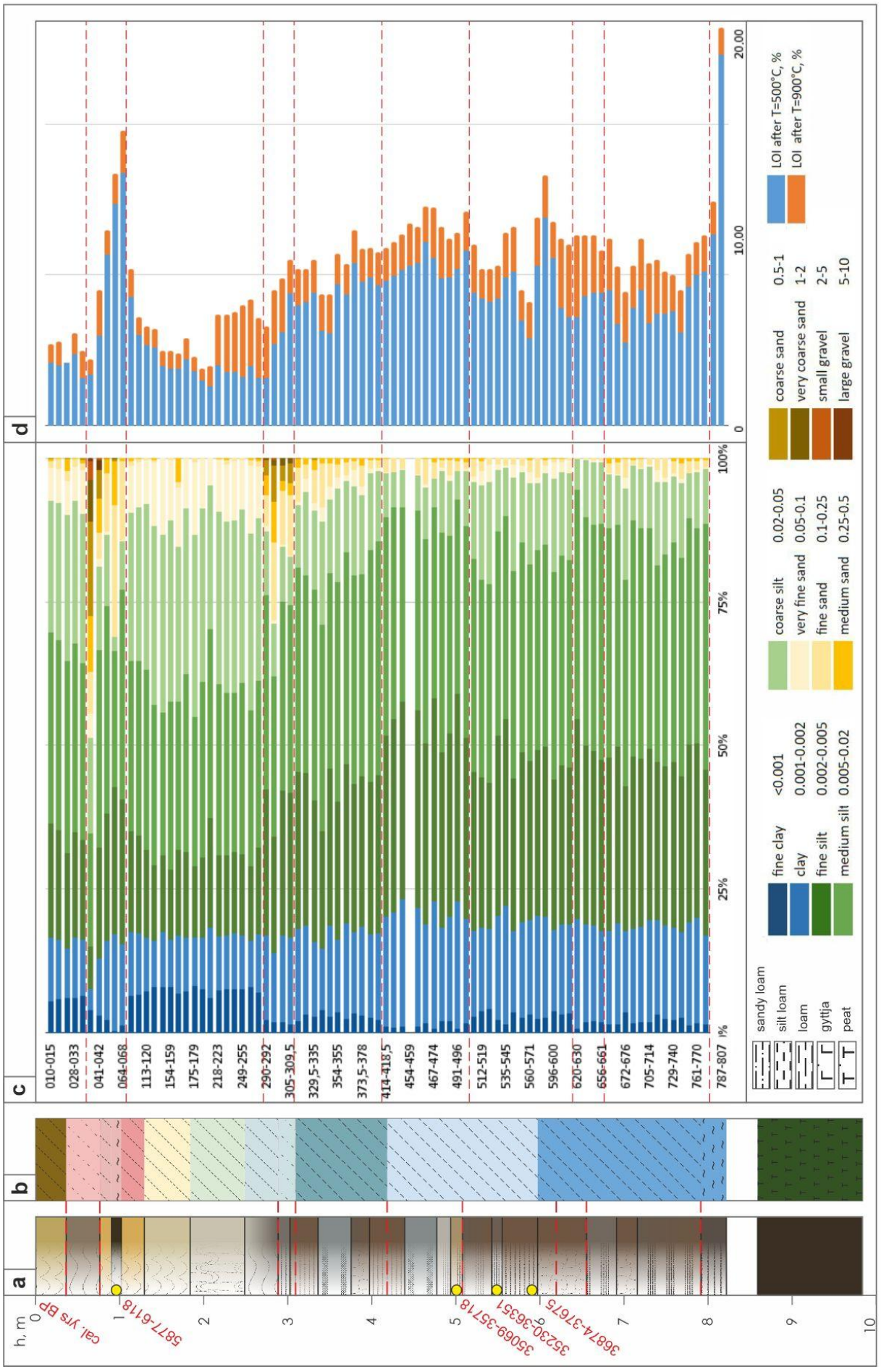

Figure 2.8. Analytical investigation of SK2 core, Solovey Kettle key site: a) structural and color (close to natural) characteristics of the core; b) lithological column (see Table 2.2 for an interpretation of color in stratigraphical legend); c) grain size distribution; d) loss on ignition (LOI) distribution.

Table 2.2. Lithology of the Solovey Kettle, SK7 core

	Depth, cm		Unit	Color	Lithology	Structure	Lower contact
[VII]	0–45(47)		$U1_{sl-agr}$	grayish-brown	fine-sandy loam	low-contrast lamination (h~5–20 mm) with large patches intercalated with whitish silt	clear wavy (A~2 mm, P~3 mm)
[VI]	45 (47) – 90 (93)	45(47)–60(63)	$U2_{sl}$	light-brown-light-gray ↓53 cm – light-yellow	sandy silt	multiphase irregular contrast large patches & low-contrast fine patches	clear tonguic (A~7 cm)
		60(63)–75		red-brown	fine-sandy loam	wavy lamination with large patches intercalated with a dense network of plane pores filled with whitish silt	noticeable
		75–90(93)		reddish-brown	loam	multiphase wavy lamination, angular disconformities with underlying layering	noticeable
[V]	90(93)–123		$U4_{sl}$	dull yellowish-light-brown	loam	large, often subvertical, multiphase patches & numerous soft dark brown Mn concretions	gradual
[IV]	123–193(196)		$U5_{(eol)sl-l}$	grayish-yellow ↓160 cm – yellow-light-gray	clayey silt loam	lenticular lamination of bright red-yellow phase, vertical deformation of lamination	clear on decrease in bright red-yellow phase
[III]	193(196)–370		$U6_{(eol)l-cryo}$	light-gray to whitish with dul reddish-yellow	clayey silt loam	multiphase wavy lamination (A~5–10 mm) with bright red-yellow lenses & soft dark brown Mn concretions	gradual on increased viscosity & decreasing bright red-yellow phase
[II]	370–425(435)		$U7_{(eol)l}$	light-gray & brownish-light-gray with red-yellow	clayey silt loam ↓410 cm – denser	non-contrast wavy lamination (A<4 mm) of gray & brownish-gray phases with dull red-yellow lenses & bright red-yellow fine to coarse concretions with dark-brown core lower 5–8 cm – darker without light red-yellow phase	clear to noticeable
	425 (435) – 520	425(435)–450	$U8_l$	gray with reddish-brown-gray	slightly sandy silt loam	low-contrast lamination of dark-gray & reddish-brown to dark-gray phases	sharp oblique
		450–455(460)	$U8_{(a)l}$	brownish-yellow	fine sand	*not preserved, core has been stretched during extraction*	sharp wavy (A~1 cm, P~1–3 cm) oblique
		455(460)–465(470)	$U8_l$	dark-gray & bluish-light-gray	slightly sandy silt loam with organic-rich layers	contrast oblique lamination of reddish dark brown interlayers (h<10 mm) ↓Isometric sand lenses with angular disconformities	sharp contrast irregular wavy-tonguic (A to 5 cm, P~1–5 cm) slightly oblique
		465(470)–490	$U8_{(a)l}$	brownish-light-gray	fine sand	*not preserved, core has been stretched during extraction*	sharp wavy (A<5 mm, P~1–2 cm) oblique
		490–510	$U8_l$	dark-gray & brownish-gray with reddish-light-brown	alternation of loam & clay loam with organic-rich fine-sandy loam	texturally contrast wavy lamination (h~0.2–1 cm) of gray & reddish-light-brown phases	sharp oblique
		510–520		dark dark-brown to reddish-brown	organic-rich fine-sandy loam	irregular lamination	clear tonguic (A~7 cm, P~10 cm)
		520–530		dark-gray & reddish-brown to dark-gray	slightly sandy silt loam	non-contrast lamination of dark gray & reddish-brown to dark-gray phases	clear wavy (A~3 mm, P~1 cm)
	530–610	530–550	$U9_l$	bluish-gray & grayish-brown	clay loam	contrast wavy lamination (h~2–4 mm, A<1 cm) of bluish-gray & brownish-gray phases	noticeable on thicker lamination

	550–610		bluish-gray & grayish-brown with brown-light-gray	clay loam	contrast irregular lenticular lamination (h~1–2 mm to 1–3 cm) of bluish-gray, brown-light-gray & dark brown phases with rare large brown-gray lenses ↓wavy lamination (A~1–3 cm)	sharp wavy (A~5–8 mm, P~5–20 mm)
	610–708	$U10_{(a)l}$	dull yellowish-light-red	fine sand ↓690 cm – silty fine sand	*not preserved, core has been stretched during extraction*	noticeable
	708–807	708–750	$U11_l$	gray & brownish-gray	clay loam with irregular sandy interlayers	non-contrast lamination (h~2–3 mm) of gray & brownish-gray phases, occasionally highlighted by soft dark-brown Mn concretions, with rare contrast sandy interlayers (h~2–25 mm)	sharp horizontal
		750–792		gray & brownish-gray	clay loam with organic-rich interlayers	texturally contrast fine lamination (h~0.5–2 mm) as in overlying subunit enriched with organic matter	noticeable on increased organic matter & lamination
		789–807		light-brownish-gray	clay loam with sandy interlayers	texturally non-contrast fine lamination	noticeable wavy (A<5 mm, P~15–20 mm)
	807–1100	807–820(822)	$U12_{(a)l}$	brownish-gray	silty fine & very fine sand with sandy-loam interlayers	irregular non-contrast lamination (h~1–10 mm)	sharp oblique
		820(822)–890		brownish-gray	fine & very fine sand with coarse-sand interlayers	texturally non-contrast lamination (*core was stretched during extraction*, h~5–15 mm)	*not clear, high water saturation*
		890–1100		brown-gray to gray↓	very fine sand with organic-rich silty patches	large dark-brown lenses & interlayers, occasionally disconform with host material	clear wavy (A<10–15 mm, P~3–4 cm)
	1100–1305	1100–1124(1127)	$U13_l$	brownish-gray	fine-sandy loam	textural lamination (h~1 mm) with superimposed contrasting interlayers of well-sorted sand (h 2 mm)	sharp oblique
		1124(1127)–1157(1160)	$U13_{bl}$	reddish-brown	organic-rich sandy material	massive with lenses of dark-brown to black phase	noticeable oblique
		1157 (1160)–1250	$U13_l$	brownish-gray	sandy gyttja with small clasts of loam	non-contrast lamination	noticeable subhorizontal on increased organic content & lamination
		1250–1305		brownish-gray	alternation of loam & fine-sandy loam with organic-rich interlayers ↓1275 cm – silty loam	irregular textural lamination (h~1–2 mm to 1–2 cm)	clear wavy
	1305–1521 (1524)	1305–1465	$U14_l$	greenish-gray & brownish-gray	fine-sandy silt loam ↓1350 cm – more plastic ↓1370 cm – denser ↓1420 cm – coarse- gravel interlayers	contrast patches of greenish-gray & brownish-gray phases ↓1415 cm – less contrast patchiness	clear on increased organic content
		1465–1521(1524)		gray with dark-brown	denser loam with organic-rich interlayers	contrast lenticular to patchy with large organic-rich lenses & interlayers	sharp wavy (A~1–2 cm)
	1521(1524) –1670		$U15_b$	reddish-brown to yellow-dark-brown	badly decomposed peat with remains of mosses, shrub & tree leaves ↓increasing density & decomposition of peat	fine lenticular lamination (h<1 mm) with organic-rich interlayers	sharp tonguic (A~3 cm, P>6 cm)

				brownish-gray to yellow	carbonate sandy sapropel with detritus	fine patchy	sharp horizontal
	1670–1674						
	1674–1700 (1703)			reddish-brown to reddish-dark-brown	carbonate sandy sapropel with organic-rich interlayers	fine lenticular lamination	sharp oblique
1670–1775		U16					
	1700 (1703)–1754			brownish-gray to brown↓	carbonate sandy sapropel ↓increasing density & organic content	fine lenticular lamination with rare sandy interlayers	sharp horizontal
	1754–1775			greenish-brown to grayish-dark-brown	carbonate fine-sandy loam, dense & slightly plastic with lenses of sandy silt & detritus	fine textural lamination (h~1–2 mm to ↓2–5 mm) ↓1755 cm – organic-rich lenses, folded deformation	clear oblique
	1775–1784			bluish-gray & dark-gray	carbonate fine-sandy loam to gyttja with small shell detritus	fine lamination (h<1 mm) of bluish-gray & dark-gray phases ↓plastic deformations ↓1785 cm – wavy (A~4 cm) sandy layers h~2–6 mm	sharp wavy (A~1.5 cm, P~2 cm)
	1784–1787			grayish-dark-brown	sapropel with varying sand content	coarse lenticular lamination	sharp oblique
	1784–1797(1799)			dark-brown with bluish-dark-gray & brownish-gray	clay loam with sapropel interlayers	oblique fine textural lamination (h~0.1–0.3 mm) lamination inclination gradually flattens out from 15° to 4–5°	sharp zip-like with angular disconformity (A~1 cm, P~1.5 cm)
1775–1925	1797–1804	U17		dark-bluish-gray & dark-gray	clay loam	multiphase fine lamination (h~0.1 mm) with microfaults & angular disconformities	sharp angular to folded (A<1 cm, P>1 cm)
	1804–1878(1879)			bluish-gray to dark-gray with dark-brown	clay loam to loam with sandy-loam interlayers	irregular fine textural lamination (h~0.3–0.5 to 1–2 mm) with plastic deformations & rare wavy interlayers (A~5–10 mm) 1830–1845 cm – rare sandy interlayers h~1–2 mm 1845–1856 cm – badly decomposed detritus ↓1856 cm – fine textural lamination ↓1870 cm – organic-rich interlayers	sharp angular (A~1 cm, P~2 cm) with microfaults & angular disconformities
	1878(1879)–1889			bluish-gray to gray with brownish-gray	clay loam to loam	multiphase lenticular lamination ↓1884 cm – sandy lenses with plastic deformations	sharp horizontal
	1889–1912		$U18_1$	gray to grayish-light-brown	clay loam to loam	texturally contrast lamination of slightly sandy interlayers (h~1–2 mm) ↑plastic deformations	sharp horizontal
	1912–1925		$U18_2$	yellowish-gray to gray	clay loam to loam	texturally non-contrast fine lamination (h~μm)	sharp horizontal
1889–2055	1925–1950		$U18_3$	gray	sand loam with coarse sand, fine gravel & rare medium-coarse gravel	massive	sharp oblique
	1950–2055		$U18_4$	gray with yellow hue	clay loam to loam with varying sand content	multi-order rhythmic lamination with microfaults alternation of sandy & loamy interlayers ↓2030 cm – large light-brown patches	sharp oblique
[1]	2055–2150	$U19_1$		gray to ↓reddish-gray	sandy silt loam with fine & rare medium gravel	massive	*not exposed*

Noteworthy that within the Solovey paleodepression, the peat top is exposed at significantly alternating depths (Fig. 2.5). From SK2 to SK7 over a distance of 380 m, it drops by more than 6 m raising a question of whether those cores reflect the joint basin or at the time two or even more small independent basins could exist in the central and northern parts of the kettle separated by glacially-laid ridges. As mentioned before, traces of such barriers are found in the present-day terrain and supported by the ERT data. Even greater elevation gradients of the buried peat top were encountered in the vicinity of the Cheremoshnik A outcrop diving 1.7 m within a distance of the first few meters from the Puzhbol Gully edge. Thus, during the Mikulino interglacial, high-amplitude glacial terrain enabled the formation of separate small bogs in its lows also possibly associated with the prolonged preservation of relict buried ice and its deferred thawing during the interglacial optimum leading to superimposed subsidences.

The sharp upper contact of peats ($U15_b$) (Fig. 2.7) suggests probable erosion and/or hiatus in the deposition record. Such breaks have been reported for the Puzhbol and Cheremoshnik exposures (Novenko et al., 2005; Rusakov et al., 2017, 2019; Sheremetskaya et al., 2022). Contrasting lenses of redeposited allochthonous organic matter at the base of the overlying unit ($U14_l$) were likely synchronous with that erosion event yet shortly followed by the recovery of lacustrine conditions. Above textural multi-order ((sub)mm to cm and tens of cm) layering and patchiness of mineral sediment with varying fine organic component (Figs. 2.7 & 2.9f), witness rhythmic cycles of lacustrine sedimentation and superimposed slope and/or alluvial input producing soft sediment clasts included in the rhythmic layers.

Thus, a position relatively close to the lake shore against periodic landscape destabilization on adjacent watersheds could be argued. A clear transition to a more organic-rich laminated gyttja ($U13_{bl}$) with peat on top records the significant increase in bioproductivity of the lake related probably to the regional climate warming. It could be correlated with analogue climatic signal in SK2 core reflected in visible gyttja and peaty lenses (Fig. 2.9e), which were ^{14}C dated 37.5–35 cal ka BP to the Middle Valday (MIS3) interstadial (Garankina et al., 2019). Dispersed organic content remained high (Fig. 2.8d) against the predominance of rather calm and stable, favorably deeper lacustrine conditions (Fig. 2.9d).

No significant input from alluvial sources is observed (Fig. 2.8c) whereas nearby, at the western edge of the kettle, thick alluvial sands at relative absolute heights are found at the mouth of the Solovey Gully (SK11) (Fig. 2.5b). That is in agreement with the glacially-laid ridge between the northern and central parts of the kettle suggested by ERT data (Fig. 2.6c), which could have diverted the solid runoff from the gully to enter only its northern part. There (in SK5, SK7, SK8) a lithologically contrast sequence (U12–U8) reflects a fairly dynamic sedimentary environment of variable energy. Against the preservation of the lacustrine conditions of an average depth the amount of terrigenous (both alluvial and colluvial) material shifted profoundly with its peaks highlighted by fine sand units (U12, U10, U8) of differentiated sorting (Fig. 2.7). Stratified fine sands ($U12_{(a)l}$) with disrupted organic lenses likely indicate increased transport capacity at the catchment both through linear and slope erosion causing some reworking to the underlying organic-rich unit (U13). The sedimentary variability and lack of rhythmicity in thick sandy layers suggest a rather high-energy sedimentary environment. It is favorable to correlate those sands with the alluvial input provided by the incision of the Solovey Gully mentioned above. The introduction of loamy layers to the sand unit (U12) substituted upwards by texturally-laminated loams ($U11_l$, Fig. 2.7) indicates the gradually reducing energy of the sedimentary environment against its yet pronounced alternations. A new phase of intense erosion in the catchment and alluvial input in the lake is highlighted by a sharp boundary with meter-thick reddish silty sands ($U10_{(a)l}$, Fig. 2.7).

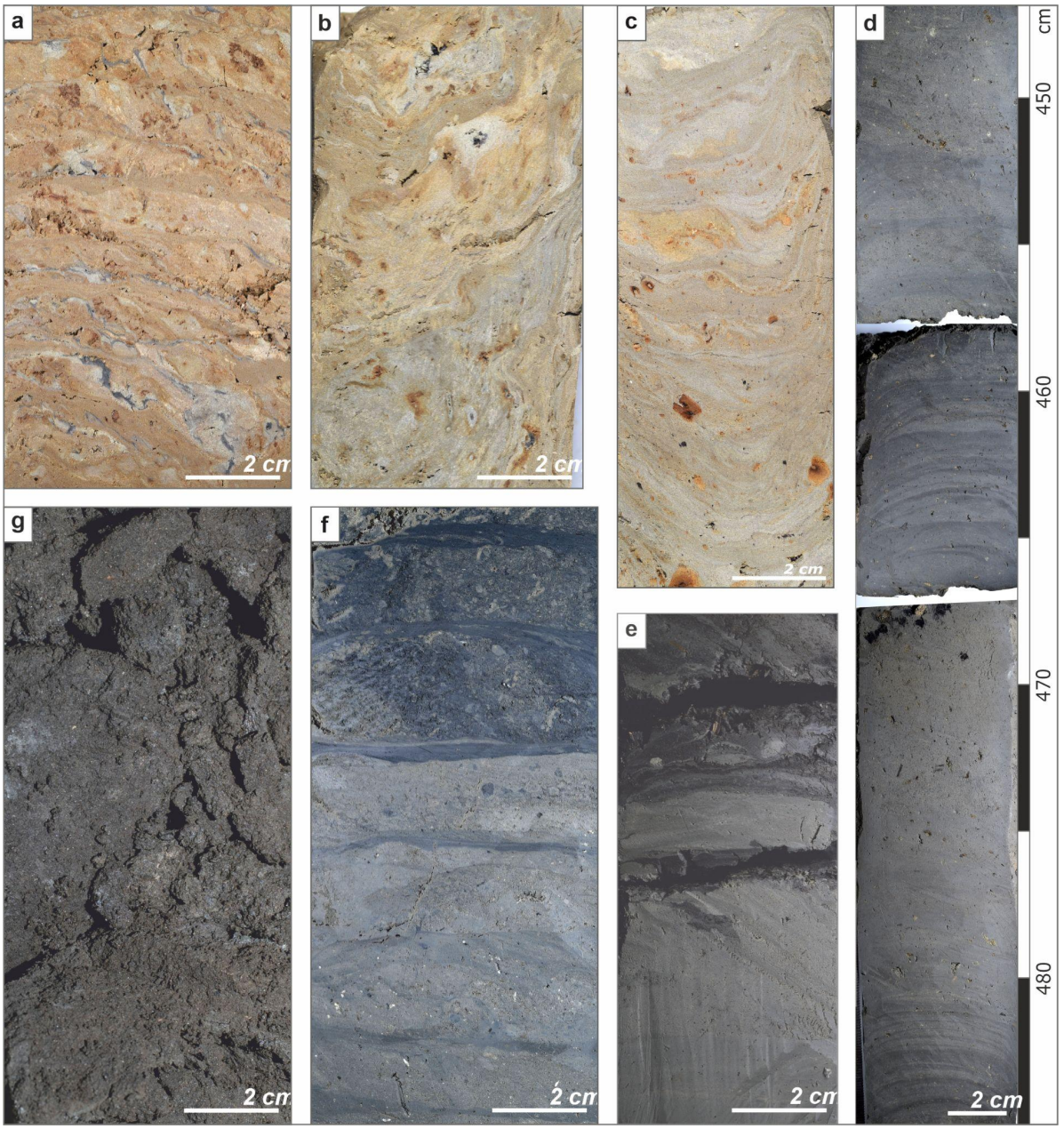

Figure 2.9. Structural features of postglacial sedimentary infill of the Solovey Kettle (SK2 core): a) colluvium ($U5_{(eol)sl-l}$) with irregular alternation of thinner wavy-subhorizontal and thicker inclined lenticular layers of highly contrasting texture; b) cryoturbation with subvertical laminae in shallow lake sediments ($U6_{(eol)l-cryo}$); c) quasi-regular wavy cm-layering with finer lamination in shallow lake sediments ($U7_{(eol)l}$); Note carbonate sand grains and ferrugineous infilling of rootlets; d) dm-stratification with superimposed cm- and mm-lamination in lacustrine unit ($U8_l$); e) dense peaty gyttja interlayer in $U13_l$; f) cm-lamination with subangular clayey clasts and finer-laminated interlayers; g) organic-rich peaty gyttja above basal peats ($U15_b$).

However, as that sandy lens is exposed at close depths in the neighboring cores (Fig. 2.5b), it likely appears to reflect an alluvial fan or slope tailing not providing sufficient evidence of significant scouring of the underlying deposit. However, its source could equiprobably be the neighboring southern slope of Career Hill or the eastern slope of Poklony Hill with its gullies. Above blueish and brown clay loams ($U9_l$) of the contrasting lenticular structure are intercalated with lenses of fine organic matter. Upwards they are substituted by sandy loams ($U8_l$) with much thinner but same reddish sandy lenses ($U8_{(a)l}$) up to 20 cm thick and peaty lenses up to 10 cm.

From there upwards the organic matter content drops significantly against the pronounced increase in the "loess" (coarse silt) fraction (Fig. 2.8c). Silt loams of lighter pale gray color ($U7_{(eol)l}$) are enriched with contrasting bright red-yellow concretions of dense brown interior indicating iron segregation in anoxic conditions along the roots of shallow-water vegetation. Gradually the deposit starts to forfeit its bluish hue ($U6_{(eol)l\text{-}cryo}$) characteristic of the deeper lacustrine thickness while the layering of cm-scale first becomes wavy (Fig. 2.9c) and then significantly distorted by plastic deformations to almost vertical lamination (Fig. 2.9b) and dissected by small-scale inclined cracks. All of the above point to the shallow lake existence, which experienced periodic shallowing or even short-term drying with the predominance of eolian sedimentary input under severe cold climatic conditions. That allowed intermittent freeze and thaw cycles to produce cryoturbations and small desiccation cracks in lake bottom sediments but prevented a more pronounced cryogenic reworking.

Upwards a gradual change to yellow-light-gray (SK7) and brownish-light-yellow (SK2) loams ($U5_{(eol)sl\text{-}l}$) mottled by reddish-yellow impregnations is accompanied by distinct signs of slope redeposition. Certain waterlogging had persisted as reflected both by traces of blueish hue and fragments of characteristic cm-mm layering. Yet the irregular oblique low-amplitude wavy-lenticular structure of subhorizontal layers suggests the predominant sedimentary input and deposition to be of initially solifluction and later slopewash nature (Fig. 2.9a) intermittent with inundation either due to water level changes in a residual shallow lake or within separate recurring ephemeral pools.

The rest of the sequence is highly variable as laterally as in each particular core. In SK2, colluvium ($U4_{sl}$) has a higher total thickness rising almost up to the surface yet only the upper 40 cm could be confidently attributed to subaerial deposition. Below it incorporates at least two organic-rich lenses showing definite signs of subaqueous deposition. The lower thin gyttja lens was dated to the Atlantic phase of Holocene (5877–6118 cal yrs BP) while the buried humus horizon of a hydromorphic soil provided even an earlier date of 6172–6680 cal yrs BP. The underlying colluvium shows multiple inclined pore planes with thick clay cutans also pointing to some landscape stabilization prior to the recurrence of lacustrine environment followed by an episode of sand, gravel, and pebble accumulation of the alluvial fan (probably from the Solovey Gully). Close ^{14}C ages were obtained for the buried gyttja in the Puzhbol alluvial fan and the base of pedosediments on the Puzbol and West Cheremoshnik gully sides suggesting a certain surface stabilization of the Holocene optimum around 6–7 ka followed by an extensive erosion and redeposition of soils around 5–6 cal ka BP (Belyaev et al., 2020).

In SK7, a transition to the predominantly subaerial deposition is associated with a rather thin unit $U4_{sl}$ presenting signs of slopewash accumulation. Light-brown phase replaces the light-gray one, and the amount of bright reddish-yellow impregnations rises noticeably. It is covered by another thin colluvium $U2_{sl}$ of a bipartite organization marked by the reddish-brown color and significant pedogenic reworking reflected in a reticulate network of plane pores with pale light-yellow siltans (ELhh and BEL horizons). Those colluvial units could be correlated with stage(s) of regional landscape destabilization associated with climatic fluctuations during the Late Glacial to Early Holocene transition followed by the Holocene surface stabilization and pedogenesis.

The final stage of sediment accumulation within the Solovey Depression can be attributed to the beginning of agricultural development of the Upper Volga region. The onset of cut-and-burn cultivation led to erosion intensification on previously forested fields and triggered the agrogenic colluvium ($U1_{sl\text{-}agr}$) accumulation on the adjacent footslopes and in local depressions commencing 0.6–1.3 cal ka BP (Belyaev et al., 2020). At the northern edge of Solovey Kettle (F11), a buried birch charcoal

lens has recorded the cut-and-burn episode at 925–976 cal yrs BP (see Fig. 3.2c).

Thus, in the Solovey Kettle, lacustrine sedimentation began at the end of MIS6 deglaciation (during the Late Moscow). Located on the macro slope of the elevated Borisoglebsk Upland the catchment of the depression weathered certain erosion episodes. Major fluvial incisions are reflected as several alluvial sand layers in the paleolake sedimentary record. Alternation of organic, organic-mineral, and mineral deposition suggests a sequence of sudden environmental shifts resulted in changes in sediment sources and agents of delivery: from predominantly colluvial input interrupted by biogenic accumulation and fluvial runoff to leading eolian input against the increasing trend of slope redeposition culminated in final transition to subaerial colluvial deposition. However, environmental rhythms are evident not solely on the level of units and subunits but are distinguishable in individual beds and laminasets. That multi-order stratification of lake sediments refers to their sensitivity to both regional environmental cyclicity (from seasonal and annual to decadal, centennial, and millennial) and irregular episodic shifts on a catchment scale. The pronounced landscape variability within the catchment was majorly influenced by large elevation differences (>50 m) of the initial glacial topography. During the glacial-to-interglacial transition (early MIS5e) high surface gradients and height amplitudes against the overall landscape instability, caused by the permafrost degradation and melt-out of buried glacial ice blocks, provoked extreme events as subaqueous slumps on steep slopes of the depression superimposed on its gradual infilling by varve-like texturally contrast sediments. Gradually decreasing deposition energy and dynamics followed by the water level drop resulted in peatland formation during the Mikulino (MIS5e). Recurred in the Early Glacial (MIS5a–d) or Early Pleniglacial (MIS4) the lacustrine environment then recorded another yet milder climatic amelioration during the Middle Valdai interstadial (MIS3) emphasized by the increased organic matter content of the stratum. However, some local but pronounced landscape differentiation has been correlated with that period as several fluvial incision episodes related to the development of branching gully systems on the adjacent eastern slope of the Poklony Hill have been recorded in the northern part of the Solovey paleodepression. Although contrastingly calm and low-energy environment had persisted in its adjacent central part corroborating the ERT-proposed hypothesis of a glacially-laid paleoridge that had, to some extent, separated the Solovey Depression into two or even several small kettle holes. Prolonged sedimentation eventually sufficiently infilled the lows of initial highly heterogeneous topography enabling the merger of those separated basins in a shallow water body. The distinct shift in eolian input to the lake marked the onset of the Last Glacial Maximum with its severe conditions reflected in cryogenic syngenetic reworking of the lake bottom sediments. Increasing colluviation trend during the Holocene gradually led to the ultimate transition from subaqueous to subaerial conditions in the kettle bottom. Some short-term water-level fluctuations marked by fragmentary thin gyttja lenses recurred during the late Atlantic phase of the Holocene. More to be said, a small residual pool, which is still identified by the darker humus-rich patches, persisted until 1984 when it was drained through the underground pipe system and open ditch towards the West Cheremoshnik Gully head. At the same time, about a millennia-old onset of cut & burn agriculture has been identified on the northern slope of the depression associated with the accumulation of agrogenic colluvium on the footslopes.

Wedding Kettle key site. Lacustrine lenses have recently been found not only in large semi-closed depressions of undulating interfluves and on the gully sides in their middle reaches but even at the modern edges of convex hillslopes seemingly unfavorable to serve as local sinks. However, the revealed highly irregular surface of glacial deposits provided suitable constraints for the widespread

existence of small lakes. It even appears that cascades of lakes had existed in isolated or semi-drained kettles at up to 190 m a.s.l. during the Late Pleistocene. In the quarry wall, an exemplary exposure of such characteristic infill of a rather small elevated (185 m a.s.l.) kettle hole (Fig. 2.10a) is presented showing patterns strikingly resembling the ones in cores of the larger Solovey Depression.

The bottom of the initial depression 4–6 m deep is of glacial stratum consisting of vertically or inclined laminated sands. It is paved by a thin reddish flow till [I``] with gradually increasing upwards signs of deposition in a water basin [I`]. The lower lacustrine subunit of bluish-gray and grayish-blue loams is found as a fairly small lens in the deepest part of the depression. It has zip-like lateral contacts with [I`] (alteration of redeposited flow till and lacustrine material). A large lens of brown sandy gravel loams with redoximorphic features and boulders is disconformly embedded in those loams. We argue that such formations (as in the Solovey Kettle and here) are a result of subaqueous slides of flow tills on steep slopes of paleodepressions. Such formations have earlier been mistaken for the younger (Valdai) glacial tills forcing the authors to protract the limits of Kalinin (MIS4) ice cover at least several hundred kilometers southward of the confirmed sites of the Early Pleniglacial ice advance.

If that or another analog slump had caused the damming of the lake it may be regarded as a trigger for the following water level rise. Above a series of laminated bluish-gray and gray sediments constitute a prominent stratum of up to 4 m thick and laterally much more widespread than the previously mentioned basal lake lens. They correlate quite well with the stratigraphical sequence of shallow lacustrine infills of the Maksimovitsy Depression (see Stop 3, Figs. 3.8i,h & 3.10c). Designated there as unit [II], covering the basal glacial complex [I] with a pronouncedly reworked water-laid subunit on top [I`], it could be distinguished into at least three subunits with occasional erosional contacts (Fig. 2.10c) and visible hiatuses emphasized by frequent (with 1.5–2 m spacing) ferruginized frost cracks (Fig. 2.10e). Occasionally the lower and middle subunits comprise darker organic-rich inclusions, which had experienced some cryogenic reworking of yet undefined cryoturbation or involution type (Murton & French, 1993). At the Maksimovitsy Depression, spheroidal structures (Fig. 2.10f) constituted of dense dark-gray gravely loams were bound to the base of the stratum [II````].

At the Wedding Glade, interlayers of much less dense but better preserved organic-rich matter (Fig. 2.10c) were found higher in the stratigraphic sequence as a part of subunits [II```] or [II``]. Interbedding of loams and gyttjas with wooden fragments is substituted by the entire tree trunks closer to lake shores. Occasionally deposits are deformed in small diapirs (Fig. 2.10d) protruding upwards into the brownish-gray loams [II``]. At the Koskovo site material organized in resembling structures was dated 34–55 ka (Rusakov et al., 2019) constraining its formation to the Middle Valdai (MIS3) interstadial.

Atop, usually with the distinct erosional undulating contact of tens of cm to meter amplitude (Fig. 2.10c) that truncate subunits [II``] and [II```], lighter gray loams [II`] lay (Fig. 2.10b). They conatain dense ferruginous concretions that inherit the reticulate network of aquatic plant rootlets. Several erosional disconformities, including sand-rich lenses, are embedded in the subunit. On top of lacustrine thickness (~1.5–2 m from the modern surface), the deposition type shifted to colluvial with the predominance of slopewash. Prior to or simultaneously large (up to 4 m deep) stratified cryostructures [D] (see Fig. 3.10) penetrated the thickness. Their light-gray to light-reddish silty infill is laminated subparallel to the inclined disconform contacts with host lacustrine loams. Reddish-brown stratified colluvium covers the erosional surface that truncates both the lacustrine stratum and [D]-structures. It bears signs of subatlantic pedogenesis leaving a rather wide gap of uncertainty between the last stage of cryogenesis and the Late Holocene landscape stabilization.

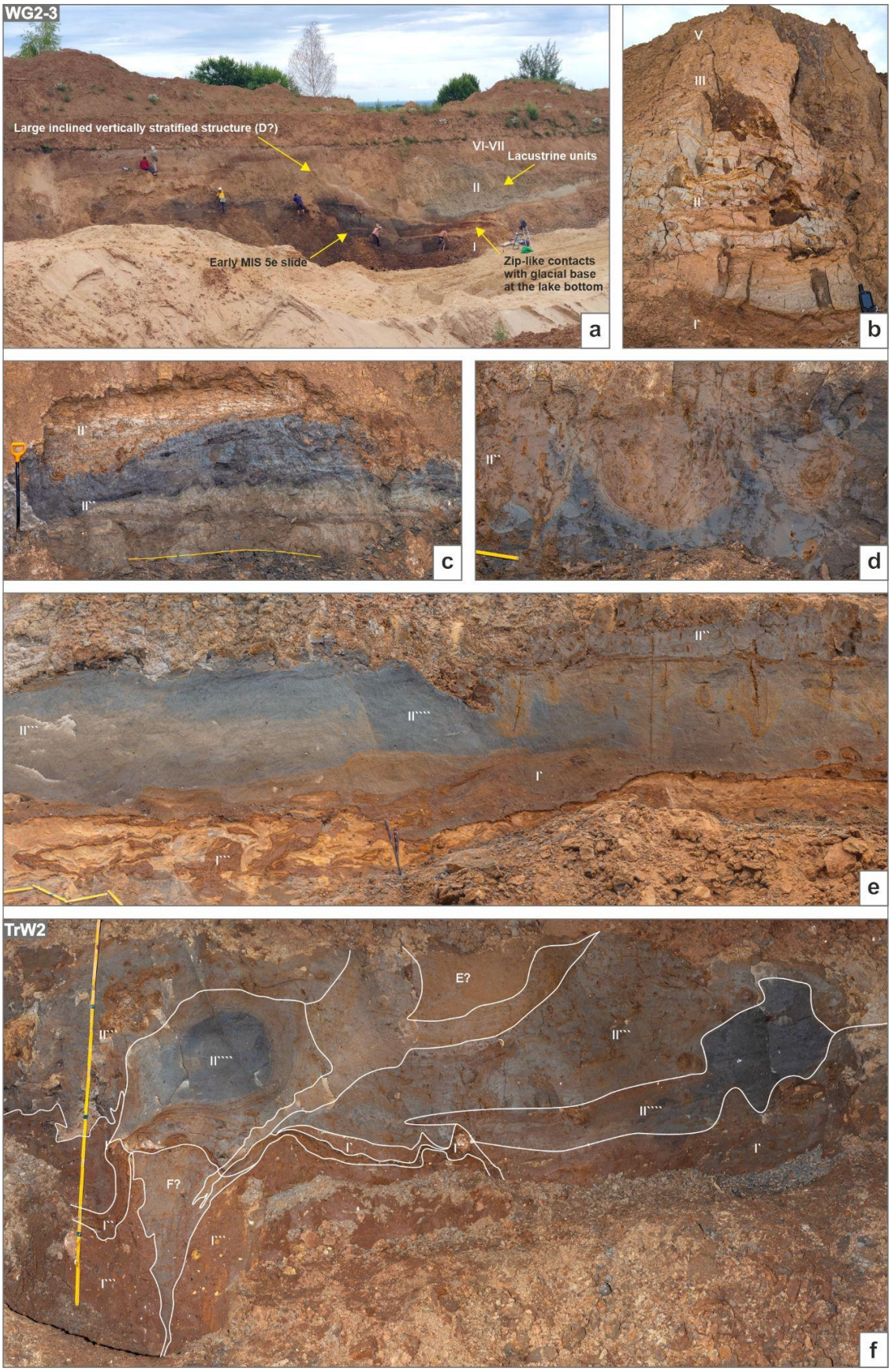

Figure 2.10. Lithological and stratigraphical organization of the Wedding Kettle lacustrine infill, 185 m a.s.l.: a) general structure of the exposure; b–e) characteristic features of distinguished units and subunits (see comments in the text); f) deposits of a similar organization in the infill of the Maksimovitsy Depression with pronounced ice-wedge casting and spheroidal structures of dark organic-rich gray loams.

Judging from the modern landscape structure of the key site the last erosion event should have been triggered by the retrogressive incision of a small Svidanka Gully head (Fig. 2.1), while during the previous stages, some minor erosion events were not powerful enough to terminate the lake regime.

DISCUSSION

Thus, numerous contacts of the major beds suggest a series of hiatuses in the sedimentary infills of the Wedding Glade and Maksimovitsy paleodepressions. As the upper subunit and its major beds show signs of a presumably erosional nature numerous subhorizontal internal boundaries in the lower and medium subunits often are conform but highlighted by the contrasting ferruginized lamination and small frost cracks. That argues for the superaqueous or even subaerial breaks in sedimentation during rather short-term lake water level shifts. Upwards the energy of both the depositional environment and of the geomorphic agents in the catchment of the depression was waxing against the fairly long-term shallowing of the water body probably due to both the sufficient infilling of the initial low and distinct deterioration of climatic conditions.

Hence it was still possible to correlate the fragmentary sedimentary record revealed at the Wedding and Maksimovitsy paleodepressions with the major environmental stages unveiled in the fuller Solovey paleoarchive. Accumulation of the basal lacustrine lens with the superimposed slumping event could be reliably corresponded to unit 18 recording the same association of depositional agents at the onset of the infill during the early stages of the Mikulino interglacial. Some episode of pronounced erosion could be hypothesized during the transition from interglacial to early glacial conditions (MIS5d–a?) as its signs were found in different geomorphic locations all over the study area (eroded tops of the Mikulino peat layers, fluvially-redeposited material of the glacial complex yet encompassing significant amount of organic matter, etc.).

However, the precise age control and interpretation of the geomorphic agents responsible for the event such widespread yet lacking any prominent linear incisions is yet to be identified. Associated with certain landscape readjustment it forced an extension of the lacustrine sedimentation areas resulting in subunit [II```] that could be tentatively correlated with unit 14 in the Solovey Kettle. Shift to the considerably organogenic deposition in more favorable climatic conditions is fixed in both the Solovey (U13) and Wedding [II```–II``] kettles. Based on the radiocarbon ages, it can be reliably enough matched with the first part and the middle of the MIS3 interstadial. The following period has manifested quite differently in the considered paleodepressions. If in the Solovey Kettle rather deep-water sedimentation has persisted against several high-magnitude episodes of the catchment erosional incisions then at the Wedding Glade only a thin subunit [II``] with distinct signs of cryogenic reworking was able to survive after the erosion episode marking the shift to vividly different sedimentary conditions. The shallow lake sedimentation of the later stages (subunit [II`] vs U7–U6) is well-identified throughout the area due to the characteristic light-bluish to whitish color of the deposit pierced by dense networks of ferruginized aquatic plant rootlets and a simultaneous noticeable rise in the "loess" (coarse silt) fraction referring to the increased eolian component of sedimentary sources. Later a general trend to the predominance of colluvial deposition expressed differently in each depression and even in their different parts greatly dependent on the actual geomorphic position in relation to the adjacent slopes.

CONCLUSIONS

– Detailed analysis of the E Borisoglebsk Upland suggests that most of the surface drift materials initially interpreted as polygenetic mantle loams were likely formed by continuous postglacial lacustrine deposition. Major arguments for such genetic interpretation are the dominance of fine-grained fractions; clear and texturally contrast multiscale lamination (up to five levels of laminae thickness); mottled colors typical for standing water environment. The Late Pleistocene age of that lacustrine sedimentation is stratigraphically evidenced by the Mikulino (Eemian) interglacial paleopedofeatures on the eroded surface of underlying Moscow glacial till and several organic-rich layers (paleosol humus horizons, peat, gyttja and plant debris lenses) in the lacustrine sequence dated to the Mikulino (MIS5) interglacial and Middle Valdai (Middle Weichselian) interstadial (MIS3).

– Despite certain lithological variability observed between cores and sections, particularly those located at different elevations and in varying paleogeomorphic positions, general structural organization and textural composition of lacustrine stratum commonly exhibit evident alternation through time reflecting the same lithodynamic (and, possibly climatic) signals. Those can, therefore, be considered typical and most common sedimentary sequences of the Late Pleistocene at the Borisoglebsk Upland. This conclusion is certainly novel in contrast with most of the previously published models of the dominantly subaerial polygenetic origin of mantle loams.

– The observed lacustrine sediments of the Late Pleistocene age systematically occur both on all studied interfluve surfaces below 190 m and in buried parts of the fluvial network. Its thickness is comparable or, at places, even exceeds local relative elevations. It means that the lacustrine sedimentation was the main and yet underestimated agent of the Late Pleistocene topography transformation in the study area.

Stop 3. MANTLE LOAMS AND POSTGLACIAL PEDOGENESIS OF BORISOGLEBSK UPLAND INTERFLUVES
August 27, 2023, afternoon

An archetypal constitution of the soil body. The soil pattern is described in accordance with IUSS Working Group WRB (2022). At the key area, all studied soils formed in thick composite postglacial loams generally represented by colluvial, loess-like, and lacustrine deposits (Garankina et al., 2022). A representative thickness varies from 2–5 m on flat hilltops, its shoulders, backslopes, and footslopes whereas on toeslopes as well as in semi-closed and partially or completely drained depressions it reaches up to 20 m. Extremely high lateral variability of the postglacial loams provides considerable spatial heterogeneity of parent material and complexity of the soil cover. *Glossic Retisols Loamic* is a natural archetype for the entire soil cover of interfluves, slopes, and depressions. Under the widespread crop fields, completely mixed light-gray to brownish-gray topsoil (plow layer, 0.20–0.45 m) with an abrupt lower boundary is due to the continuous millennia-long agricultural cultivation (Belyev et al., 2020). That reckons for applying the *Plaggic* principal qualifier to the long-term cultivated *Glossic Retisol* patterns (Fig. 3.1a). Under the pristine forests limited in area, a thick (0.4–0.5 m) completely bioturbated grayish-brown humus horizon caused by continuous windfalls and uprooting of the topsoil (Fig. 3.4) is immanent for the soil pattern. Natural and agrogenic soil patterns without evidence of soil truncation include the required group of *in situ* eluvial (EL) and subeluvial (BEL) horizons in generally silty topsoil. Its lower boundary ordinarily lays 0.35–0.45 to 0.50–0.75 m deep. Down to 3.0–3.5 m below the topsoil, a sequence of loamy and clayey layers represents illuvial "textural" (BT) horizons. They are distinguished by a distinct set of intrinsic pedofeatures: structural organization (architecture of peds), the morphology of plane, tube, and vesicular pores, and a complex of silt and clay coatings on ped and pore surfaces. That specific morphology suggests applying a *Profondic* supplementary qualifier for the majority of soil patterns.

The silty topsoil with a representative depth of 0.45 to 0.75 m and loamy "textural" horizons distinctly differ in clay content. That requires distinguishing the fabric texture supplementary qualifier as *Episiltic* for the topsoil and *Katoloamic* for deep soil horizons both applying the *Differentic* qualifier. Therefore, an archetype soil body of the entire key area could be described as *Glossic (Plaggic) Retisol Episiltic Katoloamic Cutanic Differentic Profondic Tonguic* (Fig. 3.4).

Disturbances of soil bodies and deviations of soil evolution model during the Holocene. Soil patterns with different disturbances in soil body constitution strongly prevail in the soil cover of the entire study area except for only the flattest hilltops. On slopes of any inclination, the disturbances are constrained by erosive contacts and highlighted by loamy or silty infills. However, neither prompt and deep truncation nor thick sedimentary burial are found except on the steep sides and knickpoints in gullies or in technogenic excavations and ground constructions. Distinct buried erosive contacts related to single runoff episodes and/or continuous erosion trends are revealed both in topsoil and deep textural (BT) horizons (Fig. 3.2). Yet modern erosion does not affect the sequence of BT horizons forming a surface well-resistant to slope runoff. Accumulative episodes usually closely follow the erosive ones manifesting in the redeposition of topsoil material into stratified pedosediments. That engages applying the *Solimovic* qualifier to the entire slope soil patterns. It is determined as a heterogeneous mixture of material that has moved downslope being suspended in water. It is dominated by the material that underwent soil formation at its original location.

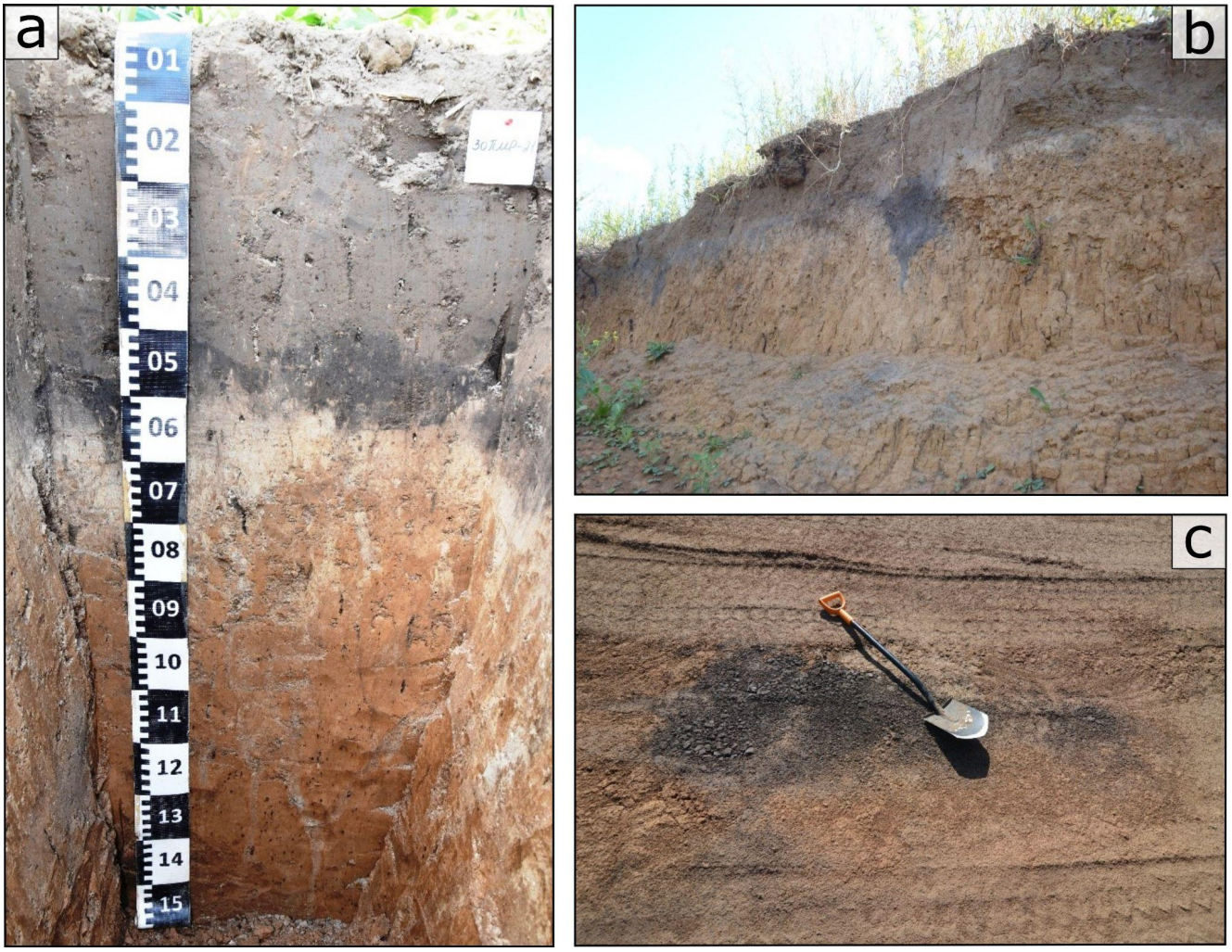

Figure 3.1. Soils with relict humus horizon (RHH): a) an archetype of the soil cover – *Glossic Plaggic Retisol Episiltic Katoloamic*; b) V-shaped infill of RHH in loess-like deposits; c) same, horizontal cross-section.

Slope soil patterns, especially in footslope and toeslope positions, have a specific architecture of "textural" thickness expressed in the set of BT horizons both with *in situ* (polygonal system of plane pores – desiccation cracks, silt and clay cutans on ped and pore surfaces) and *ex situ* (clay papules, lenticular structure) pedofeatures. *Sensu stricto*, they are products of alternating shallow slopewash erosion and subsequent deposition of pedosediment. Eventually, they become parent material for the next stage of *Luvisol* formation. Due to the lack of relict cryomorphic features, on the one hand, and the Late Atlantic ^{14}C age of the overlying relict humus horizon, on the other, the Early Holocene age of those BT horizons associated with erosive-accumulative episodes could be argued (Fig. 3.2a,b). Thus, we propose a specific polycyclic model of the Early Holocene pedogenesis. On slopes, soil bodies also contain multiple evidence of swidden agriculture implying the initial burn-beating of pristine forests at least during the early medieval times with a subsequent shift to crop-and-fallow rotation applying slash-and-burn technology (Fig. 3.2c,d). Slope soil patterns, especially in footslope and toeslope positions, could be regarded as the Holocene paleoarchives of natural and human-induced erosive-accumulative episodes either local or widely spread in the study area.

Relict pre-Holocene pedofeatures. Paleocryogenic disturbances of parent material are widespread in the study area, even in the upper 1 m of the soil body (Fig. 3.3). That obligates applying the *Relictiturbic* supplementary qualifier.

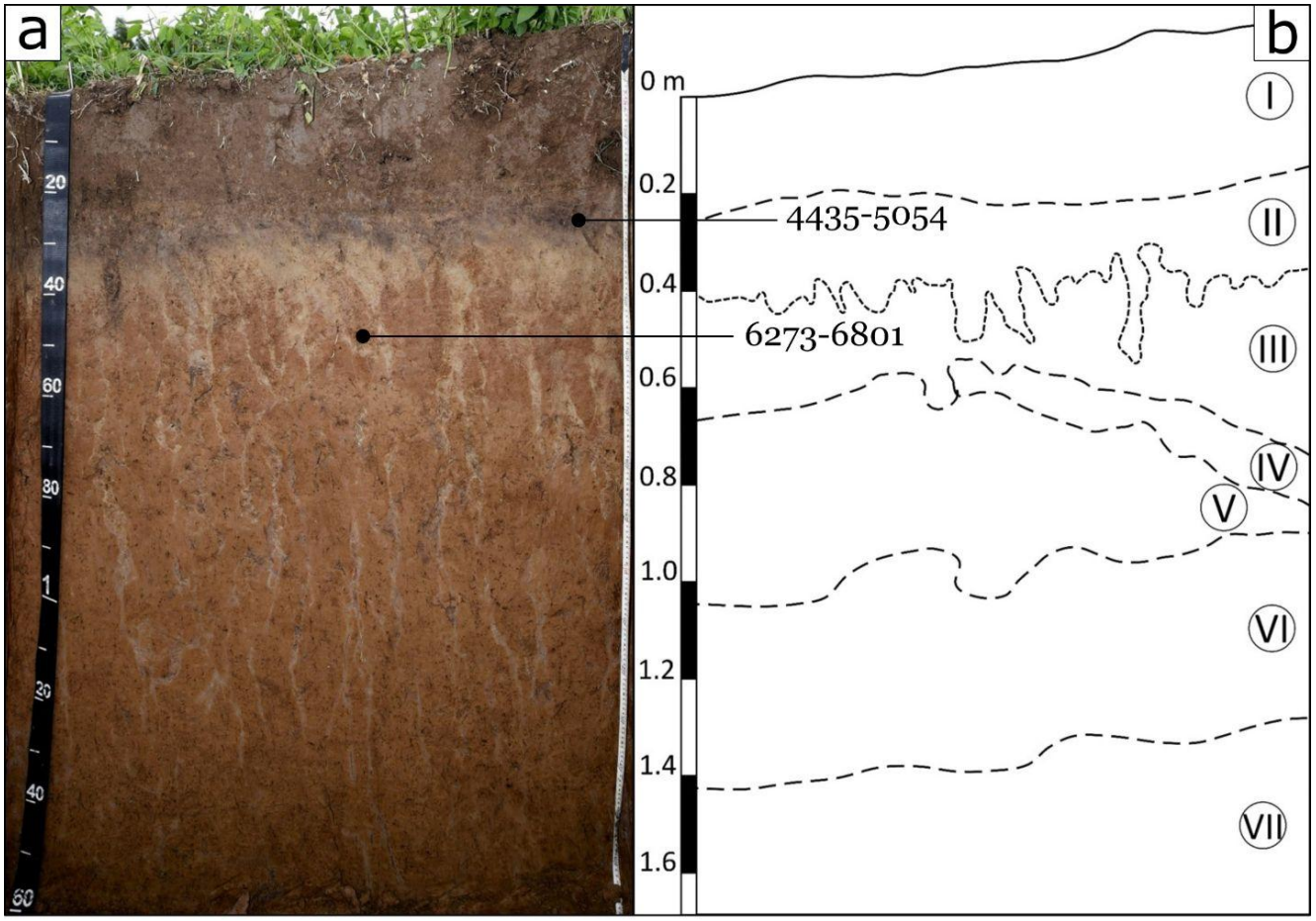
a
b
0 m
0.2
0.4
0.6
0.8
1.0
1.2
1.4
1.6
4435-5054
6273-6801
I
II
III
IV
V
VI
VII

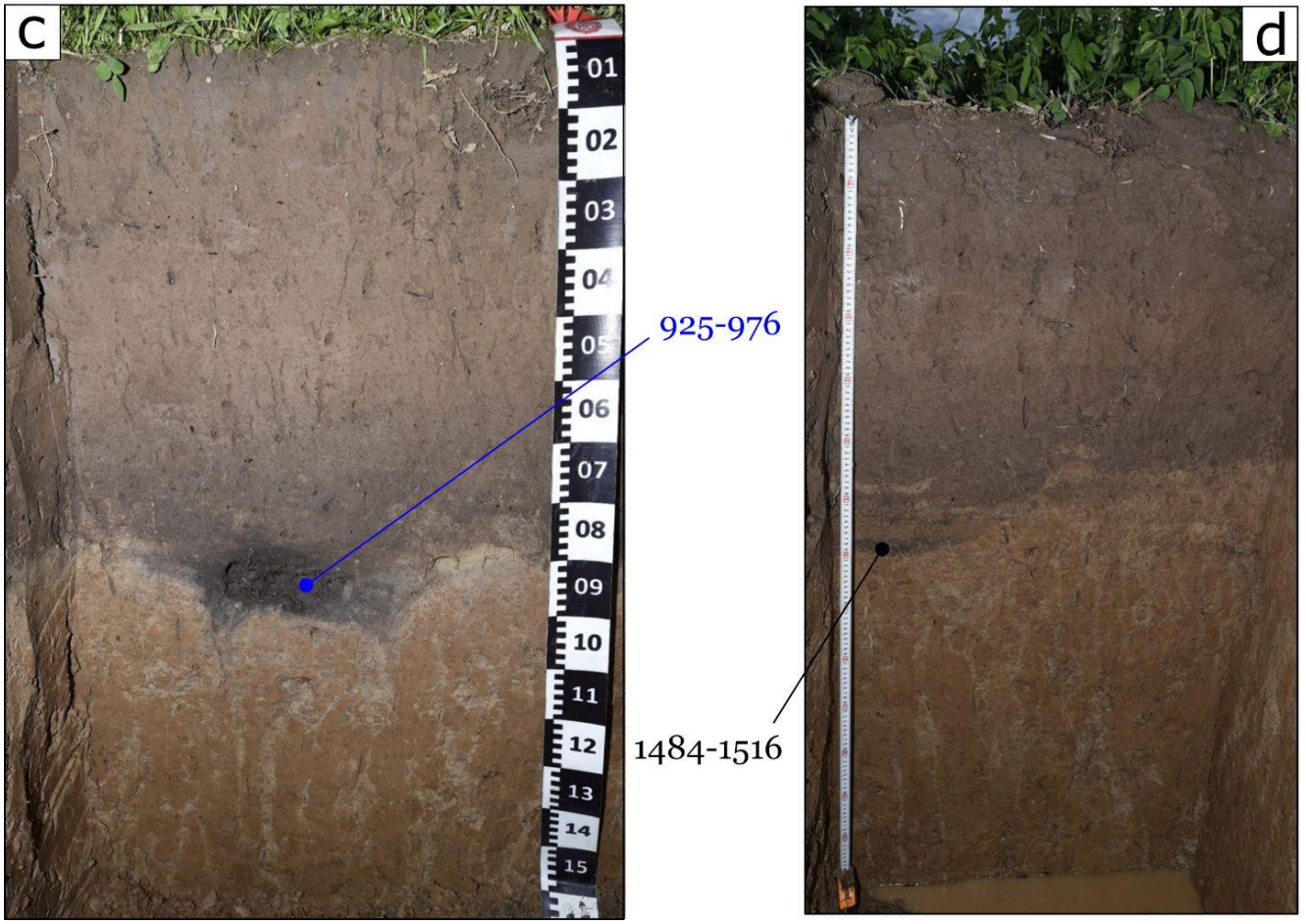
c
d
925-976
1484-1516

Figure 3.2. Soils on footslopes and toeslopes at the E Borisoglebsk Upland. Numbers represent ^{14}C dates: LSC (black, total organic carbon) and AMS (blue, birch charcoal). Dates were calibrated using IntCal20 calibration curve, the numeric range represents 2σ interval of the higher probability. Dates are used as temporal benchmarks "not earlier than … cal yrs BP". a–b) PE12 pit, vertical cross-section, toeslope position: a) Note a set of sharp contacts in brownish loams expressed both by the abrupt changes in color hue, value, and chroma and horizoning of desiccation cracks. Also note the dated RHH morphons in eluvial and subeluvial horizons; b) sketch of lithological heterogeneity: I – plow layer (P) with minor (agro) colluvial accumulation on the right; II and III – initially homogenous light-red silty pedosediment later, during Subboreal and Subathlantic, pedogenically altered into the light-gray silt of the eluvial horizon (EL, II) penetrating along the desiccation plane pores into the light-red structural metamorphic horizon (BM, III); IV – light-pinkish-brown loamy pedosediment; V – light-reddish-brown loamy pedosediment comprising the second subsurface horizon of desiccation cracks (BT1); VI – dull pinkish-brown loamy pedosediment with 3rd subsurface horizon of desiccation cracks (BT2); VII – dull reddish-brown loamy pedosediments with 4th subsurface horizon of desiccation cracks and redoximorphic pedofeatures (BT3g) (*Inclinistagnic* supplementary qualifier); c) F11 pit, vertical cross-section, toeslope position. Thick (up to 0.8 m) stratified (agro) colluvium topsoil overlies a dark lens of *in situ* charcoal-rich humified loam that evidences the burn-beating of a single birch tree under slash-and-burn cultivation at the early Medieval ages. Note the sharp contact between light-red loamy silt and light-brown silty loam at 1.10–1.15 m emphasized by the abrupt change of desiccation cracks morphology; d) PE11 pit, vertical cross-section, footslope position. Thick (up to 0.7 m) stratified (agro) colluvium with charcoal-rich loamy infill of the erosional trough at the base. Note a set of four BT horizons below the distinct erosional contact at 0.65–0.80 m contrastingly differing both by the morphology of plane pores and color, texture, and compaction of the lithomatrix.

Gleyic pedofeatures certainly related to the Holocene pedogenesis are traced exceptionally in the soil bodies of the pronounced depressions with recurrent water pools at the bottom. All other *gleyic* pedofeatures such as bluish and greenish hues are considered the Late Pleistocene relicts. Even in dry loams, concentrations of *gleyic* features are constrained by boundaries of the Late and Middle Valdai sedimentary units of lacustrine, solifluction, and eolian origin.

Contrastingly, in better-drained geomorphic positions, there is multiple evidence of buried polygonal plane pore systems of frost crack origin in the pre-Holocene parent material. Also, rare finds of pedogenic carbonates, which are relict pedofeatures of the Late and Middle Valdai loess-like and lacustrine sediments, indicate their former exposition to automorphic paleopedogenic alteration.

Relict humus horizons (RHH) are generally formed below the surface humus horizon (AY) or plow layer (P) in noncarbonate loams inside silty eluvial (EL), subeluvial (BEL) and upper "textural" (BT) horizons as gray, dark-gray to almost black-colored subhorizontal lenses, subvertical wedge infills or fragmentary patches (Fig. 3.1). Those are frequently confined to the actual and buried shallow microdepressions related to the paleocryogenic topography (Velichko et al., 1996; Alifanov, 1995; Makeev, 2012, etc.). According to the fine-scale soil mapping, the participation of those soils in the soil cover varies between 3 and 5%. Despite the controversial genetic and age interpretation of the phenomenon, we distinguish the Younger Dryas, Atlantic, Late Atlantic, Subboreal, and Early Subatlantic stages of RHH formation.

π-pedone key site. The key site represents a complex organization of parent material on the flat top of Poklony Hill elevated 212 m a.s.l. We argue the pre-Holocene origin of the entire set of sedimentary units, vertical cryostructures, and contact alterations along them (Fig. 3.3). During the Holocene, there is no clear evidence of any disturbance of the soil body except for the well-mixed topsoil developed by continuous forest windfalls and uprooting. Thereby we propose a full-Holocene evolution model of pedogenesis from the day surface. Nevertheless, a detailed investigation applying the hierarchical morphological approach (Targulian et al., 1974) revealed the peculiar strict compliance between the morphological criteria of "textural" BT horizons and lithological heterogeneity (Fig. 3.4) constrained

by the boundaries of sedimentary units (BT1, B2, BT6), contact alterations of host units along the cryostructure (BT3, BT4) and the cryostructure infill itself (BT5).

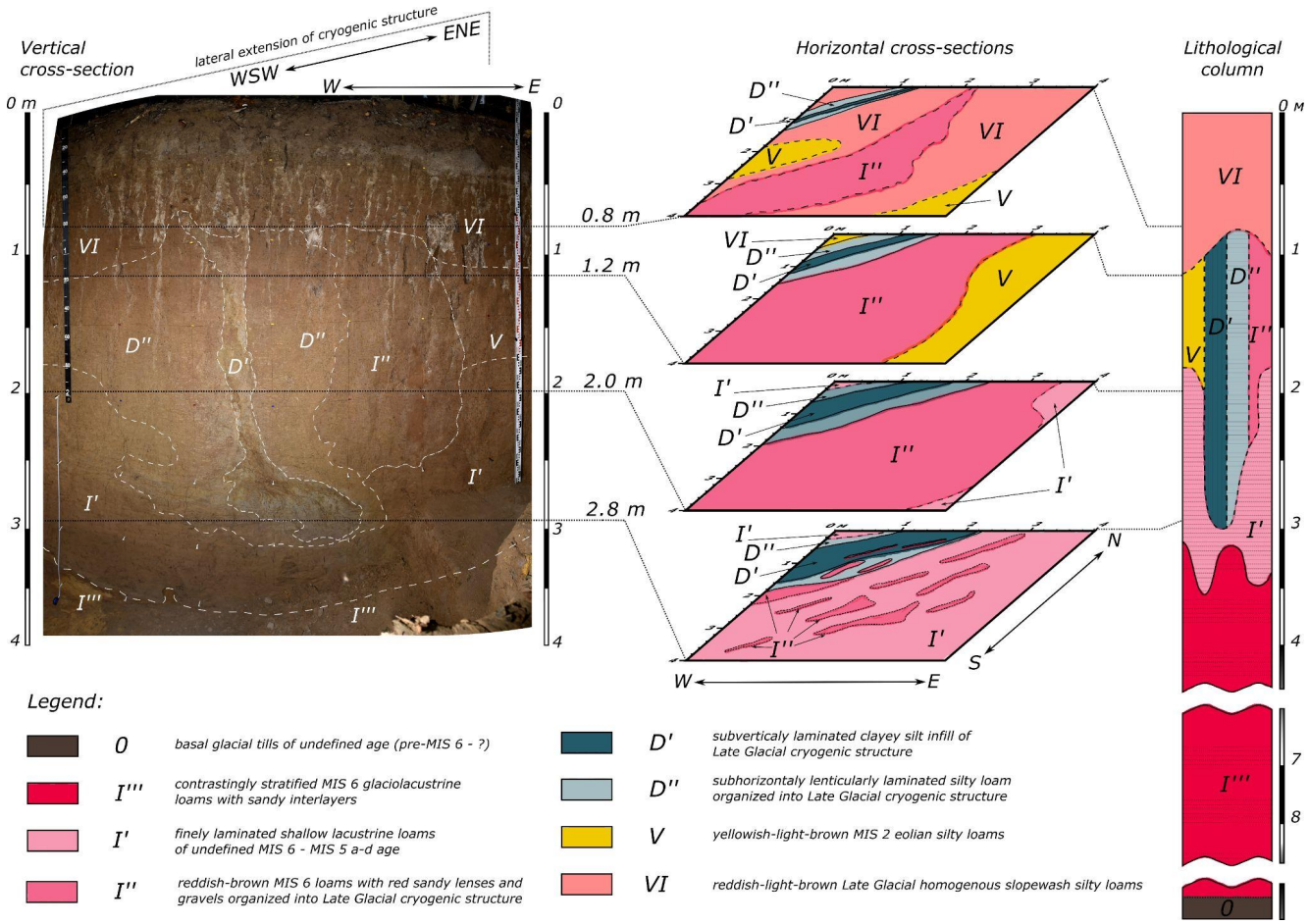

Figure 3.3. Sod-podzolic soil (*Glossic Retisol*) on the flat hilltop under pristine forest – π-pedone key site. Complex lithological organization of parent material – interfluvial mantle loams.

Direct instrumental dating of palimpsest paleoarchives such as soils is generally considered irrelevant due to the multiple superpositions of polychronous pedofeatures. Nevertheless, a detailed morphological investigation, in the frame of the hierarchical approach, allows employing the ^{14}C dating using the AMS technology with high spatial precision for the first time. The zone of contact alteration of host sediments along the cryostructure (Fig. 3.4, [D``] in BT4 "textural" horizon) has a composite lithomatrix hosting "guest" morphons (Fig. 3.5): bluish-light-gray silt patches (morphon 3, Fig. 3.5b) and specific pedofeatures – papules (morphon 4, Fig. 3.5e). That lithomatrix is split by plane pores filled with clay cutans (morphons 1 & 2, Fig. 3.5b,c,d). The age of the papule (morphon 4) is 15953–16265 cal yrs BP, which is significantly older than the age of bluish morphon 3 (12708–12752 cal yrs BP).

The former age corresponds to the Last Deglaciation time reported to be accompanied by the Trubchevsk pedogenesis (Rusakov et al., 2015). Simultaneously buried polygonal system of frost cracks with dark-gray clay infills was revealed in the host yellowish-light-brown silty loams (Fig. 3.3, unit [V], Fig. 3.4, BT2 "textural" horizon) tentatively of the MIS2 eolian origin (Garankina et al., 2022). Thereby, we suffice to guess that the Holocene soil body encompasses at least, one prominent paleosol body of the Last Deglaciation that could be attributed to the Trubchevsk geosol. The fragments of pedofeatures of that age along the vertical cryostructure suggest the later cryogenic disruption of that prominent *Luvisol*-like body.

On the other hand, the age of morphon 3, also included in the lithomatrix, rather correlates with the onset of the Younger Dryas cooling or the very end of Allerod warming. Hence the timing of the prominent superimposed cryostructure disturbing the entire volume of lithomatrix has probably even younger age. As the Younger Dryas was the last possible cryochrone in the study area we assign the formation of the cryostructure to that temporal frame. Although the origin of the slightly younger morphon 3 remains hidden either related to the Allerod organic matter accumulation or an unknown rejuvenation mechanism of the Younger Dryas cryogenesis.

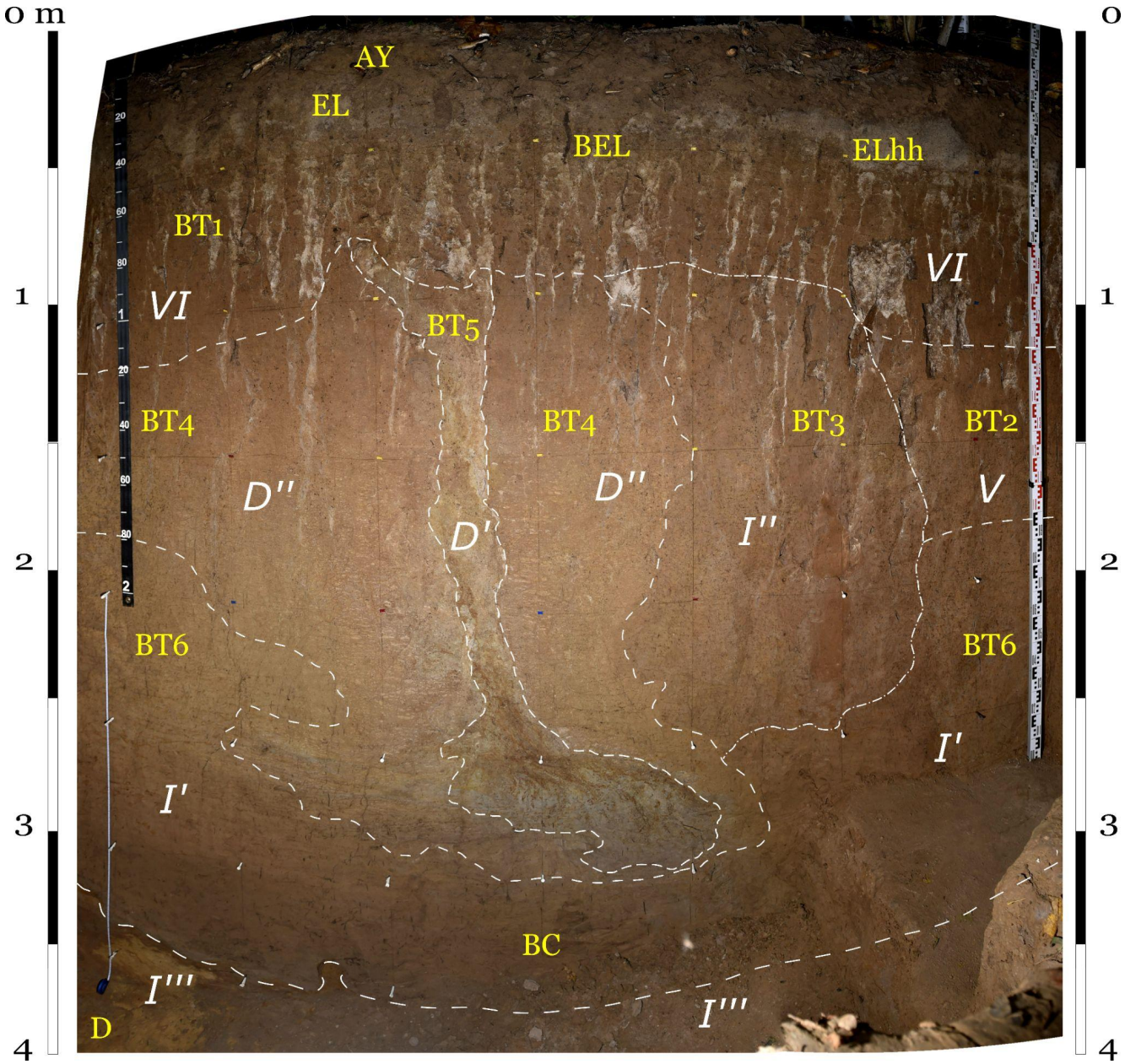

Figure 3.4. π-pedone key site: *Glossic Retisol Episiltic Katoloamic Cutanic Differentic Profondic Relictiturbic Tonguic*, subvertical cross-section. *[I`], [I``], [I```], [V], [D`], [D``],* and *[VI]* – lithological units, see Fig. 3.3. *AY* – thick grayish-brown humus horizon completely turbated by continuous forest windfalls and uprooting, *EL* – *in situ* eluvial horizon; *ELhh* – relict humic material inside the eluvial horizon; *BEL* – *in situ* subeluvial horizon; *BT1–BT6* – illuvial "textural" horizons. Note the general compliance of lithological contacts and soil horizons.

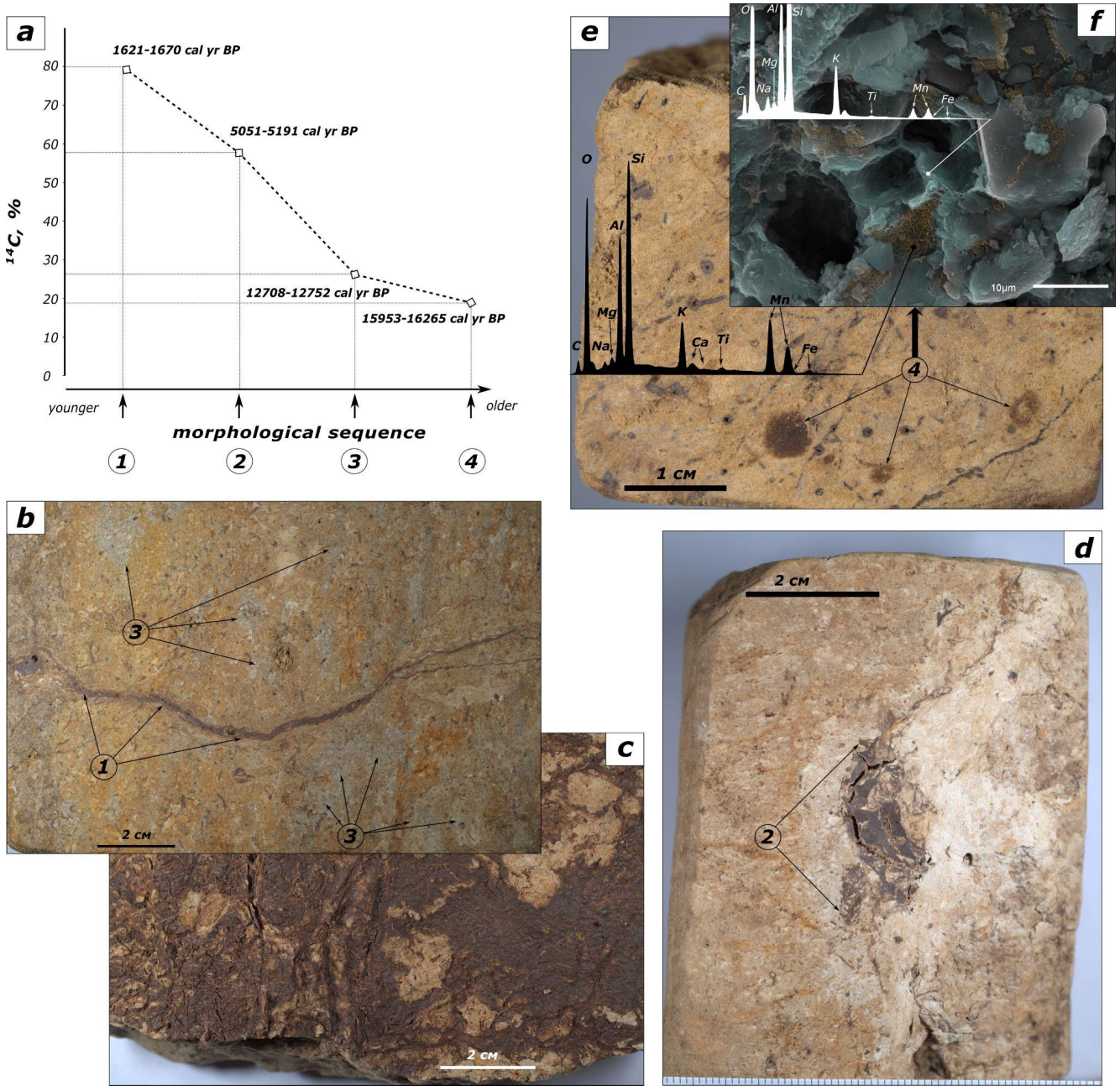

Figure 3.5. Combined hierarchical morphological and ^{14}C AMS investigation of palimpsest soil memory in the π-pedone key section: a) ^{14}C AMS ages of soil morphons in the periphery (unit [D`], see Figs. 3.3–3.4) of the Late Glacial cryostructure. *1* – brown clay cutans (subhorizontal cross-section in (b) and plane surface in (c); *2* – brown clay infillings in polygonal subvertical plane pores (b, c) and vesicular pores (d); *3* – blueish-light-gray phase of the enclosing mass; *4* – admixture of reddish-brown clay papules (e). f) false-color SEM image in secondary electrones of the papule structure.

***Sod-podzolic soil (Glossic Plaggic Retisol)* on the flat hilltop in frames of Late Pleistocene pedo-, cryo-, & lithostratigraphy (Pi5p key site).** The Pi5p key site discloses the complexity of the postglacial mantle loams in a shallow rounded microdepression at the flat top of the Poklony Hill at 210 m a.s.l. There is no clear evidence of any disturbance of the *Glossic Plaggic Retisol* body during the Holocene except for prominent mixing of the topsoil material by plowing accompanied by the upgrowth of a microgully and minor (agro) colluvial accumulation (Fig. 3.6a). Thus, it is clear to approximate soil formation by the full-Holocene evolution model of pedogenesis.


e
d
13164-13325
c
a
1
2
b

Figure 3.6. Pi5p key site (*Glossic Plaggic Retisol*), subvertical (SV) and subhorizontal (SH) cross-sections: a) SH cross-section at 0.47–0.53 m with the Pi5 borehole. Note the polygonal system of plane pores splitting the SV-oriented cryostructure with dark-gray loamy infill *(1)* and simultaneously cut by a microgully with mottled gray and brown silty infill *(2)*; b) SW wall with SH cross-section at 2.1–2.2 m; c) SW wall with SH cross-section at 2.5–2.6 m; d) SW wall with SH cross-section at 2.7–2.8 m and position of ^{14}C LSC date for total organic carbon of the dark humic material enriched with charcoal fragments at a depth of 1.90–2.05 m. Dates calibrated using the IntCal20 calibration curve, the numeric range represents 2σ interval with a higher probability; e) a fragment of SH cross-section at 2.1–2.2 m. Note the contrast SV lamination of the cryostructure infill with coarse fragments of charcoal.

Postglacial host sediments are represented by colluvial reddish-brown silty loam, eolian yellowish-brown silty loam, lacustrine bluish-light-gray sandy loam, and contrastingly laminated sandy loam with gravel of yet undefined origin. Various infills of several cryogenic structures occupy the prevailing volume of the pit.

Maksimovitsy Depression. Corona key site. Corona key site represents a local watershed of Maksimovitsy and Puzhbol streams (Fig. 3.7) with local gently sloping topography dominated by elevation of 165–175 m a.s.l. A relatively narrow (120–300 m) flat-topped slightly undulating ridge spreads eastwards from the footslope of a prominent Poklony hill. Several closed and semi-closed depressions 250–300 m in width surround the ridge, some being drained by shallow dry gullies tens of meters in width and 1–2 m deep.

Geotechnical development of the site during the 2020 summer exposed a complex structure of superficial sedimentary cover of a semi-closed depression in the west and its gentle slope and adjacent watershed in the east. The western part of the site was carved by trenches 5–7 m deep while the eastern one was exposed only in shallower trenches (1.5–3 m).

Despite postglacial deposits varying in thickness from 2.5–3.5 to 6 m (east to west), they display a reproducing sequence of eolian, colluvial, and lacustrine facies overlying the Late Moscow (MIS6) tills and glaciofluvial outwash. At least, eight host units can be distinguished (Table 3.1,Garankina et al., 2022).

The contact between reddish till rich in sand and debris (I) and light-gray lacustrine loams (II) is sharp and frequently undulating while the upper boundary of the latter is gently waving (Fig. 3.8). The upper part of II is reworked by short-distance mass-movement and cryogenic processes forming a unit of yellowish-gray loams III with ferruginous patches and laminae. The top of III is significantly truncated or completely eroded (Fig. 3.10). Its subsidences of up to 1.5 m are successively filled with colluvial brownish-gray to pinkish-brown clay loams [IV] and yellowish-brown loams [V] with steadily growing eolian component. A prominent overlying colluvial unit of reddish-brown silty loams [VI] gains thickness up to 1–1.2 m on gently inclined slopes (Fig. 3.9). Occasionally dark-gray RHH 5–20 cm thick are nested atop being best-preserved in local paleodepressions under thick (up to 1 m) lenses of stratified agrogenic colluvium [VII].

Those units host specific ***vertically oriented geological bodies*** commonly composed of silty loams and silts highly contrasting in color, texture, and fabric. Based on the shape of inclined side contacts we identified wedge casts and bulbous casts (Murton et al., 2000) (Fig. 3.13). Wedge casts propagate down from at least three depths (Table 3.1): casts [A] are buried under unit [VI]; casts [B] – under [V]; and casts [C] – under [IV]. Bulbous casts [D] are commonly associated with the roots of larger wedge casts [B] and [C] and propagate upwards from the lacustrine unit [II] up to [VI].

Wedge casts [C] run from the surface of redeposited lacustrine facies [III] or solifluction unit [IV] (Fig. 3.9c) penetrating down to the underlying till [I]. Filled with highly contrasting bluish-gray to reddish-light-brown silty to clay loams such casts are up to 2.5 m wide at the upper part and have gently sloping sides.

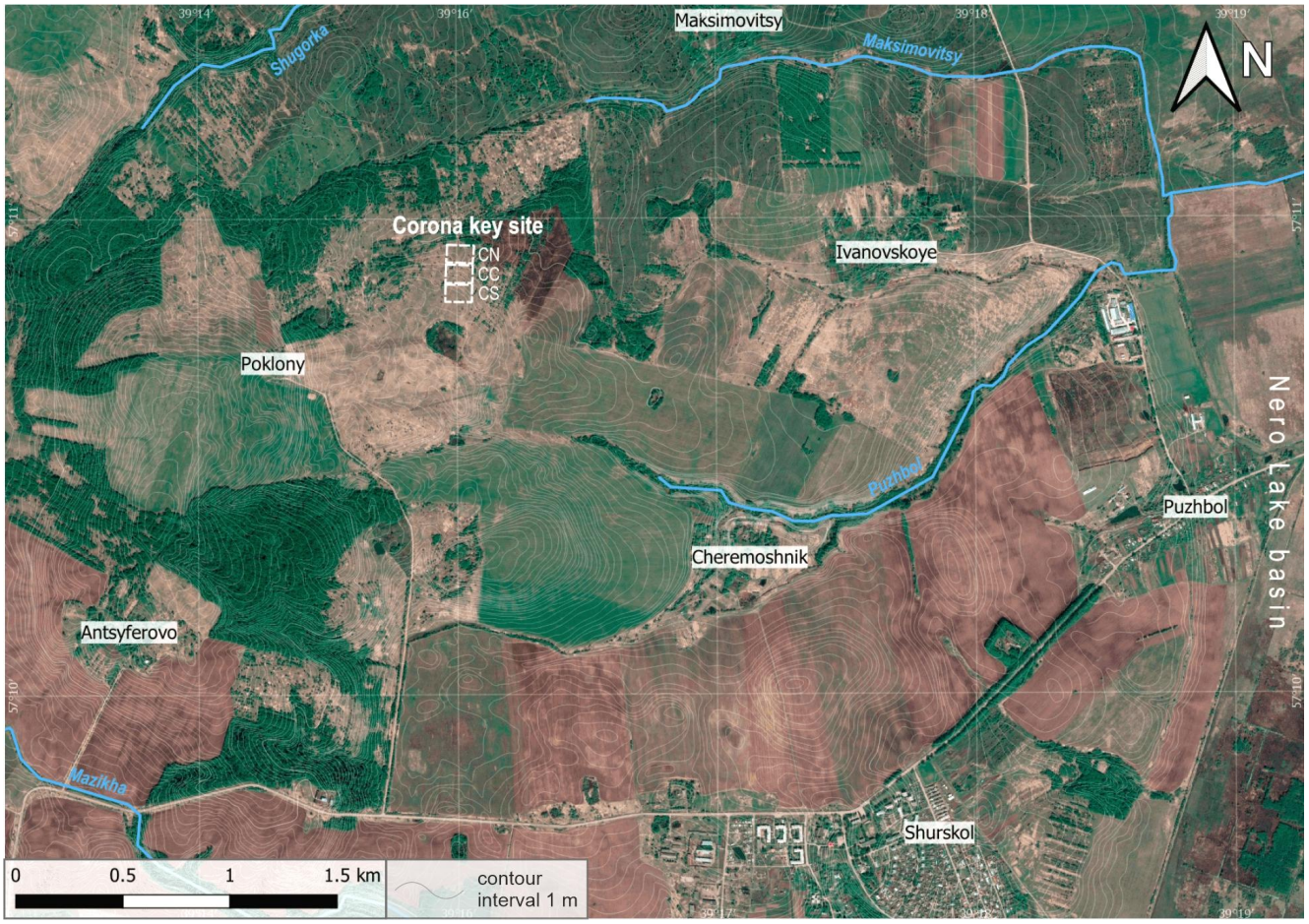

Figure 3.7. Location of the Corona key site (57.178°N, 39.260°E) (GeoEye-1 satellite image from 10.05.2019, Maxar Technologies, courtesy of Google Earth) with detailed topography based on land planning maps.

Most pronounced wedge casts [B] run in eolian [V], slope [III–IV] and lacustrine [II] loams of yellowish and grayish hue. Their infilling with high silt content, in contrast, has a dull light-reddish color (Fig. 3.9,e) and statistically higher values of apparent magnetic susceptibility (Fig. 3.9f). The width of casts [B] varies between 1–1.5 m at the top narrowing down to the first centimeters at the depth of 2.5–3.5 m (Fig. 3.9d) where they often intrude the older casts [C], thus, inheriting their spatial distribution (Fig. 3.9c).

The uppermost wedge casts [A] with dense organic-rich silty infilling have sharp angular lower contacts (Fig. 3.9a) with accommodating yellowish-brown loams [V]. Significantly truncated at the top, dark-gray casts [A``] less than 0.5 m in size are overlain by material [A`], re-deposited simultaneously with the accumulation of reddish-brown loams [VI]. They often recur under thick agrogenic slope lenses [VII] with RHH at its base (Fig. 3.9b) yet substantially differing from the latter in organic matter type and structure.

Bulbous casts [D], while nested in lacustrine deposits [II], resemble diapirs gradually narrowing upwards into thin contracted veins in [V] and even [VI] (Fig. 3.9a,). At depths of 1.4–2.3 m, they vary from 0.5 to 2 m in width being filled with vertically laminated bluish silts and silt loams noticeably gaining the clay portion downwards (Figs. 3.10 & 3.11a,b,c) .

Another type of casts commonly associated with the [D]-structures was found in the deeper sections of the Transhei key site. Yellowish casts [E] often are bound to the shallow lacustrine units having subvertical yet quite gradual contacts with abundant involutions completely disrupting the initial lake sediment structures (Figs. 3.10c, 3.11e, & 3.12).

Table 3.1. Sedimentary structure of the Corona key site

Host units	Occurrence	Depth, m min/max*	Lithology	Casts	Occurrence	Depth, m min/max*	Lithology
Plough layer	Cover layer with wavy contact	**0.0** **0.1–0.4**	**[VIII]** Grayish-brown – light yellowish-brown sandy loam with [VI] & [VII] admixture				
Agrogenic slope deposits	Thick (up to 0.9 m) wide (10 to 60 m) lenses, erosive concave contacts	**0.0–0.2** 0.2–0.9	**[VII]** Reversed lenticular sequence of redeposited soil horizons: basal dark-brown organic-rich loam, light-gray to light-yellow silty loam & brown to grayish-brown loam	**[RHH]** Relict humus horizon	Thin (5–20 cm) lenses 2–20 m wide, tonguing base, truncated top	**0.2–0.9** 0.4–1.2	**[RHH]** Dark-gray organic-rich (Ah) with light yellowish-gray (EL) fine-plated loose loam with lenticular lamination
Colluvial deposits	Thick (0.5–1.2 m) lenses tens of m wide, erosive base	**0.2–1.0** 0.4–1.5	**[VI]** Reddish-brown silt loam, compacted downwards, with scattered thin inclined lenses of light-gray silt	**[A]** Dark wedge casts	Lenses 0.3–0.7 m thick & 0.4–2 m wide, concave erosive base	**0.2–0.9** 1.0–1.3	**[A`]** Dull gray to brown-gray organic-rich dense loam, wavy lenticular oblique contrast lamination
Eolian deposits	0.6–1 m thick layer, erosive contacts	**0.2–1.5** 1.1–2.0	**[V]** Yellowish-brown loam to silt loam with thin to thick lenticular-reticulate contrast structure & dark lithified vertical rootlets at the lower contact		Lenses 0.1–0.4 m in size, sharp angular sides	**0.4–1.2** 0.8–1.3	**[A``]** Dark-gray organic-rich fine-sandy silt with inclined to vertical lenticular contrast lamination
				[B] Silty wedge casts	Lenses 1–1.5 m wide & up to 3 m deep, sharp steep to vertical sides	**0.4–1.6** 1.2–3.2	**[B`]** Dull yellowish-red patchy to lenticular non-contrast loam silt to sandy loam **[B``]** Dull light-red loam silt to fine-sandy loam with reticulate-lenticular & lenticular inclined contrast structure
Soli-fluction deposits	Lenses 0.9–1.2 m thick & 2–10 m wide, conformable base & truncated top	**0.6–2.0** 1.0–2.6	**[IV]** Mottled brownish-gray to pinkish-brown silt to clay loam with large wavy non-contrast lamination & superimposed horizontal medium wavy lamination emphasised by ferruginization	**[C]** Loamy wedge casts	Lenses >0.5–1 m deep & 1–2.5 m wide, visible to sharp inclined lower contacts	**0.8–1.8** 1.9–2.1	**[C`]** Patchy dull reddish-brown & gray loam to clay loam sometimes with superimposed lenticular to layered structure **[C``]** Dull reddish-light-brown & bluish-light-gray silty loam with large light-yellow silt lenses
Shallow lake deposits	Lenses 0.2–0.9 m thick, truncated top, conform base	**1.0–2.2** 2.0–2.6	**[III]** Yellowish-light-gray silt to clay loam with gently inclined wavy to planar layered to reticulate non-contrast structure & Liesegang				
	Layer 0.5–0.8 m thick, truncated top	**2.0–2.6** 2.5–3.2	**[II]** Light-blueish-gray non-stratified clay loam with large contrast reddish-yellow lithified ferruginous rootlets & plant remains	**[D]** Silty bulbous casts	Vertical lenses 0.5–1.3 m deep & 0.05–1 m wide, wavy sides	**0.4–2.0** 1.4–2.3	Bluish light-gray loam silt **[D`]** to silt **[D``]** with horizontal light-grayish silty lenses & vertical brownish stratification
Glacial till	Basal layer, sharp undulating top	**2.9–5.0** ...	**[I]** Brownish-red dense silt loam with coarse & medium sand lenses, gravel, pebble&boulder	**[E]** Silty wedge casts	Vertical lenses 2–3.5 m deep & 0.2–18 m wide, wavy sides	**2.5–4.0** 4.5–5.5	Yellowish silt loams **[E`]** and yellowish-gray clay loams **[E``]**, vertically stratified or largely turbared

**Depth min/max – depth of the upper and lower contacts of a unit or a cast*

Figure 3.8. Host geological units of the Corona key site: a) general stratigraphic sequence; b–c) structural organization of reddish-light-brown silt loams [VI]; d) contact of yellowish-light-brown silt loams [V] and loams [IV] highlighted by rootlets with soft organic infilling; e) contrast lenticular structure of yellowish-light-brown silt loams [V] (limon à doublets); f) wavy (A=10–15 cm, P=20–30 cm) structure of loams [IV] with superimposed low-contrast patchiness; g) contact of loams [IV] with clay loams [III] emphasized by ferrugination; h–i) shallow lake deposits with dense ferruginized rootlet networks. Distinguished host units are given by numbers, see Table 3.1 for the description and interpretation.

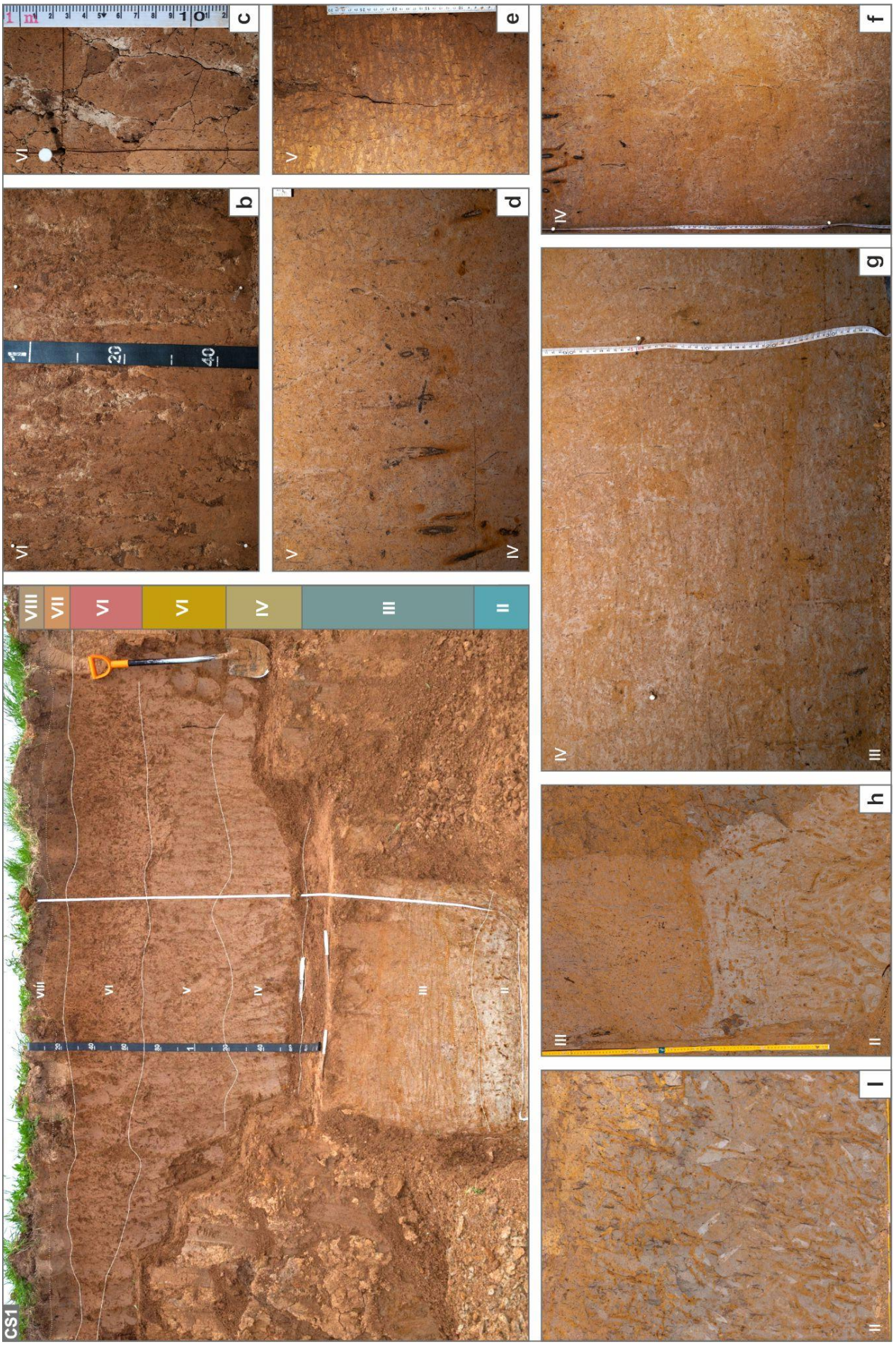
a
b
c
d
e
f
g
h
i
CS1
VIII
VII
VI
V
IV
III
II

Those casts occasionally have a typical narrow wedge shape at the lower part (Fig. 3.12f), however, sometimes extending up to 20 m laterally (Fig. 3.12a). Their interrelations with the [D]-casts are still under debate as is their age and formation mechanism requiring quite pronounced amplitudes of seasonal freeze-thaw cycles concerning both the temperatures and the influenced depth of the active layer.

DISCUSSION

The lateral distancing of the wedge cast [B] axes exposed in vertical sections and trench floors (Fig. 3.1) decreases from 15–25 to 7–10 m northward. If smaller polygons mostly have a rectangular shape then the larger ones are a combination of triangle and rectangular cells. It could be accounted for by the differences in drainage, as higher liquid-water content is one of the major factors of the contraction cracking frequency and shape. Dark lenses strongly gravitate to the widening of shallow dry gullies in the lower reaches but there is no clear relation between the courses of either buried or modern linear depressions with the polygonal network distribution.

Amplitudes of the Late Pleistocene paleotopographies used to be much higher compared to the smoothed modern one (Fig. 3.14). The initial glacial depression experienced an episode of significant reworking or even erosion prior to being infilled with shallow lacustrine deposits [II]. The highest elevation difference (of up to 1.5 m in latitudinal cross-section) was acquired upon its partial colluvial redeposition followed by linear erosion, which resulted in the highly variable thickness of unit [III]. Due to the proceeding colluvial infilling of depression, a consistent slope sedimentary sequence [IV–VI] pronouncedly reduced its height undulations. Another incision-infill cycle of lower amplitudes (up to 0.5–0.7 m) is reflected by the increased thickness of agrogenic pedosediments [VII] occasionally with contrast dark RHH lenses at the base. Such small buried linear depression 10–30 m wide extends northward in the central part of the southern trench (Fig. 3.15), further reaching the main shallow dry gully (Fig. 3.15). The modern topography does not inherit that paleolandform; on the contrary, two narrow (5–10 m) furrows run across it, downhill towards the NE.

Based on the analysis of spatial distribution and depth propagation of vertical lithostructures in superficial deposits of the NE Borisoglebsk Upland, four generations of buried casts were distinguished at its upper part, representing promising stratigraphic references for the Late Valdai (MIS2) sedimentary sequence. From the Late Pleniglacial to Late Glacial the type of cryogenesis shifted: from wide wedges with significant initial ice content against yet sufficient water saturation of sediments during the onset of LGM; through narrower yet deeper composite wedges in dryer settings of the Late Glacial onset; to relatively small earth wedges during the severe short Younger Dryas cooling.

The best-preserved silty wedge casts [B] of presumably Oldest Dryas age inherit the older pseudomorphs of the LGM ice wedges [C] while the distribution of the Younger Dryas casts [A] rich in dark organic matter is limited either by a discontinuous formation of the initial cryogenic network in lesser drained geomorphic settings or intensified erosion upon its burial.

Certain bulbous casts propagating from the underlying lacustrine deposits [II] to the uppermost colluvial unit [VI] are spatially associated with the roots of composite wedge casts [B]. That points to its younger age and certain cryogenic nature. It could have resulted either from progressive thermokarst with superimposed differential frost heaving during final permafrost degradation or more likely be related to the Younger Dryas frost cracking and earth wedge formation but of rather larger scale – reflecting the distribution of the hundred-meter polygonal wedge network of much deeper propagation than casts [A].

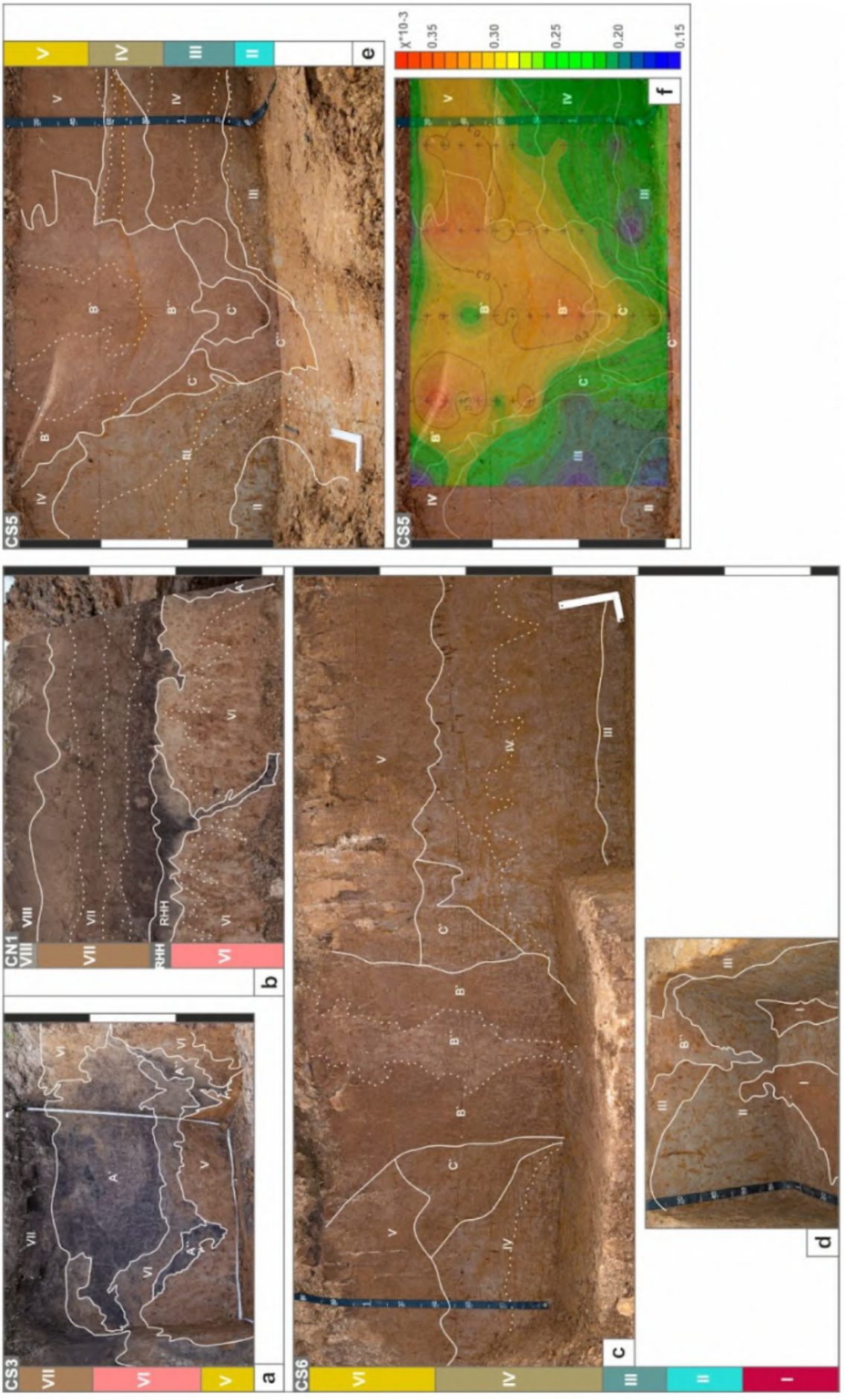

Figure 3.9. Vertical cross-sections of wedge casts in the sedimentary sequence of the Corona key site (Garankina et al., 2022): a) dark wedge cast [A``], in the upper part filled with unconsolidated polymictic deposits with inclusions of charcoal [A`]; b) agrogenic slope deposits [VII] burying the [RHH] lens; c) wedge cast [B] penetrates yellowish-brown colluvium [V] inheriting an older cast [C] that propagates from under [V]; d) protrusion of wedge cast [B] into the underlying shallow lake deposits [II] and glacial till [I]; e) wedge casts [B] inheriting wedge cast [C]. Note the amplitude of unit [III] upper contact on both sides of the cast; f) superimposed variations of apparent magnetic susceptibility (10^{-3} SI) reflect the higher values of silty infilling of the casts.

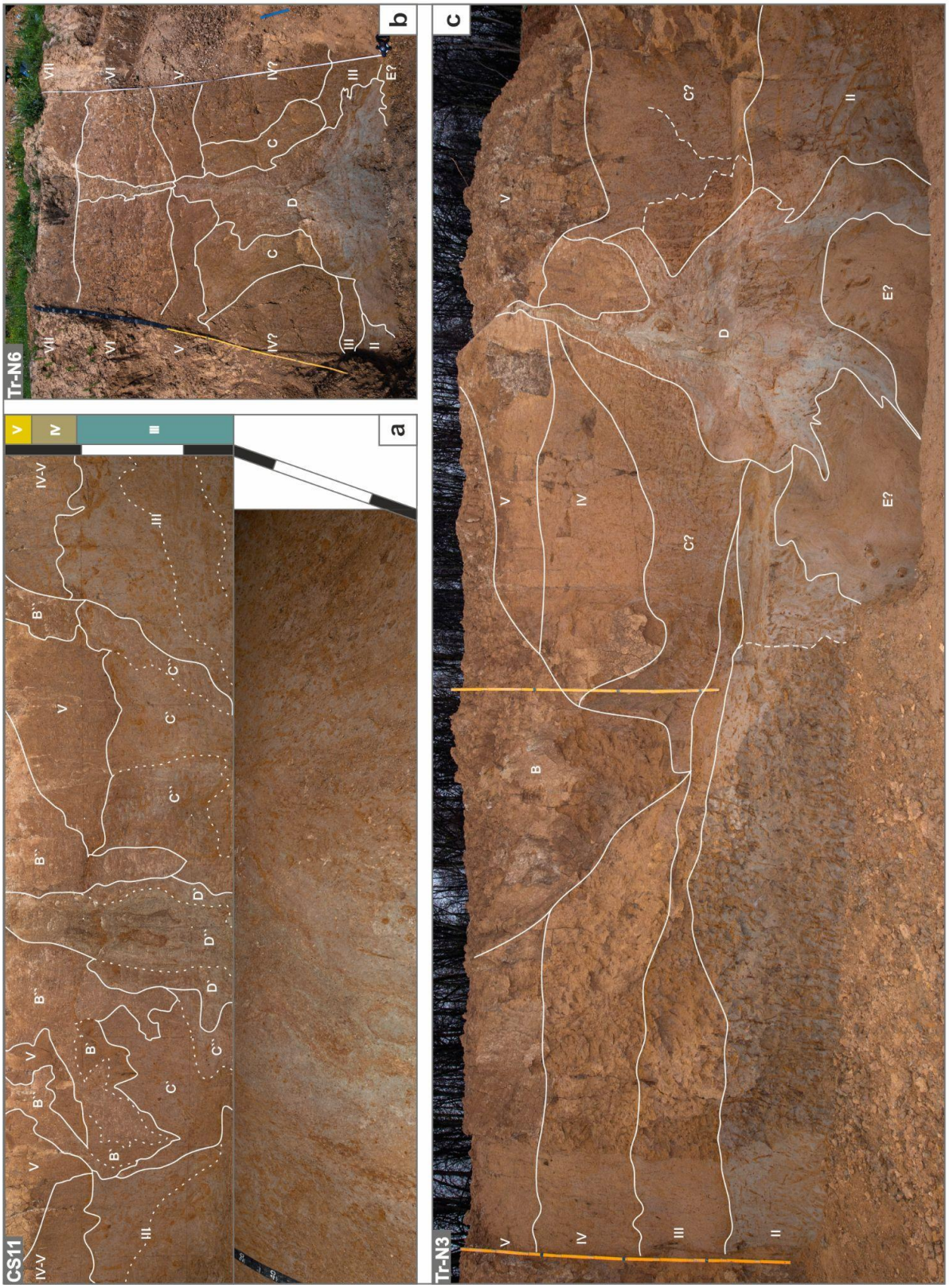

Figure 3.10. a) Vertical cross-section of bulbous cast associated with roots of wedge casts [B] and [C] and traced in the adjacent trench floor, Corona key site. Note the vertical lamination of the "bulbs" and large lenticular structures in adjacent deposits; b–c) large bulbous casts nested in lacustrine deposits narrow upwards – in the colluvial stratum up to silty loams [V] and [VI], Transhei key site. Note the specific involutions highlighted by ferrugination at the fringe-like lower contact of bulbous cast erasing the initial structures in lacustrine sediments [II] in (c).

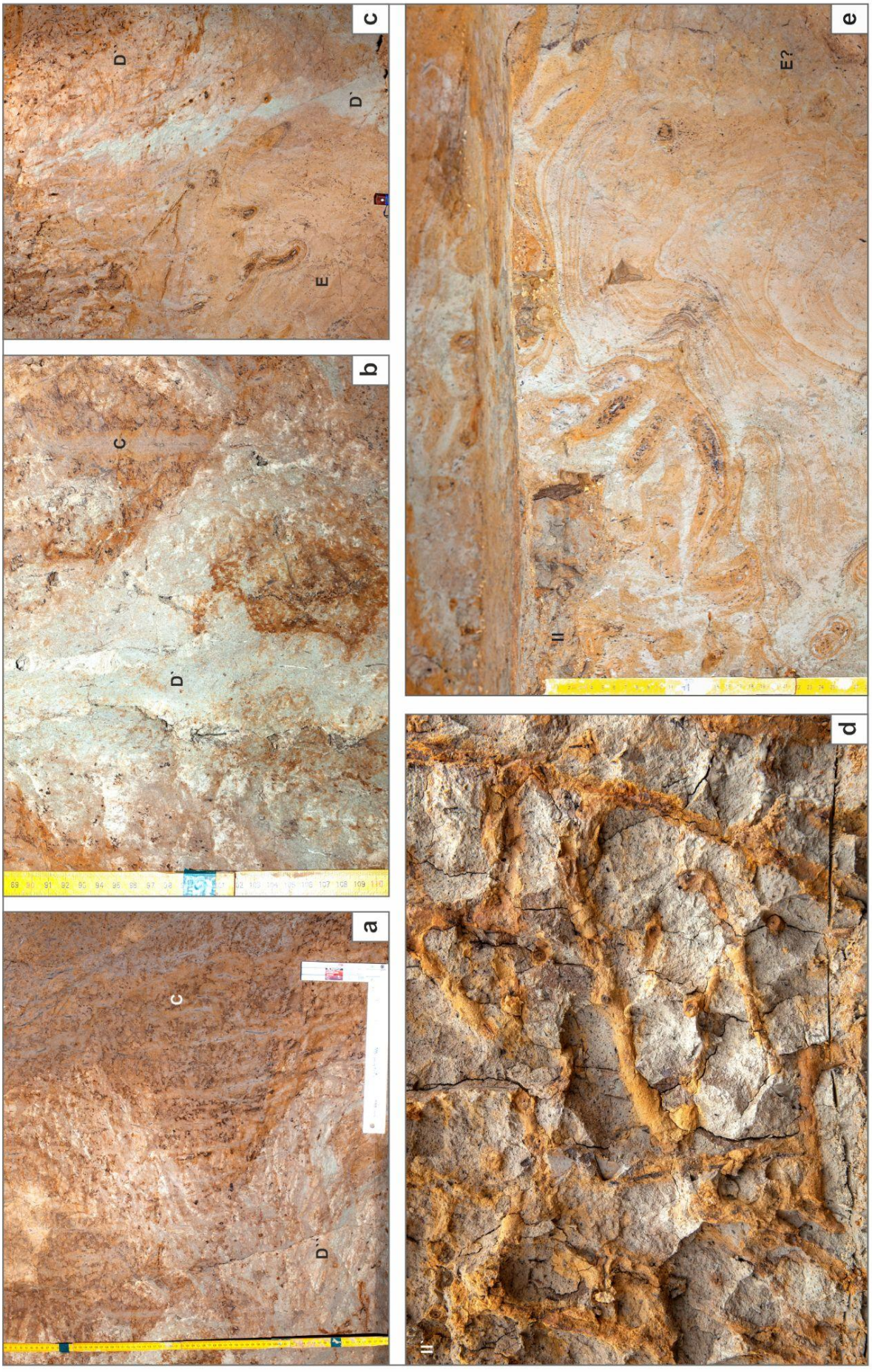

Figure 3.11. Details of the lithological organization of structures [D] (a,b,c) and transformations to the adjacent host lacustrine units [II]: d) ferruginized rootlets of shallow-water plants and e) its disturbance by plastic involutions up to entire disruption of the initial sedimentary structures. Transhei key site.

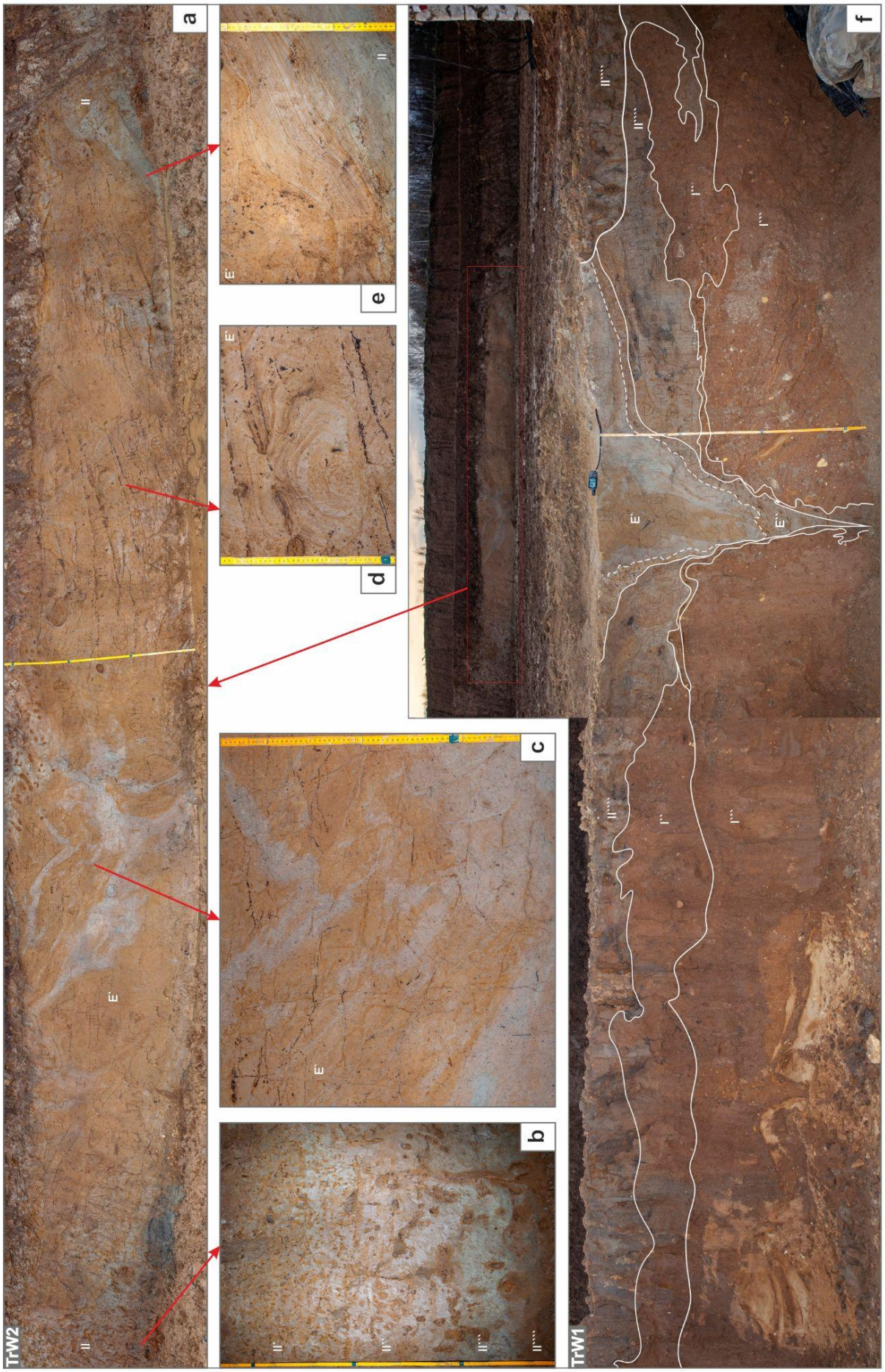

Figure 3.12. Cryogenic wedge casts [E] and associated phenomena: a) large lenticular extension (up to 20 m) of yellowish porous loams with oblique fine lamination (e), involutions (d), and superimposed post-cryogenic reticulate structure (c, d); (b) shows the sequence of finely-laminated lacustrine loams with several erosional surfaces, accommodating the above-mentioned wedge casts; f) narrow tip of the cryogenic wedge penetrating the glacial base.

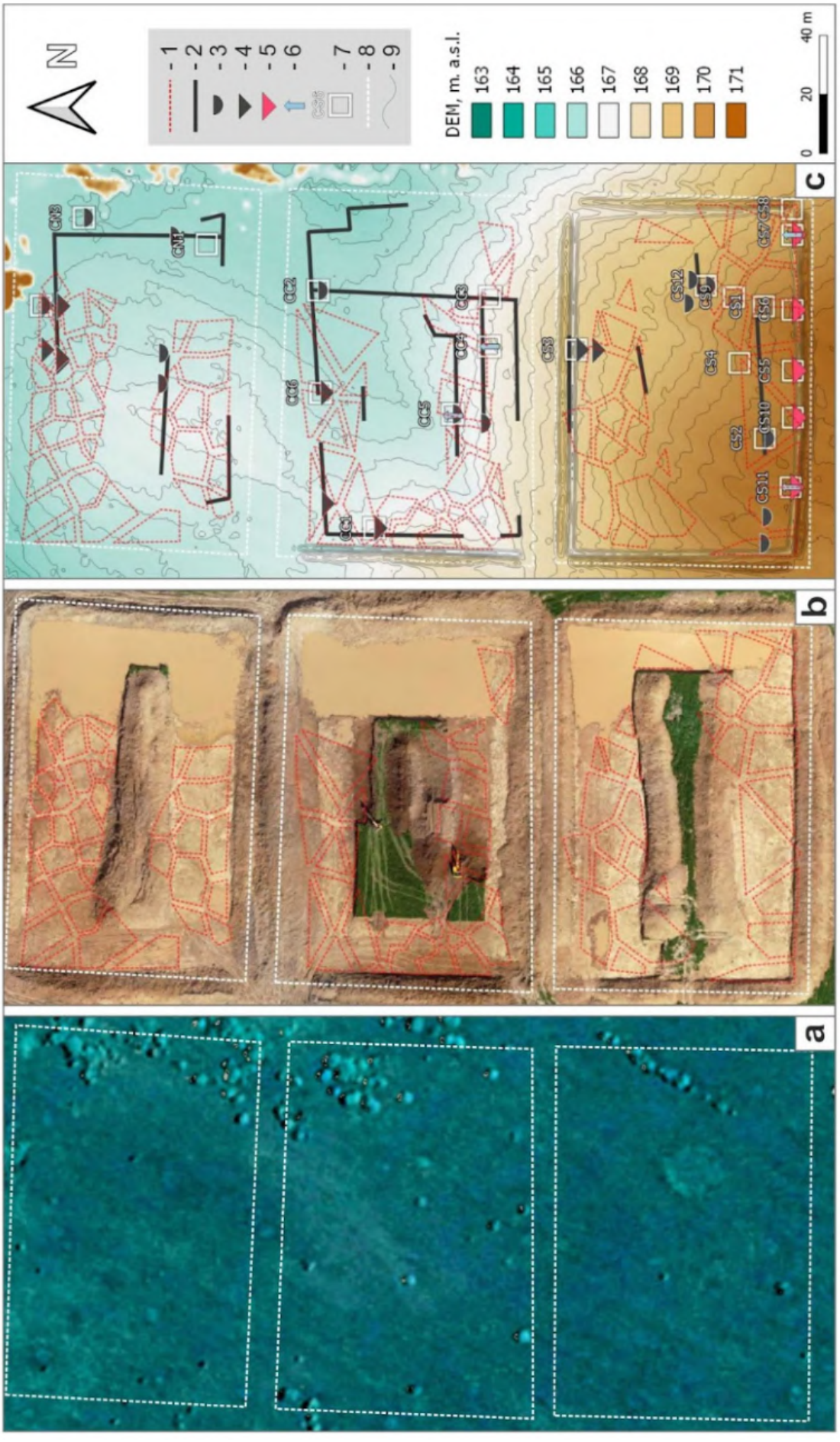

Figure 3.13. Relict permafrost features of the Corona key site combined with geodetic positions of cross-sections (after Garankina et al., 2022): a) satellite image Pleiades-1A from 03.06.2015 (CNES/Airbus, courtesy of Google Earth); b) UAV ortho mosaic (15.06.2020); c) UAV-derived DEM (02.05.2020). *1* – polygonal pattern exposed in the trench floor; *2* – relict humus horizon [RHH] found in trench walls; *3* – dark lenses [A`]; *4* – dark wedge casts [A``]; *5* – reddish wedge casts [B]; *6* – bulbous casts [D]; *7* – cross-sections; *8* – trench borders; *9* – contour lines with 0.25 m interval.

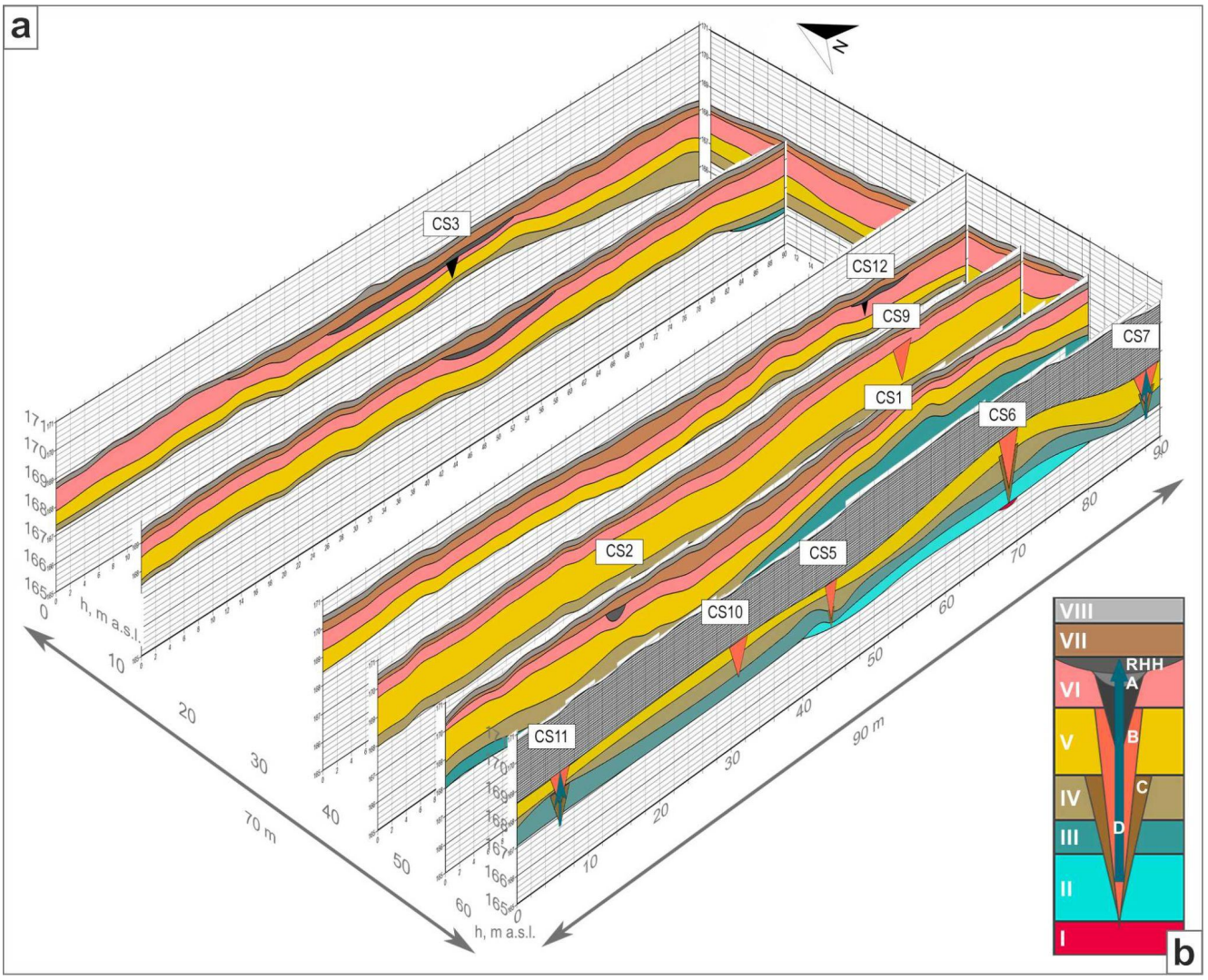

Figure 3.14. Pseudo-perspective 3D model of the geological structure at the CS trench (a) and generalized stratigraphic column of the key site (b) (see Table 3.1 for referencing) (Garankina et al., 2022). Note the top surface of [III] indicates a paleotopography of higher amplitudes (up to 1.5 m) buried and gradually leveled by the eolian and slope sequence [IV–VI]. The late incision-infill cycle of lower amplitudes (up to 0.5–0.7 m) is constrained by [RHH] or concave parts of [VII] at the base, with its top truncated by plowing.

Episodes of intensified incision followed by the colluvial infill were revealed prior to the Late Pleniglacial, then during the short Late Glacial interstadials and lately in the Early Holocene, repeatedly occurring along the inherited partially filled linear depressions. The later major hillslope erosion coincided with the onset of slash-and-burn cultivation since the Early Mediaeval Ages, which led to the simultaneous infill of pre-existing linear depressions with thick agrogenic colluvium. In-between those transformations, the second part of the Holocene was marked by landscape stabilization reflected in pronounced pedogenesis. The latest low-amplitude human-induced incision has been triggered by the intensified plowing in the mid-XX century inheriting the ancient spatial pattern.

Prevailed low-rate accumulation trend and low geomorphic connectivity of the study area provided good preservation of the repeatedly buried cryogenic casts in the watershed sedimentary cover. However, that aimed at the considerable smoothing of its exterior in the modern landscape. Thus, regular polygonal patterns representing the LGM and Late Glacial relicts are still reflected in the low-contrast patchy soil and vegetation cover of the arable fields yet are almost erased in the actual topography.

Figure 3.15. Generalized geological structure of the Corona key site (Garankina et al., 2022): a) pseudo-perspective 3D model; b–d) lower reaches of the shallow dry gully with well-defined RHH and dark wedge casts [A``] at the base; e–f) its upper reaches and sides with less prominent infilling; g) the most autonomous watershed position with the almost non-truncated sequence of host units. *1* – a larger incision crossing the central part of the site. Incised in [VI], its paleosurface is fixed by pre-arable RHH and substantially filled with agrogenic pedosediments [VII], modernly manifesting as a very smooth and shallow dry gully; *2* – a modern smaller incision into the agrogenic colluvium [VII] triggered by the intensified plowing in the mid-XX century.

MOSCOW LANDSCAPES OF UPPER VOLGA RIVER VALLEY AND BORISOGLEBSK UPLAND, AND THEIR TRANSFORMATION DURING THE LAST INTERGLACIAL-GLACIAL CYCLE

August 28–29, 2023

Glacial tills form an important landscape component within the area of Moscow (MIS6) Cryochrone. On the western slopes of the Borisoglebsk upland, they cover the uplands and slopes within the elevation range of 127–180 m a.s.l. In Kalyazin district, they also mantle bedrock terraces on the right bank of the Volga River within 117–127 m a.s.l. The glacial till is often covered only with a thin cover layer (30–50 cm on average) of veneers of sands, sandy loams, or silty loams so that surface soils (*Retisols*) are formed in the bipartite sediments: The upper soil horizons (O, Ah, AhE, E, AB, Bw, BF, 2BC) are formed in the cover layer, while the lower horizons (2Bt1–2Bt3, 2BC, 2C) are formed in the glacial till. Within the Nerl-Volga Lowland, ground moraine is presented as chains of isolated hills parallel to river valleys. Hills elevated to 135–150 m a.s.l. have gentle slightly dissected slopes while the local water base is at 108–109 m a.s.l. During MIS5a–5d (110–70 ka), MIS4 (70–35 ka), and MIS2 (24–10 ka) periods, the territory was a part of the periglacial zone of the Valday glaciation (Velichko, 1973; Gerasimov & Velichko, 1982; Kaplin, 2005; Sudakova, 2008).

The study area is characterized by a moderately humid climate with a 1 to 4 °C mean annual temperature and 550 to 650 mm mean annual precipitation with a ratio of precipitation to evapotranspiration of 1.5 (Nesmelova et al., 2007). According to the soil-ecological zonation of Russia (Shishov et al., 2001), the study area belongs to the central parts of the Middle Russian province dominated by *Retisols* (IUSS Working Group WRB, 2022), which developed as a component of southern taiga ecosystems.

Soils in bipartite sediments will be demonstrated on the bedrock terraces of the Volga River (Selishi key site), and on the top of moraine hills (Porechie key site, 145 m a.s.l., and Novoselky key site, 180 m a.s.l., Fig. F).

Two-day field tour will focus on the following issues:

– the morphology, age, and origin of the Upper Volga River valley;

– the spatial distribution of bipartite sediments on terraces and moraine uplands;

– the age of the glacial till.

– was the Moscow glacier the last in the area?

– lithic discontinuity is an indicator of the degree of post-depositional transformation of moraine uplands. Can we talk about the "secondary" moraine plains?

– long-term pedogenesis: do we have soil properties of the Last Interglacial in soils formed in the bipartite sediments?

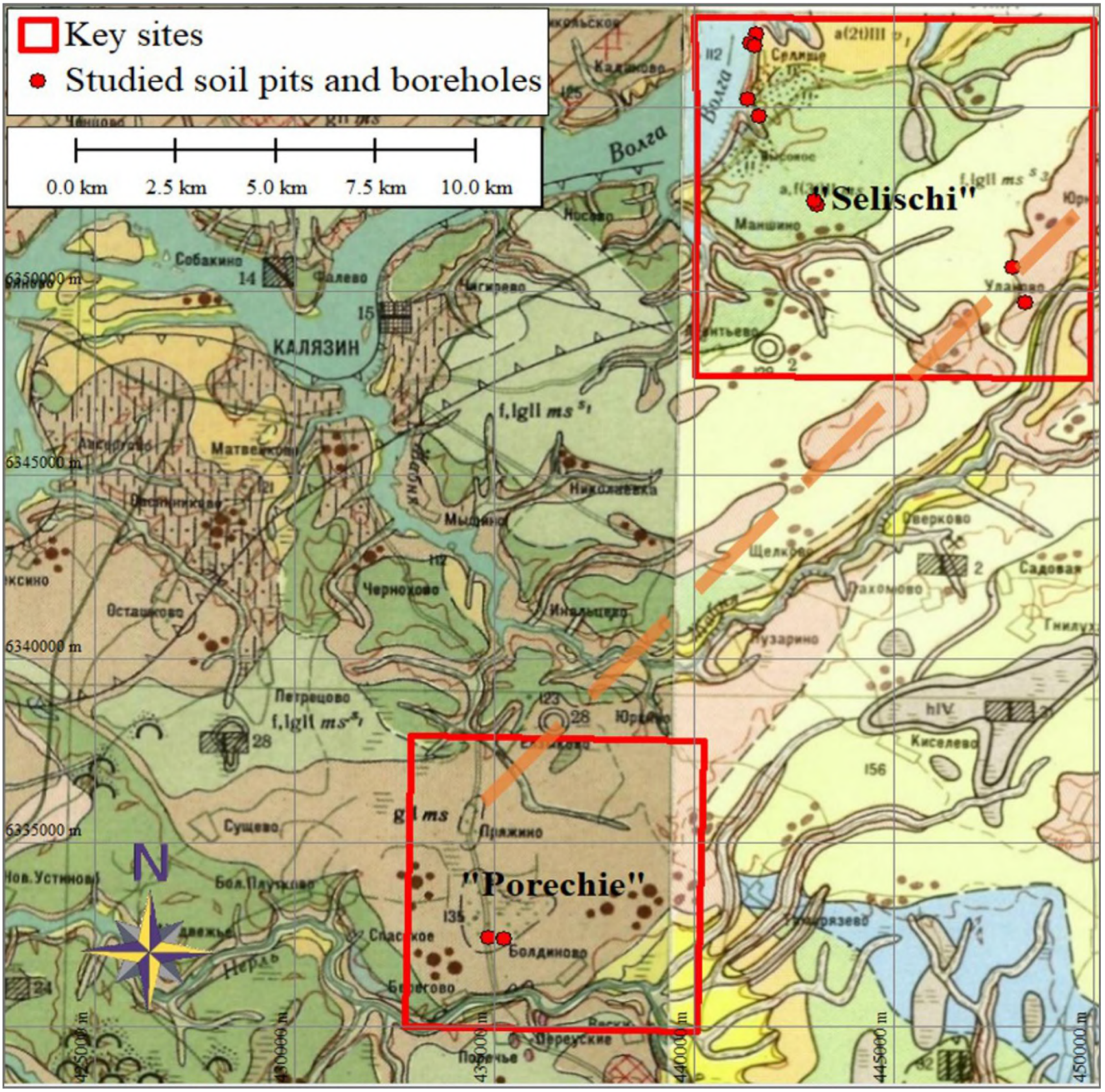

Figure F. Fragments of State geological map of USSR. Quaternary deposits, 1:200000. O-37-XXVI, 1967 and O-37-XXVII, 1969. Selishi and Porechie key sites are shown by *red rectangles*.
gIIms – glacial till, Moscow time; *f,lgIIms*^{1} – glaciofluvial deposits of glacial retreat, undistinguished, Moscow time; *os,kamIIms* – glaciofluvial deposits of eskers and kames, Moscow time; *f,lgIIms*^{s1} – glaciofluvial deposits of the early stages of glacial retreat, Moscow time; *f,lgIIms*^{s2} – glaciofluvial deposits of the late stages of glacial retreat, Moscow time; *a,f(3t)IIms* – fluvial and glaciofluvial deposits of the 3rd terrace, Moscow time; *a(2t)IIIv*$_{1}$ – fluvial deposits of the 2nd terrace, Early Valday time; *a,l IV* – floodplain deposits, Holocene.
Dashed orange line marks the Moscow hilly moraine ridge.

STOP 4. BEDROCK TERRACES ON THE RIGHT BANK OF VOLGA RIVER AND ASSOCIATED SOILSCAPES
August 28, 2023, morning

Selishi key site is located on the right bank of the Volga River ~14 km east of Kalyazin city. According to the State geological map of USSR (O-37-XXVII. 1969, Fig. F), three terraces of different ages (late Moscow, and Lower Valdai) and origins are designated within the river valley. The key site covers two terraces and reaches the upland, which is represented by moraine ridge of the Moscow age.

The exposure of the river bank, a part of the Uglich water reservoir, is located at 117 m a.s.l., 5 m above the present water table (Selishi-1 profile, 57.32569° N, 36.02571° E). The surface is a part of the 2nd terrace (117–122 m a.s.l.) elevated 14–19 m above the original water table (103–104 m a.s.l.) according to the map of flooded areas (Map of Volgostroy, 1933).

Field morphology and micromorphology of Selishi-1 exposure

The exposure exhibits glacial till that reaches the water table at 4.5 m (Fig. 4.1). It is presented by a red-brown (10 YR 4/6) massive matrix-supported unsorted diamicton that is typical for the central part of the Moscow glaciated area (Lavrushin, 1976). The lower part of glacial till is enriched in dark clay material of the underlying Jurassic deposits (sometimes deformed bodies). The till is covered by a thin cover layer of 45–50 cm. The soil formed in bipartite sediments is *Glossic Folic Albic Retisol (abruptic, loamic, cutanic, densic)*.

The content of gravels, pebbles, and stones of crystalline rocks varies considerably in soil horizons formed in the glacial till, which is typical for glacial diamicton. Coarse debris is present in an array of various rocks (granites, limestones, breccia, etc.) of different shapes, orientations, and weathering degree. Rotational structures filled with deformed material captured by the glacier are common (Fig. 4.1). Carbonate fragments are found in the 2Bt1 horizon; however, the total mass shows effervescence only from a depth of 110 cm. Concave sandy interlayers about 2 m long and 2–3 cm thick, gradually wedging out into the cover layer, mark the roof of the glacial diamicton (Fig. 4.2). The glacial till is characterized by high birefringence and porphyritic texture with a mixture of coarse grains of various sizes and roundness (Fig. 4.4d). Granostriated b-fabrics common for the glacial till are probably associated with swelling due to wetting when the ice and sediment melt. The structure is well developed in soil horizons formed in the glacial till (Fig. 4.3). The 2Bt horizons have a strong angular and subangular blocky structure ranging from fine to coarse downward. Down to 80–90 cm, the blocks are combined with plates that increase in thickness with depth (Fig. 4.3a). The sub-horizontal faces of the plates are covered by dark-brown reticulate coatings. The blocky structure is also incorporated with prismatic units. The latter become dominant below 100 cm where blocky and platy units cease. The size of prisms increases downward, and prism faces are tilted towards each other forming angular vertices.

In the 2Bt horizons, there are multi-layered complex coatings (Fig. 4.4d), roots and void channel infillings (Fig. 4.4a), and reticulate coatings on subhorizontal faces. Clay cutans may fill root channels completely. Below the 2Bt3 horizon, prism faces are uniformly covered by thin brown coatings. Thick clay cutans are dominant on the faces of trans-horizon cracks that partly follow the prism faces below the 2Bt3 horizon. In the 2Bt1 and 2Bt2 horizons, abundant white powder covers the ped faces upon clay cutans.

The cover layer is represented by sandy deposits with a large number of stones and pebbles. Sand and coarse silt grains are moderately sorted and rounded (Fig. 4.4a). The contact zone of the cover layer and glacial till is sharp and abrupt, which is well seen both on macro- and micro-levels (Figs. 2, 3, & 4.4b). It is complicated by numerous wedges.

Table 4.1. Field morphology of the "Selishi-1" exposure, 117 m a.s.l. (*Glossic Folic Albic Retisol (abruptic, loamic, cutanic, densic)*

Horizon (IUSS..., 2022)	Depth, cm	Color of general matrix (wet)	Coatings	Color of coatings (wet)	Gleyic features	Fe-Mn concr.	Structure	Carbonates	Rock fragments (stones, pebbles)	Roots amount	Horizon boundary		Consistence (moist)	Porosity
											Form	Transition		
O	0–4	5YR 2.5/2	–	–	–	–	–	N	–	abun dant	smooth	abrupt	VFR	high
Ah	4–9	10 YR 3/2	–	–	–	–	WE, FM- SB	N	–	abun dant	wavy	clear	VFR	low
AhC	9–25(27)	10 YR 4,5/6	–	–	–	–	WE, MC-SB	N	FM-C	rare	wavy	clear	VFR	low
C	25(27)–40(73)	7 YR 5/5	–	–	–	–	SG	N	FM-C + MC-F	very few	irregular	abrupt	FR	low
2Bt1/C	40–73	5YR 4/4	thin-C (P, C), thick-F (PV, SA)	5YR 4/3 7 YR 5/5	–	–	MS, FM- SA	N	FM-C + MC-C + CS-C	*	smooth	gradual	FR to FI	high
2Bt1	73–94	5 YR 4/4	thin-C (P, C), thick-F (PV, CH)	5YR 4/3 10 YR 3/2	–	–	WE, ME- PR → WM, MC-PL→ MS, VM-SN	N	FM-F + MC-V	*	smooth	gradual	FI	high
2Bt2	94–139	5 YR 4/4.5	thin-C (P, C), thick-F (PV, CH)	5YR 4/3 10 YR 3/2	–	Fine-F	WE, MC- PR → WM, MC-PL→ MS, VM-SN	+ from 110 cm	FM-C + MC-C + CS-C	*	smooth	gradual	FI	high
2Bt3	139–187	7,5 YR 4/4	thin-F (P, C), thick-F (PV, CH)	5YR 4/3 10 YR 3/2	–	–	WE, MC- PR → MS, MC-SA	+	M-C + MC-C + CS-F	*	smooth	gradual	FI	medium
2Bt4	187–244	7,5 YR 4/4	thin-V (P, C), thick-F (PV, CH)	5 YR 4/3	–	–	MS, CV-PR→ MS, MC-SA	+	FM-C + MC-C	*	smooth	gradual	FI	medium
2BC	244–280...	7,5 YR 4/4	thick-F (PV, CH)	5 YR 4/2	–	–	MS, CV-PR	+	FM-C + MC-C + CS-F	–	–	–	EFI	low

* Indexes are based on FAO guide for soil description (Jahn et al., 2006) with modifications. **Coatings**: "*thickness-abundance (location)";* thickness: very thin (<0.2), thin (0.2 – 0.5), medium (0.5 – 1), thick>1; abundance: table 64 (p. 55), location: table 68 (p. 56). **Mottlings**: *"size, abundance"*; size: table 33 (p. 35), abundance: table 32 (p. 35). **Fe-Mn concretions**: *"size-abundance"*; size: fine <3 mm; amount: F-few. **Structure**. "*Character, size class"*, character: table 47 (p. 45), size class: table 51 (p. 47); type: table 49 (p. 46); combinations: table 52 (p. 47). **Carbonates**: N (no carbonates), «+» – carbonate fragments or/and secondary pedofeatures **Rock fragments**: *"Size-Abundance"*; size: table 27; abundance: table 26 (p. 29). **Roots**: "*"* – only in trans-horizon cracks. **Boundary**. a) **form**: table 24 (p. 25) right, b) **transition**: table 24 left. **Consistence**: table 54 (p. 49). **Porosity**: table 60 (p. 52).

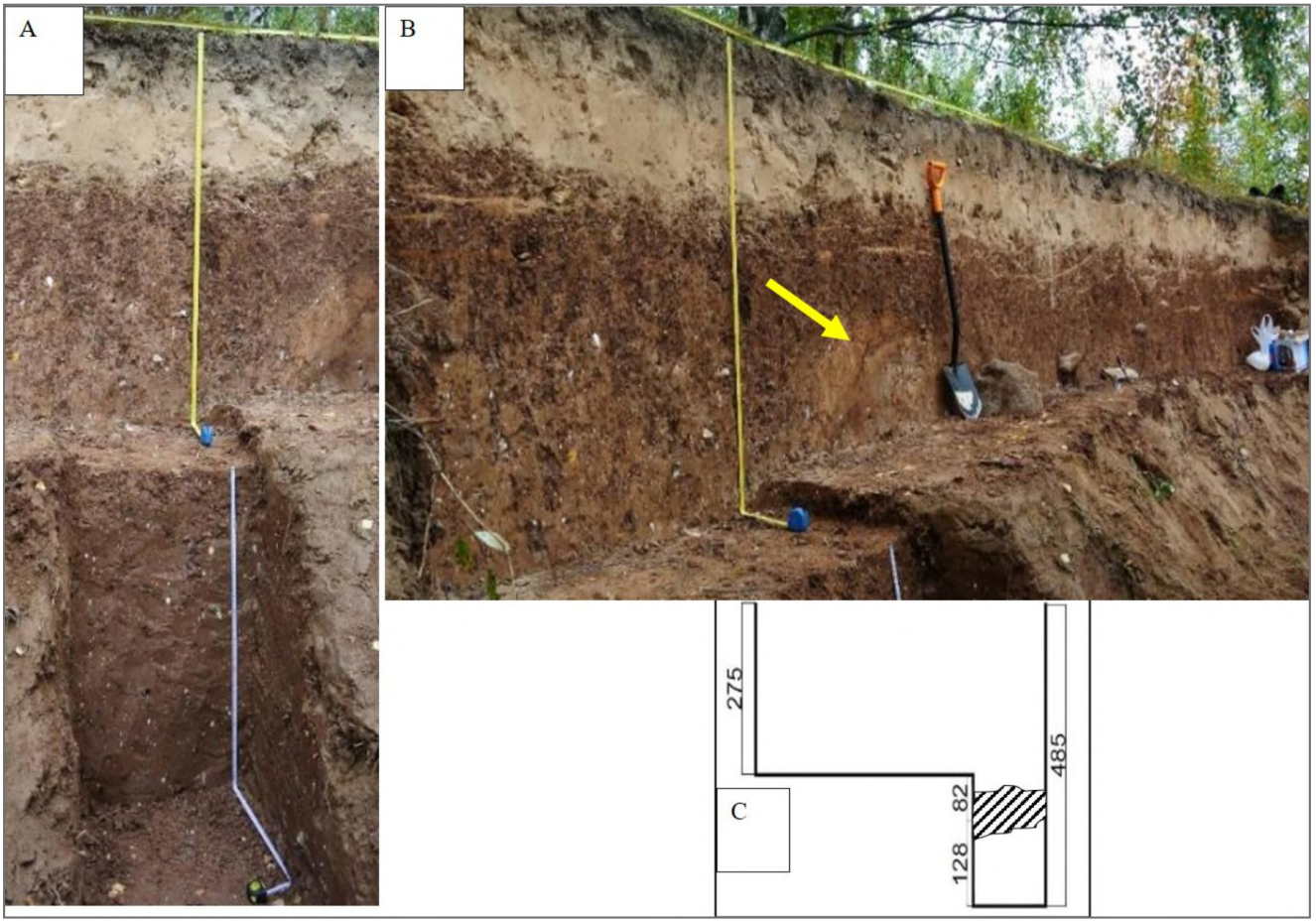

Figure 4.1. The Selishi-1 exposure: a) reference soil profile; b) general view of the outcrop. Note sandy interlayers in the uppermost part of basal till; c) Scheme of the outcrop studied down to a depth of 485 cm. Jurassic clays underlying the Moscow basal till are exposed in the right bottom corner.

Figure 4.2. The Selishi-1 exposure. Concave sand laminae marks the roof of the glacial till.

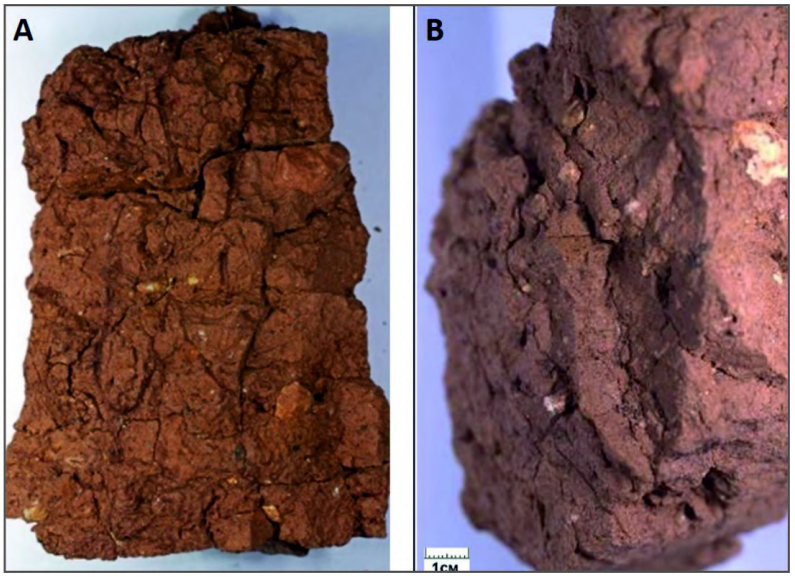

Figure 4.3. Mesomorphology of the 2Bt2 horizon formed in glacial till, Selishi-1 reference section: a) prismatic ped with irregular faces formed at the intersection of trans-horizon cracks. Note the multilayered clay coatings and voids infillings on the ped faces; b) top view on the prismatic ped with faces of a bipyramidal prism converged to a point.

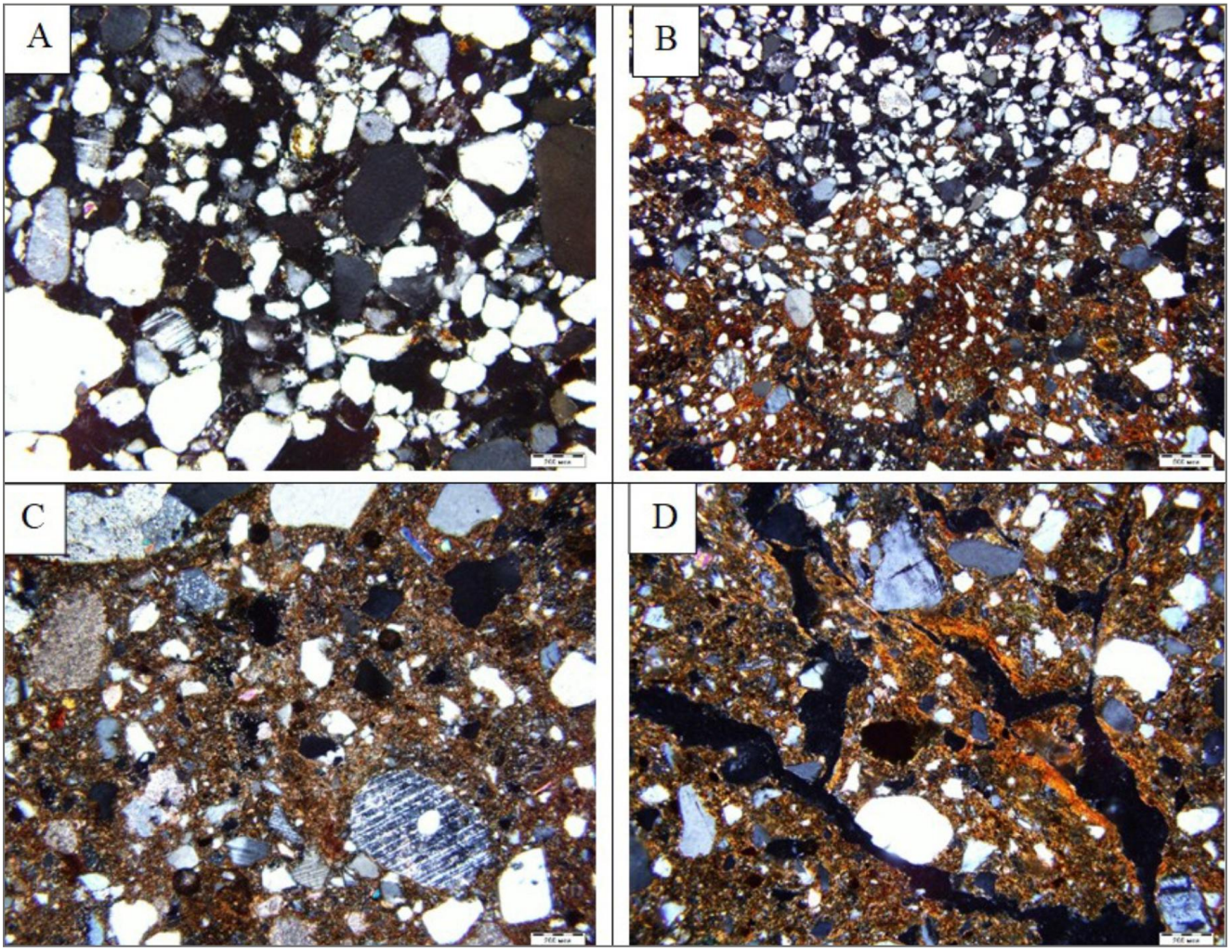

Figure 4.4. Micromorphology of the Selishi-1 section: a) cover layer close to the contact with the basal till (E/2Bt1 horizon, 35–40 cm), XPL; b) contact zone of the cover layer (single grain microstructure) and basal till (porphyritic microstructure). E/2Bt1 horizon, 38–42 cm, XPL; c) 2BC horizon (250–255 cm). Porphyric groundmass, high birefringence, and unsorted grains of crystalline rocks, XPL; d) high birefringence and multi-layered clay coatings in 2Bt2 horizon (94–139 cm), XPL.

Analytical properties of Selishi-1 exposure

Grain size distribution (Fig. 4.5). Cover layer is composed of coarse sand and loamy sand. The glacial till is represented by loam and silt loam. The difference in sand content between the cover layer and glacial till marks the bipartite sediment. Sandy interlayers at the roof of the glacial till are foreign to the cover layer indicating subglacial sedimentation. They differ in grain-size composition containing more coarse sand grains.

Chemical features (Table 4.2). Soil profiles are differentiated by acidity: the cover layer has an acid reaction while the glacial till horizons have a neutral or slightly alkaline one, which correlates to the fragments of carbonate rocks noted in them. The content of organic matter is low except for the Ah horizon. Though a certain increase in humus is noted in Bt horizons with abundant dark brown coatings. CEC is low in sandy horizons increasing in horizons with the high content of organic matter and clay. The distribution of hydrolytic acidity correlates with that of amorphous iron. Minimal values are confined to horizons with bleached sand grains. The content of iron fractions is highly heterogeneous. The content of non-silicate forms is reduced in the cover layer where amorphous iron forms comprise up to 40% of non-silicate iron (Fe_o/Fe_d). The former sharply increases in the glacial till horizons associated with the higher clay content.

Table 4.2. Chemical features of Selishi-1 exposure, 117 m a.s.l.
(*Glossic Folic Albic Retisol (abruptic, loamic, cutanic, densic)*

Horizon (IUSS..., 2022)	Depth, cm	pH	C_{org}, %	CEC, meq/ 100 g	Exch. acidity, meq/100 g	CO_2, %	MS/FS (0.25–1 mm)/ (0.05–0.25 mm)	Fe fractions, Fe_2O_3 %			
								Fe_o	Fe_d	Fe_o/Fe_d	$Fe_c=Fe_d-Fe_o$
O	0–4	5.89	–	–	–	–	–		–	–	–
Ah	4–9	4.84	1.66	7.5	3.71	–	0.57	0.12	0.40	0.30	0.28
AhC	9–25(27)	5.35	0.41	1.25	1.74	–	0.71	0.11	0.29	0.38	0.18
C	30–37	5.53	0.14	6.25	0.83	–	0.86	0.05	0.31	0.16	0.26
C	37–46	5.59	0.14	15	0.91	–	0.26	0.07	0.35	0.20	0.28
2Bt1/C	43–53	5.67	0.09	21.25	2.57	–	0.45	0.12	1.96	0.06	1.84
2Bt1	73–94	6.74	0.31	18.13	1.98	0.16	0.54	0.12	2.16	0.06	2.04
2Bt2	94–139	8.03	0.24	76.88	0.32	2.74	0.34	0.11	2.26	0.05	2.15
2Bt3	139–187	8.04	0.21	13.75	0.25	4.68	0.62	0.08	1.92	0.04	1.84
2Bt4	187–244	7.68	0.21	16.25	0.26	5.71	0.54	0.09	1.82	0.05	1.73
2BC	244–280	7.65	0.25	21.25	0.24	5.21	0.59	0.1	1.21	0.08	1.11
C	~500	8.12	0.17	11.88	<0.23	7.27	0.48	0.05	1.22	0.04	1.17
Crack	50–90	5.83	0.11	5	0.81	–	0.82	0.05	0.46	0.11	0.41
Sand lenses	60–80	5.42	0.13	3.67	0.85	–	0.83	0.05	0.40	0.13	0.35

Fe_d - non-silicate iron, diotonite-soluble; *Fe_o* - amorphous iron, oxalate soluble; *Fe_o/Fe_d* - iron activity index; *$Fe_c=Fe_d-Fe_o$* - crystallized iron content.

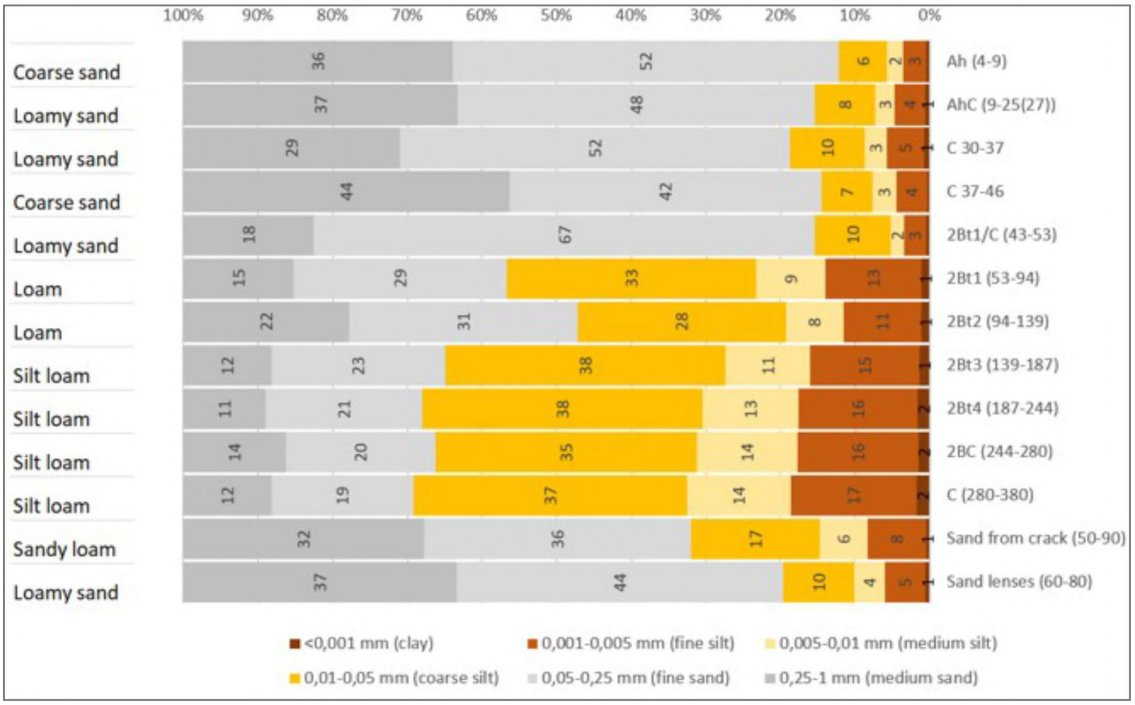

Figure 4.5. Grain size distribution in the Selishi 1 reference profile, laser diffraction method.

Soilscape pattern of the 2nd terrace, 117–122 m a.s.l. Numerous soil pits, cores, and trenches confirm the even thickness of the cover layer (Figs. 4.6 & 4.10), for instance, along the Volga riverbed from Selishi-1 exposure toward a small gully (Fig. 4.6b). In general, it varies within 50–70 cm on the terrace locally increasing to 140 cm (Fig. 4.6a). In such positions, rewashing of the upper part of the glacial till and layering in the lower part of the cover layer are observed.

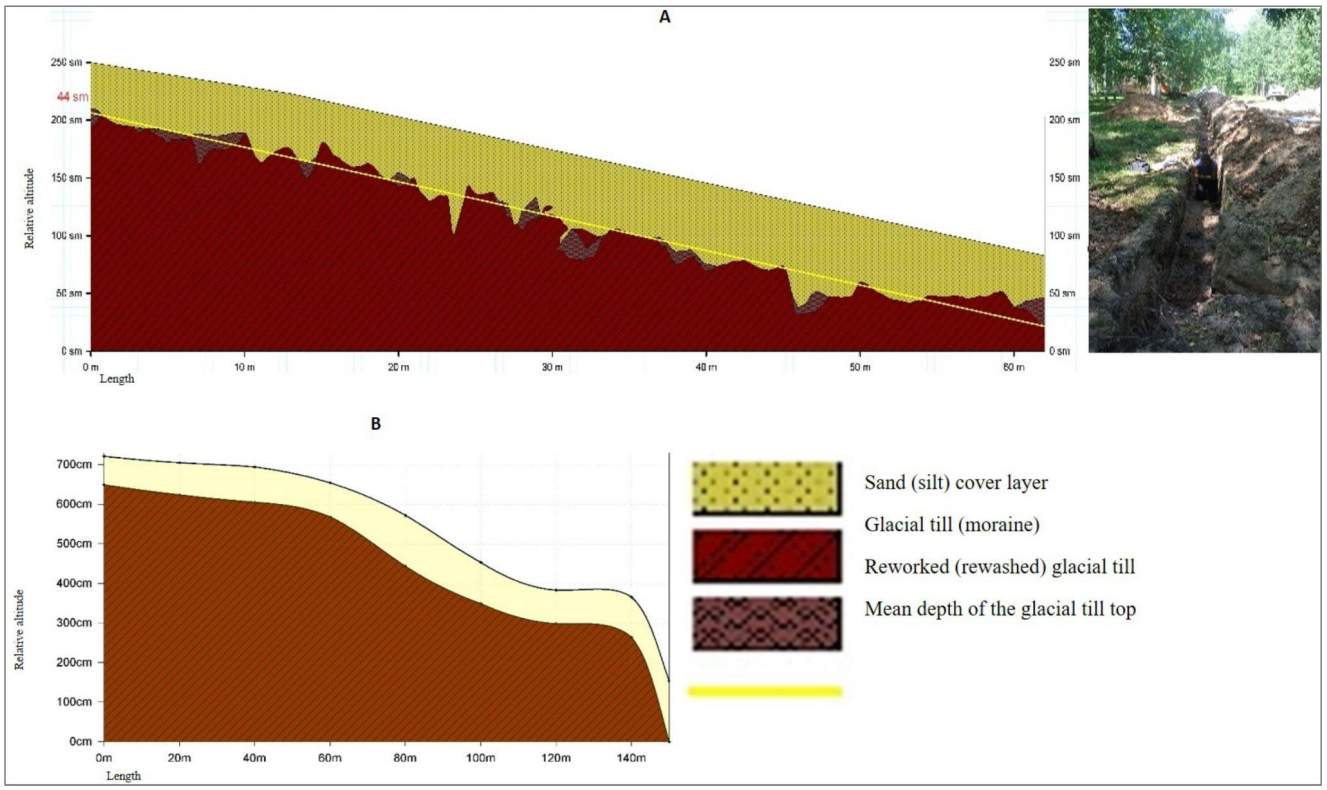

Figure 4.6. Constitution of bipartite sediments on the 2nd terrace: a) trench downsloping to the riverbank (left – a schematic image, right – photograph). Note an almost constant thickness of the silty sand cover layer, numerous wedges (mainly cryogenic) at the boundary with glacial till, and local depressions in the roof of glacial till filled with the cover layer material; b) even thickness of the cover layer along the Volga riverbed from Selishi-1 exposure toward the shallow gully with a small stream, a tributary of the Volga (based on drilling data).

Selishi-2 profile (Fig. 4.7, or WP20, 57.32535° N, 36.02745° E, Fig. 4.10) exhibits a soil with a thick cover layer: *Endostagnic Skeletic Arenosol (Bathyretic, Bathystagnic)* (IUSS working group WRB, 2022). The cover layer is 140–150 cm thick (Fig. 4.7) corresponding to the positions with its locally increased thickness (Fig. 4.6a). It is differentiated by depth (Fig. 4.7): the upper 40 cm are unstratified but layering is noticeable in the middle part of 40–130 cm depth. From 80 to 130 cm, layering is clearly expressed by the interbedding of fine and very fine sand; interlayers of medium sand appear at a depth of 120–130 cm. The middle part is characterized by a high degree of sand sorting (Fig. 4.8a). Although the lowermost part (130–150 cm) of the cover layer is unstratified consisting of stony unsorted sand (Fig. 4.8b).

Figure 4.8. General view of Selischi-2 profile (WP20, Fig. 4.10).

Redoximorphic features caused by seasonal water stagnation on the roof of massive diamicton resulted in bleached glossic zones (10 YR 7/2.5), iron stains, and single dark humus streaks (10 YR 3/1) appeared from the middle part of the cover layer. The lowermost part of the cover layer shows ferruginous covers that fill the space between the coarse grains (Fig. 4.8b).

Glacial till runs down from 146 (152) cm presented by red-brown massive matrix-supported diamicton. Similar to Selishi-1, it has abundant redoximorphic features (Fig. 4.8c). Bt horizons have the typical subangular blocky structure with ped faces covered by multi-layered clay cutans starting from the 2Bt1gb horizon (Fig. 4.8c,d). The boundary of the cover layer is characterized by sharp contact even at the micro-level (Fig. 8b).

The grain size distribution of the Selishchi-2 profile is typical for the bipartite sediments, with loamy sand, sandy loam, fine and medium sand in the cover layer, and silt loam in the glacial till. Lithic discontinuity is marked by differences in sand and silt contents. Sorting of sand particles in the cover layer and slight interlayering in its middle part are seen in the grain size distribution (Fig. 4.8).

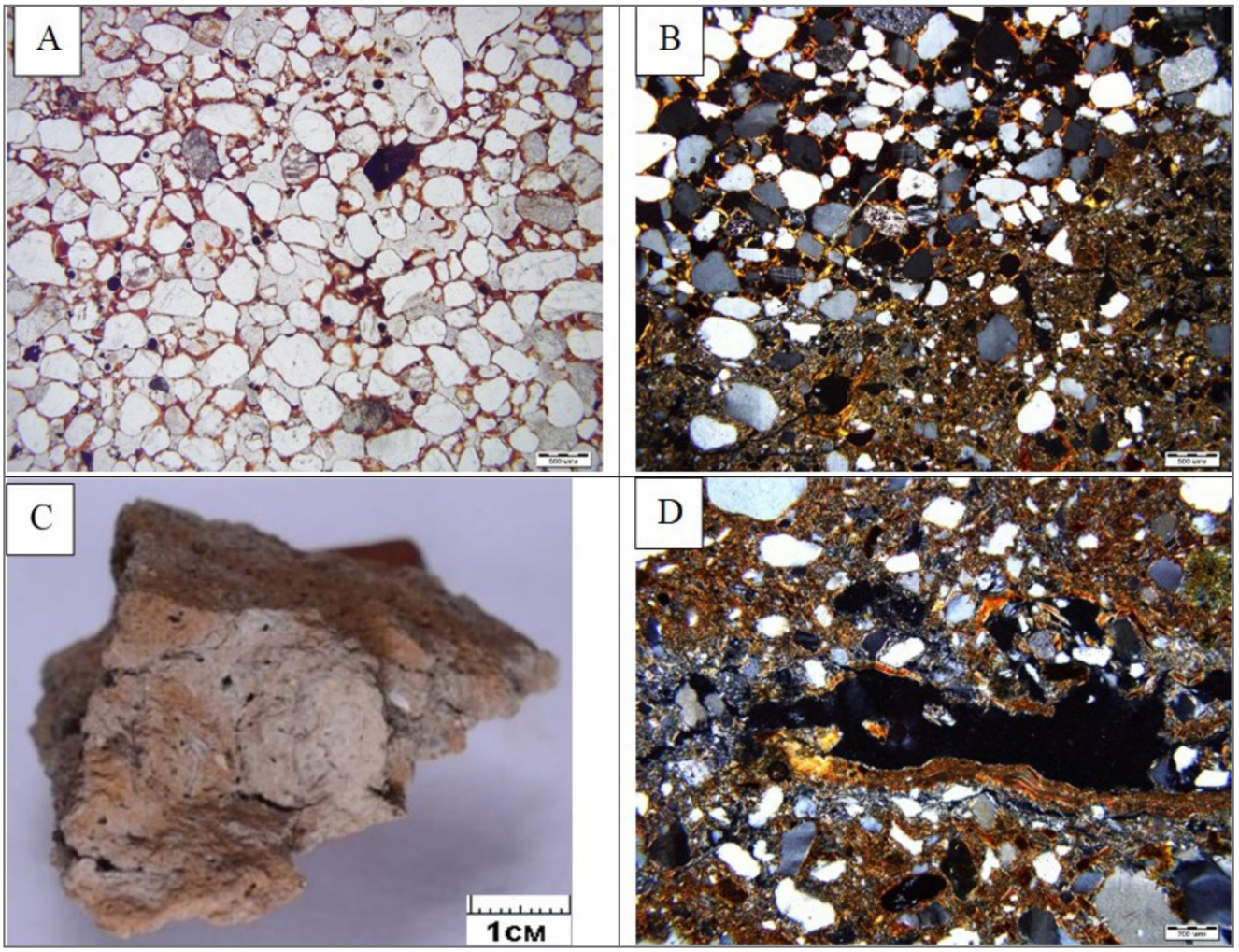

Figure 4.8. Mesomorphology (a) and micromorphology (b,c,d) of the Selishi-2 profile: a) Cc,g (E/Btb, 150–152 cm). Sorted rounded sand grains above the contact with the basal till, PPL; b) Cc,g (E/Btb) horizon (149–154 cm). Contact zone of the cover layer and basal till, XPL; c) structural units of 2Bt1gb horizon. Jointing of prismatic structures, top view; the left ped is cut off by a trans-horizon crack on the left and bottom, the right one is cleaved off by a subhorizontal plane; d) 2Bt2gb horizon (190–195 cm). Multi-layered clay coatings, XPL.

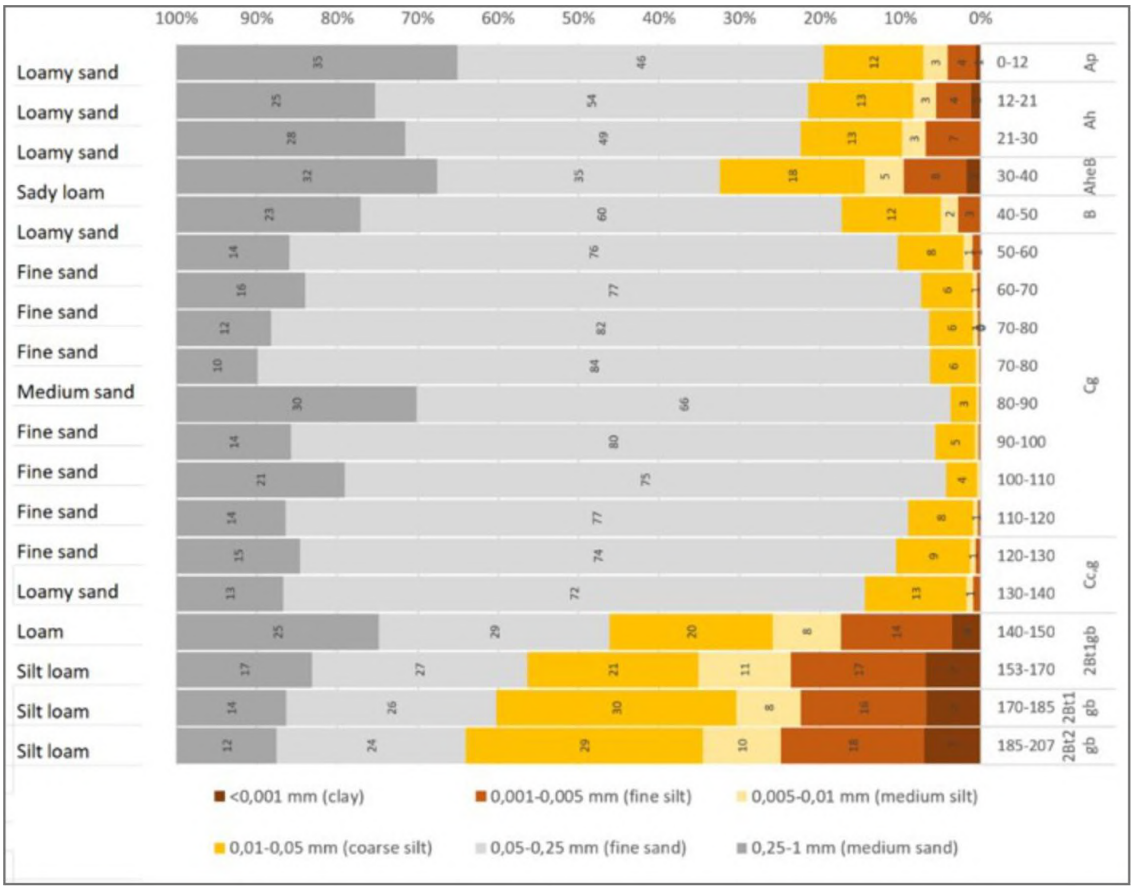

Figure 4.9. Grain size distribution of the Selishi-2 soil profile, laser diffraction method.

Soilscape pattern of the 3rd terrace (122–127 m a.s.l.) and adjacent upland (127–145 m a.s.l.). The slightly undulating surface that gradually slopes up toward the upland slopes is designated as an extensive (8 km wide) glaciofluvial plain of Moscow time (State geological map of USSR. O-37-XXVII, 1969, Fig. F). The surface is dissected by small streams and gullies and complicated by small sand dunes. The constitution of bipartite sediments was studied by soil pits, trenches, and cores from Selishi to Ulanovo settlements (Fig. 4.10, WP4–WP17). The glacial till is overlain by a sandy-loam or sandy cover layer 120 cm thick locally increasing up to 350 cm (Fig. 4.10b,c,d). The upper part of the cover layer down to 80 cm shows no signs of layering, which is visible in the lower part. Thus, the constitution of bipartite sediments on the 3rd terrace is similar to that on the 2nd one yet with the cover layer more than twice as thick. The differentiation of the cover layer with depth is also similar: the upper part is homogeneous, and the layering appears in the middle part expressed by the interbedding of fine and very fine sand or interlayers of medium sand. The grain size distribution performed using the laser diffraction method also confirms the sorting of sandy deposits and layering in the middle part of the cover layer (Fig. 4.10d). A considerable increase in the cover layer thickness is confined to sand dunes. There the cover layer consists of well-sorted sand; sequential sedimentation is evidenced by layering, weakly expressed buried humus horizons, and a network of small polygonal wedges at different levels (Fig. 4.10c).

WP10, WP11, and WP12 demonstrate the constitution of bipartite sediments on the slopes and top of the moraine ridge, a part of a chain of isolated hills confined to the watershed of Volga and Zhabnya rivers (Fig. 4.10). The thickness of cover layer varies within 30–50 cm, which is similar to that of the other moraine uplands in the area of Moscow Cryochrone (Makeev et al., 2019). The boundary between the cover layer and glacial till is complicated by frost wedges and fissures.

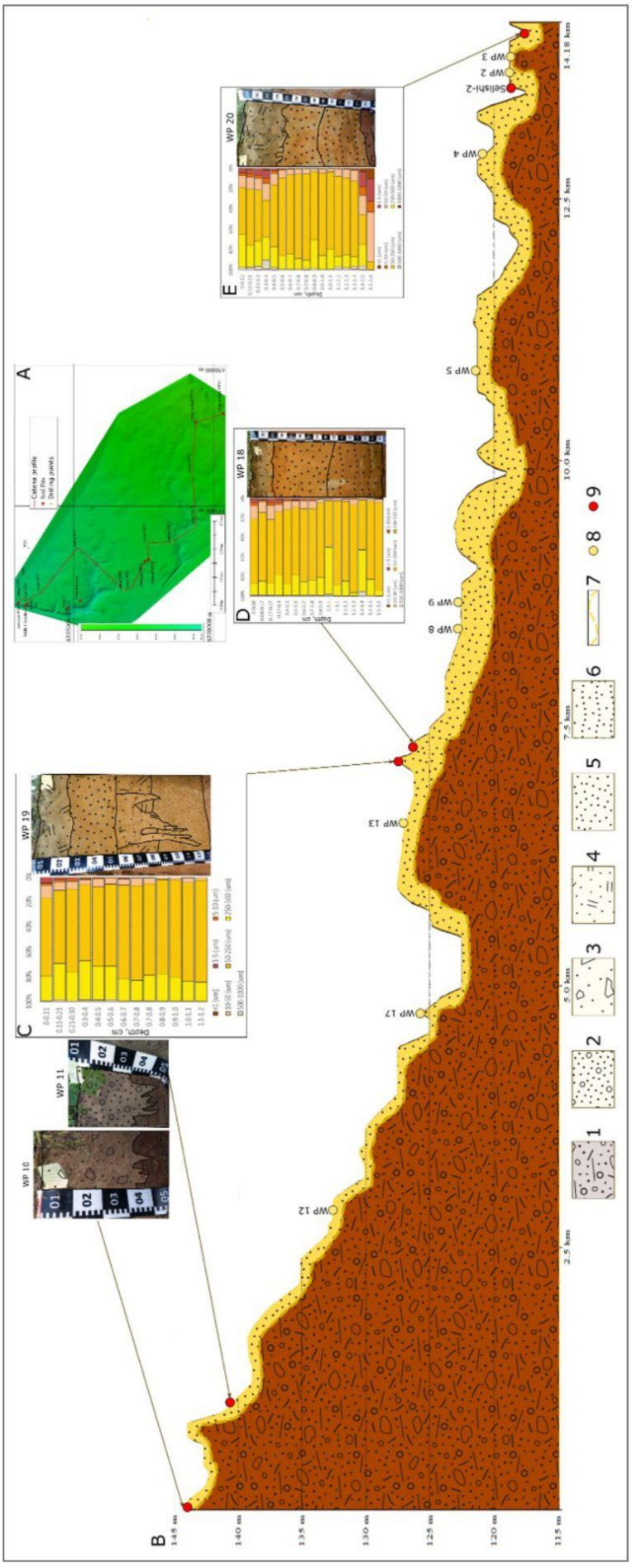

Figure 4.10. Distribution of bipartite sediments across the terraces and adjacent upland: a) position of the catena on the DEM based on a topographic map 1:10000; b) geological profile with the positions of cores and reference profiles; c–e) reference profiles with the grain size distribution on the left and the schematic diagram of the profile structure on the right: c) profile WP19 at a shallow dune. The entire profile is composed of well-sorted sediments; d) profile WP18 with layered sandy deposits in the lower part; e) profile WP20. *1* – glacial till; *2* – silty deposits with an admixture of sand, pebble, and gravel; *3* – sandy deposits with an admixture of pebble and gravel; *4* – surface soil horizons; *5* – sandy and silty sand deposits; *6* – sandy and silty sand deposits with signs of subhorizontal layering; *7* – possible depth of the glacial till rooftop; *8* – cores; *9* – reference profiles.

DISCUSSION

History of the Upper Volga River valley based on the distribution of bipartite sediments on the terraces of Selishi key site. MIS6 glaciation was the last to cover the Upper Volga basin. Bipartite sediments of the Selishi key site include the Moscow glacial till and sandy cover layer. The majority of features were acquired by the glacial till prior to deposition (Rukhina, 1973; Aparin & Rubilin, 1975; Lavrushin, 1976). Those pre-deposition features include:

– features inherited from the sediments mobilized by a glacier (older tills, weathering crusts, hard rocks, etc.): bright reddish-brown color (up to 5 YR 6/6) and strong weathering of the entire stratum.

– features indicating glacial transport: dense fabric and low porosity; homogeneous composition due to effective mixing of fine and coarse particles under the moving ice; simultaneous inclusion of heterogeneous fragments (sandy structures due to the filling of subglacial cavities; zones enriched in boulders; dispersed stones of granites, limestones, and breccia).

Deposition of the glacial till. Massive tills are formed during the plastic type of ice movement. Massive structures indicate the stable nature of sedimentation. Consolidation of till-bearing ice occurs during such movement so that the basal till layer already lacks ice under the moving glacier (Lavrushin, 1976). Glacial origin results in a very dense fabric (van der Meer et al., 1983; van der Meer, 1987; Jongsmans et al., 1989). In cases of hard lodgement, a dearth of water occurs, and, thus, frictional processes dominate leading to high consolidation, strong fabrics, and low pore contents (Ruszczynska-Szenajch et al., 2003). High meltwater content led to the formation of turbate or open structures (Hart & Boulton, 1991), which are seen well in the studied soils. The high birefringence of fine material is one of the most prominent microfeatures of the glacial till. It could be attributed to the rotation and translocation of the groundmass under the pressure of ice (Brewer, 1976; Miedema, 1987; Jongmans et al., 1989). Only one layer of glacial till is present at Selishi-1 exposure. At the bottom, it has erosional contact with the underlying Jurassic clays, as evidenced by the admixture of dark clay into the matrix of glacial till and shearing zones. At the top, the till shows a melt-out and decoupling character developed during the motion of the ice sheet. Concave sandy interlayers document multiple changes in subglacial water pressure. At the time of its increase to values balancing the pressure exerted by the ice cover, ice-bed decoupling occurred, leading to acceleration of the glacial slip, followed by a subglacial water flow responsible for the formation of thin laminae of sorted sand (Piotrowski et al., 2006; Woźniak & Czubla, 2016).

Deposition of the cover layer. On the terraces, the thick cover layer is stratified into three parts. The lower part is characterized by coarse and angular sand grains and abundant stone inclusions. Its deposition is attributed to the local rewashing of the glacial till roof by small streams that accompanied the deposition of the glacial till (Rukhina, 1973; Aparin & Rubilin, 1975; Makeev et al., 2019). The input of rewashing is evidenced by micromorphology: compared to the glacial till, the lower cover layer is enriched with slightly rounded coarse grains. The presence of angular coarse grains indicates short-term rewashing, e.g., by the streams from dead-ice bodies (Woźniak & Czubla, 2016). It is important to note that eolian activity did not influence the glacial till roof. It is evidenced by the remains of the stony layer at the cover layer bottom and concave sandy layers that are confined to the roof of the glacial till.

The cover layer was reworked by eolian processes in the cold and arid environment of the Late Valdai (Astakhov et al., 2016). That resulted in either partial deflation (as in Selishi-1 outcrop) or accumulation (as in WP20, WP18, WP19, Figs. 4.7 & 4.10) of sandy material. 7–10 m sand dunes are widespread on the terraces and are shown on the State geological map of the USSR. O-37-XXVII, 1969.

Properties of the upper cover layer confirm eolian input: well-sorted sand with silt admixture and abundant rounded grains. The study of the dune at WP19 (Fig. 4.10) showed the sequential deposition of sand. The buried soil horizon and a network of small polygonal ground wedges occur at 50 cm. Eolian transformation of the upper cover layer could be attributed to the Late Glacial (17–12.4 yrs BP), which is in line with OSL dating (Table 4.3.).

Table 4.3. OSL dates of the cover layer in soils of the Volga River valley

m a.s.l. and geomorphic position	Site	LAB no.	Depth, cm	Quartz			
				Age	Doze	Dose rate	Water content
				ka	Gy	Gy/ka	%
119 m 2nd Volga river terrace	WP 20	4089 (LIAG)	75	**15.7±1.0**	28.3±1.3	1.80±0.08	25
		4090 (LIAG)	115	**17.5±1.0**	25.9±0.8	1.48±0.06	25
127 m 3rd Volga river terrace	WP 18	4082 (LIAG)	55	**12.9±0.8**	20.6±0.9	1.6±0.07	25
		4083 (LIAG)	90	**14.5±0.7**	25.5±0.6	1.76±0.08	25
		4084 (LIAG)	120	**14.4±0.8**	23.4±0.8	1.63±0.07	25
		4085 (LIAG)	155	**12.2±0.6**	23.6±0.7	1.94±0.09	25
128 m 3rd Volga river terrace, in dune	WP 19	4086 (LIAG)	35	**15.4±0.9**	21.4±0.7	1.39±0.06	25
		4087 (LIAG)	80	**17.0±0.9**	26.6±0.8	1.56±0.07	25
		4088 (LIAG)	110	**16.9±0.9**	27.1±0.9	1.61±0.07	25

Morphology, age, and origin of the Upper Volga River valley is still a matter of debate despite its long study history (Baranov & Panin, 2021). The number of terraces varies from two to four, with different height estimates depending on the author and place. For the river valley, the age ranges from Late Moscow (MIS6) to Late Valdai (MIS2) without support of numerical dating. Following Kvasov (1975), it was considered the river basin was occupied by a large proglacial lake before MIS2, so the Upper Volga drainage network formed at the end of the Last Deglaciation. Yet no proglacial lake deposits were found on the terraces (Utkina et al., 2022) proving that the Tver proglacial lake did not exist at levels of 120–145 m a.s.l. in the Upper Volga Lowland.

Many doubts were expressed about the alluvial origin of the Upper Volga terraces. The bipartite sediments, similar to those of the Selishi key site (shallow sandy layer on top of the glacial till), are described on the terraces in various parts of the Upper Volga River valley at different levels: 120 m a.s.l. surface near Uglich (Baranov et al., 2022); 132–136 m a.s.l. surface 25–30 km downstream from Tver (Baranov, 2022); the upper (25–32 m a.s.l.) terrace near Uglich (Khimenkov, 1932; Baranov, 2022). The mantling bedding of the upper glacial till on the lower terraces was described by Velichko (Markov et al., 1969).

Based on the universal distribution of bipartite sediments, we may suggest they could in some places mantle even the river bed, indicating, according to Spiridonov (1938), the recent ongoing river incision. Obedientova (1977) and Spiridonov (1978) suggested that the Upper Volga Valley cuts mostly through till and glaciofluvial sediments. Apparently, its minimum age is MIS6 (Utkina et al., 2022). The age of small gullies is also old because the bipartite sediments mantle their slopes with the evenly distributed cover layer (Fig. 4.6b).

Thus, field and analytical data allow us to conclude that terrace levels within 117–127 m a.s.l. are old bedrock terraces mantled by bipartite sediments, with the cover layer being reworked during the Late Valdai. Alluvial terraces are absent at the Selishi site.

STOP 5. SOILS OF NERL-ZHABNYA INTERFLUVE
August 28, 2023, afternoon

Porechie key site. The area is a part of the Nerl-Volga Lowland within an elevation range of 120–140 m a.s.l. That is a vast outwash plain merged with large meltwater channels of Late Moscow time. The reference soil profile (57.107130 N, 37.922270 E) is situated 22 km SSW of the Selishchi key site (Fig. F), in the central part of the slightly undulating upland area in between Zhabnya and Nerl rivers. The upland has an aligned surface with boggy depressions formed in supraglacial meltwater channel sediments that cover the glacial till (State geological map of USSR. Quaternary deposits, O-37-XXVI, 1967, Fig. F). The soil profile is formed under spruce forest on a flat moraine hilltop elevated 135 m a.s.l. (Fig. 5.1).

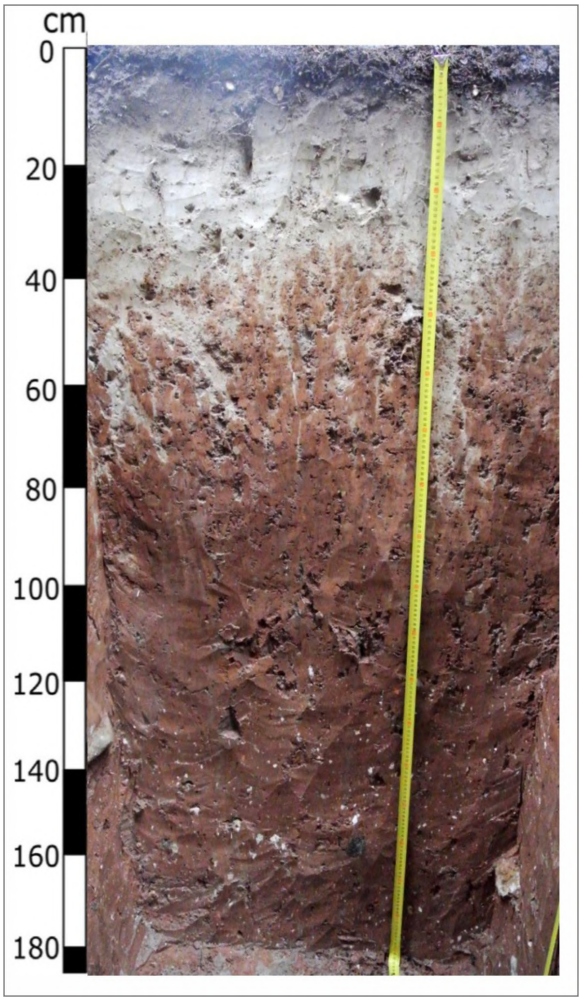

Figure 5.1. General view of the reference profile in Porechie key site. *Glossic Folic Albic Dystric Retisol (abruptic, loamic, cutanic, densic).* Carbonate gravels are well seen in the lower part of the solum (whitish spots).

Field morphology and micromorphology of the Porechie reference profile. Soil profiles have the following sequence of horizons: O (0–5 cm) AE (5–11 cm) E (11–23(40) cm) 2Bt1 (23–95 cm) 2Bt2 (95–136 cm) – 2Bt3 (136–182 cm), thus matching the criteria for *Glossic Folic Albic Dystric Retisol (abruptic, loamic, cutanic, densic).* The lower part of the solum is formed in a red-brown (5 YR 4/4) sandy clay loam: massive matrix-supported diamicton with common (~10%) gravels and stones of various shapes, orientations, and weathering degree. Carbonate gravels start from the Bt2 horizon (Fig. 5.1), though the soil matrix shows effervescence only in 2 cm around gravels. The glacial till is well-structured. Trans-horizon cracks can be seen through the solum. 2Bt horizons have strong angular and subangular blocky structures changing from fine to coarse downward. Down to 90 cm, the blocks are combined into plates that increase in thickness with depth. The blocky structure is also incorporated with prismatic units that become dominant below 100 cm where blocky and platy units cease. The size of prisms increases downward, and prism faces are tilted towards each other, forming angular vertices (Fig. 5.2a). Ped faces are covered with abundant clay cutans in the 2Bt1 and 2Bt2 horizons. Clay cutans may completely fill root channels. Below the 2Bt3 horizon, prism faces are uniformly covered by thin brown coatings. Thick clay cutans are dominant on the faces of trans-horizon cracks that partly follow prism faces below the 2Bt3 horizon. Clay-humic coatings are usually slightly darker (5 YR 4/3) than the groundmass in 2Bt1 and 2Bt2 horizons. The abundant white powder covers ped faces upon clay and clay-humic coatings forming compound silty-humic clay coatings. A wide wedge-like structure penetrates the glacial till from the top down to 160 cm being filled with different mater: yellow loamy sand with common gravels on top and fine sand at the bottom (Fig. 5.2b). Some parts of the wedge are

loose while the others are firm. A large sand wedge-like structure in the glacial till (Fig. 5.2b) was most probably formed by the filling of a subglacial cavity (c.f. Piotrowski et al., 2004; Wozniak & Czubla, 2016). It is worth mentioning that the cover layer above the wedge is silty. There are sand streaks in different parts of the glacial till. Sandy matrix interlayers, sand streaks, and wedge-like forms record the high-pressure subglacial water flow.

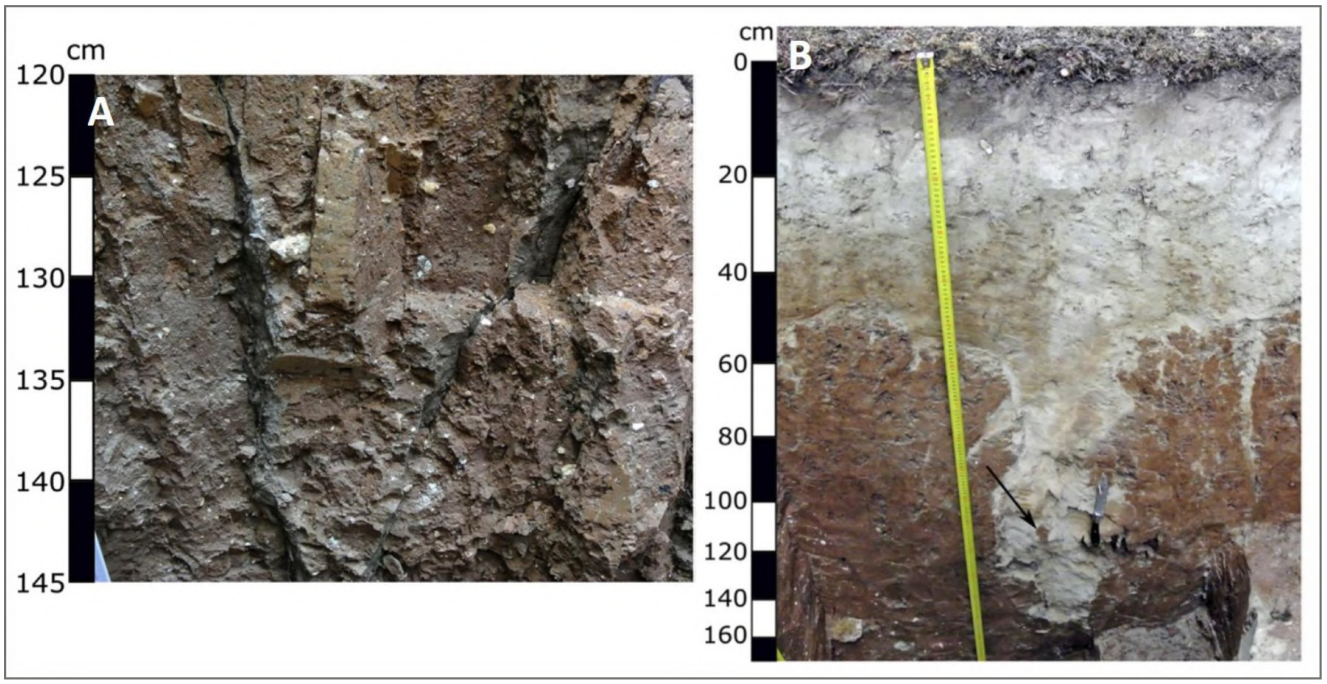

Figure 5.2. Porechie reference profile: a) prismatic structure in the lower part of the solum (2Bt3 horizon). Note tilt orientation of prisms and thick compound clay cutans on prisms faces combined with irreversible trans-horizon cracks; b) general view of the sandy wedge. Note: the till fragments with sharp boundaries are incorporated in the wedge body marked with an arrow.

The cover layer consists of silty and sandy patches, similar in color, changing from gray or even dark gray (5 YR 2.5/2) in the upper horizons to pale white (10 YR 7.5/3) at the bottom. Silt loam predominates in the upper part, with some parts forming a continuous layer. Both sandy and silty patches contain gravel, though it is more abundant in sandy patches. The boundary between the cover layer and diamicton is very abrupt and irregular, complicated by albeluvic glossae down to 50–60 cm (Fig. 5.3). The fissures are filled either with sandy or silty material depending on the overlying cover layer.

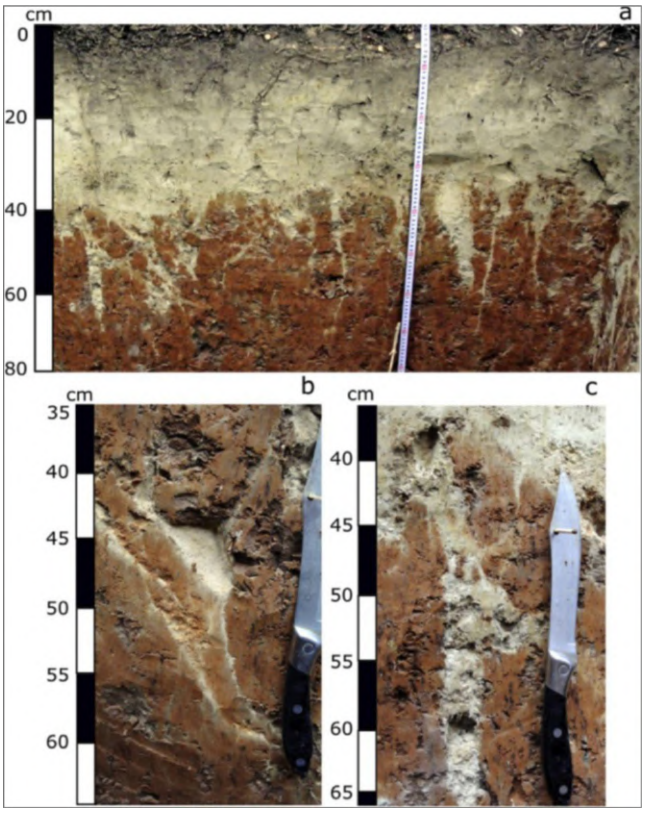

Figure 5.3. Porechie reference profile. The irregular boundary between the cover layer and basal till is complicated by the regular pattern of *albeluvic glossae* and *retic* properties: a) general view. Note that sandy (b) and silty (c) fissures are the continuations of sandy and silty parts of the cover layer.

STOP 6. RELICT LATE MOSCOW LANDSCAPES OF SW BORISOGLEBSK UPLAND AND SOILS IN BIPARTITE SEDIMENTS
August 29, 2023, morning

Novoselky key site is situated 50 km southeast of Porechie key site within an isolated moraine upland, 3 x 11 km in size, elevated 170–200 m a.s.l (Fig. 6.1a). The upland is surrounded by the outwash plain of the Moscow age (150–170 m a.s.l.). Its slightly undulating surface is superimposed by SWS – ENE oriented chains of merged kames with steep slopes and cone tops elevated 200–220 m a.s.l. The reference soil profile (56.53'58.44" N, 38.38'18.41" E, 184 m a.s.l.) is formed on a flat surface between two kames under spruce forest.

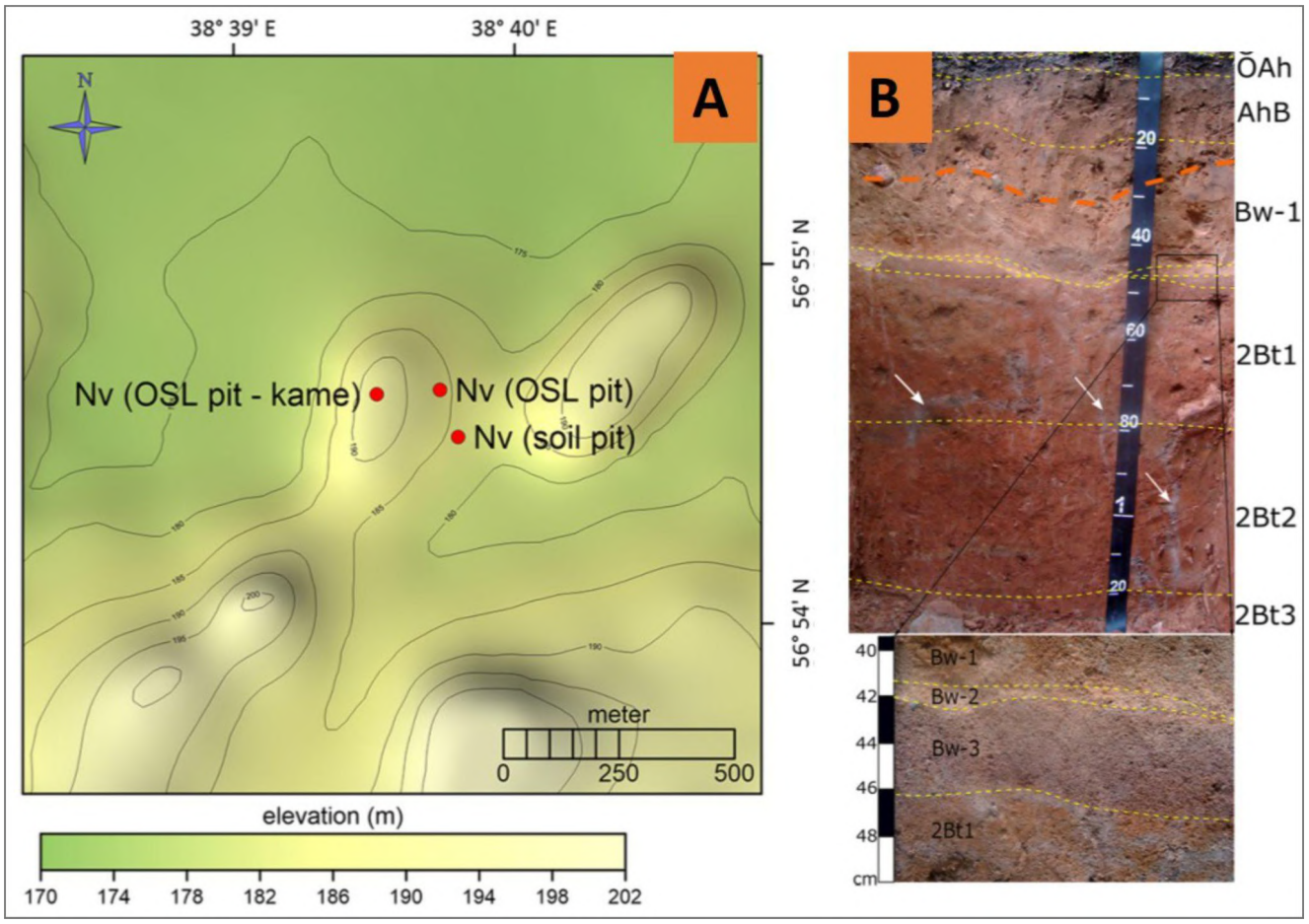

Figure 6.1. Novoselky key site: a) topographic map (1:25000) and locations of the studied pits; b) general view of the reference soil profile. Note the stoneline within the cover layer (orange dashed line). An enlarged fragment shows a bleached contact interlayer (*Bw-2*) underlined by a layer of very firm coarse sand (*Bw-3*) with abrupt boundaries.

Field morphology. The soil profile (Fig. 6.1b) has the following sequence of horizons: OAh (0–3 cm) AhB (3–18 cm) Bw1 (18–38 cm) Bw2 (38–46 cm) Bw3 (46–54 cm) 2Bt1 (54–75 cm) 2Bt2 (75–115 cm) 2Bt3 (115–128 cm) and meet the criteria for *Glossic Folic Albic Dystric Retisol (abruptic, loamic, cutanic, densic)*. The cover layer 53 cm thick is sandy with a stone line at a depth of 25–30 cm. An abrupt contact between the cover layer and glacial till shows *retic* properties with *albeluvic glossae* forming a polygonal pattern in the subhorizontal sections. The glossae have sand or silt infillings. The upper part of the contact zone is represented by a firm sandy streak at the cover layer bottom (Bw3 horizon). The cover layer hosts the Ah humus and weakly developed *Cambic* horizons marked by color.

The glacial till is well-structured. The trans-horizon cracks (Field book ..., 2012) can be seen through the solum. The 2Bt horizons have a strong angular and subangular blocky structure ranging from fine to coarse downward. Down to 80–90 cm, the blocks are combined with plates that increase in thickness with depth. The subhorizontal faces of plates are covered by dark-brown reticulate coatings. The blocky structure is also incorporated with prismatic units; the latter becomes dominant below 100 cm where blocky and platy units cease. The size of prisms increases downward, and prism faces are tilted towards each other forming angular vertices (Fig. 5.2b). The ped faces and stone surfaces in the 2Bt1 and 2Bt2 horizons are covered with abundant clay coatings. Such coatings may completely fill the root channels. Below the 2Bt3 horizon, prism faces are uniformly covered by thin brown coatings. Thick clay coatings are dominant on the faces of trans-horizon cracks that partly follow the prism faces below the 2Bt3 horizon.

Spatial distribution of bipartite sediments on moraine uplands. Similar bipartite sediments mantle uplands at the Porechie and Novoselky key sites. The depth of the cover layer varies from 30 to 75 cm with a mean depth of 45 cm. They are also similar to the one in the upper part of the Selishi key site (WP10 & WP11, Fig. 4.10b). At the Porechie key site, the depth of the cover layer increases within the supraglacial meltwater channels (Fig. 6.2a). In the cover layer, sandy patches predominate in some pits while silty ones – in others. There is a tendency that at the topmost positions of the Porechie key site (145–150 m a.s.l.) sandy material is absent and a silty cover layer uniformly mantle the glacial till. At the Novoselky key site, bipartite sediments with a sandy cover layer of even thickness mantle the upland and its slopes (Fig. 6.2b). The cover layer gradually merges with the glaciofluvial sands of the kame and outwash plain. Within approximately 300 m, the depth of the cover layer increases, sandy material becomes coarser, and the amount of gravel increases whereas the glacial till submerges deep below the thick sand layer.

Analytical properties of soils formed in bipartite sediments

Grain size distribution (Table 6.1, Fig. 6.3) confirms the bipartite character of the soil parent material. Glacial till is sandy loam, clay loam, or even loam. In both the Porechie and Novoselky reference profiles, the grain size distribution in cover layers differs significantly from that of the glacial till. The cover layer at the Novoselky is sandy loam. Silt and sandy loam patches manifest at the Porechie. All size fractions are unevenly distributed with depth. In the glacial till, sand wedges and streaks are detected on the increase in sand. For instance, the MS/FS index in the wedge-like structures differs by 1.5–5 times compared to the glacial till. It is also seen on the grain size distribution curves (Fig. 6.3a). In the Porechie reference profile, the large sand wedge (Fig. 5.2b) is not homogeneous and consists of matters that differ in the ratio of medium and fine sand indicating sequential infilling. Its upper part is more silty (loamy sand) and is closer to the cover layer overlying the wedge. The fine sand content decreases with depth. The sand wedge shows a high content of fine sand, which is much lower both in the cover layer and glacial till. On the moraine plateau at the Novoselky key site, the cover layer exhibits a clear peak in the sand fraction with grain size variation from 250 to 310 mm (Fig. 6.3c,d). In some positions, the sand peaks constitute up to 90% of the graph area (reference profile and position 13) while much less (50%, positions 12, 14) in the others. In the latter cases, the remaining area of the graphs lies within 0.5–60 mm, showing either a gradual distribution (positions 7, 17, 19, 20) or a peak in the fine silt (positions 12, 18).

Total chemical composition of the fine earth fraction (Table 6.2) attests to the fact that the differentiation of soil profiles by chemical composition is connected with the differences in the clay content between the cover layers and glacial till. Soil horizons formed in the cover layers as well as sand wedges and streaks are enriched with SiO_2 and

contain less Fe_2O_3 and Al_2O_3 compared to the lower horizons formed in the glacial till. The increase in CaO content in the lower horizons of the Porechie profile is most probably influenced by grains of carbonate rocks. The TiO_2/ZrO_2 ratios in fine earth show the difference between the cover layer and glacial till by a factor of 2 or more, confirming the lithic discontinuity. Those ratios also show the difference between sandy streaks and wedges, on the one hand, and both the enclosing till and cover layers, on the other. Other chemical elements exhibit irregular variations.

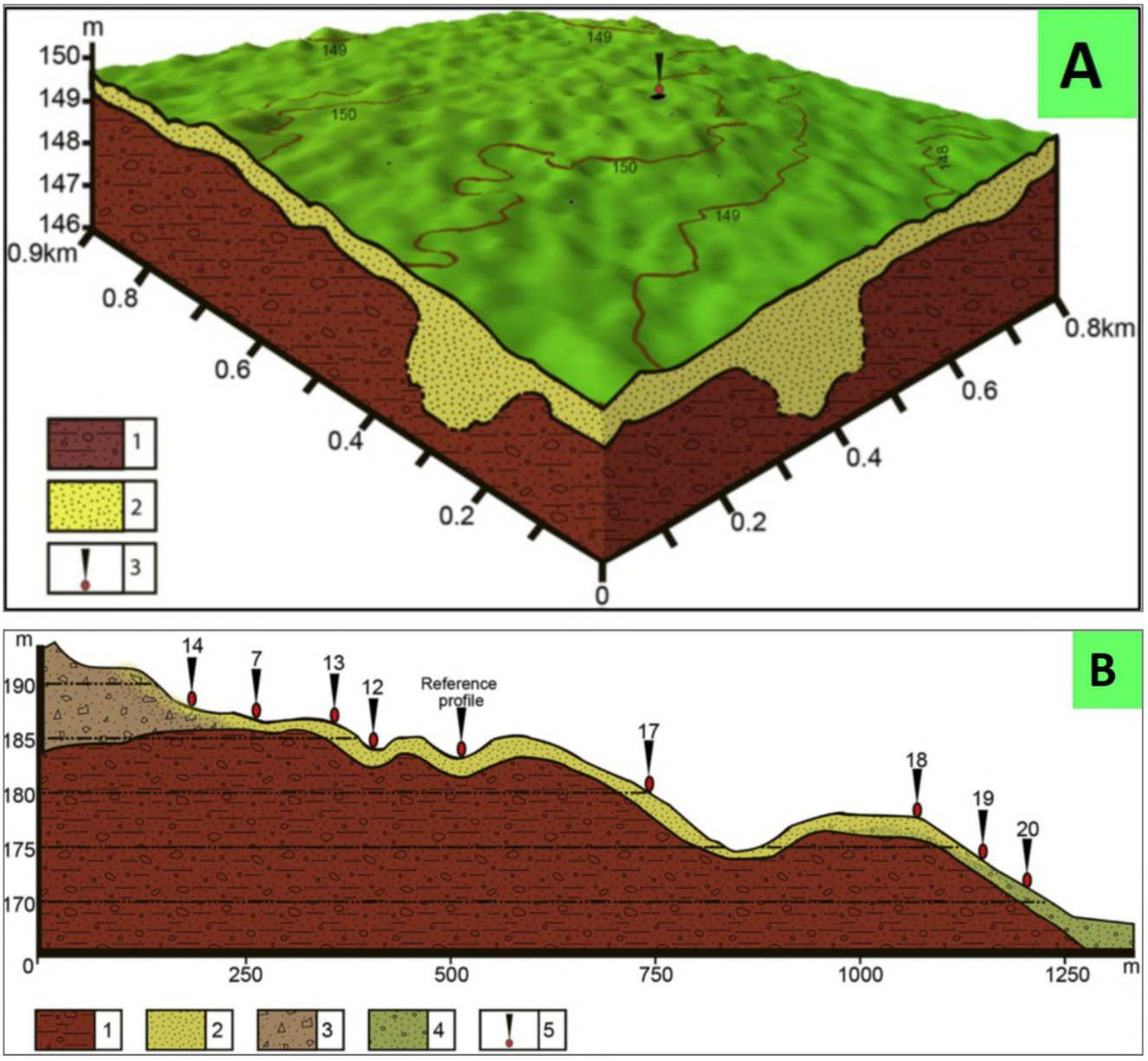

Figure 6.2. a) Porechie key site. The depth of the cover layer increases within the supraglacial meltwater channels. b) Generalized profile of the Novoselky key site. Lateral contacts of the cover layer with glaciofluvial sediments of kames and outwash plains, 165–195 m a.s.l. (SRTM30 DEM supplemented by geodetic leveling at the background). *1* – glacial till; *2* – sandy/silty cover layer; *3* – glaciofluvial sediments of kames; *4* – glaciofluvial sediments of outwash plains; *5* – position of soil pits.

Table 6.1. Grain size distribution in soils formed in bipartite sediments on the uplands (pipette method)

Horizon	Depth, cm	Particle size (mm) distribution Russian traditional fraction groups							Textural classes (IUSS..., 2022)
		1.00–0.25	0.25–0.05	0.05–0.01	0.01–0.005	0.005 – 0.001	<0.001	MS/FS (1–0.25)/(0.25–0.05)	
Porechie reference profile, 135 m a.s.l.									
AE	5–11	9	32	39	5	6	10	0.3	Silt loam
E	11–23	21	37	27	4	5	5	0.6	Sandy loam
2Bt1 (uppermost parts)	23–40	9	28	18	4	9	32	0.3	Clay loam
2Bt1	40–95	9	31	17	5	22	16	0.3	Loam
2Bt2	95–136	10	32	20	6	10	22	0.3	Clay loam
2Bt3	136–182	10	31	20	7	10	21	0.3	Clay loam
Sand streak	90–115	33	51	2	1	2	11	0.7	Sandy loam
Sand wedge upper part	40–45	34	47	9	2	4	4	0.7	Loamy sand
Sand wedge middle part	65–85	32	60	2	0	1	4	0.5	Loamy sand
Sand wedge lower part	85–160	28	64	2	0	2	4	0.4	Loamy sand
Novoselky reference profile, 180 m a.s.l.									
OAh	0–3	23	45	19	4	3	6	0.5	Sandy loam
AhB	3–18	24	44	15	5	4	8	0.5	Sandy loam
Bw-1	18–38	27	41	15	5	7	6	0.7	Sandy loam
Bw-2	38–46	39	53	3	1	1	4	0.7	Loamy sand
Bw-3	46–54	36	47	2	1	1	14	0.8	Sandy loam
2Bt1	54–75	19	33	11	4	6	27	0.6	Sandy clay loam
2Bt2	75–115	19	35	11	4	6	25	0.5	Sandy clay loam
2Bt3-1	115–123	18	36	13	3	7	23	0.5	Sandy clay loam
2Bt3-2	123–128	8	18	21	8	12	33	0.4	Clay loam

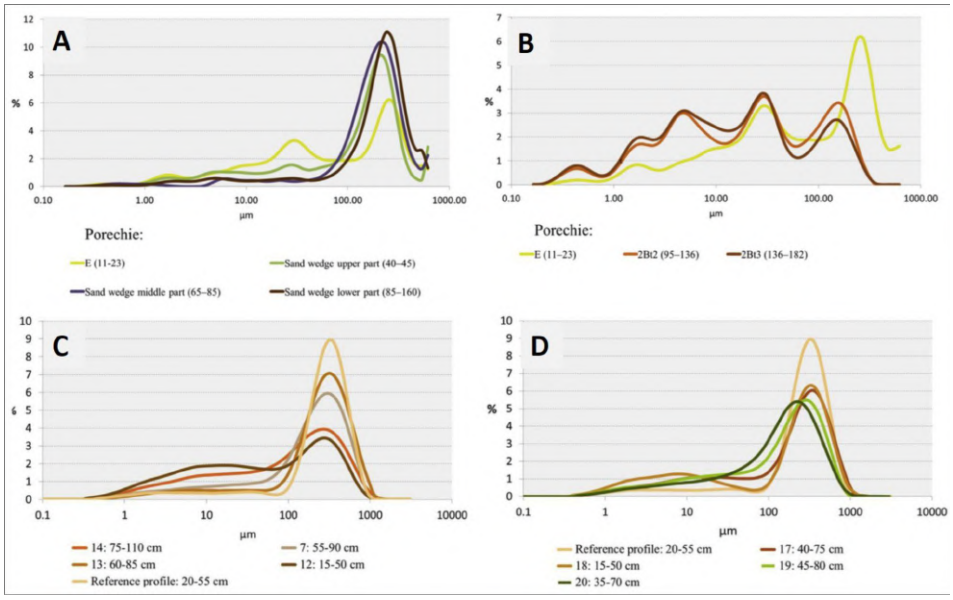

Figure 6.3. Grain size distribution, laser diffraction. a–b) Porechie key site: a) filling of the ice wedge with different materials compared to the cover layer (E horizon); b) the cover layer (E horizon) compared with the basal till (2Bt2 and 2Bt3 horizons); c–d) Novoselky key site. Grain size distribution in samples with fixed positions – 35 cm above the basal till: c) transect between the kame and moraine plateau; d) transect between the moraine plateau and outwash plain (see Fig. 6.2b for the numbers of soil pits).

Table 6.2. Total chemical composition in soils formed in bipartite sediments on the uplands, fine earth fraction, elements oxides, %

Horizon	Depth, cm	SiO_2	Al_2O_3	Fe_2O_3	CaO	MgO	MnO	TiO_2	ZrO_2	TiO_2/ZrO_2
Porechie reference profile, 135 m a.s.l.										
AE	5–11	86.62	6.87	1.41	0.63	0.37	0.02	0.68	0.09	7.936
E	11–23	88.83	5.77	1.06	0.57	0.30	0.02	0.49	0.07	6.589
2Bt1	40–95	75.51	12.11	5.55	0.80	1.59	0.11	0.72	0.04	18.631
2Bt2	95–136	69.49	10.49	4.76	7.83	3.23	0.07	0.62	0.03	21.692
2Bt3	136–182	69.23	10.65	4.25	8.03	3.63	0.06	0.58	0.03	20.464
Sand wedge middle part	65–85	92.86	3.59	0.76	0.41	0.19	0.01	0.15	0.02	8.042
Sand wedge lower part (loose)	85–160	93.20	3.46	0.68	0.39	0.20	0.01	0.14	0.02	8.286
Novoselky reference profile, 180 m a.s.l.										
AhB	3–18	88.86	5.78	1.60	0.40	0.33	0.13	0.40	0.04	10.054
Bw-1	18–38	89.02	5.52	1.56	0.43	0.33	0.13	0.40	0.04	9.682
Bw-2	38–46	93.02	3.58	0.76	0.33	0.20	0.01	0.17	0.02	7.764
Bw-3	46–54	88.79	6.24	1.70	0.29	0.49	0.02	0.31	0.02	17.244
2Bt1	54–75	82.65	8.48	3.56	1.15	0.86	0.08	0.60	0.04	13.326
2Bt2	75–115	81.39	9.78	3.85	0.58	0.88	0.03	0.57	0.04	14.228
2Bt3	123–128	79.59	11.22	3.97	0.52	0.94	0.03	0.68	0.04	15.701

Selected chemical features (Table 6.3). The profiles are medium to highly acidic, and the soil remains acidic throughout the entire solum. The humus content dramatically decreases with depth. The CEC is high in the upper horizons due to a high content of organic matter and in the 2Bt horizons due to an increase in clay. In the sandy streaks, the CEC drastically decreases. The exchange acidity shows a good correlation with pH. The differentiation of soil profiles by the total iron content is very pronounced, and it cannot be explained by the differentiation of free iron compounds. The total content of the free iron is relatively low and ranges from 20 to 40% of the total iron. The bleached horizons are slightly depleted of free iron. The oxalate-extractable iron constitutes 20–60% of the free iron (Fe_o/Fe_d). Based on the weathering index (Fe_d/Fe_t) that differs from 0.20 to 0.40 in all soils with variations less than 0.07 within the profile, we may conclude that the free iron is distributed in line with the distribution of the total iron. The distribution pattern is characterized by a distinct accumulation in the surface humus horizon and in the 2Bt horizons, especially in the 2Bt1. All sand wedges and streaks show a considerable decrease in all iron fractions. Though the sand wedge in the Porechie profile (90–115 cm) shows an increase in crystalline iron content (Fe_c).

Numerical dating of the cover layer on the uplands (Table 6.4). A large range of OSL dates is typical for the thin cover layer of bipartite sediments (Kabała et al., 2019). Thus, the sampling for OSL dating directly within the reference soil profile was rejected, and the samples were collected from pits with a higher thickness of the cover layer to avoid the influence of cosmogenic radiation and uprooting (Duller, 2008). Such positions were discovered during the field survey of the uplands. At the Porechie key site, two samples from the thick cover layer were taken in a pit within the supraglacial gully (at 37 and 63 cm, Fig. 16a). At the Novoselky key site, one sand sample was taken from the kame at 128 cm depth and the other two from the pit located in the transition zone from the moraine plateau to the kame (at 63 and 78 cm, Figs. 15a & 16b).

There the cover layer merges with the sediments of the kame gradually increasing in thickness. The dates of the cover layer vary from the Late Moscow (MIS6) for the samples below 70 cm to the Late Valdai (MIS2) for the samples above 60 cm. The relationship between the deposition of the cover layer and rewashing of the glacial till soon after its deposition suggests a time frame of 125–140 ka BP, the age of the Moscow deglaciation in the studied region (Astakhov et al., 2016; Ehlers et al., 2011; Svendsen et al., 2004).

Table 6.3. Selected chemical features in soils formed in bipartite sediments on the uplands

Horizon	Depth, cm	pH	C_{org}, g/100 g	CEC, meq/ 100 g	Exch. acidity, meq/100 g	$CaCO_3$, %	Fe fractions, g/kg		Weathering indexes		
							Fe_o	Fe_d	Fe_d/Fe_t	Fe_o/Fe_d	$Fe_c=Fe_d-Fe_o$
Porechie reference profile, 135 m a.s.l.											
AE	5–11	3.93	2.21	15.00	9.04	0	1.68	2.8	0.30	0.60	1.12
E	11–23	4.43	0.43	5.00	2.68	0	0.91	1.54	0.21	0.59	0.63
2Bt1 (uppermost parts)	23–40	5.33	0.03	16.25	5.37	0	4.41	16.59	–	0.27	12.18
2Bt1	40–95	5.14	0.15	20.00	2.68	0	3.85	14.28	0.38	0.27	10.43
2Bt2	95–136	7.10	0.15	18.75	<0.23	14.86	0.49	11.97	0.40	0.04	11.48
2Bt3	136–182	7.32	0.11	12.50	<0.23	18.27	0.42	10.43	0.39	0.04	10.01
Sand streak	90–115	5.60	0.07	6.25	0.83	0	0.08	0.56	–	0.16	2.94
Sand wedge upper part	40–45	4.68	0.19	2.50	2.25	0	0.17	1.19	–	0.52	1.12
Sand wedge middle part	65–85	5.28	0.10	2.50	1.03	0	0.06	0.42	0.30	0.26	1.19
Sand wedge lower part (firm)	85–160	5.56	0.09	2.50	0.96	0	0.08	0.56	0.19	0.62	0.35
Sand wedge lower part (loose)	85–160	6.43	0.07	6.25	0.78	0	0.03	0.21	–	0.19	0.91
Novoselky reference profile, 180 m a.s.l.											
OAh	0–3	4.92	4.61	–	11.27	0	0.36	0.59	–	–	0.61
Ah2B	3–18	4.80	1.03	–	6.11	0	0.40	0.69	11.20	0.06	0.58
Bw-1	18–38	5.06	0.5	–	4.05	0	0.37	0.62	10.92	0.06	0.60
Bw-2	38–46	5.37	0.15	–	1.63	0	0.06	0.20	5.32	0.04	0.30
Bw-3	46–54	5.38	0.34	–	5.03	0	0.23	0.70	11.90	0.06	0.33
Bt1	54–75	5.06	0.43	–	16.90	0	0.32	1.54	24.92	0.06	0.21
2Bt2	75–115	5.13	0.56	–	15.20	0	0.30	1.42	26.95	0.05	0.21
2Bt3-1	115–123	5.08	0.37	–	13.60	0	0.28	1.50	–	–	0.19
2Bt3-2	123–128	5.15	0.34	–	22.93	0	0.27	1.05	27.79	0.04	0.26

Nevertheless, we received a wider timespan with OSL dating. At the Novoselky key site, the deepest sample (170,893) has pIRIR and IR ages older than the period of deglaciation. It may be caused either by incomplete resetting of the OSL signal during the rewashing of the cover layer or by mixing of the cover layer with sediments of the kame since the sample was collected in the contact zone between the moraine plateau and kame of Moscow age. To evaluate the influence of such mixing, we dated reference sample 170,895, which was taken from the upper layer of kame. Sand from the kame showed an older age than the sample 170,893 confirming its formation before deglaciation, which is typical for sediments that

were transported subglacially in total darkness (Sidorenko, 1971). That reference sample made it possible to assert that the material of the cover layer was subject to resetting of the OSL signal during the rewashing since it shows the younger age. Otherwise, if resetting of the OSL signal was poor or absent, an older age comparable to the one of the kame sand should have been obtained for sample 170,893 as well.

Incomplete resetting of the OSL signal before the deposition is typical for the glaciofluvial deposits of the Saalian stage in Europe where OSL dates range between 150 and 190 ka BP (Lang et al., 2018). It can be caused by a specific depositional environment: turbid meltwater, high sedimentation rates, and short transport (Luthgens et al., 2010). For the cover layer, such a depositional environment is feasible due to the presence of unsorted sandy and silty patches with pebbles, the intermixture of sand and silt grains, and semi-rounded sand grains. The sandy composition of the cover layer at the Novoselky key site may indicate a rapid meltwater stream. Taking that into account, we may conclude that the OSL date for sample 170,893 confirms that the cover layer at the Novoselky key site was formed during the Moscow deglaciation.

It is important to note that the age of glacial till at the Borisoglebsk Upland where the Novoselky key site is situated is still under debate. According to the geological survey, the area was outside of the Early Valdai (Early Weichselian, MIS4) glaciation, so the glacial till was prior deposited by the Moscow glacier (State geological map of USSR. Quaternary deposits, O-37-XXVII, 1969; Shik, 2010). Another opinion is that it was deposited during the Early Valdai (Kalinin) glacial advance (Sudakova & Antonov, 2021). We believe that OSL dates for the Novoselky key site confirm the Moscow glacier to be the last in the area.

The samples from shallow depths (170,890, 170,896, and 170,894) showed younger ages for both Porechie and Novoselky key sites, which could have resulted from additional exposure of the grains to daylight caused by local rejuvenations or redeposition. One of the mechanisms is frost creep, which, according to Lorz et al. (2013), can occur on slopes of 1–2°. The authors showed frost creep to form a stoneline, with scratched faces of stones appearing between the moving layers of glacial till. Stonelines in the Novoselky profile show no scratched faces, so we suggest they appeared during the deposition of the cover layer.

The second mechanism of rejuvenation is bioturbation, especially uprooting, which may rework the upper soil horizons in the forest zone to a depth of up to 50 cm in 2000 years, penetrating locally even deeper (Karpachevsky et al., 1978; Basevich & Dmitriev, 1979; Skvortsova et al., 1983). Field morphology allows us to evaluate the uprooting impact on the initial bedding of the cover layer.

The old age of sample 170,893 from the 78 cm depth and the presence of the undisturbed sandy interlayer (Bw3 horizon, Fig. 6.1b), initially formed by meltwater rewashing, confirm that uprooting influenced only the upper part of the cover layer. The undisturbed stoneline located within the cover layer above the glacial till (Fig. 6.1b) also indicates that uprooting was not intense below the top of the latter. Glacial till stability after the deglaciation is also confirmed by vertical cryogenic wedges unaffected by shearing processes (Makeev et al., 2019). The partial resetting of the OSL signal due to the exposure to daylight by uprooting can lead to the intermixing of "young" and "old" grains. We consider the silty eolian patches of the cover layer to be the main source of such "young" grains. Those patches could be the remains of the upper cover layer that has been deposited after the deglaciation during MIS2 in a cold and windy environment and is described for the vast periglacial area of the Weichselian glaciation: the upper layer of periglacial cover beds (Lorz et al., 2013; Terhorst et al., 2013) or the landscape-wide eolian drapes (Gild et al., 2018). The exact match of the quartz and pIRIR ages also refers to the perfect resetting of the OSL signal because of the long exposure of the grains to daylight, which is typical for eolian sediments (Duller, 2008). Unfortunately, there are no

published OSL dates for such silty layers of the uplands at the Russian Plain yet a similar layer of silt was described at the Pleistocene Volga River terraces dated to the Late Glacial (Panin et al., 2018). The Late Glacial silty eolian cover layer was later disturbed by intensive bioturbations that are well seen within the upper 30 cm in both profiles: the irregular pattern of platy structure and coprolites.

DISCUSSION

Constitution and timeframe for bipartite sediment deposition and *in situ* transformation. Bipartite sediments of the Moscow age are spread almost uniformly on uplands and slopes within the area of Moscow Cryochrone covering up to 20% of the territory (State Soil Map of USSR, 1949–1958). In the area of a two-day field tour, bipartite sediments mantle the uplands and bedrock terraces of the Volga River valley. The glacial till exhibits a similar set of features related to several stages of its deposition and transformation:

1) pre-depositional features (Moscow time, MIS6): a) inherited from the material mobilized by the glacier (red-brown color, high weathered matrix, and dispersed stones); and b) resulting from sediment transport with the glacier (homogeneous matrix as a result of effective mixing; overconsolidated matrix; sand filling of glacial cavities and streaks);

2) syn-depositional (Late Moscow time, MIS6 – MIS5 transition) features: a) primary structural units that appeared in the massive glacial till with low subglacial water content during its deposition; b) cover layer of the glaciofluvial origin formed either due to the flood washing of the glacial till by streams from adjacent dead-ice bodies or due to passive imposition of the particles suspended in the dead-ice body during its degradation. Fragmentary silty patches and/or admixture of silt in the sandy cover layer are considered a result of the additional eolian input during the syn-depositional stage;

3) post-depositional features: argic horizons formed in glacial till from the Last Interglacial to the Holocene; embedded soil profiles within the cover layer; cryogenic features of the Valdai (Weichselian, MIS4 / MIS2) time.

Table 6.4. OSL dates of the cover layer on the uplands

Lab #	Depth, cm	Age ka: Quartz, preheating at 320C°, pIRIR$_{290C°}$	Age ka: IR$_{50C°}$	Quartz: Doze Gy	Quartz: Dose rate Gy/ka	Feldspar: pIRIR290C Doze Gy	Feldspar: IR50C° Doze Gy	Dose rate Gy/ka	Water content %
Porechie key site, 135 m a.s.l.									
170,896	37	**15.35±1.0**	**17.59±1.4**	**12.86±0.9**	32.7±1.6	2.13±0.08	53.92±3.93	39.42±2.29	3.07±0.10	25
170,890	63	**17.52±1.0**	**19.41±1.2**	**15.46±0.8**	24.9±1.0	1.42±0.05	45.7±2.1	36.4±1.4	2.36±0.08	25
Novoselky key site									
170,894	63	**22.58±1.28**	**22.71±1.96**	**16.86±0.83**					
170,893	78	–	**210.21±10.81**	**157.63±9.37**					
170,895	128	–	**276.50±26.81**	**214.86±10.81**					

Timeframe for the cover layer. Despite the similarity of the glacial till, the cover layer on uplands and terraces differs substantially in its transformation during the Last Glacial-Interglacial Transition (c. 20–10 ka). On the terraces, the upper part of the cover layer was substantially reworked by fluvial and eolian processes. On the uplands, a limited eolian input contributes to the deposition of silty material in the upper part of the cover layer. Due to bio-, cryo-, and pedoturbations, that thin silty layer is mixed with the sandy-silty material of the Late Glacial cover layer and remains mostly as silty patches and, in a rare case, as a silty eolian layer. For instance, silty eolian layers up to 50 cm thick on top of glacial till are described in the Netherlands (Jongmans et al., 1989) and in the Vladimir Opolie (Makeev et al., 2015). At the Porechie key site, the cover layer is a silty layer on top of a sandy one at the highest positions of the uplands. The activation of eolian activity is linked to the cold and dry Late Glacial environment. In Western Europe, the silty eolian cover layer is a mandatory member of the periglacial cover beds ("upper layer", Kleber & Terhorst, 2013; "eolian drape", Gild et al., 2018). There are no numerical dates for the cover layer in Western Europe. Based on the fact that the Lacher See tephra (12.9 ka) could underlay the upper layer, its deposition is linked to the Late Glacial.

The first OSL dating performed for the cover layer of the bipartite sediments was obtained from the frost wedge infilling, giving a date of 8.9 ka (Mokievsky et al., 2023). At Selishi and Porechie key sites, dates for the cover layer on the terraces and upland range 12–17 ka (Tables 4.3 and 6.4). Taking into account that the dating material from a shallow depth could be contaminated by both "young" and "old" grains, we may assume that the eolian input in the cover layer of the uplands and terraces happened about the same period during the Late Glacial time. It is widely accepted that the uplands in the areas of the Moscow Cryochrone have been deeply transformed by slope processes, resulting in the leveling of hills and the development of the slope mantle.

Nevertheless, the mantle distribution of bipartite sediments with the cover layer deposited during the Middle Pleistocene deglaciation indicates that moraine uplands were only locally influenced by slope processes and kept records of all depositional episodes.

The mantle distribution of bipartite sediments in other areas of the Moscow Cryochrone was described based on an interdisciplinary approach: geological, geomorphological, paleogeographic, and paleopedological methods including soil survey, GPR, and absolute dating (Makeev et al., 2019; Kust et al., 2022). OSL dates, being among the first for the bipartite sediments, in conjunction with GPR investigations, confirm the stability of the glacial till and cover layer (with only local rejuvenations) since their deposition.

In-situ transformation of the bipartite sediments. The Moscow age of glacial till and cover layer indicates that the bipartite sediments could have been subject to pedogenesis and periglacial processes since the end of Moscow time. Thus, cryogenic and polygenetic soil features of different times, from the last interglacial to the Holocene, could be recorded in soils in the bipartite sediments. If so, the bipartite sediments could have recorded paleoenvironmental trends within the last Interglacial-Glacial cycle. They keep evidence of the pedogenesis of the last Thermochrone (MIS5e) when well-developed argic horizons were formed, the frost features of the last Cryochrone, and the Holocene pedogenesis.

High stability of the intrapedal mass of the glacial till was confirmed based on morphology, micromorphology, microtomography, and clay mineralogy (Kust et al., 2022). Thus, the grain size distribution, composition of clay minerals, color, and pattern of porosity are relic pre-depositional features that have been only slightly changed by pedogenesis. Based on the AMS dating and conjoint morphology, we may conclude that clay illuviation started during the last interglacial (MIS5e). The share of Holocene illuvial clay was limited, and clay-humus

coatings originated mostly from the disintegrated glacial till fragments incorporated into the cover layer by bioturbations.

A comparison of argic horizons formed in the glacial till overlain by shallow and thick cover layers (Selishe-1 and Selishi-2 reference profiles) provides another piece of evidence of the pre-Holocene pedogenesis in the bipartite sediments. The glacial till in the Selishi-2 profile is outside the impact of pedogenetic processes since its deep burial at the Late Glacial. While in Selishi-1 and similar profiles on the uplands, it was continuously subjected to pedogenesis. Nevertheless, the argic horizons in both profiles exhibit a similar set of morphological features, in particular the complex of clay coatings that start immediately at the top of the glacial till horizons (Figs. 4.5 & 4.8). Clay coatings in both 2Bt1 and [2Bt1gb] horizons are typical for soils formed in a temperate climate (Gerasimova et al., 1996). Such a climate is known from the Last Interglacial (MIS5e, Velichko et al., 2006). Together with other similar soil properties, we may conclude that the glacial till in both profiles went through similar stages of soil formation. Recently, the Eemian age for the argic horizons was advocated for the Saalian areas in Poland (Kabala et al., 2022; Woronko et al., 2022).

The sharp boundary between the cover layer and glacial till remains undisturbed by pedogenesis (Figs. 4.5b & 4.8b). It matches the initial boundary of the cover layer, and the glacial till is also evidenced by firm sand layers and stonelines (Fig. 6.1b). However, the boundary could be disturbed by cryo- and bioturbations resulting in the mixing of the glacial till and cover layer (*retic* properties, IUSS Working Group WRB, 2022). During the Valdai (Weichselian), bipartite sediments experienced a cryogenic impact, which resulted in a network of frost wedges and fissures (Fig. 5.3).

Pedogenesis in the cover layer has resulted in a set of embedded soil profiles that developed in balance with the modern bioclimatic environment and quickly reached a steady state. Pedogenetic processes with short characteristic times include the redistribution of iron and the accumulation of organic matter while the texture and clay minerals are mostly the inherent features only slightly modified by pedogenesis.

GENERAL STRATIGRAPHY OF POSTGLACIAL SEDIMENTARY COVER OF VLADIMIR OPOLIE

August 29, 2023

At the southernmost range of mantle loams distribution, so-called loess islands (Makeev, 2012) show some resemblance to the profound loess-paleosol sequences of the extra-glacial areas (Velichko, 1990). They commonly occupy relative topographic highs that inherit pre-Quaternary erosional uplands capped with thin glacial tills (Fig. G). In contrast, surrounding lower-lying outwash plains are majorly devoid of the loamy cover representing the easternmost branch of the European eolian sand belt (Zeeberg, 1998).

Considered one of the largest loess islands on the Russian Plain, a plateau referred to as the Vladimir Opolie rises to 232 m a.s.l. (Fig. E). Its flat and gently sloping watersheds are composed of MIS6 glacial till hooded by a thick loess-like loamy cover (State geological map of Quaternary deposits, O-37-XXXV, 1968). A number of archeological sites reflect the prolonged human occupation history of the area since the Early Paleolithic (Sukachev et al., 1966; Kuzmin et al., 2014) corroborated by the high degree of anthropogenic deforestation and large plowing coverage since the Early Mediaeval time (Makarov et al., 2017, 2020; Dobrovolskaya et al., 2020). And as the former has triggered a thorough examination of postglacial sedimentary exposures in the region (Tseytlin, 1965; Sukachev et al., 1966; Moskvitin, 1967; Velichko et al., 1996a,b; Alifanov et al., 2006, etc.) the latter has presented an opportunity of investigating the spatial landscape heterogeneity of extensively cultivated fields (Velichko et al., 1996a,b; Alifanov, 1995; Zhurbin & Fedorina, 2017; Ovchinnikov et al., 2020, etc.).

Thereof intrinsic heterogeneity of loess-like mantle and soil cover was argued concerning the postglacial landscape dynamics (Makeev & Dubrovina, 1990; Gugalinskaya, 1997; Kleber & Gusev, 1998; Gugalinskaya & Alifanov, 2005; Makeev, 2009, 2012; Makeev et al., 2015). Late Pleistocene periglacial phenomena were considered to have played an important part in differentiating deposition and pedogenesis and creating fine geological and landscape patterns (Berdnikov, 1976; Velichko et al., 1996a,b; Alifanov, 1995; French, 2007; Kabała et al., 2022; Woronko et al., 2022, etc.).

A.A. Velichko distinguished three paleocryogenic horizons in the loess-like mantle. The oldest Smolensk horizon indicated mostly by solifluction features was referenced to the Early Glacial. The overlying Vladimir horizon is considered to be of the late Middle Valdai (28–23 ka) (Velichko et al., 1996a,b) or the early Late Valdai (Velichko et al., 2006, 2011) age includes both solifluction and cryoturbation footprints and wedge-shaped deformations in the southern regions. Pronounced thermal contraction cracking of the latest Yaroslavl horizon manifests in two separate phases reflecting the Late Pleniglacial (LGM) and Late Glacial (Younger Dryas) coolings respectively (Velichko et al., 1996a,b, 2006). However, Sycheva et al. (2020, 2021) argued for the LGM timing of the Vladimir horizon with both stages of the Yaroslavl horizon bound to short Late Glacial coolings.

A series of buried paleosols intercept the sedimentary sequence of cold epochs with remnants of the Mikulino (MIS5e) interglacial, Krutitsy (MIS5d), and Bryansk (MIS3) interstadial pedogenesis (Velichko, 1958; Velichko et al., 1996a,b). Velichko et al. (2011) consider two MIS5 paleosols of the Mezin soil complex to be disturbed by the Smolensk cryogenic deformations. Bryansk paleosol with low organic content, thereby, reflects the late MIS3 relative warming accompanied by Vladimir cryogenic deformations. Overlying thick MIS2 deposit hosts 2 phases of Yaroslavl wedge casts maintaining both dark relict humus horizon (RHH) and actual soil cover. Although the origin of RHH is still controversial passing

either as Late Glacial (Gugalinskaya & Alifanov, 1995; Gugalinskaya et al., 2001; Makeev, 2009; Makeev et al., 2015) or Holocene (Alexandrovskiy, 1996) in age, its contemporaneous spatial differentiation is distinctly bound to the polygonal net of Yaroslavl wedge casts. Soils with RHH qualified as *Mollic* and *Gleyic Luvisols* are associated with polygonal troughs while polygon interiors are occupied by *Calcic Luvisols* without RHH (Makeev, 2012; Makeev et al., 2015). The former have higher organic matter content and are almost devoid of carbonates compared to the latter where both the matrix is calcic and carbonate nodules occur.

Nodes of polygonal wedge troughs are often occupied by rounded depressions 30–50 cm deep and 10–20 m wide (Makeev et al., 2015). On slopes, the polygonal pattern usually transforms into soil stripes or dells (Antonov et al., 1992; Czudek, 1993; Eremenko et al., 2010; Sycheva et al., 2020; Khudyakov et al., 2020) that are thought to inherit the wedge troughs running downhill and occasionally utilized by linear erosion. However, majorly smoothed in the modern topography of gently sloping arable fields, those polygonal and linear patterns are still emphasized exclusively by soil and vegetation cover variations (Velichko et al., 1996a,b). Reflected in spectral characteristics of satellite and aerial images, such landscape patterns are addressed as cropmarks (Andrieux et al., 2016a,b; Ewertowski et al., 2017) and used as indicators of the past periglacial condition.

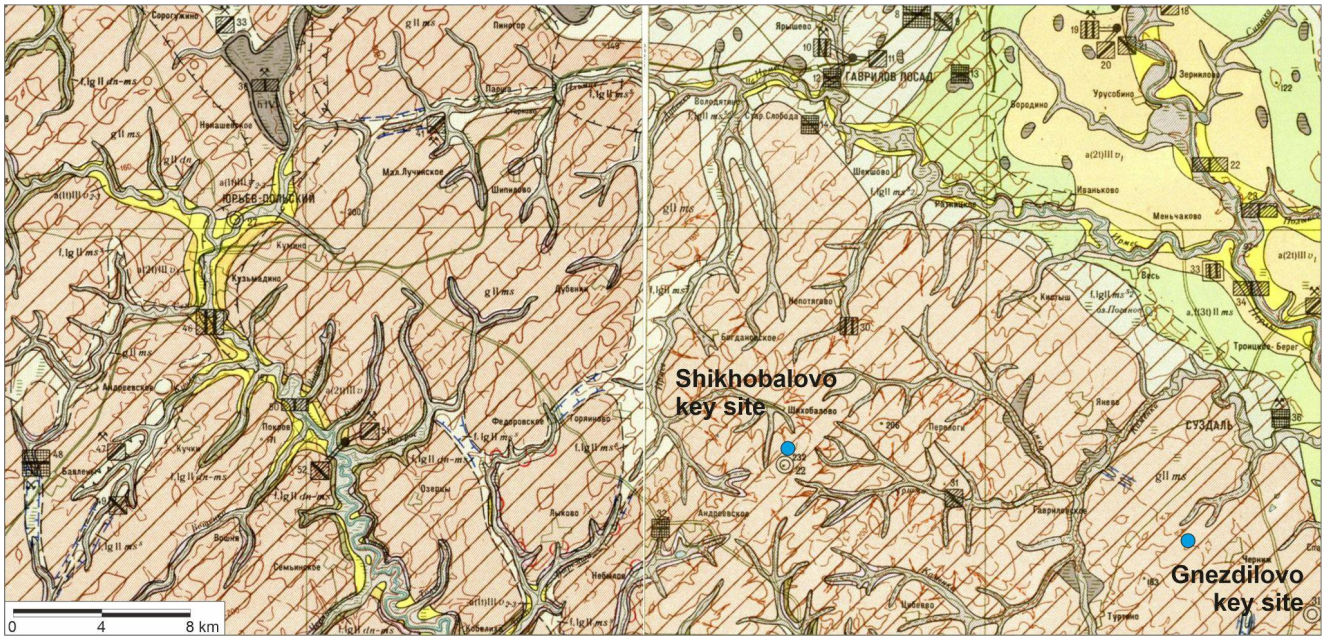

Figure G. State geological map of USSR. Quaternary deposits. 1:200000, O-37-XXXIV and O-37-XXXV, 1968. *Light pinkish color* – pre-Quaternary rocks; *gIIdn* – glacial till, Dniepr time; *f,lgIIdn* – glaciofluvial deposits of the glacial retreat, Dniepr time; *f,lgIIdn-ms* – glaciofluvial, fluvial, lacusrine, and palustrine deposits of the glacial retreat, Dniepr-Moscow time; *gIIms* – glacial till, Moscow time; os,kamII*ms* – glaciofluvial deposits of eskers and kames, Moscow time; *a,f,lgIIms*^{max} – alluvial and glaciofluvial deposits of glacial maximum, Moscow time; *f,lgIIms*^{ep} – deposits of supraglacial meltwater channels and lakes, Moscow time; *f,lgIIms*^{s1} – glaciofluvial deposits of the early stages of glacial retreat, Moscow time; *f,lgIIms*^{s2} – glaciofluvial deposits of the late stages of glacial retreat, Moscow time; a,f(3t)II*ms* – fluvial and glaciofluvial deposits of the 3rd terrace, Moscow time; *a,l,hIIImk* – fluvial, lacustrine, and palustrine deposits, Mikulino time; *a(2t)IIIv*$_1$ – fluvial deposits of the 2nd terrace, Early Valday time; *a(2t)IIIv*$_{2\text{-}3}$ – fluvial deposits of the 1st terrace, Middle–Late Valday time; *prIIId* – undistinguished complex of periglacial (watershed cover, colluvial and fluvial-colluvial) deposits, Valdai time; *hIV* – palusrine deposits, Holocene; *aIV* – floodplain deposits, Holocene.
Blue dashed double lines – glacial meltwater channels.

STOP 7. SURFACE SOILSCAPE PATTERN OF SHIKHOBALOVO PLATEAU
August 29, 2023, afternoon

Shikhobalovo key site. High flat interfluves covered by loess: opolies (from the Russian word polie, "field") are common for the periglacial area. All landscape components (parent rocks, vegetation, soil cover) in opolies differ from those in surrounding moraine plains and glaciofluvial lowlands. The Vladimir Opolie is a typical loess island, 50–60 km in diameter, located about 200 km to the east of Moscow. It is a pre-Quaternary erosional plain with an elevation of 130–230 m above sea level. The topography of the pre-Quaternary surface is very similar to the modern surface, indicating that it was only slightly influenced by the Dnieper and Moscow (Saalian I–II) ice sheets (State geological map of USSR. Quaternary deposits. O-37-XXXIV, 1968). The eroded surface of Cretaceous sediments is covered by occasional Oka deposits and more widely spread Dnieper glacial deposits. The glacial till of the Moscow (Late Saalian) ice sheet is present almost universally, forming a 10-m thick mantle. It is covered by a complex of glaciofluvial sediments from the time of the Moscow glacier retreat. They are present both on the uplands and in the bottoms of gullies, indicating that the development of modern topography was accomplished by the end of the Moscow Cryochrone. The surface sediments of the Vladimir Opolie are represented by a loess mantle, 3–5 m thick, that covers the uplands and slopes within an interval of 110–230 m a.s.l. (Fig. 7.1). Vladimir Opolie is characterized by extensive uplands with lengthy slopes, which give the impression of flat surfaces. On the other hand, the territory is incised by systems of paleogullies with a density coefficient of 0.9–2 km/km².

The common feature of the Vladimir Opolie is that it was deeply influenced by the periglacial environment (Alifanov, 1995; Alifanov et al., 2010; Velichko et al., 1996; Makeev & Dubrovina, 1990; Makeev, 2012; Makeev et al., 2015). As a result, the surface of the loess islands is complicated by thermokarst: rounded depressions 30–50 cm deep and 10–50 m wide occupy 20–30% of the terrain, forming a rectangular network. A part of depressions is more than 1 m deep. Two types of microtopography, both related to the Yaroslav cryogenic stage of the Last Glacial Maximum (Velichko et al., 1996), were identified in the Vladimir Opolie: a) polygonal blocks surrounded by gullies with pseudomorphs substituting former ice wedges. Closed thermokarst depressions are formed at the intersections of gullies; b) shallow closed depressions are supposedly related to isometric ice lenses. On most of the arable lands, the thermokarst topography is leveled by cultivation. The deep depressions are not cultivated due to perennial waterlogging.

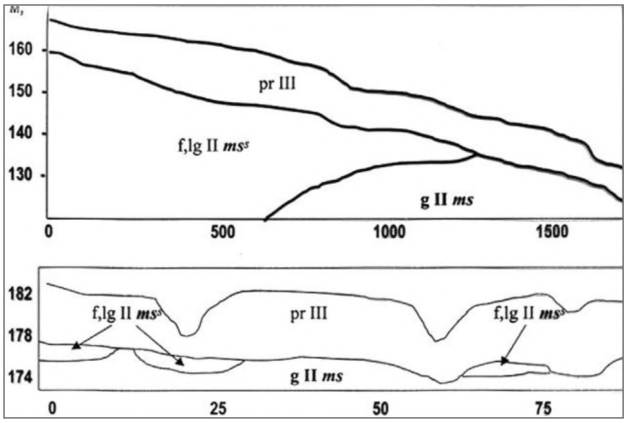

Figure 7.1. Mantle loams (pr III) on top of glacial till of Moscow (Saalian II) Cryochrone (gIIms) and glaciofluvial and limnoglacial sands of Moscow glacial retreat (f,lg IIms5). Archive of Centrgeologia geological survey, Moscow.

The climate of the area is moderately continental, with warm and humid summers, cold winters, and well-pronounced spring and autumn seasons. The mean annual air temperature is 4.5 °C. The sum of temperatures above 10 °C equals 1900–2000°. The duration of the frostless period only slightly exceeds 3 months. The soil is usually frozen to a depth of 75 cm in the second half of the winter; during extremely cold winters, the depth of freezing reaches 140–150 cm. Full thawing usually

occurs on 20–30 April. The mean annual precipitation is about 550 mm. The major part of the precipitation (70%) falls during the warm period. The maximum depth of snow cover is about 30 cm. The mean annual evaporation to precipitation ratio is about 1.3–1.4.

The Vladimir Opolie is a part of the southern taiga vegetation subzone with its mixed coniferous–broad-leaved and hardwood forests. Loess sediments predetermined high soil fertility and, hence, the ancient cultivation of the area and the lack of forest vegetation at present. Up to 80% of the terrain is represented by arable lands. Natural vegetation is preserved only in gullies and boggy depressions.

The soilscape pattern of Vladimir Opolie is determined by the topographic pattern. On cultivated surfaces under fallow, soil complexes are marked by color: microdepressions are gray and dark gray against the light gray-brown background (Fig. 7.2). Soils have texturally differentiated profiles meeting the criteria for *Luvisols* (IUSS Working Group WRB, 2022). Three soil profiles formed in different microtopographic positions are demonstrated within the high flat upland in the center of the Vladimir Opolie, 2.5 km SE of the Shikhobalovo settlement (56.410447° N, 40.111271° E).

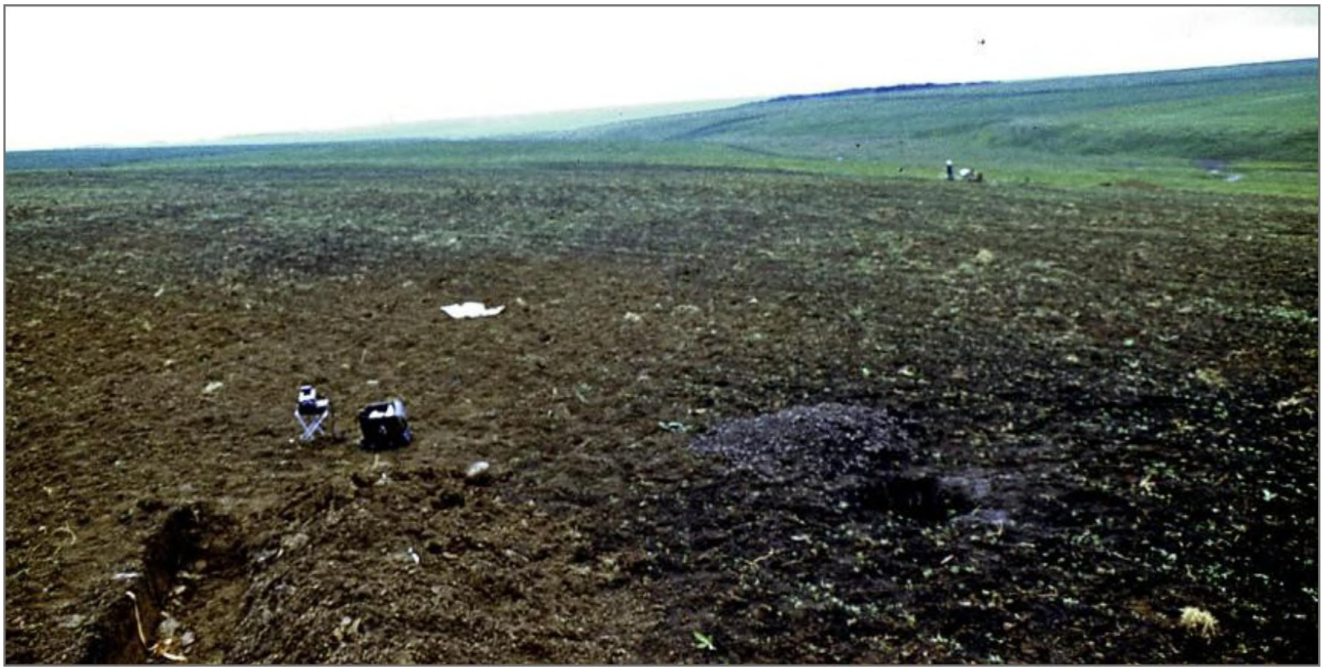

Figure 7.2. Soilscape pattern of the Vladimir Opolie. Microdepressions are marked by dark color due to the admixture of buried humus horizon into the plow layer.

Field morphology

Soils within depressions have the sequence of horizons: *Ap (Ah in virgin soils)–Ahb–[E, E/Bt]–Bt1–Bt2–Bt3–BtC–C, Haplic Luvisol Siltic, Cutanic, Thaptohumic.* Humus horizons of virgin soils are brownish-gray (10 YR 5/2), friable, with fine granular structure, about 15 cm thick, and have a wavy lower boundary. Plow layers are brownish-gray (10 YR 5/2), compact, and have an abrupt lower boundary. The presence of the buried humus horizon (Ahb; termed a "second humus horizon" in Russian publications) is a characteristic feature of soils in microdepressions. In virgin soils, it starts directly below the plow layer at a depth of 15–25 cm (Fig. 7.3a). Lenses of the buried humus horizon have a thickness of up to 40 cm (in centers of depressions) gradually wedging out toward the background surfaces (Fig. 7.4). The dark-gray to almost black (10 YR 3/1; 3/2) Ahb horizon has distinct upper and lower boundaries.

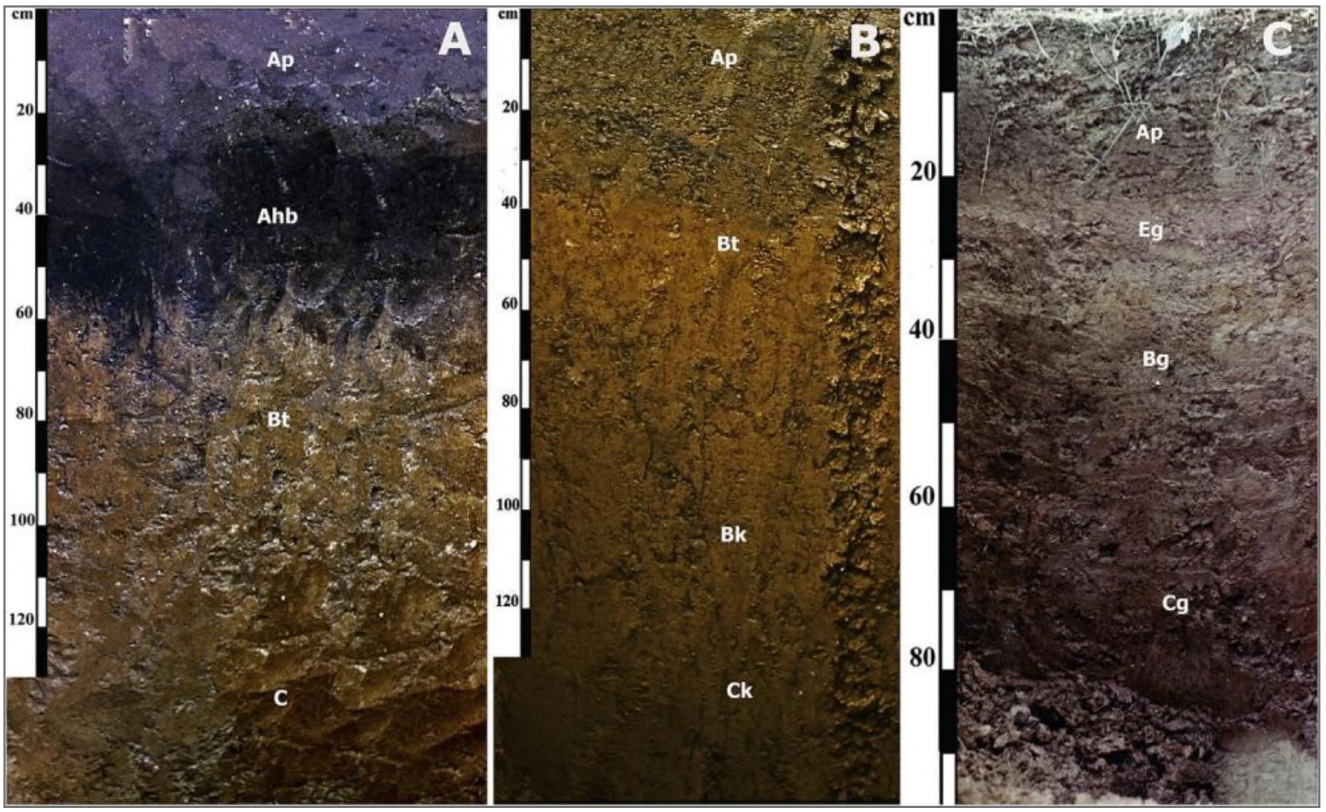

Figure 7.3. Soils of contrasting positions (Yuriev-Polsky key site): a) in the center of microdepression; b) on the polygonal block; c) in the center of deep depression.

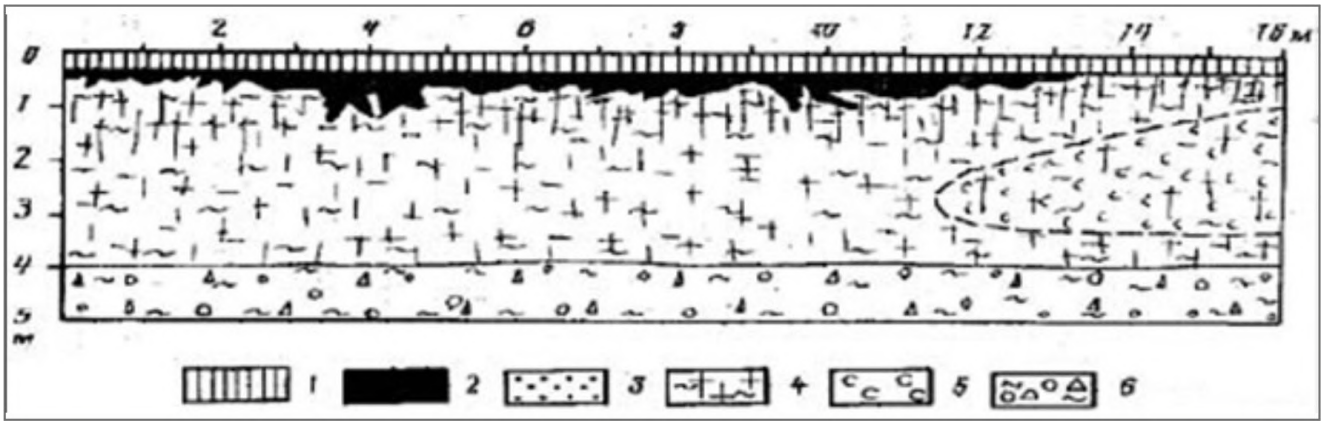

Figure 7.4. Soils of the upland with paleocryogenic microtopography formed in the upper loess layer underlain by glacial till, Shikhobalovo key site. Soil horizons: *1* – Ap; *2* – Ahb; *3* – EBt; *4* – Bt; *5* – Btk; *6* – glacial till.

Its uppermost part is often admixed into the plow layer. The Ahb horizon is characterized by granular or fine subangular blocky soil structure and high porosity. Ped faces are covered by thin skeletans. The lower boundary of the Ahb has a fringed-like shape complicated by a network of small ground fissures (moliglossic features, according to the IUSS Working Group WRB, 2022) penetrating the underlying horizon to a depth of 20–40 cm (Fig. 7.5a, b).

The width of the tongues in the upper part is about 10 cm. Somewhat bigger and deeper fissures (>1 m deep) complicated by smaller branches can also be found (Fig. 7.5a). There are also pseudomorphs on the former ice wedges filled with material from the Ahb horizon. These pseudomorphs with branching boundaries can be up to 1 m wide and may have subhorizontal branches (Fig. 7.5d, e).

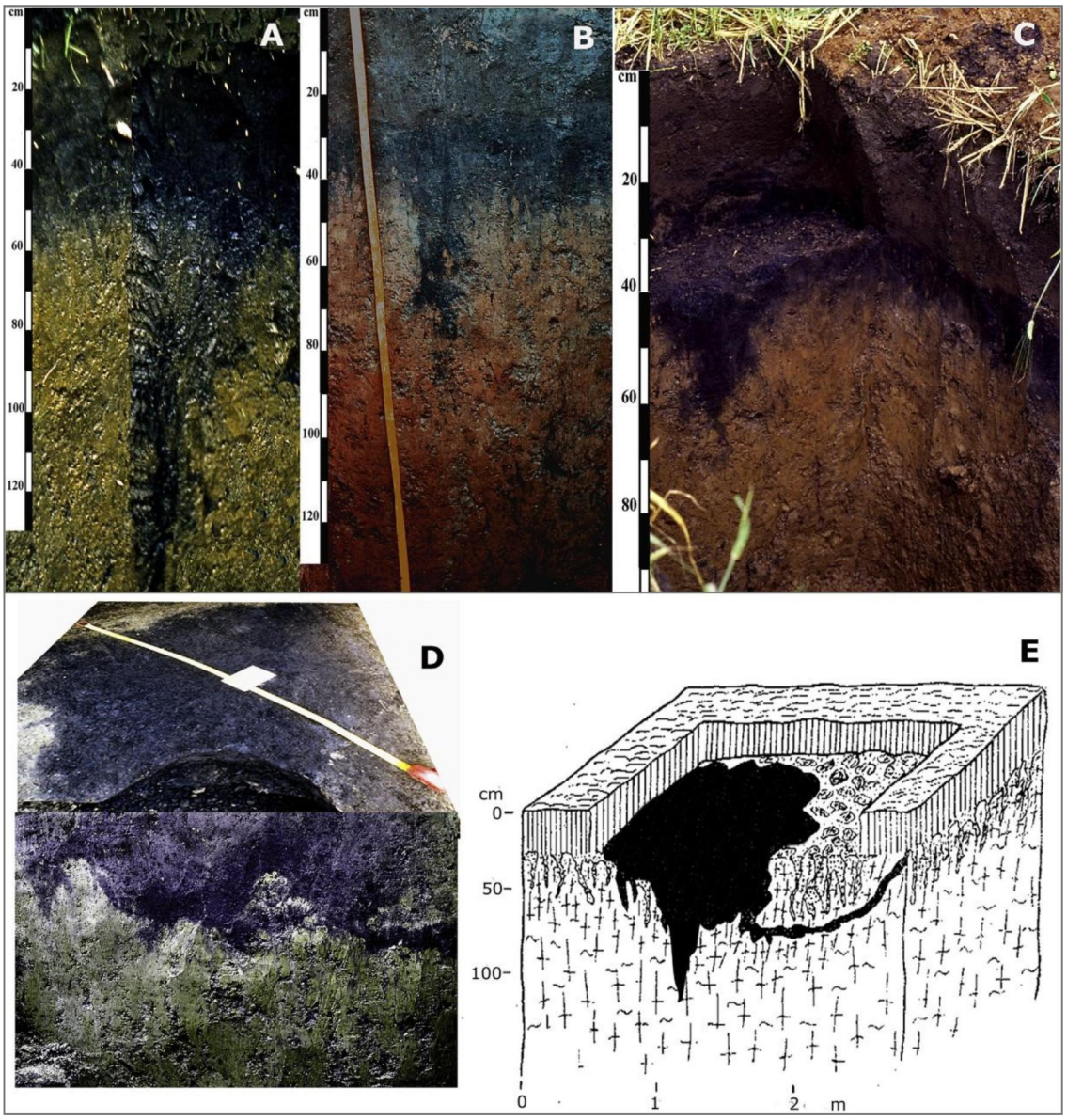

Figure 7.5. Cryomorphic features on the lower border of a buried humus horizon.

Ahb horizons are marked by a high content of phytoliths, which compose a considerable part of sand and silt particles (Makeev, 2012; Makeev et al., 2015). The microfabric of Ahb is different from that of upper humus horizons (Fig. 7.6). Ahb horizons are better aggregated (with the predominance of coagulated compound microaggregates) and have a higher porosity with the predominance of rounded pores-chambers. The microfabric is rich in black humus homogenous aggregations with distinct boundaries among light gray microfabric. Black microfissures and humus coatings on mineral grains and pore walls, as well as humus infillings, are common for the Ahb horizon. The bottom boundary of Ahb horizons is often underlain by a fringe of whitish (10 YR 7/2) material (E horizon) with a cloddy-platy structure. A sequence of argic horizons with typical diagnostic features follows below. They are silty-clay in texture, with the structure merging downward from fine to coarse subangular blocky and prismatic, with clay coatings and skeletans, especially abundant in Bt1 horizons (Fig. 7.7). Redoximorphic features are common below 120–150 cm.

Soils on polygonal blocks never have buried humus horizons, which are wedged out on the microslopes of the blocks. The soils of the blocks have the following sequence of horizons: *Ap (Ah in virgin soils) Bt1–Btk2–Btk3–BtCk–Ck, Calcic Luvisol, Siltic.*

The humus horizon of virgin soils is brownish gray, with a fine subangular blocky structure and a rather loose fabric. In arable soils, the upper part of the argic horizon is often incorporated into the plow layer. Compared to depressions, the argic horizon in soils on the blocks is lighter in color (10 YR 5/4), less aggregated, and with fewer cutans. Carbonates start at a depth of 80–100 cm (sometimes, from 50 cm). They are presented by primary (small rock debris, limestone, and dolomite grains) and secondary carbonate accumulations (hard nodules, soft segregations, calcified grassroots, and impregnation of the matrix, Fig. 7.8). On the slopes of microdepressions, the depth to carbonate table sharply increases (Fig. 7.4).

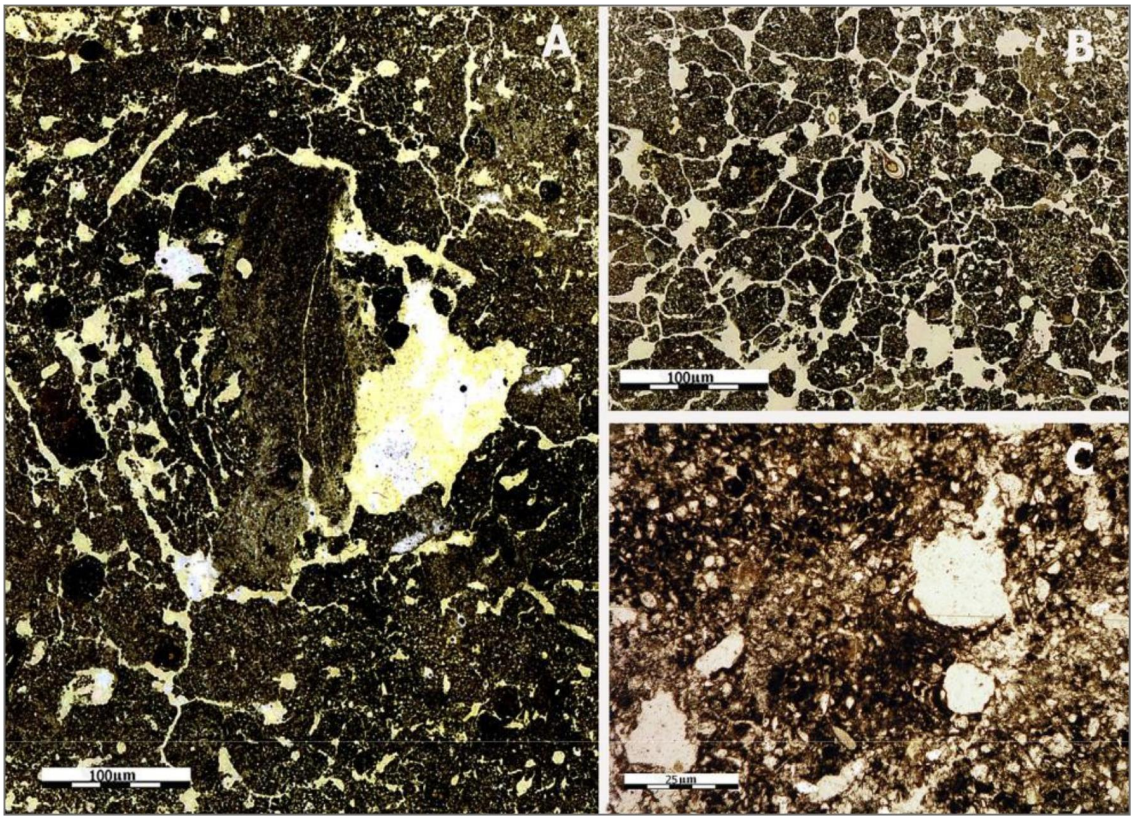

Figure 7.6. Micrographs of buried humus Ahb horizons, Shikhobalovo key site. Note heterogeneity and mobility of humus-enriched microfabric and inclusions of charcoal.

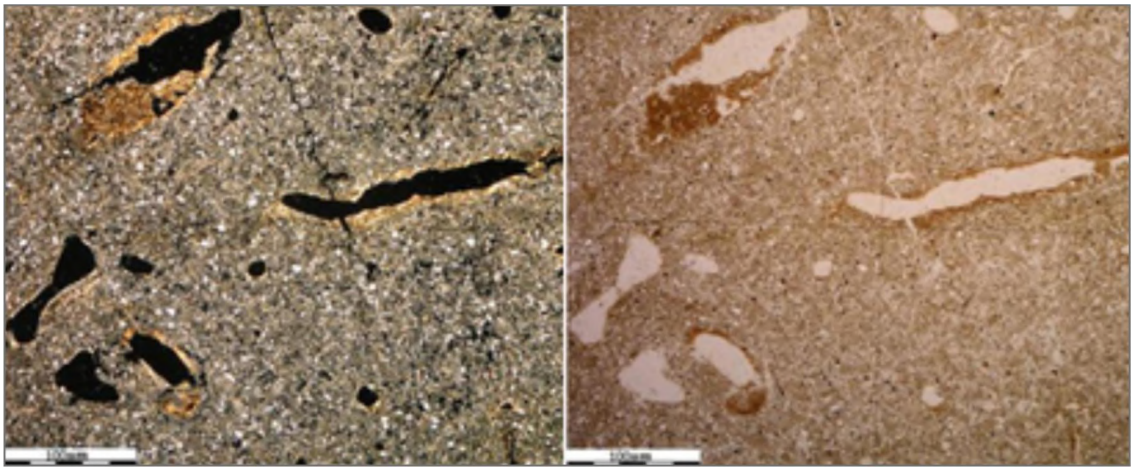

Figure 7.7. Micrographs of Bt1 horizon, Shikhobalovo key site. Note compact microfabric, high birefringence of plasma, and clay cutans. Left side – crossed polarized light, right side – plain polarized light.

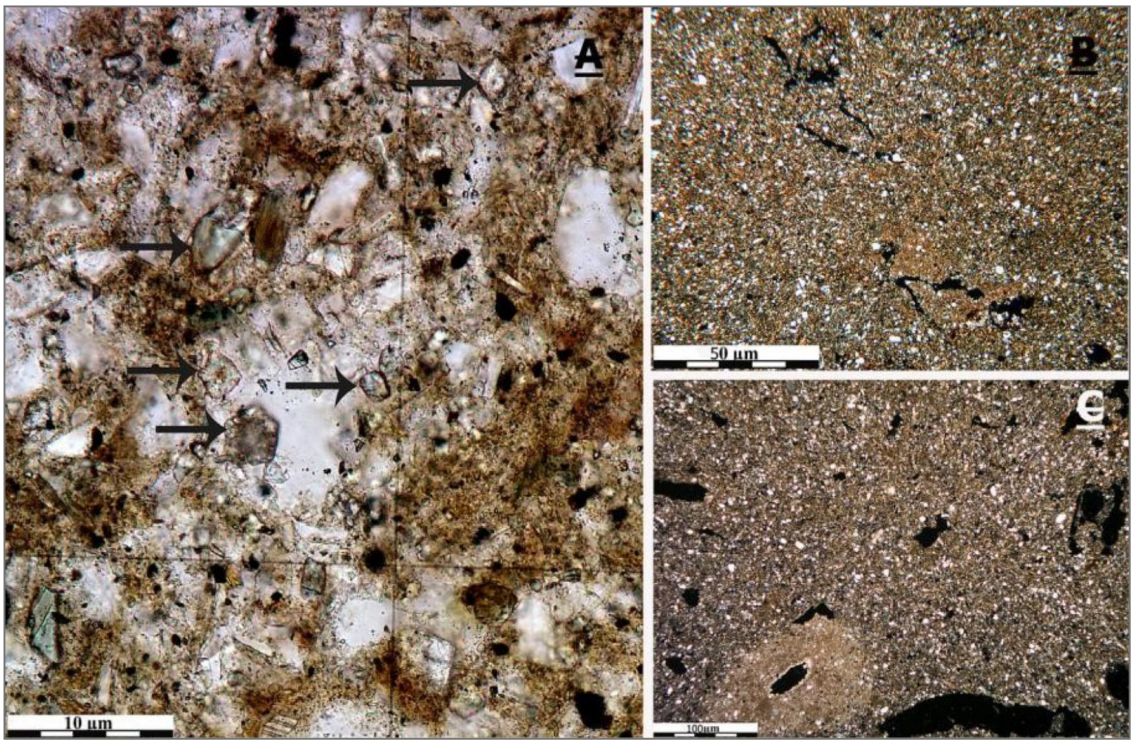

Figure 7.8. Micrographs of carbonate horizons in soils of the polygonal blocks, Shikhobalovo key site: a) calcite grains (coarse silt size, marked by arrows, plain polarized light); b–c) carbonate nodules and impregnation of microfabric, crossed polarized light: b) 100–120 cm; c) 155–200 cm.

Soils of deep depressions have neither buried humus nor carbonate horizons meeting the criteria for *Gleyic Luvisols* with the following set of horizons: *Fo–Ahg–Eg–Bt1g–Bt2g–BCg* (Fig. 7.3c). The above-described soil pattern is typical for the entire area covered by mantle loams, both in the central part and periphery of the Vladimir Opolie.

Analytical properties

Grain size distribution (Table 7.1) confirms the similarity of mantle loams with other sediments of the loess formation. The coarse silt (0.05–0.01 mm) is dominant in all horizons. Sand content is low. Textural differentiation is marked by grain size distribution, with clay content (<0.001 mm) in the upper horizons (silty clay loam) being half that in the lower part (silty clay). The clay content in the plow layers in the soils of the polygonal blocks is somewhat higher than that in the soils of depressions because of the admixture of the material in the plow layers during cultivation. For the same reason, the plow layer in depressions is enriched with the Ahb material.

Bulk chemical composition follows differences in the clay content (Table 7.2). The upper horizons are enriched in silica and contain less iron, aluminum, and manganese. These differences are less expressed in the soils of polygonal blocks due to the admixture of the Bt horizons into the plow layer. There is an increase in the CaO content in the carbonate horizons in the soils of polygonal blocks. The chemical composition of the clay fraction is uniform (Table 7.3) attesting to the fact that the differentiation of soil profiles by their chemical composition is connected with the differences in the clay content between their upper (coarser) and lower (finer) parts.

Pattern of clay minerals in the studied soils is common for the East European loess province (Gradusov & Chizhikova, 1976) with kaolinite, chlorite, illite, and smectite as the main components. Soils show clear differences in clay mineralogy between coarser and finer parts of a texturally differentiated profile (Table 7.3): surface and buried humus horizons have low contents of mixed-layered phyllosilicates compared to Bt and C horizons. The upper horizons are characterized by high

contents of hydromica, chlorite, kaolinite, and, in some cases, quartz and feldspar. The prevalence of hydromica in the upper horizons is consistent with the high K_2O content in the bulk chemical composition of the clay fraction. The presence of chlorite and vermiculite in the upper horizons is confirmed by the considerable amount of MgO. There are no significant variations in the contents of minerals in the fine and medium silt fractions (Dubrovina & Gradusov, 1993). The difference in the distribution of clay minerals is less expressed in the soils of polygonal blocks compared to the soils of depressions, which can be explained by the admixture of the Bt horizon into the plow layer.

Iron fractions. The content of oxalate extractable iron is relatively low (Table 7.4). The distribution pattern is characterized by a distinct accumulation in the surface humus horizon and, especially, in the Ahb. the latter could be of relict origin, connected with both biogenic concentrations of elements in the former surface horizon and a more hydromorphic environment of the past. The differentiation by the total content of Fe_2O_3 is not very pronounced; however, it cannot be explained by the differentiation of amorphous iron compounds. In all horizons, dithionite-extractable iron predominates and constitutes 65–75% of the total iron. The content increases with depth, contributing to the increase in total iron in the Bt and C horizons in comparison with the coarser textured upper horizons.

Table 7.1. Grain size distribution in soils of Vladimir Opolie, Shikhobalovo key site

Horizon	Depth, cm	Particle size (mm) distribution, Russian traditional fraction groups					
		1–0.25	0.25–0.05	0.05–0.01	0.01–0.005	0.005–0.001	<0.001
Center of depression, 230 m a.s.l. *Haplic Luvisol Siltic, Cutanic, Thaptohumic* (pit 12-85)							
Ap	0–33	4	12	52	10	16	6
Ahb	33–73	0	2	50	23	11	14
E/Bt	33–68	0	1	53	10	14	22
Bt1	33(73)–120	0	1	38	13	13	35
BCtg	120–150	0	2	39	9	17	33
Polygonal block, 230 m a.s.l. *Calcic Luvisol, Siltic* (pit 11-85)							
Ap	0–35	1	6	50	9	16	18
Bt1	35–50	0	1	47	6	13	33
Bt2	50–100	0	5	41	8	13	33
BtCk	100–120	0	0	43	13	17	27
BtCk	120–170	0	0	40	14	18	28
Center of deep depression 220 m a.s.l. *Gleyic Luvisol* (pit 15-85)							
Ah	2–10	2	29	41	10	15	3
AhEg	10–20	0	12	46	20	18	4
Eg	20–45	1	5	56	14	13	11
Bt1	45–75	0	1	46	7	16	30
Bt2	75–120	0	3	45	11	12	29

Table 7.2. Bulk chemical composition of soils of Vladimir Opolie, %, Shikhobalovo key site

Horizon	Depth	SiO_2	Al_2O_3	Fe_2O_3	CaO	MgO	K_2O	Na_2O	TiO_2	P_2O_5
Center of depression, 230 m a.s.l. *Haplic Luvisol Siltic, Cutanic, Thaptohumic* (pit 12-85)										
Ap	0–33	78.85	9.63	3.66	1.57	1.27	2.12	0.96	0.83	0.26
Ahb	33–73	82.15	7.51	3.64	1.32	0.65	1.76	1.13	0.82	0.17
E/Bt	33–68	73.13	14.22	5.32	1.20	1.28	2.14	0.94	0.97	0.09
Bt1	33(73)–120	72.90	14.04	5.20	1.32	1.60	2.25	1.01	0.88	0.10
Polygonal block, 230 m a.s.l. *Calcic Luvisol, Siltic* (pit 11-85)										
Ap	0–35	11.09	11.09	3.87	1.58	1.14	2.30	1.05	0.85	0.19
Bt1	35–50	13.85	13.85	5.19	1.32	1.55	2.30	0.89	0.98	0.11
Bt2	50–100	14.05	14.05	5.27	1.35	1.57	2.28	1.08	0.96	0.11
BtCk	100–120	13.72	13.72	5.06	3.67	1.36	2.49	0.85	0.90	0.13
BtCk	120–170	13.79	13.79	5.18	3.33	1.88	2.48	1.27	0.91	0.14
Center of deep depression 220 m a.s.l. *Gleyic Luvisol* (pit 15-85)										
Ah	2–10	78.08	9.45	4.06	1.59	1.02	2.61	1.12	0.92	0.31
AhEg	10–20	78.51	11.38	3.44	0.68	0.76	2.47	1.09	0.85	0.21
Eg	20–45	79.23	10.17	3.82	0.91	0.73	2.47	0.94	0.83	0.18
Bt1	45–75	72.00	15.95	4.95	0.68	1.04	2.81	0.89	0.86	0.11

The studied soils are slightly acidic, changing to alkaline within the carbonate layer in soils of the polygonal blocks, which contains free carbonates (Table 7.4). The humus content in the surface horizons is rather high for the southern taiga subzone (2.5–3.5%). On the main surfaces, it sharply decreases with depth, while in the depressions, the accumulation of organic matter extends much deeper. Humus content in buried humus horizons exceeds that in surface horizons. The composition of humus is also different, with predominant humic acids (especially its second fraction) and residual fractions, so the ratio of humic to fulvic acids is considerably higher than in surface horizons (Makeev et al., 2015).

Surface soils in various parts of the Vladimir Opolie on uplands, slopes, and within ancient gullies have similar morphology and analytical features: grain size distribution, chemical composition, and mineralogy.

Radiocarbon dating of the buried humus horizons mostly yields ages around 5–6 cal ka (Aleksandrovskiy, 1983; Parunin & Timashkova, 1984; Velichko et al., 1996). However, ^{14}C dating based on the separation of hydrophobic fractions of humic substances gave the set of dates increasing with the depth: 3880±100 cal yrs BP (39–45 cm); 9482±50 cal yrs BP (frost wedge, 50–55 cm); 12630±70 cal yrs BP (frost wedge, 75–80 cm); 12960±90 cal yrs BP (frost wedge, 100–120 cm) (Milanovsky, 2009).

During more than a century of study, a set of controversial hypotheses on the genesis of soils of the Vladimir Opolie has been developed. There are more than 20 hypotheses explaining the genesis of microdepressions, the genesis of the second humus horizon, and the differentiation of carbonates. The genesis of the soils of the Vladimir Opolie is still very acute and open to argument. The program of the field trip suggests a discussion of these issues. Let us summarize briefly the main hypotheses.

Specific soils with dark humus horizons were related to the past dominance of steppe vegetation (Nikitin, 1885; Tanfil'ev, 1902; Obruchev, 1948; Kostychev, 1949), or high content of carbonates in parent rocks and shallow table of hard groundwater (Krasyuk, 1925; Kasatkin, 1931; Yakushevskaya, 1959). Based on radiocarbon dates of the second humus horizons, Aleksandrovskiy (1983) suggested the following stages of the Holocene soil evolution: 1) textural differentiation of the soil profile since Preboreal and till the mid-Atlantic optimum;

2) dark-colored Ca-humus pedogenesis in the Late Atlantic period, development of a thick humus horizon; 3) degradation of the upper part of the dark-colored humus horizon in Subboreal and Subatlantic, resulting in the present position of the second humus horizon.

Table 7.3. Bulk chemical composition of clay and clay minerals in soils of the Vladimir Opolie, %. Shikhobalovo key site

Horizon	Depth, cm	SiO_2	Al_2O_3	Fe_2O_3	CaO	MgO	K_2O	Na_2O	TiO_2	P_2O_5	Clay minerals*, nm		
											0.7	1.0	1.7
Center of depression, 230 m a.s.l. *Haplic Luvisol Siltic, Cutanic, Thaptohumic* (pit 12-85)													
Ap	0–33	56.09	24.64	11.57	0.27	1.36	3.06	0.39	1.43	0.51	26	62	12
Ahb	33–73	55.82	22.16	14.12	0.26	1.16	3.16	0.19	1.78	0.64	24	68	8
E/Bt	33–68	55.38	24.93	12.31	0.16	2.35	2.88	0.20	1.20	0.19	16	26	58
BtCg	120–150	55.75	25.39	12.35	0.23	1.67	2.95	0.08	1.18	0.17	19	36	45
Polygonal block, 230 m a.s.l. *Calcic Luvisol, Siltic* (pit 11-85)													
Ap	0–35	56.00	25.08	12.13	0.24	1.64	2.71	0.09	1.28	0.36	20	55	25
Bt1	35–50	54.56	25.25	12.65	0.18	2.54	2.98	0.10	1.20	0.20	18	38	44
Bt2	50–100	55.35	24.96	12.47	0.16	2.36	2.98	0.10	1.18	0.18	19	28	53
BtCk	120–170	56.81	23.56	12.08	0.20	2.32	3.10	0.34	1.21	0.18	18	28	54
Center of deep depression 220 m a.s.l. *Gleyic Luvisol* (pit 15-85)													
AhEg	10–20	58.20	23.14	10.85	0.23	1.57	3.15	0.16	1.53	0.67	30	66	4
Eg	20–45	54.38	23.84	14.15	0.27	1.40	3.06	0.58	1.40	0.59	40	53	7
Bt1	45–75	55.25	25.63	12.49	0.19	1.22	3.23	0.18	1.21	0.20	18	43	39
Bt2g	75–120	55.80	25.28	11.53	0.19	2.24	2.78	0.44	1.18	0.19	25	45	30

* – 0.7 nm – kaolinite + chlorite; 1.0 nm – hydromica; 1.7 nm – smectite

Table 7.4. Selected chemical characteristics of soils of the Vladimir Opolie. Shikhobalovo key site

Horizon	Depth, cm	pH H_2O	Humus, %	$CaCO_3$, %	Ca	Mg	Al	Fe fractions, %*		
					meq/100 g soil			Fe_o	Fe_d	Fe_t
Center of depression, 230 m a.s.l. *Haplic Luvisol Siltic, Cutanic, Thaptohumic* (pit 12-85)										
Ap	0–33	6.5	2.5	–	10.6	3.3	3.0	0.52	0.52	3.66
Ahb	33–73	5.2	3.6	–	12.1	2.1	13.3	1.11	0.23	3.64
E/Bt	33–68	5.2	0.3	–	12.5	5.3	6.6	0.41	1.23	5.32
BtCg	120–150	6.0	0.3	–	14.6	6.7	4.0	0.36	1.32	5.20
Polygonal block, 230 m a.s.l. *Calcic Luvisol, Siltic* (pit 11-85)										
Ap	0–35	6.8	2.1	–	14.6	3.8	1.5	0.36	0.93	3.87
Bt1	35–50	5.7	0.5	–	14.0	3.7	3.9	0.31	1.35	5.19
Bt2	50–100	5.8	0.6	–	15.3	4.1	4.8	0.31	1.41	5.27
BtCk	100–120	7.9	0.6	4.3	e	e	0.2	0.21	1.43	5.18
Center of deep depression 220 m a.s.l. *Gleyic Luvisol* (pit 15-85)										
Ah	2–10	6.1	8.5	–	12.3	8.4	10.6	0.30	0.83	4.06
AhEg	10–20	5.9	4.2	–	1.6	0.8	10.7	0.31	0.69	3.44
Eg	20–45	5.4	0.8	–	0.5	0.3	5.5	1.12	0.41	3.82
Bt1	45–75	5.3	0.7	–	1.7	2.6	7.1	0.86	1.04	4.95
Bt2g	75–120	4.8	0.3	–	4.5	2.6	5.6	0.44	1.07	4.63

*Fe_t – bulk amount; Fe_d – dithionite-extractable; Fe_o – oxalate extractable.

The soilscape pattern is determined by microtopography. Dolgova (1964) and Rubtsova (1974) believed the uplands topography to be flatter in the past with microdepressions developed due to suffusion that accompanied the leaching of carbonates abundant in loess. Then a dark humus horizon developed in meadow soils of depressions due to the high groundwater table. Tyuryukanov & Bystritskaya (1970) considered opolies of the Russian Plain to be the remains of Late Pleistocene floodplains. The elevated position of opolies and its sufficient erosional network density were considered the result of the upward neotectonic movements.

Starting from the mid-1960s, the works of Velichko, Morozova, and, later, Berdnikov (1976) and Simakova (1984) proved the existence of relic cryogenic microtopography of the Late Pleistocene age in periglacial areas of the Russian Plain. Alifanov (1986) supported its paleocryogenic origin. He pointed out that hydromorphic features in the second humus horizons had developed in cold hydromorphic environments (cryogenic meadow-bog soils) that could have taken place immediately after the degradation of ice wedges and related landforms. Velichko et al. (1996) studied ice-wedge pseudomorphs serving as the geological basis for thermokarst depressions. Radiocarbon age of the second humus horizon was estimated at 6130±100 BP (IGAN-1141). The absence of steppe species in the pollen spectrum allowed them to consider the second humus horizon to be that of meadow soils formed during the Holocene climatic optimum.

Makeev and Dubrovina (Makeev & Dubrovina, 1990; Makeev, 2009, 2012; Makeev et al., 2015) argued that the development of paleocryogenic microtopography was accompanied by sedimentation of the upper loess layers. The lower clay content in the upper part of the texturally differentiated profile indicates a more dynamic sedimentation environment during the final stages of loess deposition. The humus horizon was formed by hydromorphic pedogenesis within thermokarst depressions during the Late Glacial and buried by the upper loess layer of 30–40 cm. Radiocarbon dates for humus material filling the ice-wedge pseudomorphs (Milanovsky, 2009) support those time estimates. Radiocarbon dates for the shallowly buried humus horizon (30–40 cm) are most probably rejuvenated due to the high input of fresh humic substances in productive ecosystems. The burial of Ahb horizons is marked by the high phytolith content in >0.01 mm fraction indicating their former surficial position. The source and differentiation of carbonates in soil profiles of the Vladimir Opolie is another crucial issue. The debris of carbonate rocks indicates it came with loess. Secondary differentiation of carbonates by microtopographic elements accompanied loess deposition following the same pattern as the differentiation of carbonates in permafrost- affected soils of arid Arctic environments.

The abundance of relict features allows us to interpret the Vladimir Opolie soils as surface paleosols (Paleopedology Glossary, 1997). For modern pedogenesis, soil-sedimentary sequences in mantle loams constitute a relict matrix that still determines soil temperature and water regimes and the redistribution of nutrients (Umarova, 2011; Arkhangelskaya, 2014). This could explain the sustainability of relict features in modern environments with contrasting bioclimatic parameters. Farming caused considerable changes to the relict soil pattern. Cultivation results in the leveling of initial microtopography and even the complete burial of depressions. However, the soil pattern became even more contrasting. Within depressions, the depth of the plow layer increases due to the redeposition of soil material from the polygonal blocks. At the same time, on the blocks, the material of argic horizons, low in humus content, is incorporated into the plow layer. The soil water and temperature patterns retain the initial heterogeneity even when the surface is flattened by cultivation.

STOP 8. FINE-SCALE LANDSCAPE HETEROGENEITY OF SUZDAL PLATEAU: DEPOSITS, PALEOSOLS, AND RELICT PERIGLACIAL FEATURES

August 30, 2023, noon

The non-contrasting lithology of loess-like mantle of the Vladimir Opolie is yet distinctly differentiated – both laterally and vertically – by superimposed sedimentary, cryogenic, and pedogenic features. We investigated fine-scale variations of the postglacial sedimentary cover, associated past permafrost and paleopedofeatures employing measurements of grain size, carbon matter content, and magnetic susceptibility juxtaposed with the thorough macromorphological interpretation of geological exposures. The study aimed to determine whether that fine-scale heterogeneity can be employed for regional stratigraphic correlation and if it has been affecting erosion and deposition trends and distribution of soil combinations. We focused on two local watersheds at the E macroslope of the Suzdal Plateau (Fig. 8.1) with different polygonal patterns reflected both in space imagery and geophysical data.

Oak Grove key site (56°22'20.6" N, 40°21'36.6" E, app. 160 m a.s.l.) is located in a small depression on a plateau-like surface 1.3 km NE from Gnezdilovo Village. Polygonal cropmarks dominate on the cultivated field gradually changing to linear ones towards the shallow dry gully of the Mzhara river catchment. The polygonal-linear pattern on the satellite image (Fig. 8.2a) is created by regular alternation of lighter rounded patches 20–25 m in diameter and darker rounded to linear patches up to 10 m wide. Polygons reflecting as tetragonal negative anomalies on the magnetic survey map (Fig. 8.2b) are rather smaller (7–20 m) and appear more clearly in the southern part where they are separated by narrow (1–2 m) positive linear anomalies. Rounded nodes of the polygonal network are both represented by positive anomalies 2–3 m in diameter. At the same time, to the north no clear patterns are to be found (Fig. 2b).

Postglacial thickness was investigated in pits to a depth of 2–2.3 m and down to 3.8 m probed by hand auger core. A relatively undisturbed sequence of host deposits in the block centers is represented by sandy loams with small debris (>3.4 m depth) overlayed by three major layers of texturally non-contrasting loams differentiated in structure and other lithological and pedogenic features. This thickness is deformed by vertical wedge- and bulbous-shaped structures representing the geological base of the polygonal system.

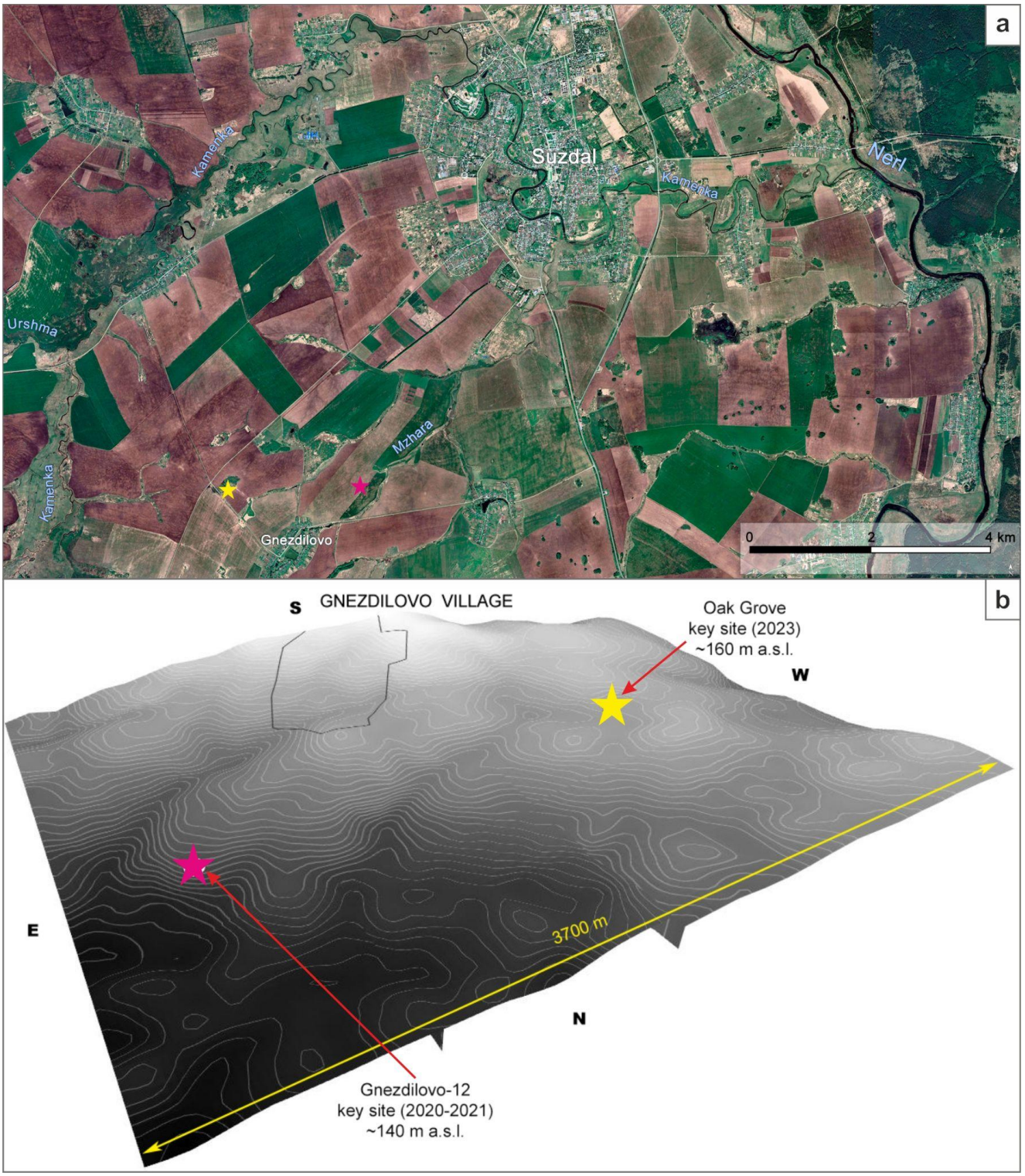

Figure 8.1. Suzdal Plateau: a) WorldView-2 satellite photoscene with Gnezdilovo Necropolis (pink star) and Oak Grove (yellow star) key sites and b) DEM SRTM perspective view of the Gnezdilovo study area from NNE.

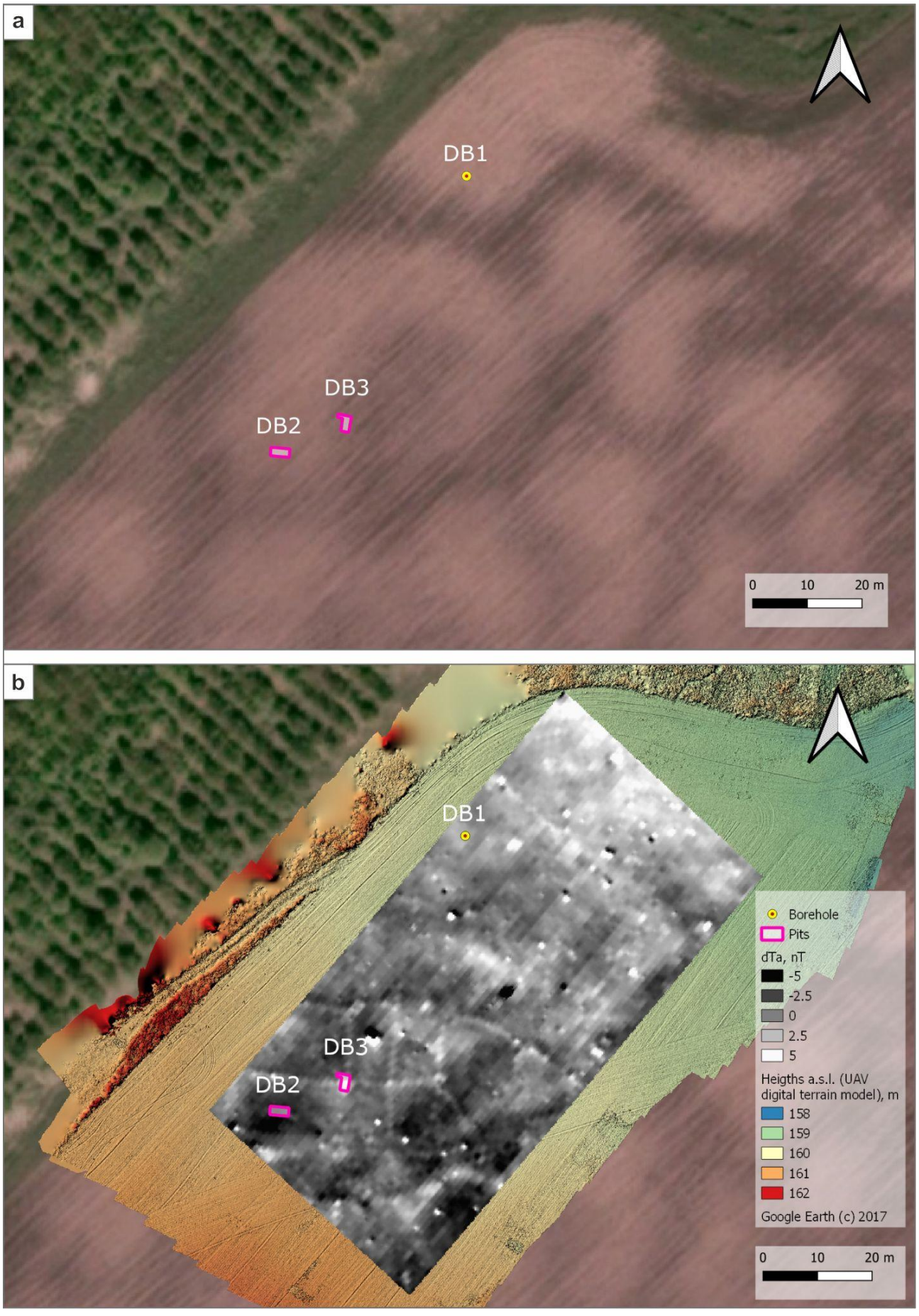
a
DB1
DB3
DB2
0
10
20 m
b
DB1
DB3
DB2
Borehole
Pits
dTa, nT
-5
-2.5
0
2.5
5
Heigths a.s.l. (UAV digital terrain model), m
158
159
160
161
162
Google Earth (c) 2017
0
10
20 m

Figure 8.2. Oak Grove key site. Positions of pits and cores are shown on the satellite image (a); b) the magnetic survey map (accomplished and processed by V. Shevchenko) superimposed on the DTM derived from the UAV survey data (accomplished and processed by V. Belyaev).

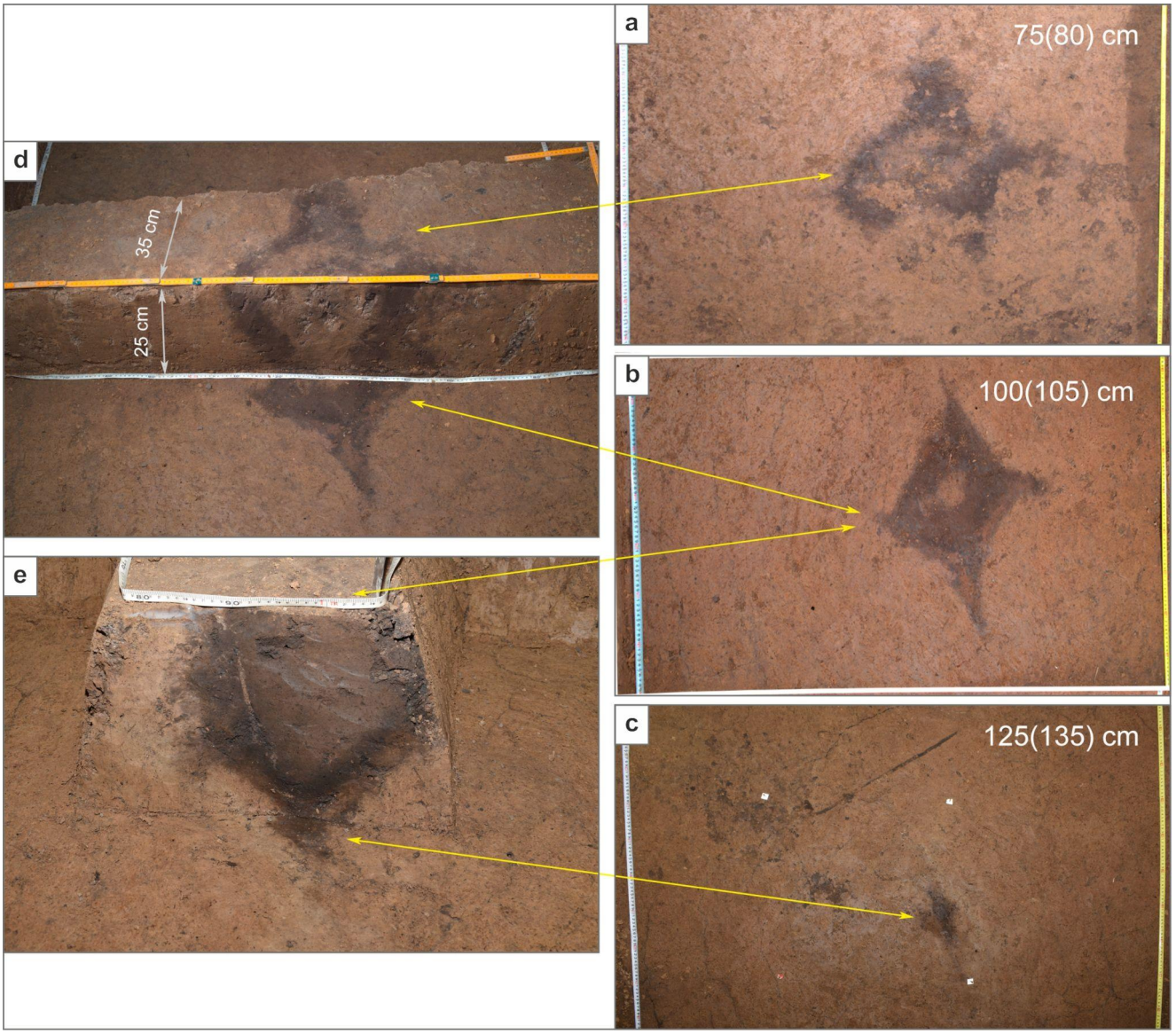

Figure 8.3. Dark wedge-shaped structure at the polygonal node, Oak Grove key site: horizontal cross-sections at depths of a) 75(80) cm; b) 100(105) cm, and c) 125–135 cm; side views of vertical steps at depths of d) 75(80)–100(105) cm and e) 100(105)–125(135). Note the intensive bioturbation of dark infill and blurred contacts in the upper part (a–b) and better preservation of the infill and sharp side contacts in the middle (a–c) and lower (d–e) parts.

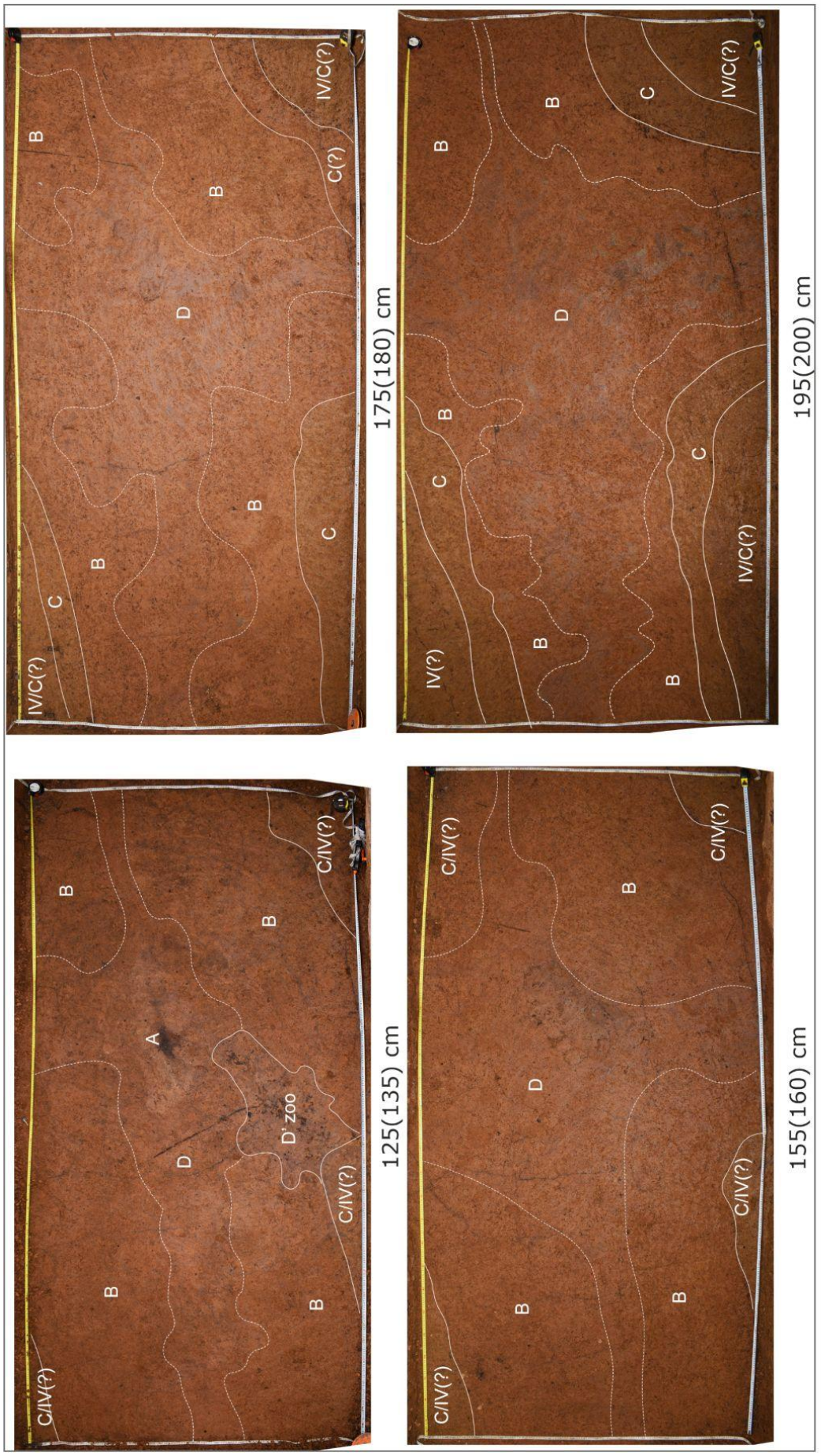

Figure 8.4. Horizontal cross-sections at different depths at the DB3 pit, Oak Grove key site. Note the gradual decrease in size of zones [B] and [C] (solid lines) versus irregular margins of the heterogeneous inner zone [D] (dashed lines) significantly increasing in size at the depth of 195(200) cm. That implies that [B] and [C]-structures narrow downwards having a wedge-like shape in the vertical cross-section versus [D]-sructure extending downwards having a "bulbous-like" shape in the vertical cross-section (see Table 8.2 for the genetic interpretation of indices).

To reliably interpret the specific patterns of the surficial sedimentary cover organization revealed at the Oak Grove key site we have to turn to the results achieved during the 2020–2021 fieldwork at another closeby site Gnezdilovo-12.

Gnezdilovo key site. Gnezdilovo-12 Necropolis (56°22'24" N, 40°23'45" E, app. 143 m a.s.l.) occupies the NE periphery of the medieval grave field Gnezdilovo-12 lately investigated by Makarov et al. (2021). The archeological site in the upper Mzhara catchment is about 6.5 km SW of Suzdal (Fig. 8.1a). Mzhara Gully with its left shallow dry tributary gully drains a local cultivated watershed with distinct linear longitudinal and less prominent transverse cropmarks (Fig. 8.5a). Those cropmarks also reflected on the ERT-data image (Fig. 8.5b) correspond to the troughs of the tetragonal paleocryogenic wedge network, yet are almost reduced in microtopography of the arable field. Longitudinal troughs are emphasized by darker dells 4–6 m wide running down a gentle (≤4°) NE slope. In-between, polygonal blocks are 22–30 m wide whereas ill-defined lighter transverse troughs could be spaced up to 40 m apart providing a lighter fragmentary pattern. Marginal zones of troughs and polygonal blocks are represented by flat rims. At polygonal nodes, darker cropmarks reach 12 m in diameter. The complexity of landscape architecture distinctly interconnects with the soil cover structure on the finest scale (Lobkov et al., 2023).

Postglacial thickness above the eroded top of Moscow (MIS6) glacial diamicts varies from 3.5 to 4 m (Fig. 8.5c, Table 8.1). Within polygonal blocks, host units are rather undisturbed while in throughs they are interrupted by a series of wedge-shaped casts penetrating even the glacial base. Lithologic and pedogenic features are assembled in Table 8.2 as field and laboratory measurements in Table 8.3, Figs. 8.9–8.12.

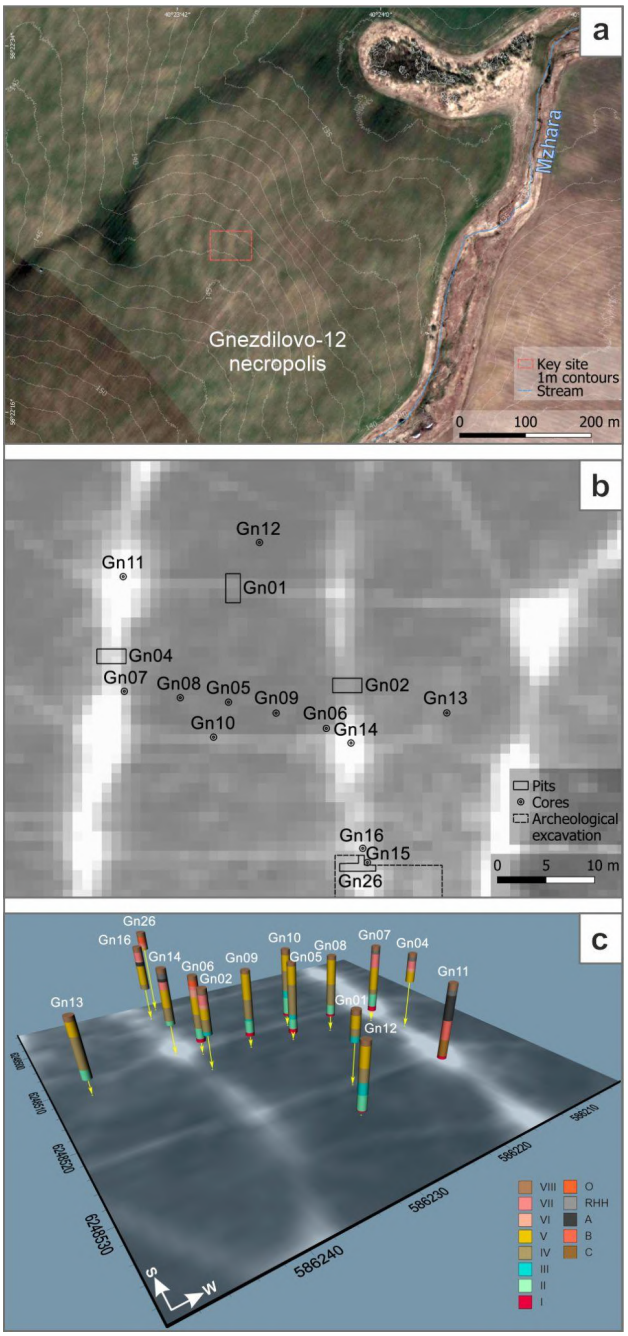

Figure 8.5. Gnezdilovo-12 key site: a) the Upper Mzhara catchment on the Pleiades-1A photo scene (25.04.2019); b) geological exposures at the NE periphery of the archeological site Gnezdilovo-12 imposed on the electrical resistivity tomography map (depth slice 61 cm) after (Makarov et al., 2021) reflecting a polygonal pattern of the higher resistivity (brighter colors); c) its 3D visualization with interpreted cores (see Table 8.2).

Table 8.1. Sampling and measurement protocol, Gnezdilovo key site

Exposure		Height,	Exposed	Number of samples collected/measured				Number of κ
name	type	m a.s.l.	thickness, m	LOI & χ	Grain size	^{14}C dating	Box samples	measurements
Gn01	**pit**	143.5	1.50	18/**10**	10/	3/	8/	770
Gn02	**pit**	143.5	2.85	35/**35**	35/	–	10/	365
Gn04	**pit**	143.5	3.05	27/**27**	27/	8/	2/	402
Gn26	**core**	144.3	0.90	1/	–	1/	1/	378
Gn09	**core**	143.7	3.65	20/**20**	20/**20**	–	–	–
Gn11	**core**	143.5	4.18	19/**19**	19/	–	–	–
Gn12	**core**	143.1	3.54	19/**19**	19/	–	–	–
Gn13	**core**	143.5	3.20	12/**12**	12/	–	–	–
			Total	143/**142**	142/**20**	12/	**21/**	**1915**

Host units. Basal sandy loam unit with debris [I] is unconformably overlayed by contrastingly stratified clay loams [II] with interlayers of better sorted silty loams at the top (Fig. 8.6b). Fragmentary lenses of laminated blueish loams [III] rest above. A sequence of loamy units follows upwards. At the bottom, dull pinkish-gray silty-clay loams [IV] up to 2 m thick (decreasing to 0.5 m at dells) with low contrasting wavy lamination have carbonate impregnations and nodules in plane pores. Upwards yellowish-brown loams [V] with contrasting lenticular-reticulate features lay. A truncated system of subvertical plane and tube pores with reddish-black thin argillans runs from its top. At polygonal blocks and transverse troughs, loams [V] outcrop directly under the plow layer [VIII].

However, at dells, U-shaped lenses of light-brown [VI] and reddish light-brown [VII] loams up to 1 m thick are incised in the top of [V]. Bright-brown bands sagging towards the trough axes are traced in [VII] due to enrichment with dark-brown argillans and lack of siltans (*Lamellae* pedofeature – Figs. 8.6b & 8.8a). On top, sporadic lenses of RHH are embedded along dells. Small polygonal systems of plane pores infilled mostly with siltans form an *albeluvic glossae* pedofeature strictly in [VII]. ~10% of those plane pores penetrate [VI] forming a sparser polygonal net with 0.2–0.4 m spacing. Only certain thick trans-horizon pores filled with multi-layered argillans and siltans penetrate down to 1.4–1.6 m in [V] forming an even sparser polygonal net with 1 m spacing. Large positive anomalies of apparent magnetic susceptibility κ correspond to U-shaped lenses of [VI–VII] and RHH at dells (Table 8.3, Fig. 8.11) while not found at transverse troughs where respective units are absent (Fig. 8.10, Gn01).

The plow layer [VIII] almost uniformly undercuts all surficial facies, especially lenses of the occupational layer [O], RHH, and eluvial horizons of *Luvisols* and *Retisols,* effectively admixing their material.

Table 8.2. Sedimentary structure of the Gnezdilovo key site

Host units	Depth, m min/**max**	Lithology	Casts and lenses	Depth, m min/**max**	Lithology
[VIII] Plow layer Cover layer with slightly wavy lower contact truncating **[VII–V]**	0.0 **0.2–0.35**	Brownish dark-gray to light-yellowish-gray silty loam with admixtures of underlying units and relocated artifacts	**[O] Occupation layer.** Isometric, elongated, and annular lenses	0.2–0.35 **0.5–0.7**	Mixed relocated material of **[RHH], [VII–V]** in backfill of graves, pits, and moats of burrow mounds; with artifacts
[VII] Reddish-light-brown colluvium Linear lenses >3 m wide along dells, with erosional concave lower contact	0.25–0.5 **0.5–1.2**	Silt loam with contrasting brighter bands (1–3cm) rich in clay cutans lacking siltans. Atop, silty EL soil horizon and ELhh&BELhh [RHH] or AU, AEL&BEL horizons, frequent multi-order small polygonal systems of plane pores with multi-layered cutans and siltans (*albeluvic glossae* pedofeature)	**[RHH] Relict humus horizon.** Lenses 3–9 m wide with tonguing base along dells and at nodes of polygonal troughs	0.2–0.35 **0.3–0.6**	Dark-gray organic-rich silty loam with mollic tonguing, *albeluvic glossae* and/or *retic* pedofeatures, occasionally mixed by pedofauna and/or translocated by mass wasting
			[A] Dark casts. Asymmetrical wedge-shaped casts at nodes of polygonal troughs	0.3–0.6 **0.7–2.0**	Dark-gray and dark-brown organic-rich clay loam with inclined up to subvertical lenticular structure
[VI] Light-brown colluvium Linear wide (>6 m) lenses along dells, with wavy undulating erosional lower contact	0.5–1.2 **0.65–1.4**	Silt loam with thin lenticular and small patchy structure of light-yellow silty loam in light-brown loam matrix with a regular net of trans-horizon plane pores – *albeluvic glossae* and/or *retic* pedofeatures	**[B] Red-light-brown casts.** Wedge-shaped linear bodies with subvertical curvilinear asymmetrical side contacts in cross-section 1–1.2 m wide atop at dells and 0.1–0.3 m – at transverse troughs	0.2–2.0 **0.7–3.1**	Silty loams to clay silts with fine sand, porosity increasing with depth. Irregular lenses (1 x 1–3 mm) of light-yellow silt loam in reddish light-brown clayey loam deformed by thin lenticular-reticulate structures, occasional low-contrasting red-yellow patches. Along cast axis, narrow (3–12 cm) red-brown veins with the small bright-red clayey lens atop
[V] Yellow-light-brown eolian loess Layer with irregular wavy (A=5–20 cm, P=0.4–1.3 m) undulating (A=up to 1 m) lower contact, small erosional features and wedge-like deformations	0.2–1.2 **0.7–2.5**	Plastic silty loam with thin pores. Contrasting light-brown clay-silty to gray-brown clay lenticular-reticulate structure (size of light yellow silty patches increases downwards). Dark-gray to reddish-black thin argillans in a truncated system of trans-horizon sub-vertical plane and tube pores running strictly from the top			
[IV] Reddish-light-gray paleocryosol Layer with sharp erosional low-amplitude irregularly wavy gently inclined lower contact	0.9–2.5 **1.15–3.15**	Dense plastic silty-clay loam with carbonate impregnations and nodules in plane pores. Non-contrast lenses of brown-yellow to light-yellow microaggregated silt loam in dull light-red loam. Low-contrasting involutions. Sand, granule and subangular pebble near wedge deformations of the top	**[C] Yellowish-light-gray casts.** Wide (1.2–1.4 m) wedge-shaped linear bodies truncated atop, with asymmetrical steeply sloping wavy side contacts in cross-section, penetrating in **[II]**	0.7–3.1 **>2.7–4.0**	At axial parts of casts, porous silty loams with non-contrasting small patches of dull yellow, brownish light-gray to light-gray silts. Further to the periphery, loam is plastic to viscoplastic with contrasting red-yellow reticulate lenses (up to 1 mm thick every 1–5(7) cm) encircled with yellowish impregnations, ellipsoidal bright red-yellow slightly cemented patches D=1–2 cm. Carbonate fines to granules and rare nodules (D=1–3 cm) along the side contacts of casts
[III] Light-gray shallow lake deposits Lenses with erosional lower and subhorizontal upper contacts	1.25–2.65 **2.55–2.8**	Microaggregated carbonate plastic to viscoplastic clayey loams with dull bluish, light-reddish and light-yellowish clayey bands and lenses. Non-contrasting wavy-lenticular lamination deformed by ferruginous lenticular-reticulate features			
[II] Variegated fluvially reworked deposits Layer with irregular amplitude wavy lower contact	2.6–3.15 **3.2–3.8**	Contrasting alternation of wavy-subhorizontal to overturned dark-yellow, yellow-gray, light-brown, gray-brown, brown-yellow, light-yellow and dull violet-gray dense plastic homogenous silt loams with thin lenticular lamination			
[I] Brown-red glacial diamicts	3.35–4.0 **n/d**	Brown-red dense very sandy loam with granules, gravels, subangular pebbles			

Figure 8.6. Sedimentary structure and morphology of the wedge-shaped casts: a) at the transverse trough with *Nudiargic Luvisol (Cutanic, Loamic, Profondic, Relictiturbic)* and b) at the dell with *Lamellic Luvisol (Cutanic, Loamic, Profondic)*.

1–2 – unit and subunit outlines; *3* – unit and subunit indices (see Table 8.2); *4* – box sample numbers; *5* – bulk sample numbers.

Stop 8. *Fine-scale landscape heterogeneity of Suzdal Plateau: deposits, paleosols, and relict periglacial features*

Compiling the grain size distribution (Fig. 8.7) with other analytical data (Figs. 8.9 & 8.10), four lithological layers (L1–L4) are traced in core Gn-9 at the polygon interior allowing to propose some genetic interpretations.

L1 – 3.45–3.65↓ m – unsorted sandy loam encompassing small carbonate debris. Granulometric fractions tend to distribute uniformly with the lowest organic matter (OM) and highest carbonate matter (CM) contents and rather medium χ values.

L2 – 2.82–3.44 m – silty and silty-clay loam (especially rich in fine silt) with sandy particles and granules, abruptly depleted of CM but significantly richer in OM with the highest χ values. Grain size distribution deviates from the overlying one (L3) by the increased sand content. The upper transition is faint over the OM content rise.

L3 – 1.74(1.84)–2.82 m – silty and silty-clay loam with profoundly higher both silt (especially coarse silt) and clay portions; higher OM and slightly higher CM contents both decreasing upwards; and the lowest χ_{LF} values with oscillating χ_{FD} curve at the background. Grain size distribution is quite similar to L4 with 100–320 μm fractions being low in content and larger particles generally lacking. Hence, at 1.84–1.92 and 2.76–2.82 m, conterminal samples in L3 are slightly enriched with medium and fine sand (630–100 μm) and rather resemble the granulometric distribution in the underlying thickness.

L4 – 0.17–1.74(1.84) m – homogeneous silt loam lacking fractions >80 μm with coarse silt portion rising upwards up to 1.5 times. CM content is the lowest while OM content and χ_{LF} values are rather medium for the column with a slight rise at the top. Layer heterogeneity is caused by alterations of sand – coarse silt to clay – fine silt ratio and subsequently generally higher structure density and plasticity of *in-situ* sediments in the lower part, with shifts of the main modal fractions from coarse (32–25 μm) to fine (3.2–2.5 μm) silt at 0.82–1.09(1.16) and 1.26(1.45)–1.74(1.84) m.

Wedge-shaped casts. At polygonal troughs, the postglacial thickness hosts wedge-shaped casts and veins, which propagate down from at least three different buried surfaces. Those vertically oriented geological bodies differ in the morphology of cross-sections and are filled with more or less contrasting material.

The lowermost wedge-shaped casts [C] cropp out in cross-sections at depths of 0.8–1.5 m (Gn01) and 1.2–2.7 m (Gn02), dipping down to 3–4 m at the polygonal node (Gn11). More than 1.5 m wide at the top and filled with mottled dull yellowish-gray porous loams, such casts propagate from the top of [IV] intruding the glacial base [I]. Along its inclined sides emphasized by carbonate nodules, the layering of the host unit [IV] is downturned.

Wedge-shaped casts [B] with bright reddish-brown silty loam infilling have sharp sub-vertical sides. They propagate from the top of [VI] down to 2.4–3.0 m intruding the wider tops of [C]-casts and inheriting their orthogonal spatial structure. At dells and nodes (Figs. 8.6b & 8.8a), [B]-casts up to 1.2 m wide are covered by lenses of [VII]. At transverse troughs (Fig. 8.6a), thin (only 0.3 m) [B]-casts were exposed almost at the day surface in [V], being significantly truncated. Cast infills [B`] are completely zooturbated due to silty texture and loose compaction (Fig. 8.14c). Diogenic redoximorphic features highlight the inner heterogeneity of the infill and its contact zones.

The uppermost wedge-shaped casts [A] are bound exclusively to nodes of the polygonal network. Dark-gray casts up to 1 m wide (Fig. 8.8b) spread directly underneath the plow pan or RHH in [VII]. Organic-rich infill is zooturbated with only the cast tips preserving sharp angular contacts. Thinner veins (1–5 cm) of the same darkish matter run as bundles on cast sides down to 1.8 m in [VI] and even [V].

Wedge-shaped cast infills showed higher apparent magnetic susceptibility (κ) values compared to host units (Fig. 8.12b), especially significant in [A]-casts.

Its zooturbated upper part [A`] is accompanied by κ values up to twice as low as

in the relatively undisturbed lower part [A``]. Lower gradients were obtained for [B]-casts (Figs. 8.10, 8.11, & 8.12a). In Gn01, κ distribution within the [B]-cast is complicated by the dark vein with values up to 0.6 and the bright-red clayey lens with extremely high positive deviation up to 20. [C]-cast infill is the least contrasting with the host [IV].

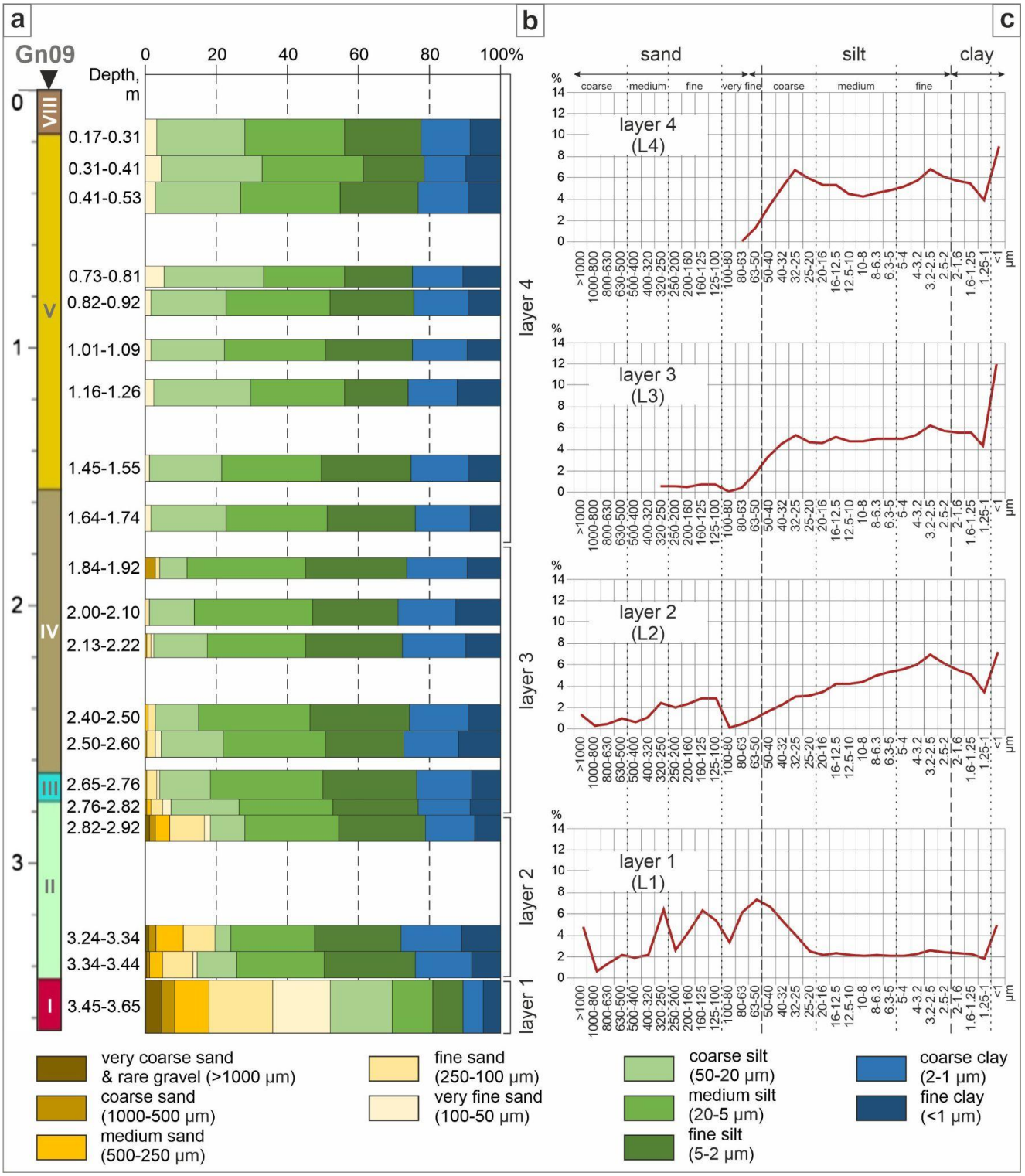

Figure 8.7. Grain size analysis of the Gn09 core, Gnezdilovo key site: a) interpretation of morphological units; b) depth-dependent granulometric histogram; c) model distribution curves of granulometric fractions for each of the distinguished lithological layers (see Sheremetskaya et al., 2023 for methodology).

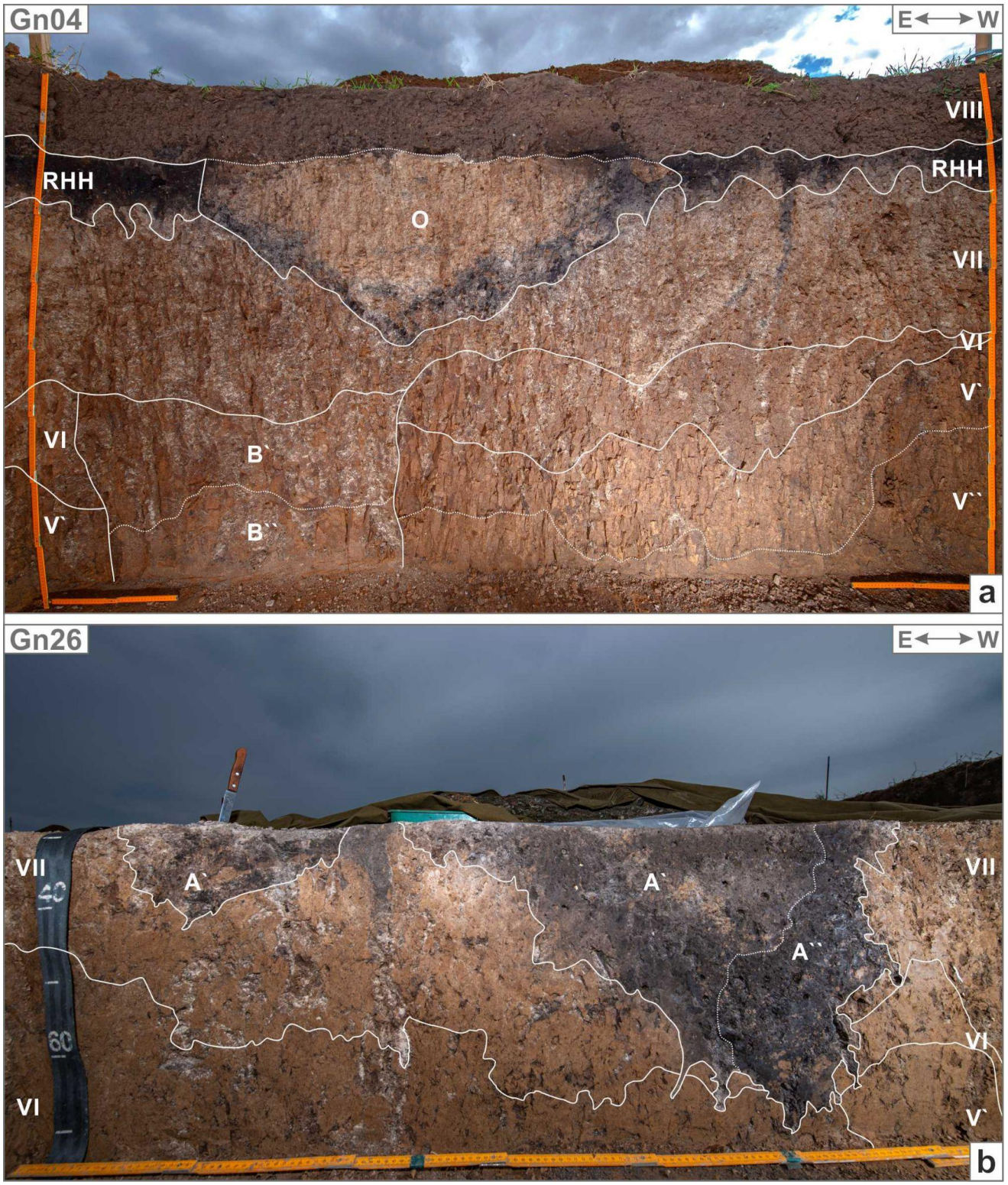

Figure 8.8. a) Prepared soil structure of the dell with a buried artificial pit marked by dark backfill and lighter colluvial infill [O] sustaining *Vermic Luvic Glossic Phaeozem (Abruptic, Loamic, Tonguic)*. Note: on the left – *Lamellae* structure in [VII] due to darker bands depleted of siltans, small erosional features at the bottom of [VI], and concentration of trans-horizon plane pores coated with siltans penetrating the wedge cast [B]; on the right – a sharp shift in prism morphology in [V] and its vertical axes tilted along the side contact of the [B]-cast – at the center. A truncated system of plane pores with dark-gray and reddish-black argillans runs from the top of [V]. b) Sedimentary structure and morphology of the asymmetrical wedge-shaped cast [A] at the polygonal node with *Vermic Luvic Glossic Phaeozem (Abruptic, Loamic, Relictiturbic)* (see Table 8.2).

Generally, mass magnetic susceptibility χ_{LF} values reflect the pattern of κ distribution. However, infills of casts [B] and [C] are rather similar in χ_{LF} values. Values in [B]-cast infills slightly exceed those in the host [V] while for the [C]-cast no clear difference is observed with host [IV]. χ_{LF} values of [A]-cast infill in Gn11 increase noticeably with depth, which reflects the same pattern as the κ-distribution in Gn26 due to zooturbation. The base of [IV] and unit [III] showed a slight but stable increase in χ_{LF} with depth. Units [II] and [I] had highly variable χ_{LF} exceeding that of the overlying thickness.

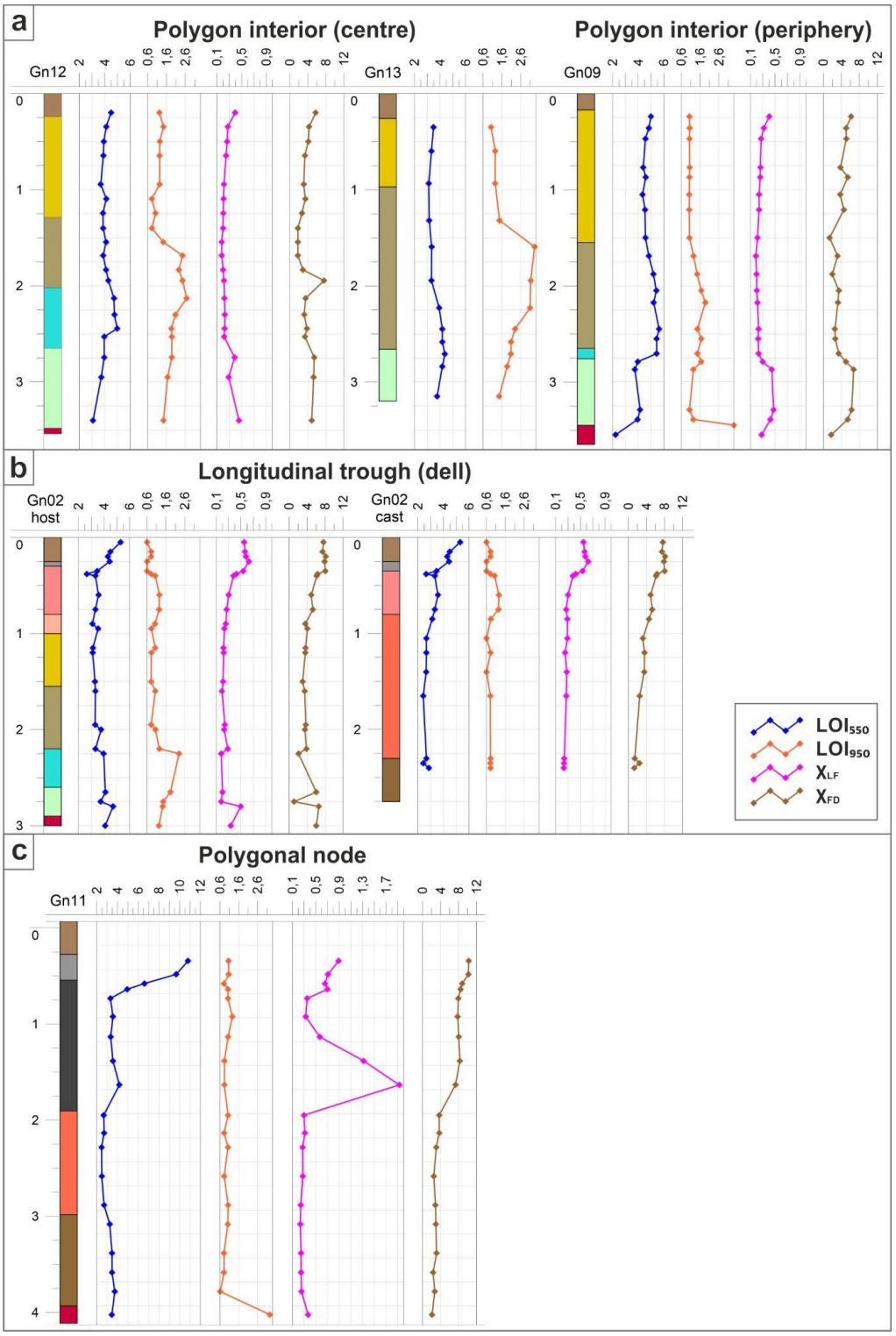

Figure 8.9. Distribution of loss on ignition and mass magnetic susceptibility values in cores at
a) interiors of polygons;
b) longitudinal troughs (dells);
c) polygonal nodes.

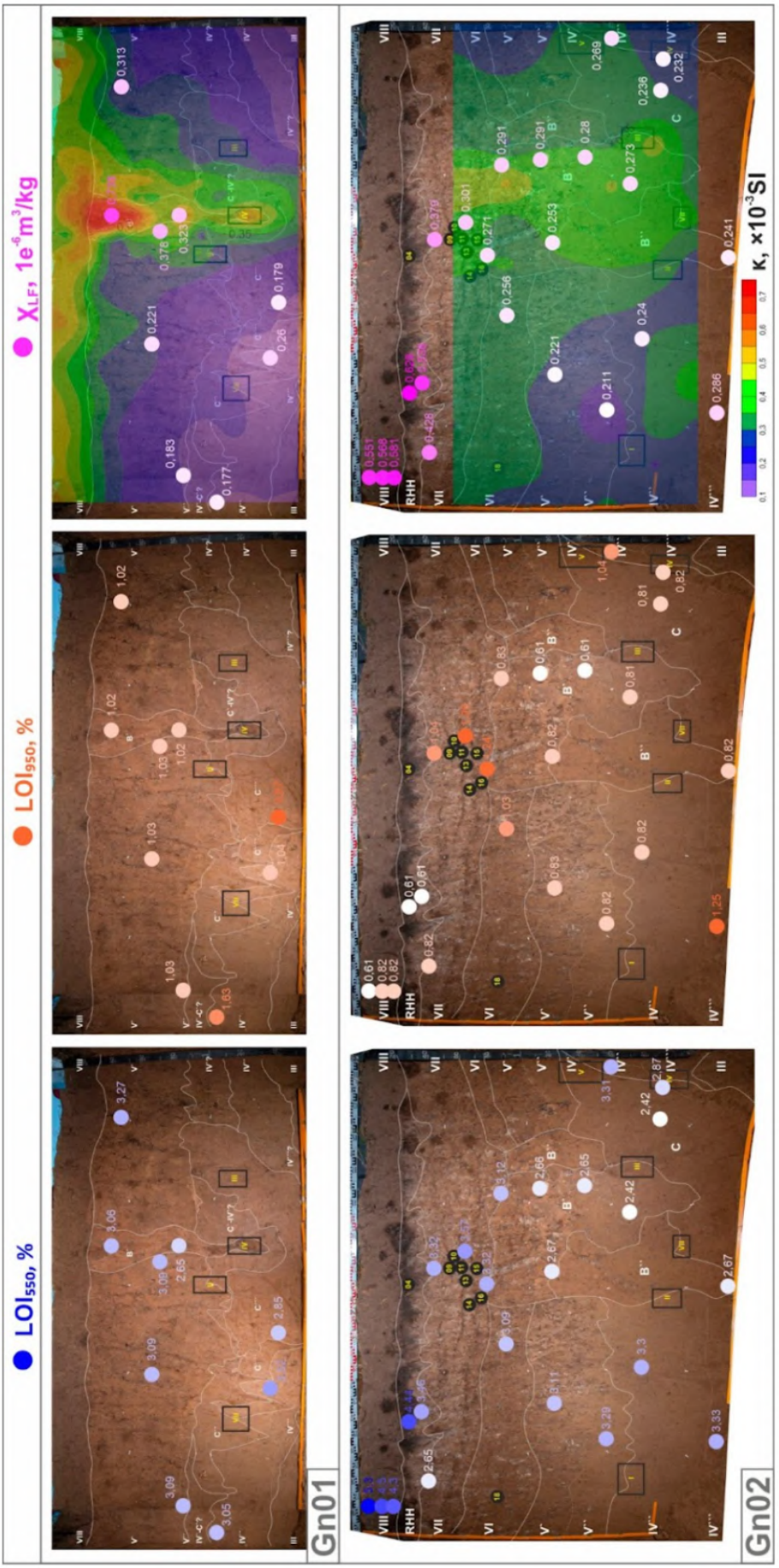

Figure 8.10. Weighted markers and values of loss on ignition – LOI_{550}, % and LOI_{950}, % – and mass magnetic susceptibility – χ_{LF}, $1e^{-6}m^3/kg$ – measurements. The latter is superimposed on variations of apparent magnetic susceptibility κ, $\times 10^{-3}$SI.

Table 8.3. Loss on ignition and magnetic susceptibility properties of morphological members distinguished at the Gnezdilovo key site with the coefficient of variations for statistically secured data given in brackets

Host units	Depth, m min/**max**	# of LOI/χ/κ samples	LOI_{550}, % (CV, %)	LOI_{950}, % (CV, %)	χ_{LF}, $1e^{-6}m^3/kg$ (CV, %)	κ, $\times10^{-3}$ SI (CV, %)	Casts	Depth, m min/**max**	# of LOI/χ/κ samples	LOI_{550}, % (CV, %)	LOI_{950}, % (CV, %)	χ_{LF}, $1e^{-6}m^3/kg$ (CV, %)	κ, $\times10^{-3}$ SI (CV, %)
[VIII] plow layer	0.00 **0.17–0.26**	4/4/77	4.3–5.3 (10%)	0.6–1.2 (29%)	0.39–0.58 (22%)	0.28–0.68 (20%)	**[O]** occupation layer	0.20–0.35 **0.50–0.70**	0/0/36	n/d	n/d	n/d	0.30–0.73 (27%)
[VII] reddish light-brown colluvium	0.25–0.50 **0.50–1.20**	5/5/104	2.7–3.6 (11%)	0.8–1.3 (20%)	0.27–0.43 (20%)	0.17–0.79 (31%)	**[RHH]** dark- gray lenses	0.20–0.35 **0.30–0.60**	4/4/12	3.5–10.8 (52%)	0.6–1.1 (31%)	0.54–0.89 (17%)	0.49–0.81 (15%)
[VI] light-brown colluvium	0.50–1.20 **0.65–1.40**	1/1/59	3.1	1.0	0.26	0.21–0.65 (27%)	**[A]** dark-gray wedge casts	0.30–0.60 **0.70–2.00**	7/7/34	3.3–6.6 (28%)	0.8–1.3 (16%)	0.33–1.93 (70%)	0.35–1.15 (25%)
[V] yellowish light-brown eolian loess	0.20–1.20 **0.70–2.50**	26/23/185	2.7–5.0 (17%)	0.8–1.4 (14%)	0.19–0.41 (21%)	0.15–0.50 (27%)	**[B]** red-light-brown wedge casts	0.20–2.00 **0.70–3.05**	12/11/51	2.4–3.1 (8%)	0.6–1.0 (18%)	0.24–0.38 (14%)	0.21–0.40 (16%)
[IV] dull pinkish-gray buried paleo cryosol	0.85–2.50 **1.15–3.15**	23/17/84	3.1–5.6 (27%)	0.8–3.3 (41%)	0.18–0.29 (15%)	0.12–0.36 (21%)	**[C]** yellowish light-gray wedge casts	0.75–3.05 **>2.70–4.00**	8/8/111	2.4–4.1 (16%)	0.6–1.2 (82%)	0.18–0.34 (17%)	0.17–0.58 (23%)
[III] blueish light-gray shallow lake deposit	1.25–2.65 **2.55–2.75**	6/6/0	4.0–5.5 (13%)	1.5–2.7 (20%)	0.18–0.23 (9%)	n/d							
[II] variegated fluvially reworked facies	2.60–3.15 **3.20–3.75**	15/12/0	3.0–4.7 (12%)	1.0–2.1 (20%)	0.18–0.50 (33%)	n/d							
[I] brownish bright-red glacial diamict	3.35–4.00 **n/d**	2/2/0	2.2–3.5 (31%)	3.3–7.1 (53%)	0.28–0.37 (19%)	n/d							

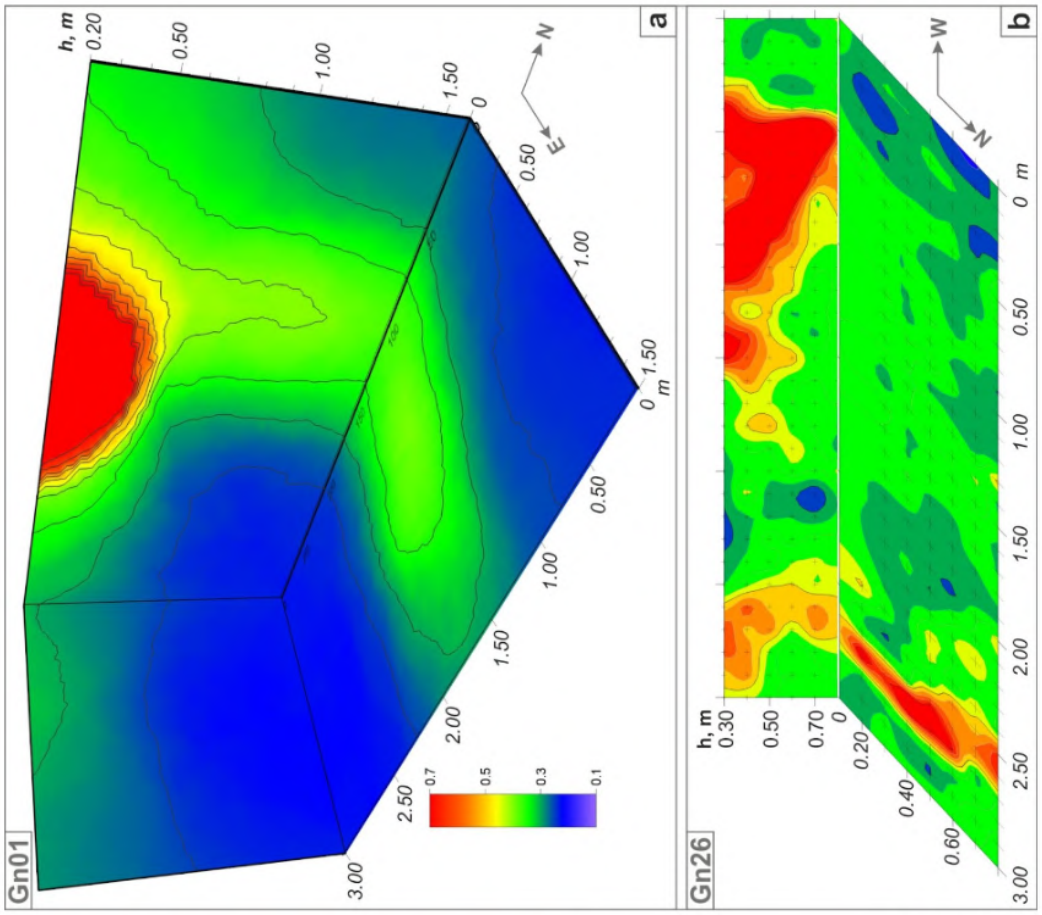

Figure 8.12. 3D visualizations of apparent magnetic susceptibility (κ, ×10⁻³SI) distribution in vertical walls and horizontal sections: a) at the latitudinal trough, wedge-shaped casts [B] are displayed in red to greenish-yellow, and casts [C] – in green and bluish-green; b) at the polygonal node, the asymmetrical wedge cast [A] and its isolated vein (apophysis) manifest in red and yellow.

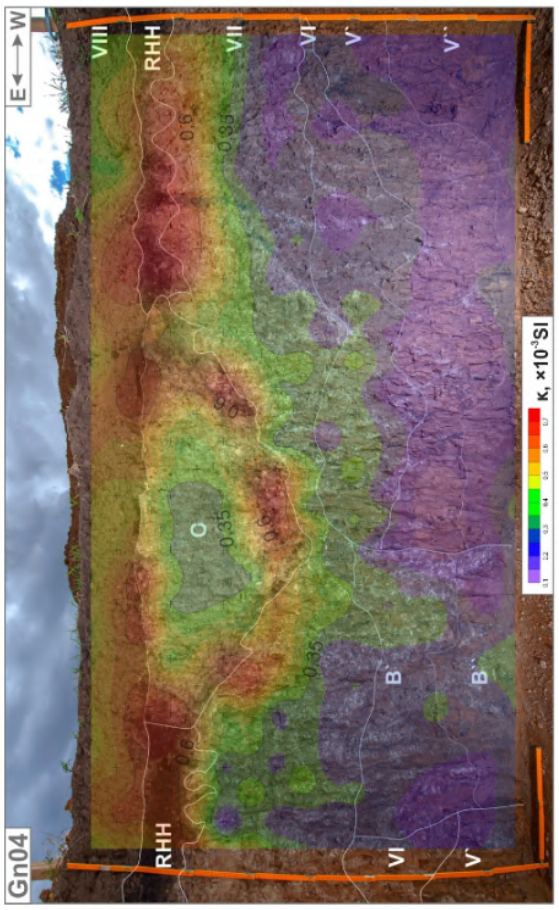

Figure 8.11. Variations of apparent magnetic susceptibility κ, ×10⁻³SI at the dell with anthropogenic buried pit.

DISCUSSION

Chronosequence and genetic interpretation. Basal unit [I] corresponds to debris-rich sandy loams of the lithological layer L1 representing the *Late Moscow glacial diamicts* (State geological map of Quaternary deposits, O-37-XXXV, 1968). L2 correlates with unit [II] of contrasting variegated beds with sharp boundaries (Fig. 8.13a,h), sand and debris inclusions, which could have been inherited due to *fluvial and/or cryogenic reworking of the glacial base* (Kleber & Gusev, 1998; Garankina et al., 2022). That is corroborated by the highest magnetic susceptibility values (χ_{LF}) against the abrupt decrease in carbonates (Fig. 8.9). Besides most samples have χ_{FD} higher than any other subsoil unit, indicating pedogenic magnetic minerals to be accountable for the χ_{LF} increase (Liu et al., 2012). Withal the raised amounts of OM and fine to medium sand grains could reflect a certain sediment input from the adjacent elevated watersheds with developed paleosols suggesting an *early period of pedogenesis followed by erosion impulse*.

Upwards, an affinity of the grain size distribution (Fig. 8.7) attests to common or close mineral sources and/or depositional mechanisms of the postglacial thickness. However, morphological alterations allowed for distinguishing rather complex sedimentary environments. L3 embraces sporadic lenses [III] and unit [IV], which lamination preserved at the bottom (Fig. 8.13g,h) and raised OM, CM, and clay contents likely represent *deposition in shallow lacustrine or pond-like environments* (Garankina et al., 2019, 2022). Stable but low sand fraction against noticeable enrichment in coarse silt point to several simultaneous or gradually changing deposition agents, of which the continued but *less dynamic sediment washout* and *inception of eolian input in colder climate conditions* are the most probable. Lamination in the unit [IV] is almost erased (Fig. 8.13g) by postdepositional subvertical involutions (Figs. 8.6b, 8.13a, & 8.14a) and possibly zooturbation aligned with slightly higher clay and fine silt contents as with impregnations, tube micropore incrustations and nodules of secondary carbonates (Table 8.3, Fig. 8.9 & 8.10), which altogether could implicate relict cryopedogenesis (Velichko et al., 1996a,b). A rather low variation of χ_{LF} in the [IV] indicates the homogeneity of the initial sediment while the highest variation of OM and especially CM reflects the differential leaching of carbonates constrained by the geomorphic position within the polygonal network: increasing from the polygon interiors to troughs and nodes.

In troughs, large wedge casts [C```] propagating from the surface of [V], on the flanks are superimposed by smaller wedge-like deformations [C`` and C`]. That suggests, at least, several episodes of thermal contraction cracking (French et al., 2003; French, 2007; Romanovskij, 1973) in changing environments producing wedge-shapped structures of different size and possibly type.

Downturned stratification of the host sediment [IV] and superimposed low-amplitude faulting at the sides of [C```]-casts (Fig. 8.14e) suggests at least some recognizable ice content in initial wedges. On the other hand, the infilling of [C]-casts resembles host sediment [IV] but is almost decalcified (Fig. 8.9, Table 8.3) and is significantly less clayey against the higher viscosity and porosity. Thus, some primary input of eolian dust during the wedge growth could be expected resulting in composite wedge formation (Ghysels & Heyse, 2006; French, 2007; Bertran et al., 2014, etc.). Later it endured apparent yet limited thermokarst reworking and sagging during thawing (Vandenberghe & Van den Broeck, 1982; Van Vliet-Lanoë, 1988; Gozdzik, 1995; Ghysels & Heyse, 2006; French, 2007; Murton, 2007) leading to some secondary infill of the voids from collapsing wedge sides. Some subordinate rejuvenation of thermal contraction cracking could be reflected in smaller wedge structures superimposed on the larger casts (Fig. 8.6a).

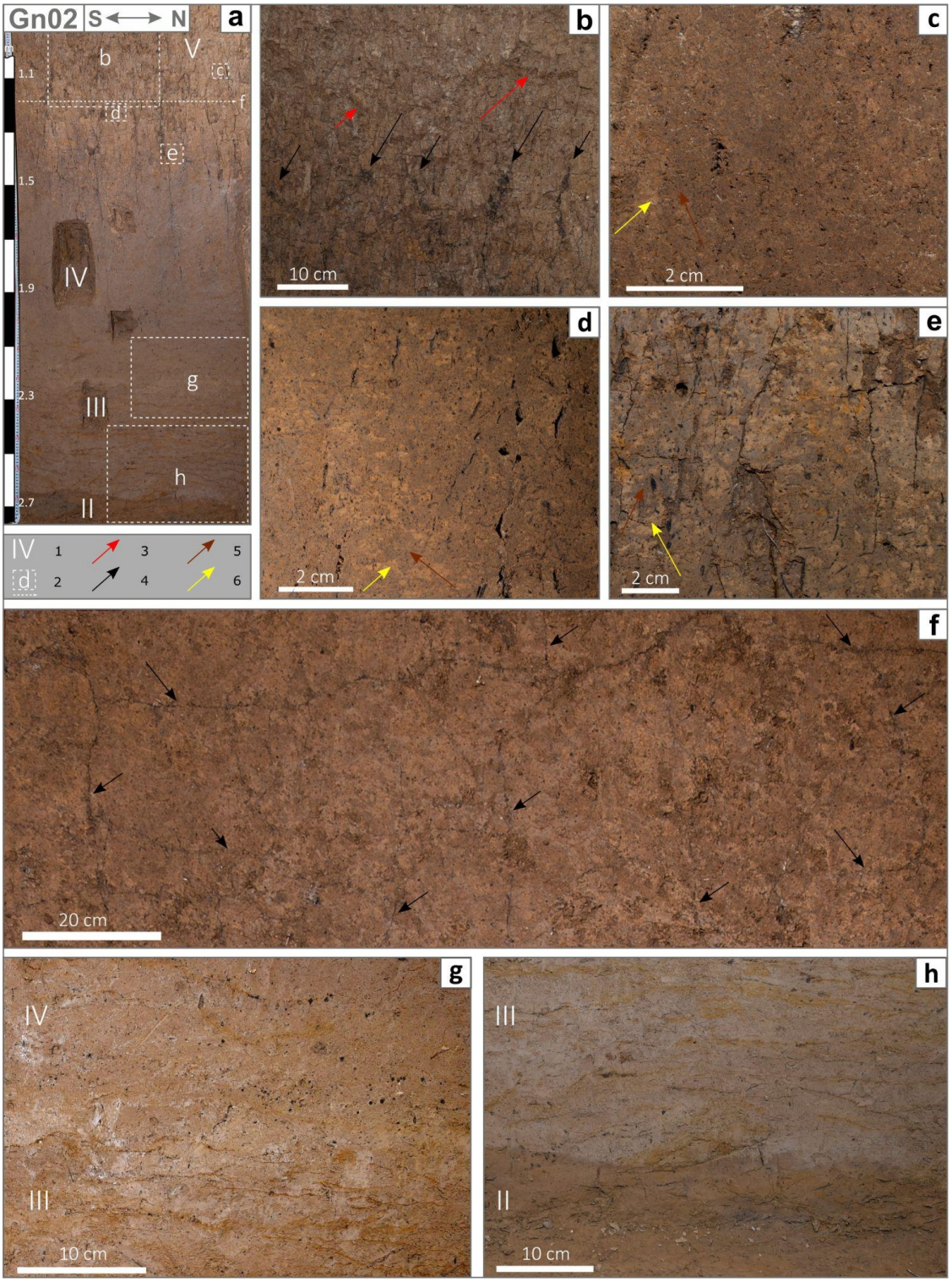

Figure 8.13. Small sedimentary and soil structures in host sediments: a) an overview; b) *Lamellae* structure of the dell infill [VII] and buried truncated network of plane pores with black argillans in [V]; c–e) mesoscale intrapedal structure of [V]; note the enlarging pattern of light silty patches downwards and the dominance of the darker clay phase at the top; f) orthogonal network of plane pores with black argillans in [V]; g) subsoil of buried paleo cryosol [IV] rooted in shallow lacustrine silty clays [III]; h) eroded contact of contrastingly stratified fluvially reworked deposits [II] with laminated shallow lacustrine silty clays [III].
1 – unit indices (see Table 8.2); *2* – location of horizontal (f) and vertical (b)–(e),(g),(h) cross-sections in sidebars; *3* – *Lamellae* structures; *4* – the buried network of truncated plane pores with black argillans; *5* – darker clay phase; *6* – light silty phase of bipartite lenticular-patchy structure.

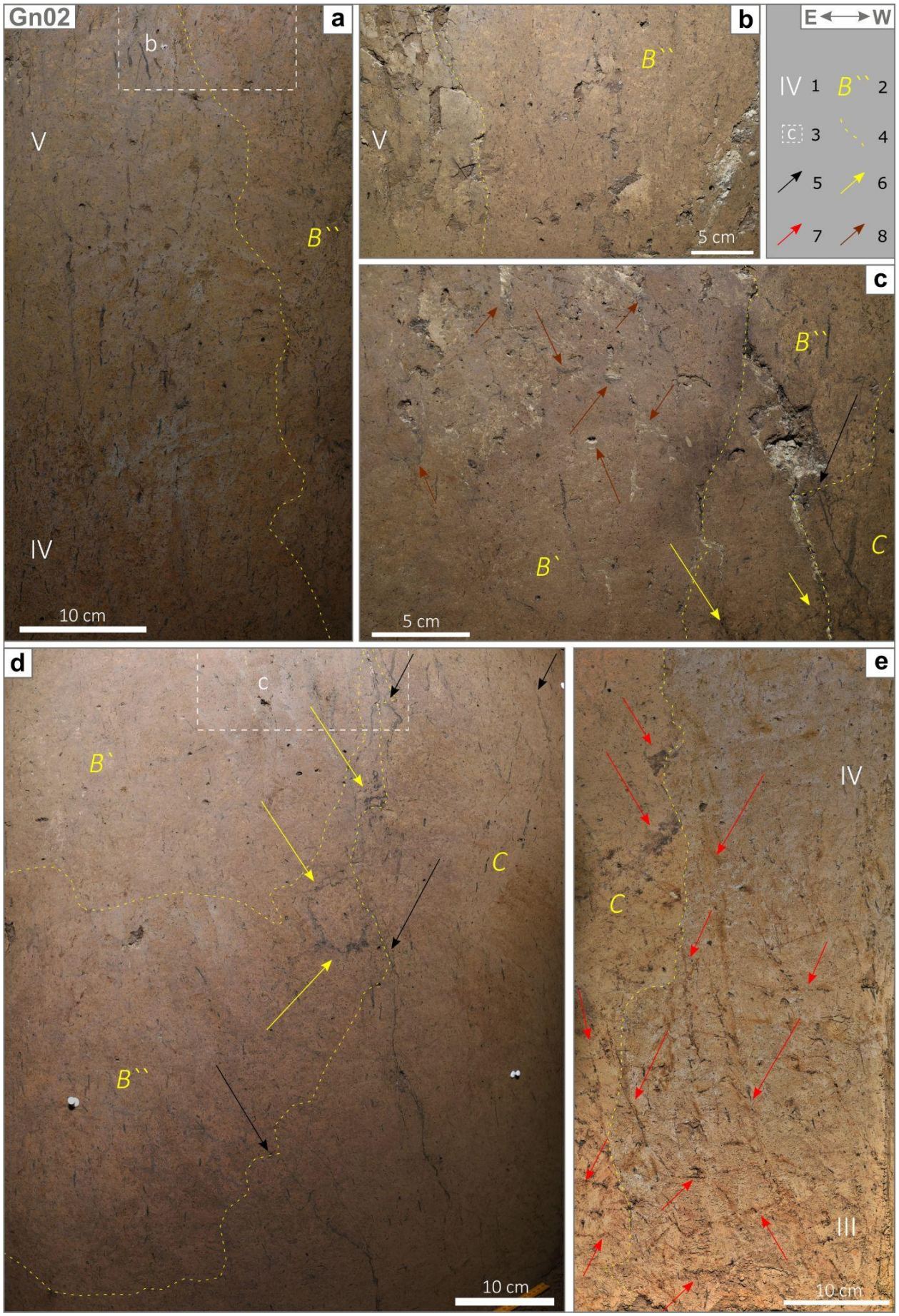
Gn02
a
b
V
B``
IV
10 cm
b
B``
V
5 cm
E ⟷ W
IV 1 B`` 2
c 3 4
5 6
7 8
c
B``
B`
C
5 cm
d
c
B`
C
B``
10 cm
e
IV
C
III
10 cm

Figure 8.14. Small sedimentary and soil structures in wedge casts: a) the eastern contact of the composite-wedge cast [B] with host sediments; b) intrapedal microstructures at the contact of the host [V] and cast [B``]; c–d) interiors of casts [B] and [C]. Note the abundance of light silty phase in the [B`]-cast interior and zoogenic tubes and cavities infilled with dark-brown argillians and light siltans (c); Note that plane pores infilled with black argillans are *in situ* only in the pseudomorph [C] but deformed at the side contact with the cast [B``] (d); e) the western contact of ice-wedge pseudomorph [C] with host sediments of post-cryogenic reticulate structure. Note the subhorizontal structure immanent in [IV] and [III] broken by inclined microfaults running from inside the [C]-cast. Indices of: *1* – host units and *2* – casts (see Table 8.2 for referencing); *3* – location of vertical cross-sections shown in sidebars; *4* – sedimentary contacts; *5* – the buried network of truncated plane pores with black argillans in [C]-casts; *6* – deformed plane pores with slightly redeposited black argillians at the contact zone of casts [C] and [B``]; *7* – post-cryogenic reticulate structures; *8* – relict and actual infills of soil macro- and mesofauna burrows.

The gradual transition from [IV] to [V] in polygon interiors is marked by the admixture of light silty phase (Fig. 8.13e) and prominent rise in coarse silt fraction (Fig. 8.7, L4) while in throughs the undulating lower contact of [V] is rather sharp and also has wedge-like features of a larger period but smaller amplitude. Low variations of both LOI and χ_{LF} in [V] argue for the spatially monotonous deposition and diagenesis. That implies a lasting eolian input as the prevailing deposition agent, commonly attributed to mantle loams at the marginal zone of the MIS6 glaciation (Spiridonov, 1960; Kriger, 1965; Moskvitin, 1967; Gerasimov & Davitaya, 1973; Sergeeva et al., 1986; Kleber & Gusev, 1998; Trofimov et al., 2001; Velichko et al., 2006). A rather unstable rise in sand and coarse silt fractions upwards suggests a slight increase in the energy of the main depositional agent. On the other hand, a syn-sedimentary reworking of host sediment is expressed in the formation of a darker clayey phase that gradually increases upwards causing a specific lenticular-reticulate structure of the entire unit (Fig. 8.13c–e). Such features were attributed to the short-distance solifluction and frequent freeze-thaw cycles (Grigor'eva et al., 2012; Van Vliet-Lanoë, 1988, etc.) occasionally referred to as limon a doublettes (i.a. Lauttridou & Sommé, 1974; Antoine et al., 1999;Guette-Marsac et al., 2009).

Black argillans, which infill the network of truncated plane pores (Fig. 8.13b,f) running down straight from the eroded top of [V] and penetrating as host sediments [V–II] as [C]-casts (Fig. 8.14d), are consistent with another surface stabilization. It could be matched with the ceased eolian accumulation in deeply degraded or non-permafrost conditions yet with no distinct signs of thermokarstic activity. That enabled the development of the deep plane pores network occupied by vertical migration of suspensions indicating the distinct automorphic pedogenic stage resulted in the *Luvisol* formation. Organic-rich topsoil of the time could have been truncated by a certain erosion episode preceding or simultaneous with the accumulation of [VI].

Unit [VI] is distinguished generally on its morphology differing, on the one hand, by the termination of *albeluvic glossae* and *lamellae* structures from overlying [VII] and by vanishing of the bipartite intrapedal structure (darker and lighter matter o lenticular-reticulate structure) and black argillans characteristic of underlying [V], on the other. Hence that specific interstitial unit bears the most prominent casts [B] (Fig. 8.6b) serving as an important stratigraphical reference.

[B]-casts do not contain but cut and deform the network of subvertical plane pores with black argillians, the latter being slightly redeposited at the contact with [C]-casts (Fig. 8.14c,d). They start from the top of [VI] faintly differing from the host but displaying sharp and clear subvertical side contacts with underlying [V]. That could point to the formation of [B]-casts either upon the deposition of [VI] or even concurrently with it.

The amount of initial ice probably was very low due to the absence of thermokarstic reworking as of the infill as of the side contacts. Those contrasting structures of silty texture

with thin multiphase patches and lenses of even better-sorted coarse silts (Fig. 8.14b–d) could be argued to have experienced a strong eolian input that partially relates it to typical sand wedges widespread in Central and Western Europe and Northern America. Yet [B]-casts explicitly differ by the main mode fraction of infilling and certain reworking by slope processes probably upon thawing of low ice content. Rather clear wedge shapes of the sharp-sided structures are often compared to bulbous or bundle or irregularly shaped sand wedges (Worsley, 2016; Murton et al., 2000; Andrieux et al., 2016a; Ewertowski et al., 2017, etc.), allowing to consider them a variation o composite wedge casts with low initial ice content (Ghysels & Heyse, 2006; French, 2007; Bertran et al., 2014, etc.).

Lenses of lamellic silty loams [VII] with very thin lenses of intrapedal structure are incised in [VI] and occasionally cut the top of [B]-casts (Figs. 8.6, 8.8a, & 8.13a,b) displaying distinct footprints of fluvial and/or slope redeposition of [VI] and even [V].

Dark asymmetric wedge casts [A] with thin apophyses filled with organic-rich fine loamy matter (Fig. 8.12b) are bound to [VII] reflecting the last impulse of cryogenesis at the key site. It is often problematic to distinguish if such fragmentary structures required deep-seasonal freezing with frost cracks or permafrost conditions (Black, 1976; Murton et al., 2000; Murton, 2007; Ewertowski et al., 2017). However, preserved angular contacts at the tips of [A]-casts (Fig. 8.8) (Garankina et al., 2022) and their substantial sizes (1–2 m deep at the Gnezdilovo key site) provide quite an argument for its formation in the presence of dry permafrost. Thus, it is possible to correlate the [A]-casts formation with rather mild thermal contraction cracking focused in the most susceptible polygonal nodes. As to the question of whether they developed after or during the dark topsoil formation a simultaneous ground fill during pedogenesis is supported by a rather low OM content of [A]-casts compared to the overlying RHH or modern humus horizon.

The other type of organic-rich matter present at the top of [VI] and [VII] usually is referred to as the relict humus horizon. RHH lacks any signs of cryogenic disturbances or hydromorphic pedofeatures representing a period of past *Mollic* horizon formation and/or its derivates.

Regional stratigraphic correlation. *Wedge casts*. The stratigraphical model proposed by A.A. Velichko and colleagues (1996a,b, 2006, 2011) distinguished three paleocryogenic horizons: Smolensk being of MIS5 – MIS4 age and Vladimir and Yaroslavl both of MIS2 age: the former related to the onset of LGM and the latter corresponding majorly to the Late Glacial. If footprints of the latest cryogenesis at the Russian Plain center are commonly assumed to be ice-wedge pseudomorphs of two phases (a and b) of wedge infilling, the older paleocryogenic horizons (Vladimir and Smolensk) were thought to have manifested only as involutions, cryoturbation and solifluction features formed in the seasonally-frozen layer (whereas substituted by small wedge casts further south). However, in the Sungir section near Vladimir (Makeev & Velichko, 2000) there was a mention of a large "earth vein" penetrating from underneath the MIS2 loess as opposed to more widely found footprints of its superimposed reworking since the LGM.

Morphologically studied [B]-casts quite resemble the reported structures of the Yaroslavl cryogenic horizon (Velichko et al., 1996a,b). Although our findings support neither its interpretation as ice-wedge pseudomorphs nor attribution to the latest cryogenesis episode of the Younger Dryas. Those presumably earth wedges are separated both from even younger wedge-shaped structures [A] above by the deposition of [VII] and from the older casts [C] by the pronounced deposition of [V] (Garankina et al., 2022) and even a stage of *Luvisol* formation.

In some previously studied sections as Bogolubovo, a misinterpretation of such inherited paleocryostructures of two different horizons could be expected as some differences

in the infilling of the upper and lower parts of the casts have been reported. Yet they were assumed to result from the sequential phases of the initial ice-wedge degradation and not two separate stages of cryogenesis. However, the affinity of [C]-cast infilling to its clayey host [IV] and the sharp upper boundary separating it from the overlying mantle of silty loams [V] forces us to attribute its development to the Vladimir cryogenic horizon referencing the Sungir section. Its timing most confidently can be attributed as following the onset of LGM due to the increasing influence of eolian input over quite ceasing slope processes. Yet composite-wedge casts [C] with higher initial ice content have formed in cold but relatively wet (bogs in depressions) environments (Makeev & Velichko, 2000) against the composite wedges [B] with low ice content that reflect severely dryer and harsher conditions of the Late Glacial reported from the paleoflorisic data (Borisova, 2021).

The upper dark casts [A] have not been separately regarded as paleocryogenic structures by Velichko et al. (1996a,b), being assumed a tonguic part of the Holocene RHH. Yet the authors briefly mentioned gray-brown loamy casts of the late Yaroslavl phase. V.M. Alifanov (1995) followed by Makeev et al. (2015) suggests the Late Glacial age for dark casts implying they were formed during the Older and/or Younger Dryas on top of the Bølling–Allerød "cryohydromorphic" paleosol, which served as a source for the organic-rich infilling. A.L. Alexandrovskiy (2011, 2014) showed the Allerød stratigraphic position of the dark cryosols later buried by slope sediments at the Borisoglebsk Upland with similar relative age interpretations recently obtained by Garankina et al. (2022).

Thus, it is possible to correlate the formation of wedge casts [A] with short permafrost aggradation during the Younger Dryas (late Yaroslavl stage) predeceased by pedogenesis of the Allerød or even concurrent with it at some point (Sedov et al., 2022). Casts [B] reflect the previous stage of the Late Glacial cooling (probably the Oldest Dryas) being initially composite wedges with low ice and high eolian components. Therefore, casts [C] indicate significantly wetter conditions of the LGM onset and could reliably be correlated with the ice-wedge networks of the Vladimir cryogenic horizon (Sycheva et al., 2021).

Paleosols. As of buried paleosols, the key site provides a more comprehensive picture than was previously suggested (Velichko et al. 1996a,b, 2006). Stable stages of relict pedogenesis consistent with negligible sedimentation are reflected, on the one hand, in the accumulation of secondary carbonates at polygon interiors in [IV] and ubiquitous formation of a tetragonal system of thin subvertical plane pores filled with illuvial organo-argillans in [V], on the other. The former pedofeature can be reliably attributed to the Bryansk pedogenesis during the end of MIS3 (Velichko et al., 1996a; Sycheva et al., 2020, 2021) both due to its stratigraphic position and morphological resemblance.

Although the latter pedofeature being clamped between the LGM and Late Glacial wedge casts [B] and [C] was rarely reported in the previous studies of the Vladimir Opolie except for rarely mentioned traces of another soil unit or fissures filled with dark (humified) clayey films (Paleosols..., 2000), incorporated organic lenses (Velichko et al., 1996a,b, 2006). However, the developed morphology of that paleopedofeature allows correlation with the Trubchevsk paleosol bound to the substantial permafrost degradation. According to the paleofloristic data (Borisova, 2021) such conditions first occurred during the main deglaciation at the end of the Late Pleniglacial, which is corroborated by the findings both at the southern (Gololobovo, Trubchevsk, and Khotylevo sites – Velichko et al., 2006, 2011; Stolpnikova et al., 2018) and northern (Borisoglebsk Upland – Rusakov et al., 2015) regions. In the Kursk region, the younger age estimation for that paleosol is provided correlating it with Allerød paleosols of Western Germany (Sycheva et al., 2020, 2021). Nevertheless, such rejuvenation of that

pedogenesis is not plausible as it was followed by at least two more pronounced episodes of cryogenesis (casts [B] and [A]) that deform the discussed pedofeatures. Footprints of the past pedogenesis can also be found in the lower-lying loamy heterogeneous facies [II], which could tentatively be correlated with redeposited material of one of the Mezin (MIS5) paleosols (Velichko et al., 1996a,b, 2006) found at the Bogolubovo site. While the distinct age and type determination of the pedogenesis is of the further research goals, the timing of its redeposition may be referred to as the beginning of the Early Glacial.

Host units. Following the proposed relative stratigraphy, the first manifestation of paleocryogenic topography should have occurred before the eolian deposition of [V] as it coats the undulating top of [IV] and [C]-casts. Amplitudes are not traced between the tetragonal blocks and the secondary generation of wedges (transverse troughs) (Fig. 8.15b) inside the block ridges. Or even an opposite trend of a slightly concave upper contact of [C]-cast with [V] is displayed on the E wall of Gn01 (Fig. 8.6a). Thus, the origination of longitudinal dells along the primary wedges (Fig. 8.15a) was rather not attributed to thermokarst of the ice contained in wedges and accompanied sagging. Feasibly they occurred due to some runoff concentration along the wedges following the general slope, which provided there a sharper concave contact with the overlying [V] against the gradual transition at the polygon interiors.

Later another deepening of dells occurred on top of [V], which deposition probably had almost completely reduced the preceding dell microtopogrphy. It is not possible to discern if the major erosive episode preceded or postdated the *Luvisol* formation in [V]. However, juxtaposed with the paleoenvironmental reconstructions (Borisova, 2021), at least some erosion could have been expected around 19 ka BP matching the intensification of the surface runoff in still-permafrost conditions. Also subsequent to *Luvisol* formation, an increase in slope mobility could be associated with the accumulation of [VI]. The further infilling of dells with loams [VII] occurred after the wedges [B] formation in the Oldest Dryas yet before the Allerød (cryo)sol formation (Alexandrovskiy, 2011) and the Younger Dryas final cryogenic stage (earth wedges A). Thus, it could correspond to the Bølling warming or the transition to an elusive cold stage of Older Dryas.

Deposition of loams [V] with footprints of repeated freeze-thaw cycles and short-distance slope processes may be confidently referred to as the second part of LGM with reported increased continentality of the climate (Borisova, 2021) followed by superimposed Trubchevsk interstadial *Luvisol* formation.

Shallow lacustrine sedimentation of [III] preceding the Bryansk paleocryosol development and turbation of its upper part or even the entire depth of unit could tentatively be referred to as the Early Pleniglacial preceded by the redeposition of the last interglacial soil at the onset of the Early Glacial.

Relict humus horizons and organic-rich casts. The concept of RHH ("second humus horizon") has been used quite presumptuously accounting for several different phenomena. Commonly it refers to all buried or eluviated relicts of *Phaeozems* developed during the Atlantic climate warming, which is corroborated by the richest pool of radiocarbon dates (Velichko et al., 1996a; Alexandrovskiy, 2011, 2014; Alexandrovskiy et al., 2022, etc.). However, there are some cryomorphic features of the lowest parts of such dark morphons and rare pre-Holocene radiocarbon dates related to them (Velichko et al., 1996a; Alexandrovskiy, 2011, 2014; Alexandrovskiy et al., 2022), which occasionally were referred to as "third humus horizon" or Allerød cryomorphic paleosols. For the Vladimir Opolie, Alifanov (1995) and Makeev et al. (2015) suggested the formation of the entire dark morphons as a major impact of the Late Glacial cryopedogenesis regarding the major Holocene pool of radiocarbon dates as being significantly rejuvenated by the superimposed Holocene pedogenesis. The Late Glacial age of *Chernozems* that evolved into

Luvisols after the Neolithic is also reported from Southern Poland (Kabała et al., 2019).

As signs of both such phenomena are manifested at the key sites, in our opinion, they represent separate stages of pedogenesis. The older one (Allerød) being affected by the Younger Dryas frost and thermal contraction cracking ([A]-casts) despite the dark-gray color shows a rather low organic matter content. The younger ones comprise the highest amounts of OM reflecting milder conditions of the Holocene optimum. We assume the latter *in situ* horizon and its redeposited derivates to serve as the middle Holocene RHH while the former to be regarded as an even older cryosol relict of the Late Glacial.

Spatial distribution of wedge-shaped casts and associated landscape transformation. The regular linear pattern of longitudinal cropmarks correlates well with the lateral distribution of evenly spaced large wedge-shaped casts [B] buried by the associated lenses of reddish-brown loams [VII] with embedded RHH in dells. Besides, transverse wedge-shaped casts [B] truncated by plowing were found spaced ~15 m across the slope (between Gn01 and Gn10) (Fig. 8.5c). Put together, orthogonal wedge casts build up a rectangular block ~25 m x 15 m in size (E – W and N – S respectively, Fig. 8.7). Thus, the longitudinal extension of that block is two times shorter than displayed by the faint patchy latitudinal cropmarks on the arable surface. Yet the distribution of transverse wedge casts corresponds well to the narrow but distinct latitudinal anomalies of electrical resistivity (Fig. 8.5b) and magnetic field (Makarov et al., 2021; Modin et al., 2021) introducing a high potential for detailed correlations of landscape characteristics with geophysical data (Erokhin et al., 2011; Zhurbin & Fedorina, 2017).

Nodes of the polygonal network, well displayed both in satellite and aerial imagery and electrical resistivity maps (Fig. 8.5c,d), are occupied by the rounded filled depressions (Gn11, Gn26). Resembling features bound to polygonal trough intersections but rather topographically prominent (up to 1.5–3 m deep) were detected elsewhere in the Vladimir Opolie earlier (Alifanov, 1995; Velichko et al., 1996a,b; Makeev et al., 2015, etc.). While confirming the primary post-cryogenic (thermokarstic) origin of such depressions against the degrading permafrost (Murton et al., 2000; Ewertowski et al., 2017; Van Vliet-Lanoë et al., 2019) yet it points to the significant Holocene reworking of the initial landscape (Garankina et al., 2022).

The polygonal network of the Late Glacial wedge casts [B] is not reflected in the modern microtopography of the key site yet inherits buried microlows of the unit [IV] upper surface. Moreover, our investigation revealed (Fig. 8.15) an obligatory replication of wedge cast [C] by wedge cast [B], with the latter propagating along the axial part of the former despite the thick eolian stratum [V] in-between (Figs. 8.6 & 8.9b). The same relationship is fair for the [A]-casts inheriting the [B]-casts, yet well-manifested only at the intersections of polygonal troughs (nodes) (Fig. 8.9c).

Longitudinal transects both along the dell axis (Fig. 8.15c) and subparallel block ridge (Fig. 8.15b) demonstrate that the top surfaces of all sedimentary units starting from [IV] are conform with the modern slope reflecting rather steady trends of erosion and accumulation. On the opposite, the pronounced past topographic elevation of blocks above the troughs is well reflected in the high-amplitude and deformed top of paleocryosol [IV] on the latitudinal transect (Fig. 8.15a). The top of [V] had been repeatedly eroded with the first episode recorded in the linear incision along the axes of longitudinal buried casts [C]. The next stage associated with the composite wedges [B] thawing and casting is reflected in the continuous slope erosion and mass wasting at blocks and transverse troughs versus linear incision and redeposition in dells along the main slope. That stage yielded the major infilling of dells. Hence local sediment sinks – nodes and adjacent fragments of dells – enabled the repeated accumulation and preservation of organic-rich casts [A] and relict

horizons (RHH) both at the end of the Late Glacial and through the Holocene. And since the Mediaeval ages, the lowered amplitudes of the periglacial landscape have been almost completely leveled due to prolonged tillage both at polygonal interiors and transverse troughs, leading to the burial of the RHH.

At the block ridges including polygon interiors and transverse troughs plow layer is enriched with admixtures of [V] and is directly underlaid by BT horizon without eluvial topsoil (Makeev et al., 2015). On average it is thinner due to higher compaction of the underlying layer [V] compared to [VI] at rims and [VII] with RHH at dells.

Implications of fine-scale heterogeneity of magnetic properties in the postglacial sedimentary cover. Field magnetic susceptibility measurements proved to be a powerful tool for identifying fine-scale heterogeneities of sediments low-contrasting in texture and structure, such as paleocryomorphic features and soil horizons including paleosols (Vagapov et al., 2013), zoogenic disturbances and anthropogenic modifications, solid runoff variations (Jordanova et al., 2011, 2014).

κ-mapping of the vertical and horizontal sections highlights the buried casts inheriting both ice and composite wedges, which values, though to a varying degree, statistically exceed those of the host sediments. Supported by the laboratory χ_{LF}-measurements (Fig. 8.10, Table 8.3), that probably hints at the more redox conditions accompanying its formation in lower geomorphic, thus, more waterlogged positions.

Due to the general increase of magnetic susceptibility in soils compared to parent material (Maher, 1998, Babanin et al., 1995) the dark lenses of organic-rich loams (RHH) associated with dells and nodes stand out on the maps of κ-distribution (Fig. 8.11). At polygon interiors (Fig. 8.19b), the topsoil is significantly lower in κ-values, which is associated with the exposure of underlying units [V] and indicates the prevalence of slopewash at such geomorphic positions.

Generally, *κ*-values received for host thickness and RHH (Table 3) appear to be at similar ranges as shown by recent studies in the area (Kosnyreva & Zolotaya, 2011). E.g., κ maximum (up to 0.8 10^{-3}SI) associated with arable horizons P and ELhh (RHH) significantly exceeded values in underlying deposits (0.20–0.25 10^{-3}SI). The same pattern was found further to the south where magnetic susceptibility parameters reached the second maximum at the AU/AU-B boundary in *Chernozem* profiles (χ up to 0.4 $1e^{-6}m^3/kg$ and κ up to 0.35 10^{-3}SI) indicating humus paleosol horizons thickening in microlows of paleocryogenic topography (Alifanov et al., 2010, 2012; Vagapov et al., 2013; Ovchinnikov et al., 2020). Notably lower κ-values (0.05–0.3 10^{-3}SI) for RHH and dark casts with organic-rich infill [A] were found northwards at the Borisoglebsk Upland (Garankina et al., 2022). It was considered to reflect specifics of relict paleosols formation and/or subsequent humus degradation due to regional differences throughout the Late Glacial and Holocene or other factors as local drainage settings (Dearing et al., 1985) or fluvial redeposition of both RHH and [A]-cast material. As shown above intense zooturbation of the [A]-cast infills can also reflect in the decrease of magnetic susceptibility apparently due to the extra input of low-magnetic clastic matter by the pedofauna (Figs. 8.9c & 8.12b).

At the dell in the Gn04 section (Fig. 8.11), a contrasting concave lens interrupts the zone of higher κ-values associated with RHH. Such a localized infill low in κ-values but lined up with displaced RHH residues of increased κ-values at the bottom suggests an anthropogenic origin of the small pit later filled up by the material of underlying clastic units. Yet the cause of such ancient excavation at the grave field periphery and the timing of its infill remain obscure.

Another anomaly is bound to the bright-red loamy lens atop the [B]-cast (Figs. 8.10a & 8.12a), which greatly surpasses the entire sedimentary thickness in κ-values. Such increased magnetic susceptibility is reported to be caused by high temperatures

during wildfires (Le Borgne, 1960; Maher, 1998). However, the localized surficial manifestation of the anomaly could be indicative of a local pyrogenic event, most probably a regular bonfire found close to the Mediaeval necropolis (Makarov et al., 2021).

Soil variability and microcombinations. At the axial part of block ridges, comprising both transverse troughs and polygon interiors, *Nudiargic Luvisols (Cutanic, Loamic, Profondic, Relictiturbic)* are regular while substituted by *Haplic Luvisols (Cutanic, Loamic, Profondic)* at longitudinal rims closer to the dells (Figs. 8.6a & 8.15a,b). *Nudiargic* principal qualifier implies the significant admixture of argic horizon [V] in the entire volume of the relatively thin (up to 20 cm) plow layer. That corresponds with both modern tillage and pronounced microslope erosion during the Holocene soil formation at block ridges. *Relictiturbic* supplementary qualifier infers either the shallow depth (≤1 m) of cryoturbated upper contact of the buried paleocryosol [IV] at blocks or [B]-casts truncated by plowing at transverse troughs.

At the dells, the banded structure of [VII] caused by fluvial and colluvial infill (Figs. 8.6b, 8.8a, & 8.15a,c) conditions the development of *Lamellic Luvisols, although* limited to positions dominated by recent erosion. In contrast, at accumulative positions (proximity of the polygonal nodes), the exclusive preservation of RHH constrains the *Luvic Glossic* and *Vermic Luvic Glossic Phaeozems* distribution. Low-contrast microcombinations of *Luvic Glossic Phaeozems (Abruptic, Loamic, Pachic, Tonguic)* and *Vermic Luvic Glossic Phaeozem (Abruptic, Loamic, Tonguic, Relictiturbic)* gravitate to the node's center (Fig. 8.8b) whereas *Vermic Luvic Glossic Phaeozem (Abruptic, Loamic, Tonguic)* and *Luvic Glossic Phaeozem (Abruptic, Loamic, Tonguic)* sprout at the periphery. *Pachic* supplementary qualifier implies a maximum thickness up to 0.6 m of *Mollic* horizon and/or RHH while *Relictiturbic* – a sharp transition of *Mollic* or RHH to dark casts [A] in the upper 1 m.

Thereby, the soil cover along the dell axis is quite puzzled by sporadic patches of *Lamellic Luvisols (Cutanic, Loamic, Profondic)* (Fig. 8.6b), *Lamellic Luvisols (Cutanic, Differentic, Loamic, Profondic), Luvic Glossic Phaeozems (Abruptic, Loamic, Tonguic)* and *Vermic Luvic Glossic Phaeozems (Abruptic, Loamic, Tonguic)* (Fig. 8.8a).

Rims along the dells are designated by a gradual transition from *Glossic Retisols (Abruptic, Aric, Cutanic, Differentic, Loamic, Profondic)* to *Abruptic Luvisols (Cutanic, Differentic, Loamic, Profondic)*. We attribute the limitation of *Retisols* to the rims as a result of the unit [VI] cropping out straight under the plow pan (Fig. 8.15a) where *albeluvic glossae* are significantly reduced compared to neighboring dell infills [VII] with *Luvisols* and *Phaeozems*.

Therefore, the facial variability of postglacial lithological structure at the key site is essentially defined by the historical inheritance of buried wedge-cast networks (Kabała et al., 2022; Woronko et al., 2022) and associated cryogenic deformations of host sediments. The actual soil cover generally succeeds that surficial lithological heterogeneity. Although its modern complexity is caused by the differences in erosion and accumulation trends on the finest spatial scale. In turn, those trends were limited by the distribution of cryogenic and post-cryogenic landforms during the entire postglacial landscape development.

A.O Makeev (2009, 2015) regarded soils of the Vladimir Opolie as surface paleosols due to the abundance of relict pedofeatures particularly in the topsoil. Our findings, au contraire, reveal the continuous postglacial pedogenesis (incl. both the full-Holocene and actual soil formation) that conditioned the specific welded architecture of the soil body. Thus, the interfluvial soils of the region can be regarded as the Late Pleistocene – Holocene pedocomplexes.

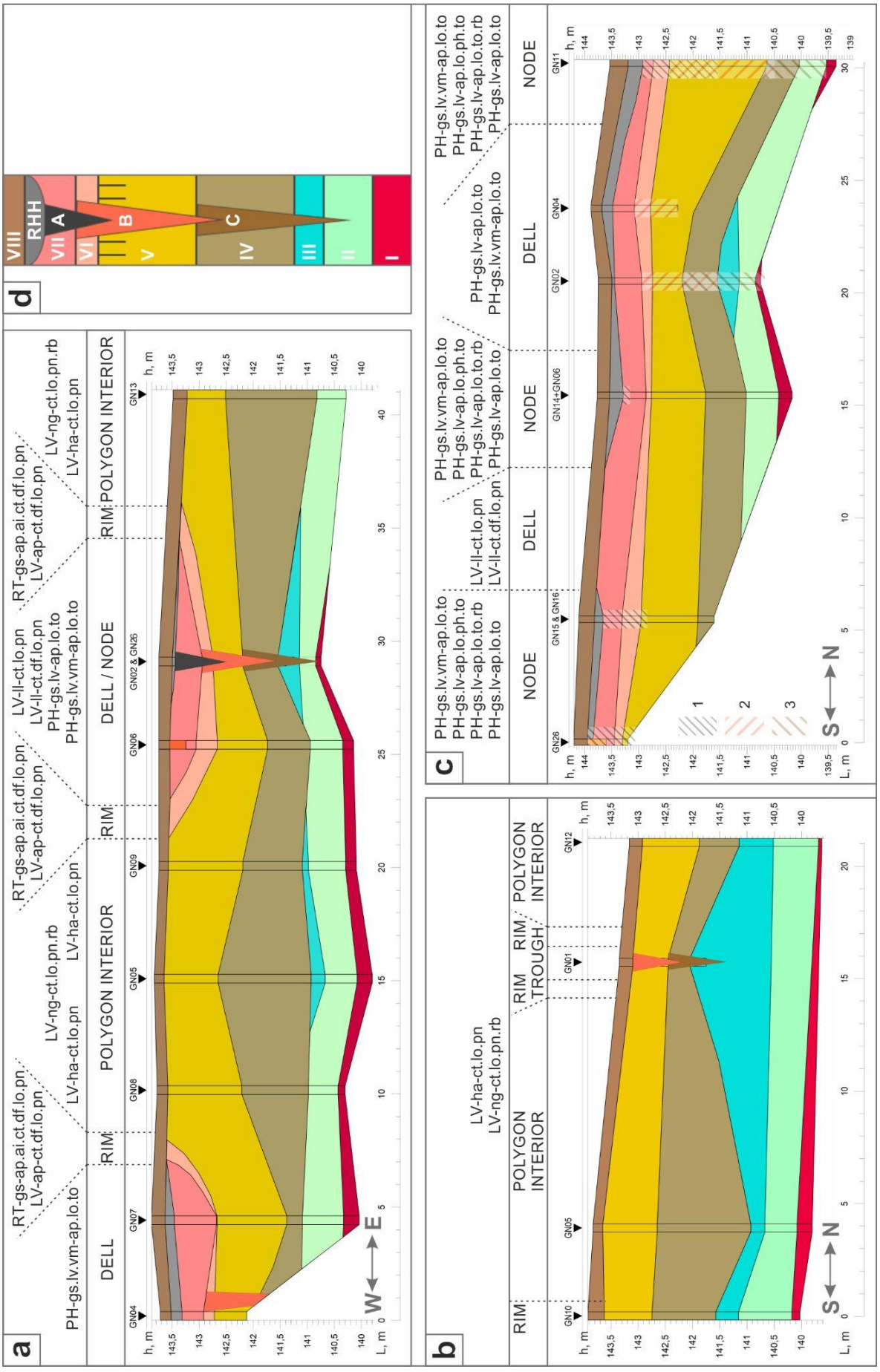
a
RT-gs-ap.ai.ct.df.lo.pn
LV-ap-ct.df.lo.pn
PH-gs.lv.vm-ap.lo.to
LV-ng-ct.lo.pn.rb
LV-ha-ct.lo.pn
LV-ll-ct.lo.pn
LV-ll-ct.df.lo.pn
PH-gs.lv-ap.lo.to
PH-gs.lv.vm-ap.lo.to
LV-ng-ct.lo.pn.rb
LV-ha-ct.lo.pn
DELL
RIM
POLYGON INTERIOR
RIM
DELL / NODE
RIM
POLYGON INTERIOR
GN04
GN07
GN08
GN05
GN09
GN06
GN02 & GN26
GN13
h, m
L, m
W
E
b
LV-ha-ct.lo.pn
LV-ng-ct.lo.pn.rb
RIM
POLYGON INTERIOR
RIM
TROUGH
RIM
POLYGON INTERIOR
GN10
GN05
GN01
GN12
h, m
L, m
S
N
c
PH-gs.lv.vm-ap.lo.to
PH-gs.lv-ap.lo.ph.to
PH-gs.lv-ap.lo.to.rb
PH-gs.lv-ap.lo.to
LV-ll-ct.lo.pn
LV-ll-ct.df.lo.pn
PH-gs.lv-ap.lo.to
NODE
DELL
NODE
DELL
NODE
GN26
GN15 & GN16
GN14-GN06
GN02
GN04
GN11
h, m
L, m
S
N
1
2
3
d
VIII
RHH
VII
A
VI
B
V
C
IV
III
II
I

Figure 8.15. Generalized stratigraphic and spatial structure of the key site: a) latitudinal transect and two longitudinal transects across the polygon interiors (b) and along the dell axis with nodes (c) of the key polygonal blocks. Abbreviations for naming soil individuals are given following the Rules for the use of the codes for naming soils and Rules for the use of the codes for creating map legends (IUSS Working Group WRB, 2022). *1* – wedge casts [A], *2* – wedge casts [B], *3* – wedge casts [C], shown only at certain cores and pits on the longitudinal transect along the dell. (d) Generalized stratigraphic column (see Table 8.2 & Fig. 1c for units and spatial referencing).

Vladimir Opolie was considered one of the "loess islands" (Makeev, 2009; Makeev et al., 2015) due to the significant involvement of silt – "loess fraction" – in the postglacial mantle. Combined with the manifold succession of paleogeographic events shown above that relates the opolie to loess-paleosol series of extra-glacial uplands southwards. However, the revealed welded architecture of Late Pleistocene and Holocene soil bodies as well as numerous superimposed sedimentation agents and intervening cryogenic horizons determine a specific palimpsest type of the environmental record more likely comparable with the palimpsest one (Targulian et al., 1974) in mantle loams of the uplands northwards (Shishkina et al., 2019).

CONCLUSIONS

Integration of thorough morphological investigation supported by analysis of spatial and depth distribution of textural, magnetic susceptibility, organic and carbonate matter properties at the key sites at the Borisoglebsk Upland and Vladimir Opolie allowed us to reveal the high heterogeneity of sedimentary and soil cover conditioned by relict periglacial features yet demonstrating sufficient reproducibility across the entire marginal zone of the MIS6 (Moscow) glaciation.

– Postglacial thickness show contrasting stratigraphic sequence reflecting stable sedimentary environments at each stage of landscape development. The predominant colluvial trend of re-deposition shifts upwards to local shallow lacustrine sedimentation with increasing eolian input. During the Late Pleniglacial, the eolian agent prevails as both sediment source and deposition mechanism. Since the Oldest Dryas, the colluvial re-deposition once again takes the leading part in the Late Glacial landscape transformation and Holocene soil cover evolution. The main patterns of spatial heterogeneity were enabled at stages of surface stabilization due to negligible sediment transfer when cryogenic and pedogenic processes repeatedly transformed the postglacial stratum.

– At the key site, the first *in situ* soil body is a buried paleocryosol correlated with the regional MIS3 pedogenesis (Bryansk or Sungir paleosol). The overlying pronounced loess unit reflects a contrastingly dry cold sedimentation environment strongly affected by another interstadial pedogenesis in a rather warmer climate presumably at the time of the Main Deglaciation (end of the Late Pleniglacial, Trubchevsk paleosol).

– Three wedge-cast horizons each separated by pronounced loess or colluvial deposition represent distinct changes in the periglacial environment from the formation of wider composite wedges in host sediments with higher water capacity to severely dryer settings enabling the development of more narrow composite wedges and initial earth wedges. The cryogenic sequence culminated with the occurrence of smaller but organic-rich soil wedges reflecting the last cold episode of the Late Glacial (the late phase of Yaroslavl cryogenic horizon, Younger Dryas). Therefore, two older wedge-cast horizons at the base and on top of the thick loess stratum are correlated with two separate cold stages – the onset of LGM (Vladimir cryogenic horizon) and the Oldest Dryas (early (main) phase of Yaroslavl cryogenic horizon). That points to a period of

warm *Luvisol*-like pedogenesis in-between suggesting distinct climate warming during the Trubchevsk Late Pleniglacial interstadial.

– Late Glacial elevation amplitudes of the polygonal wedge cast networks are almost completely leveled due to the prolonged erosion trend at the key site. Despite that, the differentiation of the actual soil cover inherits that polygonal pattern. Polygon interiors, adjacent rims, and dells occupying the polygonal troughs running downhill display the high contrast of soil microcombinations. However, the transverse troughs where wedge casts are exposed and significantly truncated show no distinction in soil distribution from polygon interiors. Thus, the actual soil cover is not sensitive to the cryogenic pattern *per se* but reflects the surficial deposit re-distribution with respect to buried cryogenically constrained erosional landforms.

– Postglacial thickness of the Vladimir Opolie replicates the same stratigraphic sequence of sedimentation, pedo-, and cryogenesis typical of loess-paleosol series of extraglacial southern regions. Simultaneously its type of environmental record with the welded architecture of Late Pleistocene and Holocene soil bodies and intervening erosion episodes is more comparable with the palimpsest record of mantle loams at the neighboring glacial uplands. Interfluvial soils of the region can be regarded as Late Pleistocene – Holocene pedocomplexes.

REFERENCES

Aleshinskaya, Z.V., Gunova, V.S. 1997. Recent deposits and paleogeography of Lake Nero. Moscow *University Bulletin. Series 5. Geography,* ***1***, 49–52 (in Russian).

Aleksandrovskiy, A.L. 1983. *Holocene Evolution of Soils of East-European Plain*. Nauka, Moscow (in Russian).

Alexandrovskiy, A.L. 1996. The Holocene evolution of the soil cover of the Russian plain. *Eur. Soil Sci.,* ***28***, 20–32.

Alexandrovskiy, A.L. 2011. Soil evolution on the low terraces of Lake Nero. *Eur. Soil Sci.,* ***44***, 1055–1067. https://doi.org/10.1134/S1064229311100024

Alexandrovskiy, A.L. 2014. Soil evolution and natural environment of Eastern Europe in the Holocene. In: Proceedings of All-Russian scientific conference on archaeological soil science. ISSP PBC RAS, Pushchino, 9–14 (in Russian).

Alexandrovskiy, A.L., Chendev, Y.G., Yurtaev, A.A. 2022. Soils with the second humus horizon, paleochernozems, and the history of pedogenesis at the border between forest and steppe areas. *Eur. Soil Sci.,* ***55***, 127–146. https://doi.org/10.1134/S1064229322020028

Alifanov, V.M. 1986. Gray forest soils in the center of the Russian Plain. Historic and genetic analyses. In: I.V. Ivanov and V.A. Demkin (Eds.) *Evolution and Age of Soils of USSR*. Scientific center of biological research, AS USSR, Pushchino. 155–162 (in Russian).

Alifanov, V.M. 1995. *Paleocryogenesis and Modern Pedogenesis*. ONTI PNC Russian Academy of Sciences, Puschino (in Russian).

Alifanov, V.M., Gugalinskaya, L.A., Ivannikova, L.A., Ovchinnikov, A.Y. 2006. Soil polygenesis in the northeast part of Vladimir opolie. *Eur. Soil Sci.,* ***39***, 31–39. https://doi.org/10.1134/S1064229306130072

Alifanov, V.M., Gugalinskaya, L.A., Ovchinnikov, A.Yu, 2010. *Paleocryogenesis and Soil Variability in the Center of East European Plain*. GEOS, Moscow (in Russian).

Alifanov, V.M., Vagapov, I.M., Gugalinskaya, L.A. 2012. Distribution of magnetic susceptibility in profiles of complex palaeocryomorphic soils. *Bull. of the Samara Scientific Centre of RAS,* ***14***, 2028–2031 (in Russian).

Andrieux, E., Bertran, P., Antoine, P., Deschodt, L., Lenoble, A., Coutard, S., et al. 2016. Database of Pleistocene periglacial features in France: description of the online version. *Quaternaire,* ***27***(4), 329–339. https://doi.org/10.4000/quaternaire.771

Andrieux, E., Bertran, P., Saito, K. 2016. Spatial analysis of the French Pleistocene permafrost by a GIS database. *Permafrost Periglac. Process.,* ***27***, 17–30. https://doi.org/10.1002/ppp.1856

Antoine, P., Rousseau, D.-D., Lautridou, J.-P., Hatte´, C. 1999. Last interglacial-glacial climatic cycle in loess-palaeosol successions of north-western France. *Boreas,* ***28***, 551–563. https://doi.org/10.1111/j.1502-3885.1999.tb00241.x

Antonov, S.I., Bolysov, S.I., Myslivets, V.I. 1992. Cryogenic relicts in the topography and loose sediments of the Middle Protva drainage basin. *Geomorfologia,* ***1***, 41–49 (in Russian).

Aparin B., Rubilin E. 1975. *Specific of Soil Formation in Two-layered Sediments of the North-Western Part of the Russian Plain*. Nauka, Leningrad (in Russian).

Arkhangelskaya, T.A. 2014. Diversity of thermal conditions within the paleocryogenic soil complexes of the East European Plain: the discussion of key factors and mathematical modeling. *Geoderma,* ***213***, 608–616. https://doi.org/10.1016/j.geoderma.2013.04.001

Astakhov V., Shkatova V., Zastrozhnov A., Chuyko M. 2016. Glaciomorphological map of the Russian Federation. *Quat. Int.,* ***420***, 4–14. https://doi.org/10.1016/j.quaint.2015.09.024

Babanin, V., Trukhin, V., Karpachevskii, L., Ivanov, A., Morozov, V. 1995. *Soil Magnetism*. YSTU, Yaroslavl (in Russian).

Baranov D.V., Panin A.V. 2021. Dynamics and causes of incision of the Upper Volga River according to OSL dating of terrace staircases. In: *Materials of the II All-Russian Conference "Puti evolyucionnoj geografii"*, 22–25 November 2021, Moscow, 761–764 (in Russian).

Baranov, D.V. 2022. Geomorphology of the upper Volga River valley: study history and state of the problem (paper 2. The Upper Volga Lowland). *Geomorfologiya,* ***52***, 4, 3–14. https://doi.org/10.31857/S0435428122010047

Baranov, D.V., Utkina, A.O., Panin, A.V. 2022. Tver proglacial lake (Tver region, Russia): myth or reality. *Limnology and Freshwater Biology,* ***4***, 1383–1384. https://doi.org/10.31951/2658-3518-2022-A-4-1383

Barysheva, A.A. 1953. Nero Lake basin: physico-geographical characteristics. Extended abstract of doctoral thesis in geography. MOPI, Moscow (in Russian).

Basevich, V.F., Dmitriev, E.A. 1979. Impact of uprooting on the soil cover. *Pochvovedenie,* ***9***, 134–142 (in Russian).

Belyaev, V.R., Garankina, E.V., Shorkunov, I.G., Konstantinov, E.A., Rusakov, A.V., Shishkina, Y.V., Andreev, P.V., Verlova, T.A. 2020. Holocene erosion and deposition within a small catchment of the northeastern Borisoglebsk Upland (Central European Russia). In: *IOP Conf. Ser.: Earth Environ. Sci.*, V Int. Conference on Ecosystem dynamics in the Holocene, 11–15 November 2019, Moscow, 438. https://doi.org/10.1088/1755-1315/438/1/012002

Berdnikov, V.V. 1976. *Palaeocryogenic Topography of the Center of the Russian Plain*. Nauka, Moscow (in Russian).

Bertran, P., Andrieux, E., Antoine, P., Coutard, S., Deschodt, L., Gardère, P., Hernandez, M., Legentil, C., Lenoble, A., Liard, M., Mercier, N., Moine, O., Sitzia, L., Van Vliet-Lanoë, B. 2014. Distribution and chronology of Pleistocene permafrost features in France: database and first results. *Boreas, **43***, 699–711. https://doi.org/10.1111/bor.12025

Bikbulatov, E.S., Bikbulatova, E.M., Litvinov, A.S., Poddubniy, S.A. 2003. *Hydrology and Hydrochemistry of Lake Nero*. Rybinsk Publ. House, Rybinsk (in Russian).

Black, R.F. 1976. Periglacial features indicative of permafrost: ice and soil wedges. *Quat. Research, **6***, 3–26.

Borisova, O.K. 2021. Landscape and climatic conditions in the Central East European Plain in the last 22 thousand years: Reconstruction based on paleobotanical data. *Water Resour., **48***, 886–896. https://doi.org/10.1134/S0097807821060038

Borisova, O., Konstantinov, E., Utkina, A., Baranov, D., Panin, A. 2022. On the existence of a large proglacial lake in the Rostov-Kostroma lowland, north-central European Russia. *J Quat. Sci., **37***(8), 1442–1459. https://doi.org/10.1002/jqs.3454

Brewer R. 1976. *Fabric and Mineral Analysis of Soils*. R.E. Krieger, Huntington, New York.

Chizhikov, N.V. 1956. Geomorphology and soils of the Nero Lake basin and Ustje-Kotorosl' rivers. In: N.V. Sukachev and N.V. Korde (Eds.) *Treatises of the laboratory of sapropel deposits, **6***, AS USSR, Moscow, 130–144 (in Russian).

Czudek, T. 1993. Pleistocene periglacial structures and landforms in Western Czechoslovakia. *Permafrost Periglac. Process., **4***, 65–75. https://doi.org/10.1002/ppp.3430040106

Dearing, J.A., Maher, B.A., Oldfield, F. 1985. Geomorphological linkages between soils and sediments: the role of magnetic measurements. In: K.S. Richards, R.R. Arnett, and S. Ellis (Eds.) *Geomorphology and Soils*. Allen & Unwin, London, 245–266. https://doi.org/10.4324/9780429320781

Dobrovolskaya, M.V., Makarov, N.A., Samorodova, M.A. 2020. Mobility of the Suzdal Opolye settlers in 900–1150 AD. *Archaeol. Ethnol. Anthropol. Eurasia, **48***, 106–115. https://doi.org/10.17746/1563-0110.2020.48.4.106-115

Dokuchaev, V.V. 1884. On so-called Yuriev Chernozem. *Papers of Saint-Petersburg Nature Society, **15***, 48–77 (in Russian).

Dolgova, L.S. 1964. On the necessity of soil cover structure study using fine-scale soil mapping. In: *Soil-Geographic and Landscape-Geochemical Research*. Moscow University, Moscow, 104–121 (in Russian).

Dorosh, Ye.Ya. 1973. *Rain in-Twain with Sun: Village Diary*. Sovetskij pisatel', Moscow.

Dubrovina, I.V., Gradusov, B.P. 1993. Chemical and mineralogical characteristics of soils of Vladimir Opolie. *Pochvovedenie, **3***, 64–73 (in Russian).

Duller, G.A.T. 2008. *Luminescence Dating: Guidelines on Using Luminescence Dating in Archaeology*. English Heritage, Swindon.

Ehlers, J., Gibbard, L.P., Hughes, D.P. 2011. *Quaternary Glaciations – Extent and Chronology: A Closer Look*, 1st ed. Dev. Quat. Sci., Elsevier, 15.

Eremenko, E.A., Karevskaya, I.A., Panin, A.V. 2010. Postglacial transformation of glaciofluvial channels in the marginal zone of the Moscow (MIS6) glaciation. *Moscow University Bull. Series 5, Geography, **2***, 56–70 (in Russian).

Erokhin, S.A., Modin, I.N., Palenov, A.Yu., Shevnin, V.A. 2011. Mapping of relict cryogenic polygonal structures using geophysical methods. *Engineering Surv., **11***, 30–34 (in Russian).

Ewertowski, M., Kijowski, A., Szuman, I., Tomczyk, A., Kasprzak, L. 2017. Low-altitude remote sensing and GIS-based analysis of cropmarks: classification of past thermal-contraction-crack polygons in central-western Poland. *Geomorphology, **293***, 418–432. https://doi.org/10.1016/j.geomorph.2016.07.022

Field Book for Describing and Sampling Soils. 2012. NSSC, NRCS, USDA.

Fortunatov, M.A., Moskovskiy, B.D. 1970. Lakes of the Yaroslavl region. In: *Lakes of the Yaroslavl Region and Prospects for Their Economic Use*. Yaroslavl State University, Yaroslavl, 3–183 (in Russian).

French, H. (ed). 2007. *The Periglacial Environment*, 3rd ed. Wiley.

French, H.M., Demitroff, M., Forman, S.L. 2003. Evidence for Late-Pleistocene permafrost in the New Jersey Pine Barrens (Latitude 39°N), Eastern USA. *Permafrost Periglac. Process., **14***, 259–274. https://doi.org/10.1002/ppp.456

Garankina, E.V., Belyaev, V.R., Shorkunov, I.G., Shishkina, Yu.V., Andreev, P.V., Sheremetskaya, E.D. 2019. Lake sedimentation as an underestimated agent of postglacial transformation of interfluves and fluvial landscapes of the Borisoglebsk Upland, Central European Russia. In: *Land Use and Climate Change Impacts on Erosion and Sediment Transport*. Proceedings of IAHS, 27–31 August 2018, Moscow, 381, 13–20. https://doi.org/10.5194/piahs-381-13-2019

Garankina, E.V., Lobkov, V.A., Shorkunov, I.G., Belyaev, V.R. 2022. Identifying relict periglacial features in watershed landscape and deposits of Borisoglebsk Upland, Central European Russia. *J of Geological Society, **5***, 179. https://doi.org/10.1144/jgs2021-135

Gerasimov, I.P., Davitaya, F.F. 1973. Subaerial origin of mantle loams. *Izvestiya AS SSSR, Series 3, Geography* (in Russian).

Gerasimov, I.P., Velichko, A.A. (Eds.). 1982. *Paleogeography of Europe during the Last 100000 yrs*. Nauka, Moscow, 81–92 (in Russian).

Gerasimova, M.I., Gubin, S.V., Shoba, S.A. 1996. *Soils of Russia and Adjacent Countries: Geography and Micromorphology*. Moscow State University, Wageningen Agricultural University, Moscow, Wageningen.

Ghysels, G., Heyse, I. 2006. Composite-wedge pseudomorphs in Flanders, Belgium. *Permafrost Periglac. Process.*, ***17***, 145–161. https://doi.org/10.1002/ppp.552

Gild, C., Geitner, C., Sanders, D. 2018. Discovery of a landscape-wide drape of late-glacial aeolian silt in the western Northern Calcareous Alps (Austria): First results and implications. *Geomorphology,* ***301***, 39–52. https://doi.org/10.1016/j.geomorph.2017.10.025

Gorlova, R.N. 1968. Change of vegetation cover during the Mikulino interglacial according to studies of peat bogs in the Yaroslavl region. In: N.I. Pyavchenko (Ed.) *History of Development of Vegetation Cover in Central Regions of European Part of USSR in Anthropocene*. Nauka, Moscow, 45–91 (in Russian).

Gozdzik, J. 1995. Permafrost evolution and its impact on deposition conditions between 20 and 10 ka BP in Poland. *Biuletyn Peryglacjalny,* ***34***, 53–72.

Gradusov, B.P., Chizhikova, N.P. 1976. Clay minerals of loess. *Reports of AS USSR,* ***229***, 1433–1435 (in Russian).

Grigor'eva, T.M., Sycheva, S.A., Belyaev, Y.R., E.D. Sheremetskaya. 2012. Textures and micromorphology of the early Valdai pedosediments and their importance for the reconstruction of the natural conditions in the period of the first Post-Mikulino cooling (MIS5d). *Eur. Soil Sc.,* ***45***, 172–181. https://doi.org/10.1134/S1064229312020111

Guette-Marsac, C., Lautridou, J.-P., Cliquet, D., Lechevalier, C., Schwenninger, J.-L., Lamothe, M., Mercier, N., Fosse, G. 2009. Les occupations du Paléolithique moyen et supérieur d'Épouville (Pays de Caux) en contexte loessique. *Quaternaire,* ***20***(3), 389–404 (in French). https://doi.org/10.4000/quaternaire.5269

Gugalinskaya, L.A. 1997. Morpholithopedogenesis of the center of the Russian Plain. Extended abstract of doctoral thesis in biology, Pushchino (in Russian).

Gugalinskaya, L.A., Alifanov, V.M. 2005. Late Pleistocene morpholithogenesis of Holocene soils in the center region of the Russian Plain. *Bull. Comm. Study Quat.,* ***66***, 33–41 (in Russian).

Gugalinskaya, L.A., Ivannikova, L.A., Alifanov, V.M., Antoshechkina, N.A. 2001. Pedocyclites in Grey Forest and buried Bryansk soils of the Vladimir Opol'e and biological methods of their diagnostics. *Eur. Soil Sci.,* ***34***, 1031–1042.

Gunova, V.S. 1975. The history of Lake Nero according to paleobotanical data. Doctoral thesis. Moscow State University, Moscow (in Russian).

Gunova, V.S., Leflat, O.N. 1997. Holocene and current state of the ecosystem of Lake Nero. *Moscow University Bull. Series 5. Geography,* ***5***, 42–45 (in Russian).

Hart, J.K., Boulton, G.S. 1991. The interrelation of glaciotectonic and glaciodepositional processes within the glacial environment. *Quat. Sci. Rev.,* ***10***, 335–350. https://doi.org/10.1016/0277-3791(91)90035-S

Ivanova, I.K. 1972. In the Commission for Study of the Quaternary at the Environmental Science section, AS USSR (1969 and 1970). *Bull. Comm. Study Quat.,* ***38***, 156–164.

IUSS Working Group WRB. 2022. *World Reference Base for Soil Resources. Int. Soil Classification System for Naming Soils and Creating Legends for Soil Maps* (4th ed.). Int. Union of Soil Sciences (IUSS), Vienna.

Jongmans, A.G., Feijtel, T.C., Bouma, J.A. 1989. Micromorphological and chemical study of a buried Saalian till deposit in the northern part of The Netherlands. *Catena,* ***16***, 559–574. https://doi.org/10.1016/0341-8162(89)90042-8

Jordanova, D., Jordanova, N., Atanasova, A., Tsacheva, T., Petrov, P. 2011. Soil tillage erosion estimated by using magnetism of soils — a case study from Bulgaria. *Environ Monit Assess.,* ***183***, 381–394. https://doi.org/10.1007/s10661-011-1927-8

Jordanova, D., Jordanova, N., Petrov, P. 2014. Pattern of cumulative soil erosion and redistribution pinpointed through magnetic signature of Chernozem soils. *Catena,* ***120***, 46–56. https://doi.org/10.1016/j.catena.2014.03.020

Kabała, C., Musztyfaga, E., Waroszewski, J. 2019. Modern and sub-fossil clay-illuvial soils with albeluvial tonguing in SW Poland. In: *XXX Congress of the Soil Science Society of Poland. Soil – Source of Life*, Lublin, 2–7 September 2019. Book of Abstracts. Polihymnia Sp. z o.o., 55.

Kabała, C., Musztyfaga, E., Jary, Z., Waroszewski, J., Gałka, B., Kobierski, M. 2022. Glossic planosols in the postglacial landscape of central Europe: Modern polygenetic soils or subaerial palaeosols? *Geoderma,* ***426***, 116101. https://doi.org/10.1016/j.geoderma.2022.116101

Kaplin, P.A., 2005. Continental ice formations and peripheral sea basins of Russia in the Pleistocene. *Moscow University Bull. Series 5. Geography,* 55–65 (in Russian).

Karpachevsky, L.A., Dmitriev, E.A., Skvortsov, E.A., Basevich, V.F. 1978. Windfall part in shaping the structure of soil cover. In: *Structure of Soil Cover and Use of Soil Resources*. Nauka, Moscow, 37–43 (in Russian).

Kasatkin, V.G. 1931. *Soils and Landforms of Ivanovo Industrial Area* (in Russian).

Khimenkov, V.G. 1932. *Essay on Geological Structure of Volga River Valley and Its Tributaries between Staritsa and Kalinin*. Mosgeorazvedka Trust, Moscow (in Russian).

Khudyakov, O.I., Alifanov, V.M., Pletenev, P.A., Ovchinnikov, A.Yu., Reshotkin, O.V., Bukhonov, A.V. 2020. Palaeocryogenesis as a factor of heterogeneity of agro-grey soil. *Eur. Soil Sci.*, ***53***, 1437–1445. https://doi.org/10.1134/S1064229320100099

Kleber, A., Gusev, V.V. 1998. Soil parent materials in the Moshaysk district, Russia. *Catena*, ***34***, 61–74. https://doi.org/10.1016/S0341-8162(98)00082-4

Kleber, A., Terhorst, B. (Eds.), 2013. *Mid-Latitude Slope Deposits (Cover Beds)*. Dev. Sedimentol., Elsevier.

Konstantinov, E.A., Karpukhina, N.V., Zakharov, A.L., Bricheva, S.S., Ukraintsev, V.Yu., Lazukova, L.I., Rudinskaya, A.I. 2023. Fluctuations of Nero Lake during the Holocene. *Geomorfologiya i Paleogeografiya*, ***54***, 2, 51–60 (in Russian). https://doi.org/10.31857/S2949178923020044

Konstantinov, E.A., Karpukhina, N.V., Zakharov, A.L., Bricheva, S.S., Ukraintsev, V.Yu., Lazukova, L.I., Rudinskaya, A.I. 2022. Fluctuations of Nero Lake in the Holocene. *Doklady Earth Sciences*, ***506***, Suppl. 1, S48–S54. https://doi.org/10.1134/S1028334X22700258

Kosnyreva, M.V., Zolotaya, L.A. 2011. *Geophysical Methods in Soil Science. Developing a Complex of Geophysical Methods for Solving Applied Problems of Soil Mapping*. Lambert Academic (in Russian).

Kostychev, P.A. 1949. *Soils of Chernozemic Area of Russia. Genesis, Composition, and Features*. State Agricultural Publ., Moscow (in Russian).

Krasyuk, A.A. 1925. *Soil Areas of Ivanovo-Voznesensk, Kostroma, and Vladimir Regions*. Moscow–Leningrad (in Russian).

Kriger, N.I. 1965. *Loess, Its Properties and Relationship with Geographical Environment*. Nauka, Moscow (in Russian).

Kust, P., Makeev, A., Lessovaya, S., Milanovsky, E., Rusakov, A., Abrosimov, K., Belyaev, V., Ryazantsev, P. 2022. Polygenetic features in Retisols formed in Moscow (Late Saalian) glacial till. *Catena*, ***214***, 106245. https://doi.org/10.1016/j.catena.2022.106245

Kuzmin, Y.V., van der Plicht, J., Sulerzhitsky, L.D. 2014. Puzzling radiocarbon dates for the Upper Paleolithic site of Sungir (central Russian Plain). *Radiocarbon*, ***56***, 451–459. https://doi.org/10.2458/56.17038

Kvasov, D.D. 1975. *Late Quaternary History of Eastern Europe's Large Lakes and Inland Seas*. Nauka, Leningrad (in Russian).

Lang, J., Lauer, T., Winsemann, J. 2018. New age constraints for the Saalian glaciation in northern central Europe: Implications for the extent of ice sheets and related proglacial lake systems. *Quat. Sci. Rev.*, ***180***, 240–259. https://doi.org/10.1016/j.quascirev.2017.11.029

Lautridou, J.-P., Sommé, J. 1974. Les loess et les provinces climato-sédimentaires du Pléistocène supérieur dans le Nord-Ouest de la France. Essai de corrélation entre le Nord et la Normandie. *Quaternaire*, ***11***, 3–4, 237–241 (in French).

Lavrushin, Yu.A. 1976. *Composition and Genesis of Basal Tills of Continental Glaciers*. Nauka, Moscow (in Russian).

Lavrushin, Yu.A., Chistyakova, I.A. (Eds.). 2001. *Problems of Stratigraphy and Paleogeography of Quaternary Deposits of the Yaroslavl' Volga Region*. Materials of symposium, Yaroslavl, July 2001. GEOS, Moscow (in Russian).

Le Borgne, E. 1960. The influence of iron on the magnetic properties of the soil and on those of schists and granite. *Amer. geophys.*, ***16***, 20.

Liu, Q., Roberts, A.P., Larrasoaña, J.C., Banerjee, S.K., Guyodo, Y., Tauxe, L., Oldfield, F. 2012. Environmental magnetism: Principles and applications. *Rev. Geophys.*, ***50***, RG4002. http://dx.doi.org/10.1029/2012RG000393

Lobanov, A.I. 2001. Specifics of glacial sediments structure and glaciotectonics in the vicinity of Yaroslavl'. In: *Problems of the Quaternary Stratigraphy and Paleogeography of the Yaroslavl' Volga Region*. Materials of symposium, Yaroslavl, July 2001. GEOS, Moscow (in Russian).

Lobkov, V.A., Shorkunov, I.G., Garankina, E.V., Sheremetskaya, E.D. 2023. Spatial organization of soil cover at a model site of Vladimir Opolie. In: *Periglacial of East-European Plain and Western Siberia*. Materials of All-Russian scientific conference, Rostov, 25–26 August 2023, IG RAS, Moscow (in Russian).

Lorz, C., Frühauf, M., Mailänder, R., Phillips, J.D., Kleber, A. 2013. Influence of cover beds on soils. *Dev. Sedimentol.*, ***66***, 95–125. https://doi.org/10.1016/B978-0-444-53118-6.00003-9

Lüthgens, C., Krbetschek, M., Böse, M., Fuchs, M.C. 2010. Optically stimulated luminescence dating of fluvioglacial (sandur) sediments from north-eastern Germany. *Quat. Geochronol.*, ***5***, 237–243. https://doi.org/10.1016/j.quageo.2009.06.007

Maher, B.A. 1998. Magnetic properties of modern soils and loessic paleosols: Implications for paleoclimate. *Palaeogeogr. Palaeoclimatol. Palaeoecol.*, ***137***, 25–54. https://doi.org/10.1016/S0031-0182(97)00103-X

Makarov, N.A, Krasnikova, A.M, Zaytseva, I.E., Dobrovolskaya, M.V. 2020. The Shekshovo medieval burial ground: "Vladimir mounds" in the light of new field research. *Russian Archeology,* ***4***, 121–140 (in Russian). http://dx.doi.org/10.31857/S086960630012630-2

Makarov, N.A., Fedorina, A.N., Shpolyanskiy, S.V. 2017. Large settlements of the X–XI centuries and structures of resettlement of the XII–XIII centuries in Suzdal Opolie: problems of continuity. In: *Archaeology of Vladimir-Suzdal Land*. Materials of scientific-practical seminar, IA RAS, 8 (in Russian).

Makarov, N.A., Krasnikova, A.M., Erokhin, S.A. 2021. First results of new studies of the Gnezdilovo cemetery near Suzdal. *Brief Comms. Inst. Archaeol.,* ***264***, 7–29 (in Russian).

Makeev, A.O. 2009. Pedogenic alteration of aeolian sediments in the upper loess mantles of the Russian Plain. *Quat. Int.,* ***209***, 79–94. https://doi.org/10.1016/j.quaint.2009.03.007

Makeev, A.O. 2012. *Surface Paleosols of Loess Areas in the Center of Russian Plain*. Molnet, Moscow (in Russian).

Makeev, A.O., Dubrovina, I.V. 1990. Geography, genesis, and evolution of soils of Vladimir Opolie. *Pochvovedenie, 7*, 5–25 (in Russian).

Makeev, A., Kulinskaya E., Yakusheva, T. 2015. Surface paleosols of the loess island within Moscow glacial limits: Vladimir Opolie. *Quat. Int.,* ***365***, 159–174. http://dx.doi.org/10.1016/j.quaint.2014.09.038

Makeev, A., Kust, P., Lebedeva, M., Rusakov, A., Terhorst, B., Yakusheva, T. 2019. Soils in the bipartite sediments within the Moscow glacial limits of the Russian Plain: Sedimentary environment, pedogenesis, paleolandscape implication. *Quat. Int.,* ***501***, 147–173. https://doi.org/10.1016/j.quaint.2017.09.017

Makeev, A.O., Panin, A.V., Subetto, D.A. (Eds.) 2023. *Periglacial of East-European Plain and Western Siberia*. Materials of All-Russian scientific conference, Rostov, 25–26 August 2023, IG RAS, Moscow (in Russian).

Makeev, A.O., Velichko, A.A. (Eds.). 2000. Paleosols and modern soils as stages of continuous soil formation. *Abstracts and Field Excursion Guidebook of V Int. Symposium on Paleopedology*, Suzdal, 10–16 July 2000. Dokuchaev Soil Science Society, RAS, Moscow.

Map of Volgostroy, 1:10000. O-37-101-A-a-1. Archived copy. 1933.

Markov, K.K., Velichko, A.A., Sudakova, N.G., Breslav, S.L., Berdnikov, V.V. (Eds.). 1969. *Guidebook "Moscow – Upper Volga"*. Int. Symposium on Paleogeography and Periglacial Phenomena of Pleistocene. Moscow State University, Moscow (in Russian).

Miedema, R. 1987. Soil Formation, Microstructure and Physical Behaviour of Late Weichselian and Holocene Rhine Deposits in the Netherlands. Doctoral thesis. University of Wageningen.

Milanovsky, E.Yu. 2009. *Soil Humus Substances as Natural Hydrophobic-hydrophilic Compounds*. GEOS, Moscow (in Russian).

Modin, I.N., Erokhin, S.A., Krasnikova, A.M., Shorkunov, I.G., Shevchenko, V.A., Skobelev, A.D. 2021. Geophysical studies of the visually imperceptible Shekshovo-9 medieval necropolis in Suzdal Opolie. *Moscow University Bull., Geology series.* ***76***, 1–13 (in Russian). https://doi.org/10.3103/S0145875221010087

Mokievskiy, N.V., Makeev, A.O., Rusakov, A.V., Lebedeva, M.P., KusT, P.G. 2023. The final stage of loess accumulation and its role in textural differentiation of Retisols on the Petrovskaya Ridge. In: *Periglacial of East-European Plain and Western Siberia*. Materials of All-Russian scientific conference, Rostov, 25–26 August 2023, IG RAS, Moscow (in Russian).

Moskvitin, A.I. 1967. *Pleistocene Stratigraphy of European Part of USSR. Transactions of AS SSSR*, Geological Institute, Moscow (in Russian).

Moskvitin, A.I. 1976. *Pleistocene Reference Sections of Russian Plain*. Nauka, Moscow (in Russian).

Murton, J. 2007. Periglacial landforms. Ice wedges and ice-wedge casts. In: S.A. Elias (Ed.) *Encyclopedia of Quaternary Science*. Elsevier, 2153–2170.

Murton, J., Worsley, P., Gozdzik, J. 2000. Sand veins and wedges in cold aeolian environments. *Quat. Sci. Rev.,* ***19***, 899–922. https://doi.org/10.1016/S0277-3791(99)00045-1

Murton, J.B., French, H.M. 1993. Thermokarst involutions, Summer Island, Pleistocene Mackenzie delta, Western Canadian Arctic. *Permafrost Periglac. Process.,* ***4***, 217–229. https://doi.org/10.1002/ppp.3430040304

Nesmelova, E.I., Sorokina, V.I., Surkova, G.I. 2007. *General Geographic Field Practice in the Moscow Area*. Faculty of Geography, Moscow State University, Moscow (in Russian).

Nikitin, S.N. 1885. Vladimir chernozem. *News of Geological Committee,* ***4***, 36–54 (in Russian).

Novenko, E., Velichko, A., Zyuganova, E., Junge, F., Boettger, T. 2005. Dynamics of vegetation at the late Pleistocene glacial/interglacial transition (new data from the center of the East European Plain). *Polish Geological Institute Special Papers,* ***16***, 77–82.

Novsky, V.A. 1975. *Pleisocene of Yaroslavl Volga Region*. Nauka, Moscow.

Obedientova, G.V. 1977. *Erosion Cycles and Formation of the Volga River Valley*. Nauka, Moscow (in Russian).

Obruchev, V.A. 1948. Loess as a specific type of soil, its genesis and goals of assessment. In: *Genesis and Geography of Soils: Selection of Scientific Papers*. AS USSR, Moscow – Leningrad, 23–38 (in Russian).

Ovchinnikov, A.Y., Alifanov, V.M., Khudyakov, O.I. 2020. The impact of palaeocryogenesis on the formation of grey forest soils in central Russia. *Eur. Soil Sci.*, ***53***, 1354–1364. http://dx.doi.org/10.1134/S1064229320100142

Palacios, D., Hughes, P.D., García-Ruiz, J.M., Andres, N. (eds). 2022. *European Glacial Landscapes: Maximum Extent of Glaciations*. Elsevier. https://doi.org/10.1016/C2020-0-00404-4

Paleopedology Glossary. 1997. Paleopedology Commission Newsletter.

Panin, A., Baranov, D., Moska, P. 2018. Rates of postglacial incision of the Upper Volga River estimated by luminescence dating of the terrace staircase. In: *Practical Geography and XXI Century Challenges*. Int. Geographical Union Thematic Conference dedicated to the Centennial of the IG RAS, 4–6 June 2018, Moscow. Conference Book, 1, 626–631 (in Russian).

Panin, A., Matlakhova, E. 2015. Fluvial chronology in the East European Plain over the last 20 ka and its palaeohydrological implications. *Catena,* ***130***, 46–61. https://doi.org/10.1016/j.catena.2014.08.016

Parunin, O.B., Timashkova, T.A. 1984. List of radiocarbon dates of the laboratory of recent deposits and paleogeography of Pleistocene, Faculty of Geography, Moscow State University. *Bull. Comm. Study Quat., 169*–172 (in Russian).

Piotrowski, J.A., Larsen, N.K., Junge, F.W. 2004. Reflections on soft subglacial beds as a mosaic of deforming and stable spots. *Quat. Sci. Rev.*, ***23***, 993–1000. https://doi.org/10.1016/j.quascirev.2004.01.006

Piotrowski, J.A., Larsen, N.K., Menzies, J., Wysota, W. 2006. Formation and subglacial till under transient bed conditions: deposition, deformation, and basal decoupling under Weichselian ice sheet lobe, central Poland. *Sedimentology,* ***53***, 83–106. https://doi.org/10.1111/j.1365-3091.2005.00755.x

Romanovskij, N. 1973. Regularities in formation of frost-fissures and development of frost-fissure polygons. *Biuletyn Peryglacjalny, 23*, 237–277.

Rubtsova, L.P. 1974. On the genesis of soils of Vladimir Opolie. *Pochvovedenie,* ***6***, 17–27 (in Russian).

Rukhina, E.V. 1973. *Lithology of Glacial Sediments*. Nedra, Leningrad (in Russian).

Rusakov, A., Nikonov, A., Savelieva, L., Simakova, A., Sedov, S., …, Titova, D. 2015. Landscape evolution in the periglacial zone of Eastern Europe since MIS5: Proxies from paleosols and sediments of the Cheremoshnik key site (Upper Volga, Russia). *Quat. Int.,* ***365***, 26–41. https://doi.org/10.1016/j.quaint.2014.09.029

Rusakov, A.V., Nikonov, A.A., Savelieva, L.A., Simakova, A.N., Maksimov, F.E., …, Starikova, A.A. 2017. Chronostratigraphy of the Cheremoshnik key section (Yaroslavl Volga Region) based on new geochronological, palynological, and paleosol data. *Doklady Earth Sciences,* ***472***, 244–247 (in Russian). https://doi.org/10.1134/S1028334X17020271

Rusakov, A., Sedov, S., Sheinkman, V., Dobrynin, D., Zinovyev E., Trofimova, S., Maximov, F., Kuznetsov, V., Korkka, M., Levchenko, S. 2019. Late Pleistocene paleosols in the extra-glacial regions of Northwestern Eurasia: Pedogenesis, post-pedogenic transformation, paleoenvironmental inferences. *Quat. Int.,* ***501***, 174–192. https://doi.org/10.1016/j.quaint.2018.03.020

Ruszczynska-Szenajch, H., Trzcinski, J., Jarosinka, U. 2003. Lodgement till deposition and deformation investigated by macroscopic observation, thin-section analysis, and electron microscope study at site Debe, central Poland. *Boreas,* ***32***, 399–415. https://doi.org/10.1111/j.1502-3885.2003.tb01093.x

Samus, A.V., Konstantinov, E.A. 2022. Vegetation dynamics in the Rostov lowland (Yaroslavl oblast) during the Late Glacial and Holocene based on new pollen data. *Limnology and Freshwater Biology,* ***4***, 1565–1567. https://doi.org/10.31951/2658-3518-2022-A-4-1565

Sedov, S., Sheinkman, V., Bezrukova, E., Zazovskaya, E., Yurtaev, A. 2022. Sartanian (MIS2) ice-wedge pseudomorphs with hydromorphic pedosediments in the north of West Siberia as an indicator for paleoenvironmental reconstruction and stratigraphic correlation. *Quat. Int.,* ***632***, 192–205. https://doi.org/10.1016/j.quaint.2022.05.002

Serebryanny, L.R. 1965. *Progress in Radiocarbon Dating in Quaternary Geology. For the VII INQUA Congress, USA*. Nauka. Moscow (in Russian).

Sergeeva, E.M., Larionova, A.K., Komissarova, N.N. (Eds.). 1986. *Loess Deposits. Vol. 1. Engeneering-Geological Specifics and Problems of Sustainable Management*. Nedra, Moscow (in Russian).

Sheremetskaya, E.D., Garankina E.V., Shishkina, Yu.V., Zhuravlyeva, V.I., Bogdanova, O.A., Shorkunov I.G., Lobkov, V.A. 2023. Methodological aspects of grain size analysis applied for detailed studies of watershed deposits. In: *Periglacial of East-European Plain and Western Siberia*. Materials of All-Russian scientific conference, Rostov, 25–26 August 2023, IG RAS, Moscow (in Russian).

Sheremetskaya, E.D., Karevskaya, I.A., Samus, A.V., Garankina, E.V., Shorkunov, I.G. 2022. New data on the stratigraphic importance of the Cheremoshnik section (Yaroslavl region). *Moscow University Bull. Series 5. Geography,* ***4***, 88–100 (in Russian).

Shik, S.M. 2010. On the glaciers distribution boundaries in the central part of European Russia. *Bull. Comm. Study Quat.,* ***70***, 100–107 (in Russian).

Shik, S.M., Tseytlin, S.M. (Eds.). 1981. *Guidebook for A–2 and C–2 excursions (Upper Volga and the Golden Ring)*. XI INQUA Congress, Moscow.

Shishkina, Y., Garankina, E., Belyaev, V., Shorkunov, I., Andreev, P., Bondar, A., Potapova, V., Verlova, T. 2019. Postglacial incision-infill cycles at the Borisoglebsk Upland: Correlations between interfluve headwaters and fluvial network. *Int. Soil and Water Conserv. Res.,* ***7***, 184–195. https://doi.org/10.1016/j.iswcr.2019.02.001

Shishov, L.L., Komov, N.V., Rodin, A.S., Fridland, V.M. 2001. *Soil Cover and Land Resources of the Russian Federation*. V.V. Dokuchaev Soil Science Institute, Moscow (in Russian).

Sidorenko, A.V. (Ed.). 1971. *Geology of USSR. 4. Center of the European Part of USSR (Moscow, Vladimir, Ivanovsk, Kalinin, Kaluga, Kostroma, Ryazan, Tula, Smolensk and Yaroslavl Regions), Part 1 – Geological Description*. Nedra, Moscow (in Russian).

Simakova, M.S. 1984. Reflection of ancient cryogenic processes in the structure of soil cover of limnoglacial plains in the western part of Yaroslav district. In: *Soil Cover Structure and Regional Planning*. Moscow, 157–165 (in Russian).

Skvortsova, E.B., Ulanova, N.G., Basevich, V.F. 1983. *Ecological Role Of Windfalls*. Forest industry, Moscow (in Russian).

Somov, E.I. 1939. Geological structure of the northern part of the Yaroslavl region. In: *Treatise of Mosk. Geol. Upravleniya,* ***31*** (in Russian).

Spiridonov, A.I. 1938. Geomorphology of the northeastern part of the Kalinin Region. *Uchenye zapiski of Moscow University, Geografiya*, ***23***, 112–157 (in Russian).

Spiridonov, A.I. 1960. Significance of the problem of the origin of mantle loams. *Zemlevedenie,* ***5***, 61–67 (in Russian).

Spiridonov, A.I. 1978. *Geomorphology of the European Part of USSR*. Higher School, Moscow (in Russian).

State geological map of USSR. Quaternary deposits. 1:200 000. O-37-XXVI. VSEGEI. 1967.

State geological map of USSR. Quaternary deposits. 1:200 000. O-37-XXVII. VSEGEI. 1969.

State geological map of USSR. Quaternary deposits. 1:200 000. O-37-XXVIII. VSEGEI. 1968.

State geological map of USSR. Quaternary deposits. 1:200 000. O-37-XXXIV. VSEGEI. 1968.

State geological map of USSR. Quaternary deposits. 1:200 000. O-37-XXXV. VSEGEI. 1968.

State Soil Map of USSR. 1:1 000 000. N-36, N-37, O-36, O-37, O-38. 1949–1958.

Stolpnikova, E.M., Kovaleva, N.O., Kovalev, I.V. 2018. The carbon isotope composition of organic matter and the age of paleosols from Wurm glaciations interstadials to Holocene (Bryansk region, Russia). *IOP Conf. Ser.: Earth Environ. Sci.,* ***107***, 012123. https://doi.org/10.1088/1755-1315/107/1/012123

Sudakova, N.G. 2008. Actual questions of interregional correlation of glacial horizons. Lithological concept. *Bull. Comm. Study Quat.,* ***60***, 50–58 (in Russian).

Sudakova, N.G., Antonov, S.I. 2021. Regional features of the geomorphological structure of previously glaciated region in the center of the Russian Plain. *Geomorfologia,* ***52***, 1, 100–108 (in Russian). https://doi.org/10.31857/S0435428121010120

Sudakova, N.G., Dashevskiy, V.V., Pisareva, V.V., Chebotaryeva, N.S., Shik, S.M. 1984. *Quaternary Deposits near the Town of Rostov-Yaroslavsky. Excursion 10–B Guidebook*. XXVII Int. Geological Congress, Moscow.

Sukachev, V.N., Gromov, V.I., Bader, O.N. 1966. Upper palaeolithic site Sungir. In: *Transactions of GIN,* ***162***, Nauka, Moscow (in Russian).

Svendsen, J.I., Alexanderson, H., Astakhov, V.I., Demidov, I., Dowdeswell, J.A., Funder, S., Gataullin, V., Henriksen, M., Hjort, C., Houmark-Nielsen, M., Hubberten, H.W. 2004. Late Quaternary ice sheet history of northern Eurasia. *Quat. Sci. Rev.* ***23***(11–13), 1229–1271. https://doi.org/10.1016/j.quascirev.2003.12.008

Sycheva, S., Frechen, M., Terhorst, B., Sedov, S., Khokhlova, O. 2020. Pedostratigraphy and chronology of the Late Pleistocene for the extra glacial area in the Central Russian Upland (reference section Aleksandrov quarry). *Catena,* ***194***, 104689. https://doi.org/10.1016/j.catena.2020.104689

Sycheva, S.A., Khokhlova, O.S., Pushkina, P.R. 2021. Structure of the Late Pleistocene climate rhythm inferred from the detailed soil-sedimentation archive of the extraglacial region of the East European Plain (Aleksandrovka quarry). *Stratigraphy and geological correlation,* ***29***, 368–387. https://doi.org/10.1134/S0869593821030084

Tanfil'ev, G.I. 1902. On pre-historic steppes of Vladimir Region. *Pochvovedenie,* ***2***, 393–396 (in Russian).

Targulian, V.O., Sokolova, T.A., Birina, A.G., Kulikov, A.V., Tselishcheva, L.K. 1974. *Arrangement, Composition, and Genesis of Sod-Pale Podzolic Soil Derived from Mantle Loams. Morphological Investigation.* X Int. Congress in Soil Science. AS USSR, Moscow (in Russian).

Terhorst, B., Kleber, A., Bibus, E. 2013. Relative Dating with Cover Beds. *Dev. Sedimentol.,* ***66***, 229–251. https://doi.org/10.1016/B978-0-444-53118-6.00007-6

Trofimov, V.T., Balykova, S.D., Bolikhovskaya, N.S. et al. (Eds.). 2001. *Loess Cover of the Earth and Its Properties*. Moscow University, Moscow (in Russian).

Tseytlin, S.M. 1965. Geology of the area of the Upper Paleolithic site Sungir in the Vladimir region. In: *Stratigraphy and Periodization of the Paleolith of Eastern and Central Europe*. Moscow, 66–85 (in Russian).

Tyuryukanov, A.N., Bystritskaya, T.L. 1971. *Opolies of Central Russia and Their Soils*. Nauka, Moscow (in Russian).

Ukraintsev, V.Y., Konstantinov, E.A., Zakharov, A.L. 2020. Drainage changes in the Nero Lake basin, Central European Russia. *Limnology and Freshwater Biology,* ***4***, 476–477. https://doi.org/10.31951/2658-3518-2020-A-4-476

Umarova, A.B., 2011. *Preferential Flow in Soils: Formation Regularity and Significance of Soil Functioning*. GEOS, Moscow (in Russian).

Utkina, A.O., Panin, A.V., Kurbanov, R.N., Murray, A.S. 2022. Unexpectedly old luminescence ages as an indicator of the origin of the upper Volga River valley sediments. *Quat. Geochronol.,* ***73***, 101381. https://doi.org/10.1016/j.quageo.2022.101381

Vagapov, I.M., Gugalinskaya, L.A., Alifanov, V.M. 2013. Spatial variations of the magnetic susceptibility in the profiles of palaeocryomorphic soils. *Eur. Soil Sci.,* ***46***, 291–296. https://doi.org/10.1134/S1064229313030113

Van der Meer, J.J.M. 1987. Micromorphology of glacial sediments as a tool in distinguishing genetic varieties of till. In: *INQUA Till Symposium, Finland, 1985*. Geological Survey of Finland, 77–89.

Van der Meer, J.J.M., Rappol, M., Semeijin, J.N. 1983. Micromorphological and preliminary X-ray observations on a basal till from Lunteren, The Netherlands. *Acta Geologica Hispanica,* ***18***, 199–205.

Van Vliet-Lanoë, B. 1988. The significance of cryoturbation phenomena in environmental reconstruction. *J Quat. Sci., 3*, 85–96.

Van Vliet-Lanoë, B., Pissart, A., Baize, S., Brulhet, J., Ego, F. 2019. Evidence of multiple thermokarst events in northeastern France and southern Belgium during the two last glaciations. *Geomorphology,* ***327***, 613–628. https://doi.org/10.1016/j.geomorph.2018.08.036

Vandenberghe, J., Van den Broeck, P. 1982. Weichselian convolution phenomena and processes in fine sediments. *Boreas,* ***11***, 299–315.

Velichko, A.A. 1958. Periglacial structures of the middle Desna River basin and their significance for stratigraphic and palaeogeographic constructions. *Biuletyn Peryglacjalny,* ***6***, 361–372.

Velichko, A.A. 1973. Environmental process in Pleistocene. Nauka, Moscow (in Russian).

Velichko, A.A. 1990. Loess-paleosol formation on the Russian Plain. *Quat. Int., 7*, 103–114. https://doi.org/10.1016/1040-6182(90)90044-5

Velichko, A.A., Faustova, M.A., Pisareva, V.V., Gribchenko, Yu.N., Sudakova, N.G., Lavrentiev, N.V. 2011. Glaciations of the East European Plain: Distribution and Chronology. In: J. Ehlers, P. Gibbard, and P. Hughes (Eds) *Dev. Quat. Sci.,* ***15***, Elsevier, 337–359. https://doi.org/10.1016/B978-0-444-53447-7.00026-X

Velichko, A.A., Morozova, T.D., Nechaev, V.B., Porozhnyakova, O.M. 1996. *Palaeocryogenesis, Soil Cover and Agriculture*. Nauka, Moscow (in Russian).

Velichko, A.A., Morozova, T.D., Nechaev, V.B. Porozhnyakova, O.M. 1996. Late-Pleistocene cryogenesis and modern soil formation in the southern Taiga zone (with special reference to Vladimir Opolie). *Eur. Soil Sci.,* ***29***, 984–991.

Velichko, A.A., Morozova, T.D., Nechaev, V.P., Rutter, N.W., Dlusski, K.G., Little, E.C., Catto, N.R., Semenov, V.V., Evans, M.E. 2006. Loess/paleosol/cryogenic formation and structure near the northern limit of loess deposition, East European Plain, Russia. *Quat. Int.,* ***152–153***, 14–30. https://doi.org/10.1016/j.quaint.2005.12.003

Wohlfarth, B., Tarasov, P., Bennike, O., Lacourse, T., Subetto, D., Torssander, P., Romanenko, F. 2006. Late glacial and Holocene palaeoenvironmental changes in the Rostov-Yaroslavl' area, West Central Russia. *J of Paleolimnology,* ***35***, 543–569. https://doi.org/10.1007/s10933-005-3240-4

Woronko, B., Zagorski, Z., Cyglicki, M. 2022. Soil-development differentiation across a glacial-interglacial cycle, Saalian upland, E Poland. *Catena, **211***, 105968. https://doi.org/10.1016/J.CATENA.2021.105968

Worsley, P. 2016. Sand wedges in England and arctic Canada. *Mercian Geologist, **19***, 7–17.

Woźniak, P.P., Czubla, P. 2016. Unraveling the complex nature of the Upper Weichselian till section at Gdynia Babie Doły, northern Poland. *Geologos, **22***, 15–32.

Yakushevskaya, I.V. 1959. Soils of Vladimir Opolie. *Science reports of higher school. Biological Sciences, **1***, 194–200 (in Russian).

Zeeberg, J.J. 1998. The European sand belt in eastern Europe – and comparison of Late Glacial dune orientation with GCM simulation results. *Boreas, **27***, 127–139. https://doi.org/10.1111/j.1502-3885.1998.tb00873.x

Zhurbin, I.V., Fedorina, A.N. 2017. Complex geophysical surveys of the Suzdal Opolie settlements. *Archaeol. Ethnol. Anthropol. Eurasia, **45***, 62–70 (in Russian).

ACKNOWLEDGMENTS

The field tour sites were investigated and prepared with the support of the Russian Science Foundation, project # 23-17-00073.
The scientific data employed in the guidebook was acquired with the support of the Russian Science Foundation, projects # 23-77-10063 and # 19-77-10061.

We are deeply grateful to the Deputy Director for Science Alexander G. Morozov and Alexander V. Kiselev for the opportunity to hold the conference at the historical venues of the State Museum-Reserve "Rostov Kremlin" and particularly to Dmitry E. Leonov for the warm welcome, heartfelt assistance, and enthralling excursions around the exhibitions of the Rostov Stable Yard and Kekin City Estate.

Special acknowledgments are expressed to the CEO of agricultural enterprise Krasny Mayak LLC Vasily Finogeev and especially to the Chief Engineer Sergey Guzev for the help provided in preparation of the field sites and transportation during the Symposium.

We highly appreciate the help of Veronika Smirnova, Polina Verevkina, Vadim Ukraintsev, Roman Shukhvostov, Nikolay Mokievsky, Ilya Boyko, Ivan Petrovnin, and Dmitry Baranov in preparing the key sections shown during the Symposium and also their active involvement in the maintenance of both the in-doors conference events and field tour additionally supported by Lidia Shasherina and Vitalia Posazhennikova.

Complex logistics of the field part would not be accessible without the assistance of Vitaly I. Mitckevitch, the head of transportation division.

Elena D. Sheremetskaya has executed the most challenging part of the event preparation dealing with the remote logistics and bureaucracy, which exclusively allowed the participants to fully enjoy the field tour and accommodations.

Finally, we recognize the entire *π-pedone united* © team for assistance in the field and lab work during the preceding period of scientific data acquisition and interpretation, which made the Valdai Periglacial Symposium possible and successful as it was.

ISBN 978-5-89658-071-3